THE CITY UNIVERSITY

DEPARTMENT OF CHEMISTRY

THE SOLID STATE AND CATALYTIC PROPERTIES OF SOME TIN CONTAINING COMPOUNDS

by

Anna Nicolaides

A thesis submitted for the degree of Doctor of Philosophy in the Faculty of Science, The City University, London.

Department of Chemistry,
The City University,
Northampton Square,
London EC1V OHB.

May 1984.

for

Mum , Dad

and

CONTENTS

ACKNOWLEDGEMENTS

First of all I would like to thank my supervisor, Professor John Donaldson, for his help and guidance throughout the course of this work.

I should also like to acknowledge the help and support of friends and colleagues at The City University, especially [redacted] for the carbon and hydrogen microanalysis, [redacted] for his hard work in running ^{13}C NMR spectra, [redacted] for advice on spectroscopic techniques, [redacted] for her technical assistance and the Physics Department of The City University for the use of their X-ray facilities.

I wish to thank the Science and Engineering Research Council (SERC) and the International Tin Research Institute (I.T.R.I.) for their financial support. Thanks are due to [redacted] and to colleagues at I.T.R.I. for making the time I spent there both enjoyable and productive.

Finally, my gratitude is owed to my parents for their continuous encouragement and support throughout the years I have spent studying, and to [redacted], for the excellent quality of the typing and diagrams in this thesis and for relieving me of the very painful job of proof-reading.

DECLARATION

The experimental work in this thesis was carried out in the Department of Chemistry of The City University between October 1980 and September 1983. This work has not been previously presented and is not being presented for any other degree.

I grant powers of discretion to the University Librarian to allow this thesis to be copied in whole or in part without further reference to me. This permission covers only single copies made for study purposes, subject to normal conditions of acknowledgement.

A. Nicolaides

May 1984

PUBLICATIONS

Some of the work contained in this thesis has previously been published, as detailed below:

(1) Preparation and Spectroscopic Studies of Diorganotin Oxycarbonates.

P.J. Smith*, R. Hill, A. Nicolaides and J.D. Donaldson, J. Organomet. Chem., (1983), 252, 149.

(2) The Crystal Structure Determination of Potassium[Hydrogen-bis-(maleato)]-Stannate(II).

J.D. Donaldson*, S.M. Grimes and A. Nicolaides, Polyhedron, In Press.

ABSTRACT

A series of normal and complex tin(II) carboxylates are prepared and fully characterised by infrared and Mössbauer spectroscopy, differential thermal analysis, thermogravimetric analysis and chemical analyses. Crystal structure determinations are carried out on two of these compounds, viz. potassium [hydrogen-bis-(maleato)]-stannate(II) and tin(II) malonate. Both structures show unusual features, the maleato complex has Sn in a trigonal pyramidal environment but contains two types of maleate ligands and the malonate has tin in a site intermediate between the common trigonal- and square- pyramidal environments.

The catalytic activity of the tin(II) carboxylates is tested in a number of polymerisation systems and the results obtained compared with those achieved using known catalysts. In all cases, the tin(II) species performed well. Mechanisms for the polymerisations are postulated on the basis of analytical measurements on the systems. In the case of propylene oxide polymerisation, both crystalline and amorphous polymers are obtained via cationic and anionic mechanisms, respectively. In the polymerisation of trioxane, the reaction pathway is cationic. A study of the curing of a commercial silicone resin shows that the cure time is dependent on (1) the catalyst used, (2) its concentration and (3) temperature, but is independent of the solvent used.

The spectroscopic characterisation of a series of diorganotin(IV) oxycarbonates provides evidence that they adopt a polymeric structure made up of intermolecularly bridging carbonate groups and four membered Sn_2O_2 rings. The solid and gaseous thermal decomposition products of the carbonates are studied and their decomposition pathways determined. The final solid residue is normally a dark coloured powder whose major component is tin(IV) oxide.

For the SnF_2:MoS_2 system, the removal of the distortion effects of the tin(II) lone pair electrons is shown to occur via the donation of the 5s electrons into conduction bands. Similar results are obtained for the tin(II) halide - tin(IV) sulphide systems.

CHAPTER ONE

INTRODUCTION

1.1. INTRODUCTION.

Tin is a group (IV) element with the outer electronic configuration $5s^2 5p^2$ and can exist both in the II+ and IV+ oxidation states, with the latter being far more stable. Whilst in general, Sn(IV) compounds are covalently bonded with a strong tendency towards complex formation, Sn(II) compounds are more electrostatic in their bonding and the tendency for complex formation is somewhat reduced. The presence of the non-bonding electron pair in the outer electronic configuration of Sn(II), usually results in its compounds being lone pair distorted.

1.1.(1). Tin(IV) Compounds.

There are three ways in which the element in its IV+ state can form derivatives:

(a) By loss of all four valence electrons to form the stannic ion, Sn^{4+}.

(b) By hybridisation of all the available atomic orbitals in a suitable configuration to form four equivalent covalent bonds.

(c) By complex formation, i.e. making use of the empty 5d orbitals which are of similar energy to the valence electron orbitals. This is represented as the overlap of empty hybrid orbitals on the metal with filled orbitals on a suitable ligand, to form dative covalent bonds.

This would suggest a spherical ion for ionic bonding, tetrahedral coordination for covalent bonding and octahedral coordination for complex formation. This data is summarised diagrammatically in Figure 1.(1).

Bond Type	Electronic Configuration	Shape Of Ion Or Hybrid	Typical Ion Or Compound	Ref.
	5s 5p 5d			
Tin	↑↓ ↑ ↑ □			
Sn^{4+} Stannic ion	□ □ □ □	spherical ion	SnO_2	(1)
Covalent Sn	↑ ↑ ↑ ↑		$SnCl_4$	(2)
			most organo-tin(IV) compounds	(3)
Complex formation	□ □ □ □ □ □ sp^3d^2		$SnCl_6^{2-}$	(4)

Filled Orbital ↑↓ Half-filled Orbital ↑ Empty Orbital □

FIGURE 1.(1). Bonding in Tin(IV) Species.

1.1.(2). Tin(II) Compounds.

In tin(II) compounds only two valence electrons are available for bonding. This means that the outer electronic configuration of the element in this oxidation state must contain a completely filled 5s orbital, and if this orbital obtains any p-character, it becomes a directional lone pair leading to the distortion found in the structures of Sn(II) compounds. Tin in its lower oxidation state also has empty 5p and 5d orbitals which could be utilised in compound formation.

The four possible ways in which a Sn(II) species can be formed from tin are as follows:

(a) By loss of two valence 5p electrons to form the stannous ion, Sn^{2+}.

(b) By the use of two 5p electrons to form a covalent bond.

(c) By complex formation, involving the use of the empty 5p and 5d orbitals in the hybridisation, as acceptor orbitals.

(d) By overlap of the lone pair of electrons with an empty orbital on an acceptor species.

1.1.(2).1. The Stannous Ion.

Tin can readily lose its two 5p electrons to form a dipositive ion of configuration $5s^2$.

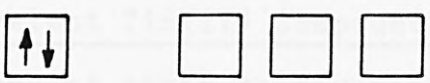

This ion does not have spherical charge distribution because,

unlike spherical ions which have a closed shell configuration it has a pair of s electrons beyond a completed shell (the lone pair), this ultimately leads to a lowering of the symmetry of coordination of the negatively charged ligands around the element and a distorted environment for the ion.

The first excited state of the stannous ion, which is $5s^1 5p^1$, lies very near to the ground state, and so it is possible to gain extra crystal field stabilisation by s-p orbital mixing, effectively promoting one of the s electrons into a p orbital. Since the s orbital is spherically symmetrical and the p orbital is not, the only way in which this stabilisation may be achieved, is by the unsymmetrical distortion of the environment of the ion. In ionic materials containing oxide and fluoride ions, tin should be in an octahedral environment, but if the stabilisation energy gained by s-p mixing is greater than that for a regular octahedral arrangement, then a distorted octahedral structure will be obtained. The stabilisation energy decreases as the tin-anion bond distance increases and this means that the crystal field distortion should be greatest in materials containing small anions.

There are three ways in which an octahedron can be distorted unsymmetrically, resulting in three, four and five nearest neighbours for the stannous ion, as shown below in Figure 1.(2).

1.1.(2).2. Covalent Tin(II) Compounds.

Since the ground state configuration of tin metal is $5s^2\ 5p^2$, it can form covalent compounds in the II+ state, by using the two unpaired 5p electrons for bonding. The stereochemistry of the molecule formed is dependent upon the

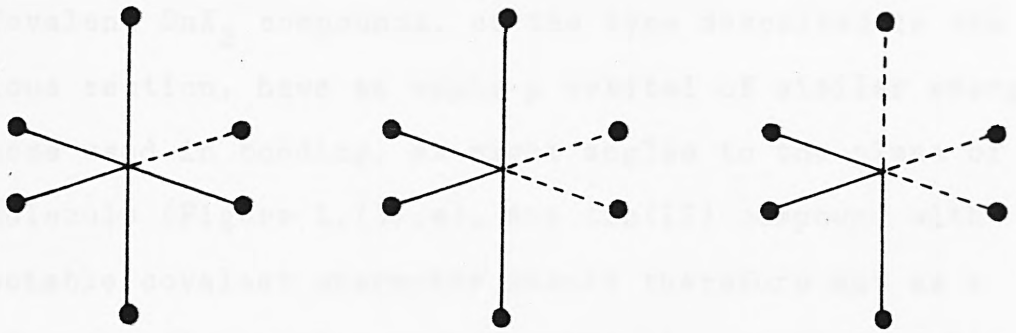

FIGURE 1.(2). Distorted Octahedral Environment for the Tin(II) Ion with Three, Four and Five Nearest Neighbours.

hybridisation of the valence shell electrons, mixing of the 5p electrons and the lone pair electrons leads to sp^2 hybridisation of the molecule, with bond angles approaching 120°.

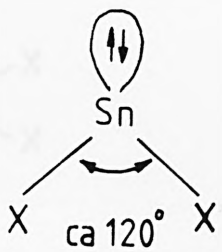

In practise, the bond angle also depends upon the extent of the repulsion between the lone pair orbital and the bonds formed, the greater the repulsion the smaller the bond angle. In anhydrous tin(II) halides[5] in the vapour phase for example, the X-Sn-X bond angle is reduced to about 95°.

Thus, covalent bonding is of importance in tin(II) compounds in the vapour and liquid phases and in solids where the bonding cannot be explained in terms of an electrostatic interaction alone.

1.1.(2).3. Tin(II) Complexes.

Covalent SnX_2 compounds, of the type described in the previous section, have an empty p orbital of similar energy to those used in bonding, at right angles to the plane of the molecule (Figure 1.(3).a). Any tin(II) compound with appreciable covalent character should therefore act as a mono-functional acceptor towards suitable monodendate ligands to form compounds of the type SnX_2.(Ligand). The stereochemistry of such a material depends on the overlap of a lone pair orbital from the ligand with the empty p orbital on the tin and there is a tendency for the structure to be distorted towards sp^3 hybridisation (Figure 1.(3)b).

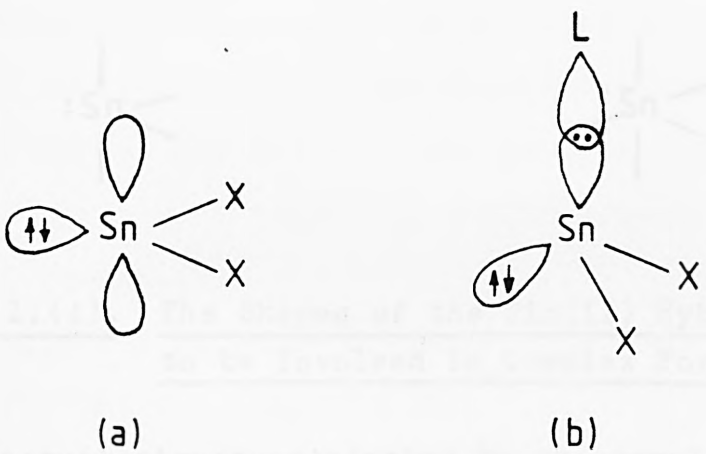

FIGURE 1.(3). The Orbital Arrangement of Molecular Tin(II) Compounds (a) Before and (b) After Adduct Formation.

The stannous ion with empty 5p and 5d orbitals can also act as an acceptor towards certain ligands. It is possible to predict, from the electronic configuration of the ion, the hybridisation of the tin which is likely to be adopted in these complexes. In each case, the lone pair must be included in the hybridisation (Figure 1.(4).). Again, these

complexes would be formed by the overlap of lone pair orbitals on the ligands with the empty hybrid orbitals on the tin.

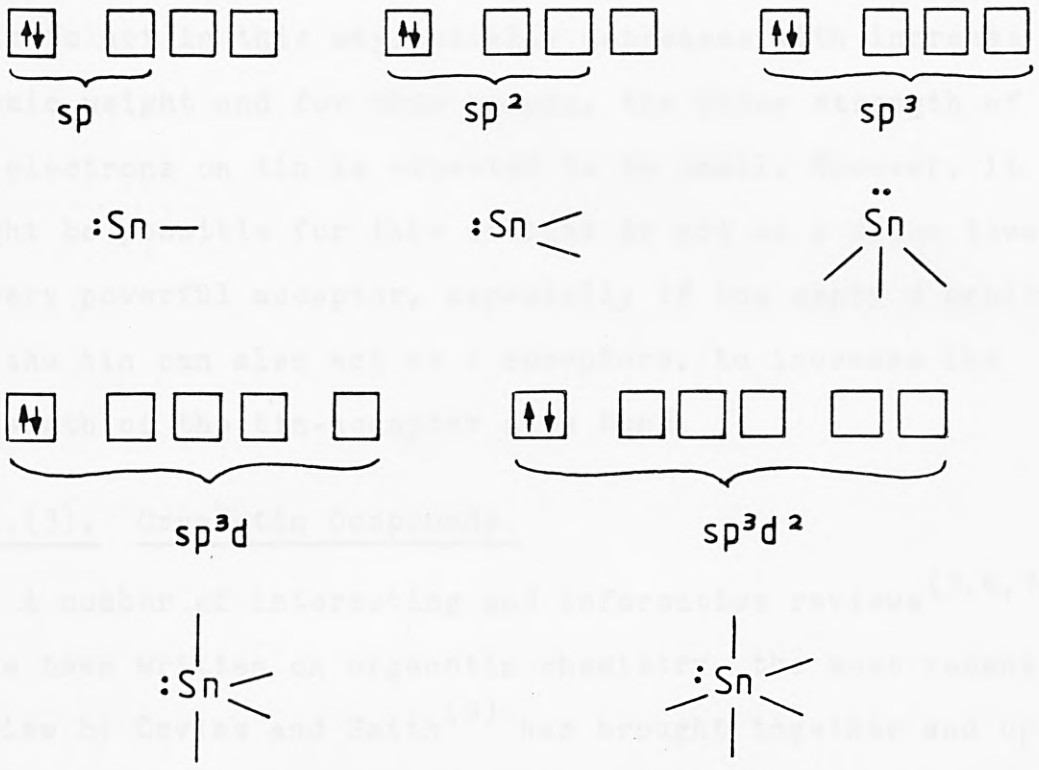

FIGURE 1.(4). The Shapes of the Tin(II) Hybrids Likely to be Involved in Complex Formation.

The actual structure adopted by the complex, will depend upon the relative stability of the available configurations. Since the energy separation between the s and p orbitals is small, all p orbitals should be included in the hybridisation if possible and so the sp^3 configuration should be very stable. The inclusion of d character in the hybridisation, will depend upon the s-d separation as well as the s-p separation, thus these configurations will be less likely.

1.1.(2).4. Stannous Tin As A Donor Species.

The lone pair of electrons on the tin in molecular and complex stannous compounds, is sterically active and as such, could act as a σ donor species. The ability of a lone pair to act in this way, usually decreases with increase in atomic weight and for this reason, the donor strength of the 5s electrons on tin is expected to be small. However, it might be possible for this orbital to act as a donor towards a very powerful acceptor, especially if the empty d orbitals on the tin can also act as π acceptors, to increase the strength of the tin-acceptor atom bond.

1.1.(3). Organotin Compounds.

A number of interesting and informative reviews[3,6,7,8] have been written on organotin chemistry, the most recent review by Davies and Smith[9] has brought together and updated the syntheses, reactions and structures of most organotin compounds.

The majority of known organotin compounds are derivatives of tin(IV), the few organotin(II) compounds that are known are usually unstable.

The simpler organotin(II) compounds of the type R_2Sn, where R is an alkyl or an aryl group, are generally polymeric[10], or polymerise rapidly after preparation as a monomer. The polymerisation results in the formation of Sn-Sn bonds, such that each Sn atom is surrounded by two R groups and two Sn atoms in approximately tetrahedral coordination. The effect of the polymerisation is to oxidise the tin to tin(IV) by making use of all four valence electrons in covalent bond formation.

1.2. THE USE OF TIN(II) CARBOXYLATES IN CATALYSIS.

Although some tin(II) carboxylates have been known for nearly one hundred and fifty years, their use as homogeneous catalysts has developed over the last forty years. Their industrial application has been the subject of a great number of reports, particularly in the patent literature.

Stannous Formate.

Tin(II) formate $Sn(CHOO)_2$, is the simplest stannous carboxylate, but although this compound has been known since 1836, when it was reported by Liebig[11], its use in the field of catalysis has been limited to the preparation of fibre-forming poly(ethyleneterephthalate)[12].

Tin(II) Acetate.

Stannous acetate is a polymerisation catalyst in the preparation of several types of polyurethanes. It is used in the preparation of polyurethane elastomers[13], based on the reaction of polyesters or polyethers with polyhydroxy compounds and diisocyanates. The elastomers produced, have improved tear resistance, abrasion and permanent set properties. The composition of the polyol may vary and the acetate has been used to prepare a glutarate containing polyol[14] which is then reacted further to produce a polyurethane. This catalyst has also been used to promote the foaming process, in which large amounts of carbon dioxide gas are evolved causing the polyurethane to foam[15,16].

Other applications include the preparation of transparent polyesters with high heat distortion temperatures[17], highly crystalline poly(vinylchloride)[18] polymers and epoxide resins[19]. The curing of epoxides for example, can

occur using concentrations of only 0.98-4.0 wt.% catalyst. By modifying the catalyst with polyfunctional organic hardeners, resins with a wide range of varying and preselected properties can be synthesised[20,21].

Recent studies carried out by this group, have shown that transition metal derivatives of the triacetatostannate (II) ion, $Sn(CH_3COO)_3^-$, will catalyse the polymerisation of propylene oxide[22], to give polymers which have properties comparable to those reported in the literature.

Tin metal promoted by chloroacetic acid, dichloroacetic acid and trichloroacetic acid has been found to be excellent at catalysing the hydrogenation of coal[23], giving an 84-87% conversion of coal to liquid fuel. This compares very favourably with the 86% conversion rate achieved using stannous chloride, a tin species with an inbuilt promoter, as the catalyst.

Tin(II) Oxalate.

The simplest dicarboxylate, stannous oxalate (SnC_2O_4), has been widely utilised in industry. It is an ideal catalyst for esterification reactions, since it limits the destructive side-reactions which are responsible for the degradation of the esters at their preparation temperatures. A wide variety of polyesters have been prepared, including linear polyesters[24] and unsaturated polyesters with improved colour, heat and chemical resistances[25,26].

Other systems catalysed by stannous oxalate are:

(a) the polyurethanes, giving elastomers with improved resistive properties[13],

(b) the preparation[19] and cure[20,21] of epoxide resins,

(c) the liqiud-phase polymerisation of acrylonitrile[27]

(d) the preparation of trioxane polymers and copolymers[28]

One of the most important applications of tin(II) oxalate is as a catalyst in the hydrogenation of coal[23]. The oxalate is preferred to the tin metal, because it is less expensive and easier to disperse, the most efficient method of dispersion involving the impregnation of the coal with a solution of the catalytic components. Further studies showed an increase in the performance of the catalyst following promotion with chlorine, bromine or iodine and in these cases, impregnation by special techniques was not required. Stannous oxalate was reported to have an efficiency of 85% in the conversion of coal to liquid fuel.

Tin(II) Octoate.

Stannous octoate (stannous 2-ethyl-hexanoate) is the most readily available stannous carboxylate commercially, and as such, is used most widely in industry, especially in the production of polyurethanes. Depending on the conditions and starting materials used, polyurethanes may be made to various specifications and having a variety of properties, ranging from foams with great strength[29] to polymers which are suitable for paper impregnation[30]. Modification of the catalyst with a mixture of antimony or bismuth carboxylates, antimony oxide and zinc oxide in a one-shot polymerisation process[31] with a PVC copolymer, produces a foam which has improved heat and discolouration stability. Varying the starting materials can result in foams with flexibility[32], hydrophilic properties[33] or adhesive properties[34].

Other important applications of stannous octoate are in

the preparation of polyesters with low acid numbers, which are free from discolouration[35-37], the preparation[9,38,39] and curing of epoxide resins[20,21] and the polymerisation of caprolactam[40]. In the preparation of poly(vinylchloride) moulding compositions[41], the catalyst has the added advantage of stabilising the PVC.

Stannous octoate has been utilised in the preparation of polysiloxanes. Organosiloxane elastomer foams[42] and cold and water resistant rubbers are prepared by grafting styrene onto methyl-vinyl siloxane rubber, followed by curing with ethyl silicate and stannous octoate[43]. Linear poly(diaryl-siloxanes)[44] and functional organosilicon oligourethane preparations are also carried out in the presence of this catalyst[45].

Tin(II) Octanoate.

The polyurethane production can also be catalysed by stannous octanoate[16,45,46]. Bulygin and his co-workers[47] have also determined the percentage of tin remaining in the polyurethane foams by a polarographic technique. The procedure involved the extraction of the Sn by refluxing the foam in a 1:1 aqueous 3N HCl-ethanol solution for 15 minutes followed by polarographic analysis. The technique is reported to have a sensitivity of 0.01% with an average relative standard deviation of 0.067.

If the catalyst is modified with a tertiary amine-benzoyl peroxide mixture, it can be used as a cross-linking agent to prepare unsaturated polyester adhesive compositions which are stable and are exceedingly strong[48]. Initial tests have shown that they are able to fix anchor bolts to rocks and concrete walls.

Tin(II) Caproate.

This compound is utilised in the preparation of poly-(vinylchloride) moulding compositions[41], in the production of urethane modified isocyanurate foams[16], by the reaction of a polyfunctional isocyanate with a polyol, the synthesis of polyurethanes using glutarate containing polyester polyols[14] and in the polymerisation of epoxides[20].

The chemical state of the tin atom during the polymerisation of formaldehyde using tin(II) caproate as catalyst in an organic medium has been studied by Kessler and his colleagues, using Mössbauer spectroscopy[49,50]. During the polymerisation of formaldehyde in either air or argon, the catalyst undergoes partial oxidation from Sn(II) to Sn(IV), either because of the atmospheric oxygen or because of the impurities present in the gaseous HCHO. This is said to result in the formation of a catalytically inert hexa-coordinated binuclear complex

$$[CH_3(CH_2)_4CO_2]_2\ Sn\begin{matrix}O\\ \diagup\ \diagdown\\ O\end{matrix}Sn\ [O_2C(CH_2)_4CH_3]_2$$

and $Sn(O_2C(CH_2)_4CH_3)_4$. The oxidised complex loses its catalytic activity and a decrease in polymer yield and viscosity are observed. The catalytically active compound in the system is said to form a complex with the formaldehyde, viz. $(CH_3(CH_2)_4CO_2)_2Sn.HCHO$, in the initial stages of the polymerisation, whilst in the final stage, the tin species are reported to form a complex with the polymer chain.

Tin(II) Stearate.

The literature reveals that the main catalyst utilised in the polymerisation of the glycolides is stannous stearate. The polymerisation, which takes place in an extruder, is

rapid and continuous and requires only 0.01-2.0% catalyst[51]. The polyglycolide produced may be extruded as a filament, wire, ribbon, film or tube[52]. The glycolide may also be polymerised continuously in a screw press[53].

Stannous stearate has also been used as a catalyst in the preparation of polyesters[35], in the preparation[19] and cure[21] of epoxides and as a heat and light stabiliser of polyvinylhalide resins[54].

Other Tin(II) Carboxylates.

The hydrogenation of coal has been efficiently catalysed by stannous naphthenate[23], impregnation of 0.1wt.% of the catalyst caused 88% of coal conversion at 500°C and about 7500 psig hydrogen pressure. The metal naphthenates are the most effective catalysts in coal hydrogenation, but so far they have only technical significance, because of their high costs.

Polyurethane foams have been prepared using the following tin(II) carboxylates as the catalyst: tartrate[55], oleate[14, 29], propionate, butyrate[16,14] and dodecanate[16]. The preparation[19] and curing[20,21] of epoxides has been catalysed using stannous oleate, propionate, butyrate, laurate, valerate and palmitate. Heat stabilisation of vinyl resins[54] has been achieved in the presence of the stannous derivatives of the following acids:- phthalic, naphthenoic, tartaric, oleic, lauric, benzoic, succinic, salicylic and palmitic.

At this point, it is useful to list various carboxylic acids with their systematic and trivial names and to characterise them in terms of the number of carbon atoms present in each acid. This is shown in Table 1.(1).

$C_nH_{2n}O_2$	Systematic Name	Trivial Name	Examples of the Use of Tin(II) Salts as Catalysts
1	methanoic	formic	polyethylene terephthalate
2	ethanoic	acetic	coal hydrogenation, PVC polymerisation
3	propanoic	propionic	epoxide cure
4	butanoic	butyric	polyurethane production
5	pentanoic	valeric	epoxide cure
6	hexanoic	caproic	formaldehyde polymerisation
8	octanoic	caprylic	preparation of polyurethane foams, aids cross-linking of polyesters
8	2-ethyl-hexanoic	octoic	polyurethane production, cure of silicone rubbers, PVC and polyesters preparation
12	dodecanoic	lauric	preparation and cure of epoxides
16	hexadecanoic	palmitic	
18	octadecanoic	stearic	glycolide polymerisation

TABLE 1.(1). Systematic and Trivial Names of Some Commonly Used Carboxylic Acids.

1.3. EXPERIMENTAL TECHNIQUES.

Several experimental techniques have been used in the course of this work, in order to characterise the compounds and polymers prepared. Because of the importance of the results obtained from both Mössbauer spectroscopy and differential thermal analysis (DTA), a detailed account of the theories involved in their usage is given in this chapter. For other techniques used, the description is simply limited to details of the apparatus utilised.

1.3.(1). Mössbauer Spectroscopy.

1.3.(1).1. Introduction.

The phenomena of the emission and absorption of a γ-ray photon, without loss of energy due to the recoil of the nucleus and without thermal broadening, is known as the Mössbauer effect. It was discovered by R.L. Mössbauer[56] in 1957, as a result of a study of the recoilless resonant absorption in ^{191}Ir, but the first indications of hyperfine interactions in chemical compounds were obtained by Kistner and Sunyar[57] in 1960.

The unique feature of the Mössbauer effect is the production of monochromatic radiation with a very narrowly defined energy spectrum, so that minute energy differences can be resolved. Thus, slight variations in the energy of interaction between the nucleus and the extra-nuclear electrons can be detected.

Over 40 elements have had their Mössbauer spectra recorded, but of these, information of chemical significance is restricted to about 12 elements, e.g. Fe, Sn, Sb, Te and I. In this work, only ^{119}Sn Mössbauer spectra were recorded.

1.3.(1).2. Theory.

Mössbauer spectroscopy involves the recoilless emission and resonant reabsorption of γ-radiation between the ground state and usually the first excited state of the nucleus; the transitions involved are of the order of $10^8 cm^{-1}$.

When the nucleus has emitted its γ-ray, it will experience recoil in the opposite direction to which it is radiating. Absorption of the γ-radiation by an identical nucleus will cause this second nucleus to recoil also. Since in the gas phase, the γ-ray will experience a loss of energy due to the recoil of the first nucleus, it will have insufficient energy to cause a transition between the ground state and the first excited state of the second nucleus and so a Mössbauer spectrum will not be observed. When the nuclei are in the solid state, the recoil associated with the emission or absorption of the γ-ray, is taken up by the lattice as a whole. Under these conditions, the γ-radiation has sufficient energy to cause a transition between the ground state and excited state of the absorbing nuclei and an absorption and hence a Mössbauer spectrum will be obtained as in Figure 1.(5).

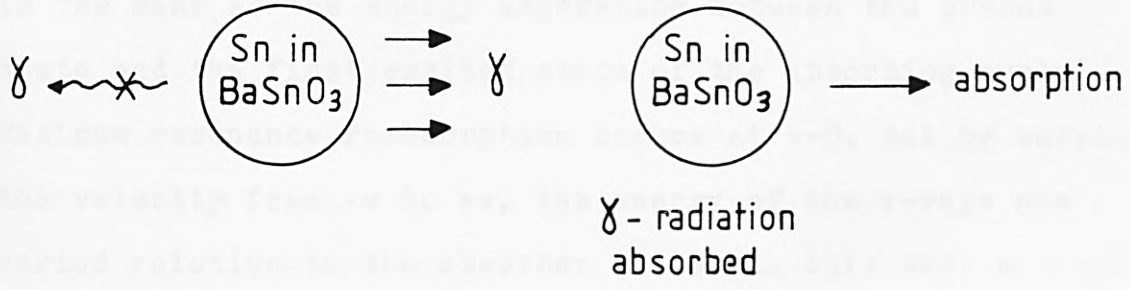

FIGURE 1.(5). Absorption of a γ-Ray to Give a Mössbauer Transition.

To obtain a Mössbauer spectrum, the source (emitting

γ-radiation of energy E) is subjected to a Doppler motion (velocity v) relative to a stationary absorber scanning through the absorption so that it can be observed.

This is shown in Figure 1.(6).

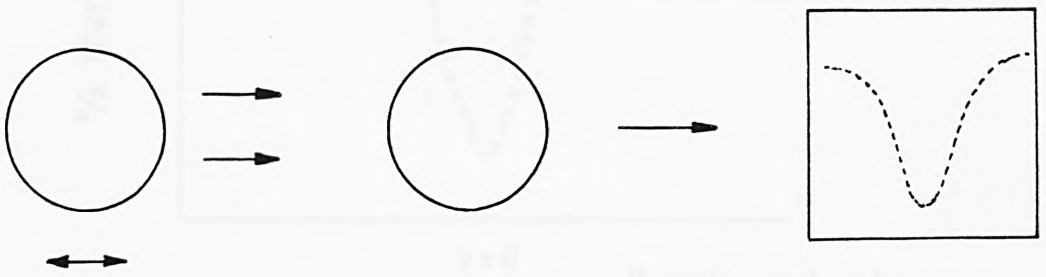

FIGURE 1.(6). Simple View of Doppler Motion.

The effect of this Doppler motion, is to vary the γ-ray energy relative to the absorber, and to produce a γ-ray energy shift ΔE, which is given by the expression below,

$$\Delta E = \frac{v}{c} E_{\gamma}$$

where c= velocity of light.

When both the emitting and absorbing nuclei are in the same chemical environment, the energy of the emitted γ-ray is the same as the energy separation between the ground state and the first excited state of the absorbing nuclei. Maximum resonance reabsorption occurs at v=0, but by varying the velocity from -v to +v, the energy of the γ-rays are varied relative to the absorber and so in this way, a Mössbauer spectrum may be observed. Figure 1.(7)., shows the Mössbauer spectrum of a $BaSnO_3$ absorber, relative to a $BaSnO_3$ source.

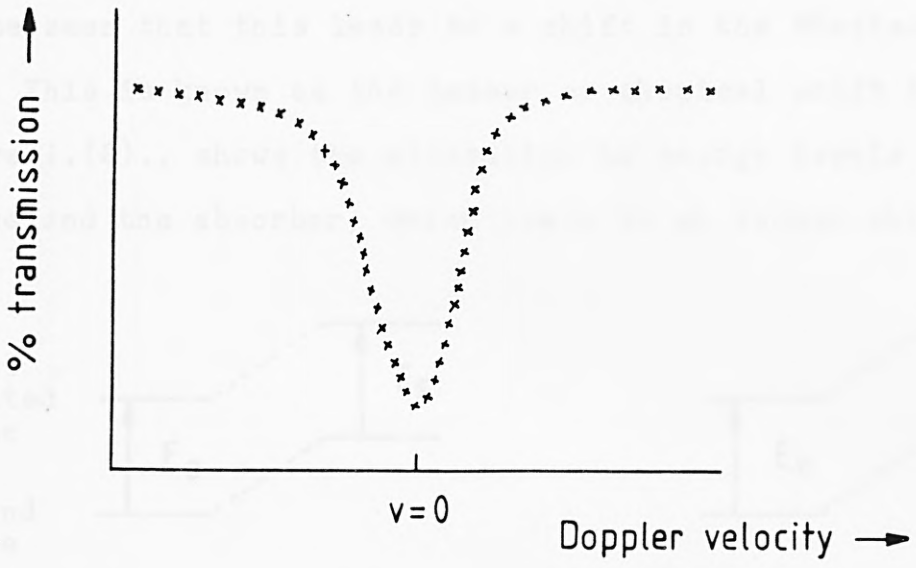

FIGURE 1.(7). Mössbauer Spectrum of $BaSnO_3$ Relative to a $BaSnO_3$ Source.

The Mössbauer spectrum is plotted as percentage transmission (number of counts registered by the detector) versus Doppler velocity and therefore energy. The motion of the source towards the absorber, is taken as positive velocity (+v) and motion away from the absorber, as negative velocity (-v).

Information on chemical structure and bonding is obtained by studying the shifts and splittings which occur in the Mössbauer spectral line, resulting from changes in the chemical environment of the emitting and absorbing nuclei.

1.3.(1).3. The Isomer Shift.

When the source and absorber are not in the same chemical environment, the energy gap between the ground state and excited state in the nuclei of the source, is different to that in the absorber. Under these circumstances, the energy of the γ-radiation must be modulated by the Doppler motion applied to the source, until the conditions of maximum

resonance are fulfilled and at this point, v≠0. Thus, it can be seen that this leads to a shift in the Mössbauer line. This is known as the isomer or chemical shift δ. Figure 1.(8)., shows the alteration in energy levels of the source and the absorber, which leads to an isomer shift.

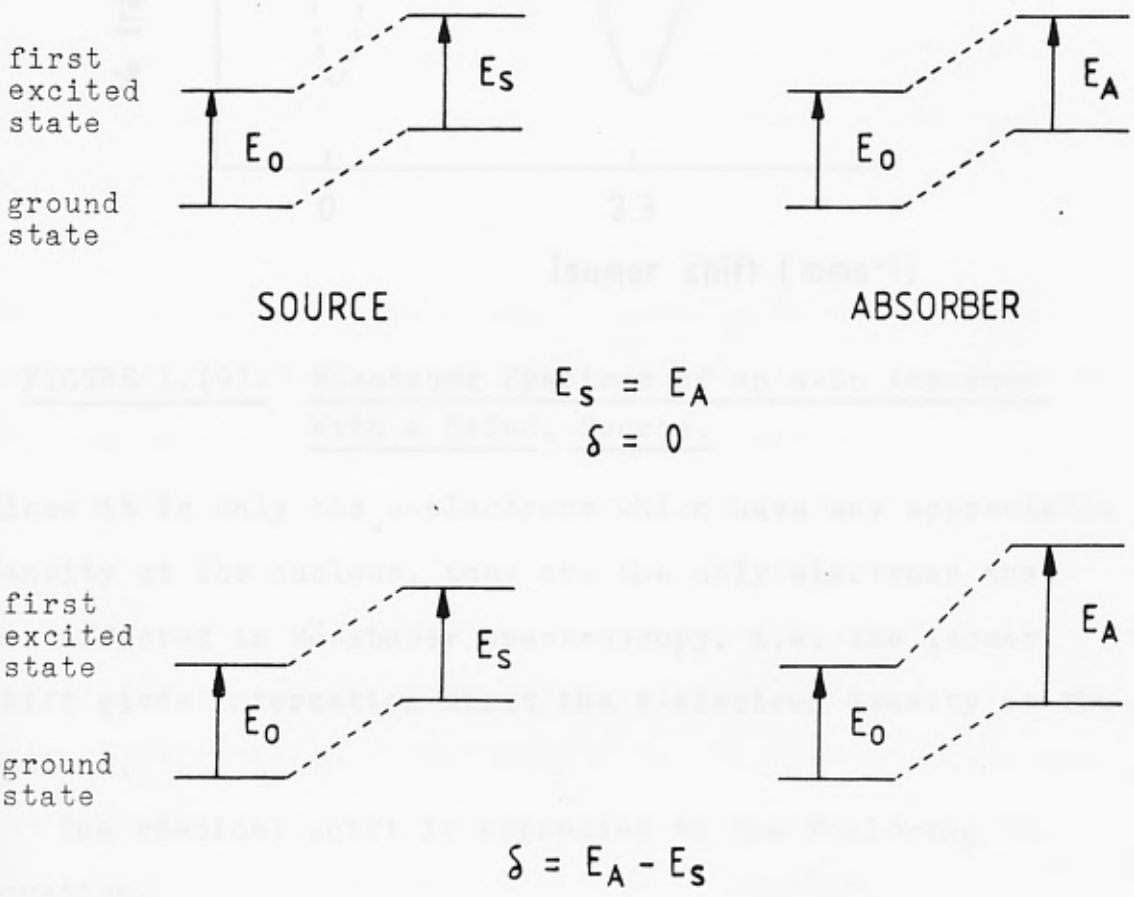

FIGURE 1.(8). Energy Level Diagram Showing the Occurrence of the Isomer Shift.

Therefore, if the Mössbauer spectrum of an α-Sn absorber is recorded relative to a $BaSnO_3$ source, we see the spectrum shown in Figure 1.(9).

The change in electronic environment about the nucleus produces a change in the interactions between the electrons around the nucleus and hence the isomer shift provides information about the electron density about the nucleus.

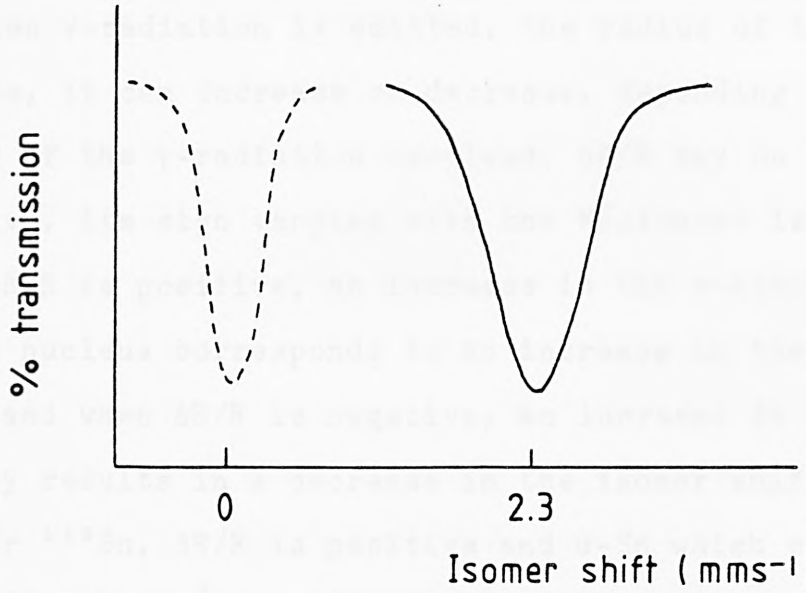

FIGURE 1.(9). Mössbauer Spectrum of an α-Sn Absorber With a $BaSnO_3$ Source.

Since it is only the s-electrons which have any appreciable density at the nucleus, they are the only electrons that are affected in Mössbauer spectroscopy, i.e. the isomer shift gives information about the s-electron density at the nucleus.

The chemical shift is expressed by the following equation,

$$\delta = k \cdot \frac{\Delta R}{R} \cdot \left\{ |\Psi_0|^2_A - |\Psi_0|^2_S \right\}$$

where k = constant

R = radius of the nucleus in the ground state

ΔR = change in the radius of the nucleus on going from the ground state to the excited state.

$|\Psi_0|^2$ = wavefunction defining the s-electron density at the nucleus.

ΔR/R arises because of nuclear factors and the term associated with the s-electron density at the nucleus is

due to electronic factors.

When γ-radiation is emitted, the radius of the nucleus changes, it can increase or decrease, depending upon the energy of the γ-radiation involved. ΔR/R may be positive or negative, its sign varying with the Mössbauer isotope used. When ΔR/R is positive, an increase in the s-electron density at the nucleus corresponds to an increase in the isomer shift and when ΔR/R is negative, an increase in the s-electron density results in a decrease in the isomer shift.

For ^{119}Sn, ΔR/R is positive and α-Sn which can be assumed to be sp^3 hybridised, is usually taken as the reference point. Therefore, as the s-electron density at the nucleus increases, the shift also increases relative to α-Sn i.e. Sn(II) compounds have a greater shift than α-Sn. Conversely, a decrease in the s-electron density, corresponds to a decrease in the shift of the Mössbauer spectral line and Sn(IV) compounds have a smaller shift relative to α-Sn. This is illustrated in Scheme 1.(1)., which also shows how the ionicity of a compound can affect the isomer shift.

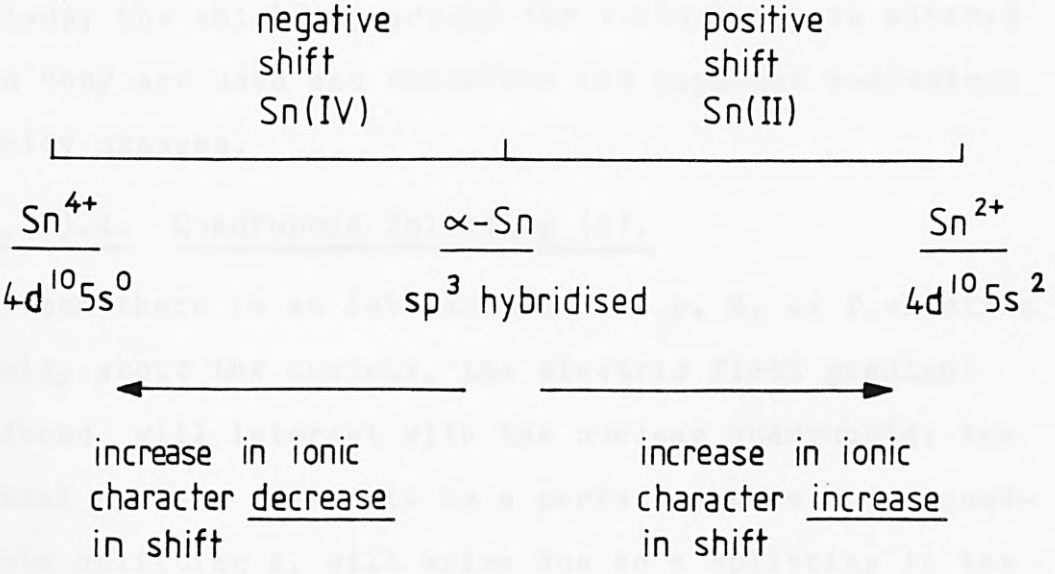

SCHEME 1.(1). Schematic Representation of the Effect of the s-electron Density on the Mössbauer Isomer Shift for ^{119}Sn Nuclei.

In general, compounds which approach the ionic configuration Sn^{4+} ($5s^0$) have the smallest chemical shift. In covalent Sn(IV) compounds, the hybridisation approaches $5s^1 5p^3$, with some electron withdrawal from the tin, therefore their isomer shifts lie between those of ionic Sn^{4+} and α-Sn in which the tin is surrounded tetrahedrally by four other tin atoms.

With stannous compounds in which the tin is covalently bonded, the non-bonding lone pair of electrons ($5s^2$) on the tin, results in a large positive chemical shift, which increases as the compounds become more ionic.

Thus, the increase of chemical shift follows the sequence $Sn^{4+} < Sn(0) < Sn^{2+}$ and this is directly related to the s-electron density about the tin nucleus: $s^0 < s^1p^3 < s^2$.

There are two ways in which the s-electron density at the nucleus may be altered:

(1) direct use of s-electrons in bonding.

(2) use of p, d, or f electrons in the bonding.

Although in (2), the electrons have zero density at the nucleus, the shielding around the s-electrons is altered when they are used and therefore the apparent s-electron density changes.

1.3.(1).4. Quadrupole Splitting (Δ).

When there is an imbalance in the p, d, or f electron density about the nucleus, the electric field gradient produced will interact with the nuclear quadrupole; the central nucleus ceases to be a perfect sphere and a quadrupole splitting Δ, will arise due to a splitting in the nuclear energy levels. Figure 1.(10). shows the quadrupole split doublet spectrum for tin(II) acetate.

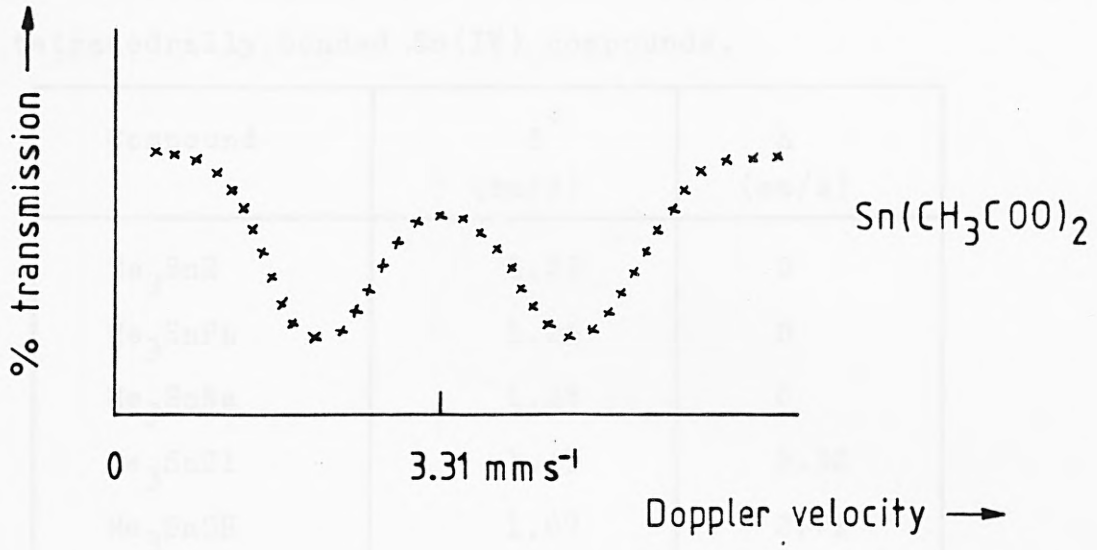

FIGURE 1.(10). Quadrupole Split Mössbauer Spectrum of Stannous Acetate Relative to a Barium Stannate Source.

In tin, the d and f orbitals are empty, consequently it is only the imbalance in the p electrons which will cause a quadrupole splitting. The imbalance arises from the fact that nuclear states with spin I > 1/2 can align themselves either with or across the electric field gradient and this removes the degeneracy of the nuclear sublevels. In this way, valuable information about the imbalance in the p, d and f electron density can be obtained. The splitting of the nuclear sublevels is shown diagrammatically in Figure 1.(11). below.

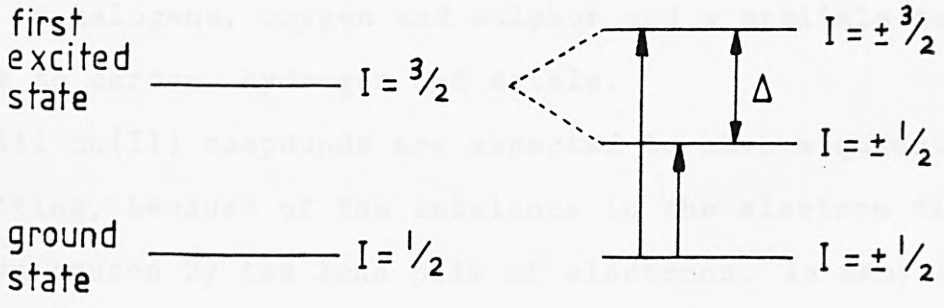

FIGURE 1.(11). Removal of the Degeneracy of Nuclear Sublevels to Give a Quadrupole Splitting Δ.

Table 1.(2). gives the Mössbauer parameters for a range of tetrahedrally bonded Sn(IV) compounds.

Compound	δ^* (mm/s)	Δ (mm/s)
Me_3SnH	1.23	0
Me_3SnPh	1.25	0
Me_3SnNa	1.28	0
Me_3SnCl	1.43	3.32
Me_3SnOH	1.07	2.71
Bu^n_2SnS	0.90	1.90

* Chemical shifts relative to Barium Stannate ($BaSnO_3$).

TABLE 1.(2). Mössbauer Parameters for a Selection of Organotin(IV) Compounds.

The tin in Sn(IV) compounds, is capable of adjusting the electron distribution around itself, so that all bonds have the same electron density. It can do this with ligands which use similar orbitals for bonding, e.g. Cl and Br, or Ph and H, but with ligands which use different orbitals for bonding, as with Cl and Ph, the tin cannot adjust the electron distribution. In this case, an imbalance then arises and a quadrupole splitting is obtained.

In general, it is found that tin uses p orbitals to bond to halogens, oxygen and sulphur and s orbitals to form bonds to carbon, hydrogen and metals.

All Sn(II) compounds are expected to have a quadrupole splitting, because of the imbalance in the electron distribution caused by the lone pair of electrons. In many cases however, e.g. $SnCl_2$ and $SnBr_2$ Δ=0, due to the fact that p electrons are also used in bond formation, enabling a balance

to be achieved between the p-electron density in the bonding orbitals and that in the lone pair orbital.

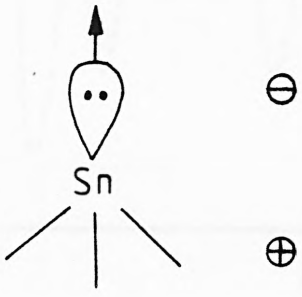

For compounds of the type MA_2B_4, the Mössbauer quadrupole splitting can be used to distinguish between cis- and trans-isomers. In general, Δ is expected to be two times greater in the trans isomer and of the opposite sign to that of the cis isomer.

1.3.(1).5. Magnetic Hyperfine Splitting.

The Mössbauer line can also be split as a result of a magnetic hyperfine interaction, which will occur if there is a magnetic field at the nucleus. This magnetic field can arise within the atom itself, can be produced by paramagnetic electrons or it can result from placing the compound in an external applied magnetic field. Figure 1.(12). shows the magnetic hyperfine split spectrum of ^{57}Fe, with the energy level diagram showing how these splittings arise. ^{57}Fe has been utilised as the standard to calibrate the Mössbauer spectrometer during these studies.

1.3.(1).6. The Spectrometer.

The spectrometer used throughout this work was a Cryophysics MS-102 Microprocessor Mössbauer Spectrometer. The basic set-up of this instrument is shown diagrammatically in Figure 1.(13).

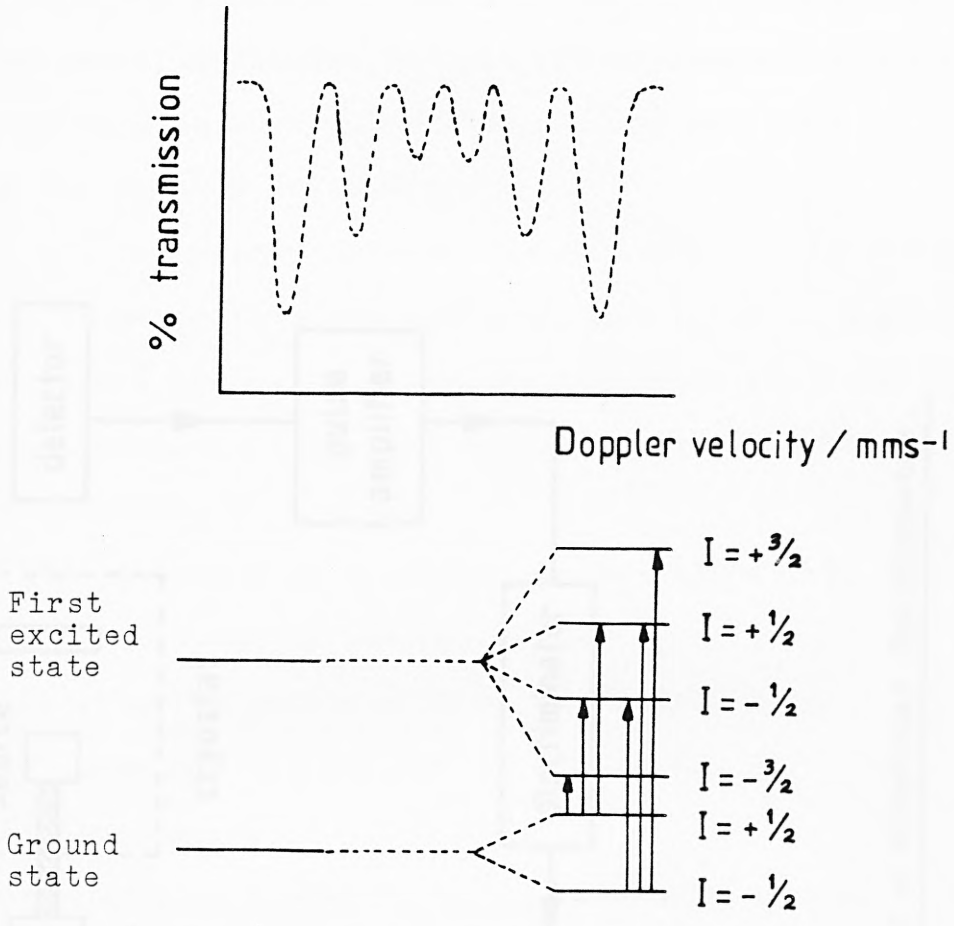

FIGURE 1.(12). Magnetically Split ^{57}Fe Spectrum and How it Originates.

The major component of the spectrometer is the multi-channel analyser which can store an accumulated total of γ-counts in a binary memory store, in one of 512 channels. Each channel is held open for a short period of time by a very stable constant frequency clock, any γ-counts detected by the system during this time interval are added to those counts already accumulated in the store.

The time pulses from the clock may also be used to synchronise a voltage waveform, which is used as a command signal to the servo-amplifier controlling a vibrator. The vibrator moves the source relative to the absorber. The voltage increases linearly with time so that the source moves with constant acceleration and spends equal time intervals

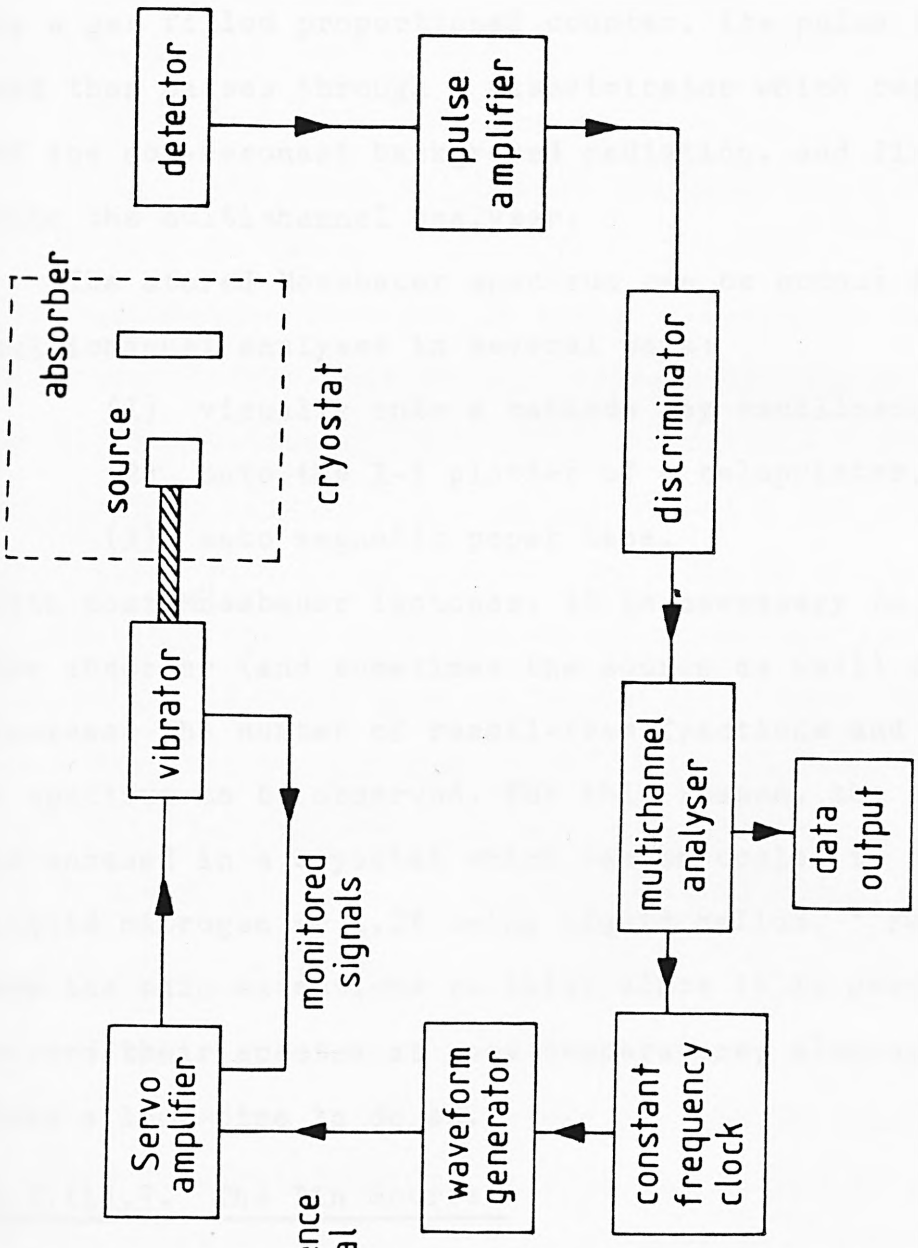

FIGURE 1.(13). Diagrammatic Representation of a Mössbauer Spectrometer.

at each velocity increment. The multichannel analyser and the drive are synchronised so that the velocity increases from -v to +v with increasing channel numbers. This is also known as the Doppler drive mechanism.

When a γ-ray passes through the absorber, it is detected by a gas filled proportional counter, its pulse is amplified and then passes through a discriminator which reflects most of the non-resonant background radiation, and finally is fed into the multichannel analyser.

The stored Mössbauer spectrum can be output from the multichannel analyser in several ways:

(1) visually onto a cathode ray oscilloscope,

(2) onto the X-Y plotter of a teleprinter,

(3) onto magnetic paper tape.

With most Mössbauer isotopes, it is necessary to cool down the absorber (and sometimes the source as well) so as to increase the number of recoil-free fractions and to enable a spectrum to be observed. For this reason, the absorber is encased in a cryostat which can be cooled to 80K using liquid nitrogen or 4.2K using liquid helium. ^{57}Fe and ^{119}Sn are the main exceptions to this, since it is possible to record their spectra at room temperature, although it may take a long time to do so.

1.3.(1).7. The Tin Source.

^{119}Sn Mössbauer spectroscopy, observes the 23.8KeV decay transition from the first excited state of the metastable tin-119m nucleus to the ground state. The source matrices used in the past have been metallic tin[58], stannic oxide[59], tin-palladium alloys[60] and the alkaline earth metal stannates[61].

In this work, a 5mCi $Ca^{119}SnO_3$ source was utilised, which had a natural line width, $\Gamma_{1/2}$ = 0.38mm/s. The isomer shifts were recorded relative to a $BaSnO_3$ standard source.

1.3.(1).8. Calibration of the Spectrometer.

In interpreting any Mössbauer spectrum, two constants must be known:

(1) the calibration constant,

(2) the point in channel numbers, which corresponds to 0mm/s.

The calibration constant is obtained using an iron enriched absorber, because the energy separations between the peaks of a ^{57}Fe Mössbauer spectrum are accurately known[62]. The calibration constant is a number by which the observed separation must be multiplied, in order to derive the true separation. Since in Mössbauer spectroscopy, an identical source and absorber give an isomer shift equal to zero, the room temperature spectrum of $Ba^{119}SnO_3$ is recorded relative to a $Ba^{119}SnO_3$ source, and the point in channel numbers at which the Mössbauer peak occurs, is called the zero position.

1.3.(1).9. Experimental Conditions.

Normally, the absorber materials were ground into fine powders, pressed into hollow perspex sample holders and wrapped in aluminium foil to keep the sample in place. Many of the polymers prepared however, were very viscous liquids and for these a thin layer of the polymer was smeared over the holder (a detailed discussion on the polymers is given in Chapter (4).). The absorber was then encased in a cryostat and cooled to 78K, using liquid nitrogen. Typically, spectra took between six and twenty four hours to record, depending upon the percentage of tin in the sample and its

recoil free fraction.

1.3.(1).10. Curve Fitting Program.

The Mössbauer spectra recorded, were fitted with an iterative least squares program. Two programs were utilised for the fitting process, either the curve fitting PARLOR program or that written by Dr. F. Woodhams[63], which is an integral part of the microprocessor spectrometer. In the PARLOR program, estimates of the Mössbauer parameters are input with the data in the form of punched cards. The program then outputs the position and half-width of the peaks, as well as the areas under the minima, percentage absorption and a plot of the original and the fitted spectrum.

1.3.(1).11. Applications to Tin Chemistry.

As mentioned earlier in Section 1.3.(1).3., $\Delta R/R$ is positive for ^{119}Sn, therefore an increase in the s-electron density at the nucleus gives rise to an increase in the isomer shift. Since Sn^{4+} compounds typically have the electronic configuration $4d^{10}5s^{0}$ and Sn^{2+} compounds the configuration $4d^{10}5s^{2}$, a change in valency from +4 to +2 is associated with an increase in the s-electron density and consequently an increase in the isomer shift values occurs.

e.g. Sn^{4+} : $SnCl_4$ δ = 0.85mm/s

Sn^{2+} : $SnCl_2$ δ = 4.07mm/s

Mössbauer spectroscopy can also give an indication of the bonding to the tin nucleus, i.e. is it ionic or covalent. Taking α-Sn as the reference point, for Sn(II) compounds, an increase in the isomer shift corresponds to an increase in the s-electron density about the nucleus and hence an increase in the ionicity. Conversely, for Sn(IV) compounds it is a decrease in the isomer shift (increasing negative

shift from α-Sn) that corresponds to an increase in the s-electron density and ionicity. In each case, the actual value for the isomer shift will give an indication of the ionicity or covalency in the bond to the tin.

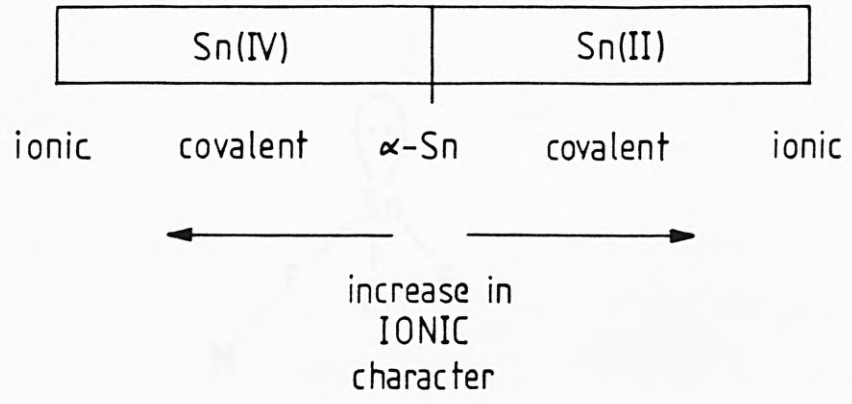

When the coordination of a molecule alters, a corresponding change in the Mössbauer spectrum is observed.

i.e. $SnCl_4$ δ = 0.85mm/s

$SnCl_6^{2-}$ δ = 0.48mm/s

Effectively, on going from $SnCl_4$ to $SnCl_6^{2-}$, the coordination has changed from tetrahedral to octahedral, there is an increase in the coordination number and ionic character of the bonding and therefore, the isomer shift decreases.

Conversely, it is found that upon forming a tin(II) complex, the bonds to the Mössbauer nucleus are strengthened and become shorter, increasing the covalent character of the bonding. This means that for Sn(II) compounds, the isomer shift decreases on formation of a complex, for example,

$Sn(CH_3COO)_2$ δ = 3.21mm/s

$Sn(CH_3COO)_3^-$ δ = 2.80mm/s

Another factor affecting the isomer shift in complexes is the nature of the co-cation in the solid derivative of

the complex.

SnF_2	δ = 3.20mm/s
SnF_3^- Na^+	δ = 3.07mm/s
SnF_3^- K^+	δ = 3.02mm/s
SnF_3^- Rb^+	δ = 2.97mm/s
SnF_3^- Cs^+	δ = 2.93mm/s

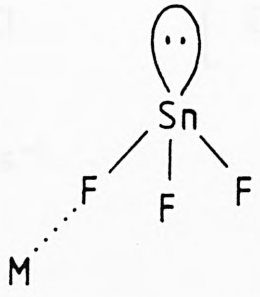

The strongest interaction occurs with the Na cation, which is the smallest and most polar atom. It forms the strongest bond to the fluorine atom, pulling electron density away from the tin and giving the weakest Sn-F covalent bond. As the Na is replaced by a less polar cation, the interaction between the metal (M) and the fluorine decreases and the degree of covalency in the Sn-F bond increases, leading to a decrease in the isomer shift. Since the polar nature of the ions follows the trend,

$$Na^+ < K^+ < Rb^+ < Cs^+$$

the isomer shifts follow the reverse trend as shown below,

$$\delta_{Na} > \delta_K > \delta_{Rb} > \delta_{Cs}$$

Finally, the lone pair on the tin nucleus can be donated to another metal atom, such as platinum, during complex formation. This results in a net decrease in the s-electron density around the tin nucleus and therefore the isomer shift decreases. The fact that the non-bonding electrons are

now being used in bonding, makes the complex formally a Sn(IV) species and this is reflected in the value of the isomer shift.

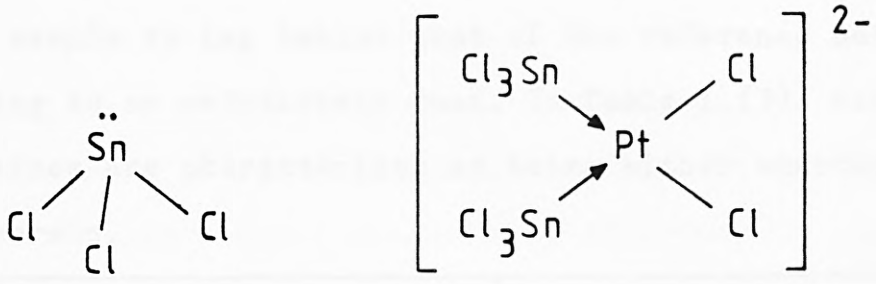

$\delta = 3.47\ mms^{-1}$ $\delta \sim 1.90\ mms^{-1}$

Thus, Mössbauer spectroscopy is shown to be a very valuable technique. It provides information on the effects of the electronic environment on the tin nucleus with great precision and accuracy and helps to elucidate problems on both bonding and structure. In the present work, Mössbauer spectroscopy has been used to characterise new compounds and to reinvestigate some known tin(II) carboxylates. In the field of catalysis, it has provided many interesting results which help to explain the mechanisms of the polymerisation processes, which would have been very difficult to explain using any other technique.

1.3.(2). Differential Thermal Analysis.

Differential thermal analysis (DTA), is a technique which involves heating (or cooling) a test sample and an inert reference material, e.g. alumina, under identical conditions and recording any temperature difference that develops between them. Any physical or chemical change occurring in the test sample which produces heat, will cause

the temperature to rise temporarily above that of the reference sample, thus giving rise to an exothermic peak on the DTA plot. Conversely, a process which is accompanied by the absorption of heat, will cause the temperature of the test sample to lag behind that of the reference material, leading to an endothermic peak. In Table 1.(3). various processes are characterised as being either endothermic or exothermic.

Process	Type of Reaction
Melting point	Endothermic
Cooling point	Exothermic
Boiling point	Endothermic
Decomposition	Endothermic
Solid - solid phase transitions	Endothermic or Exothermic

TABLE 1.(3). Endothermic and Exothermic Processes.

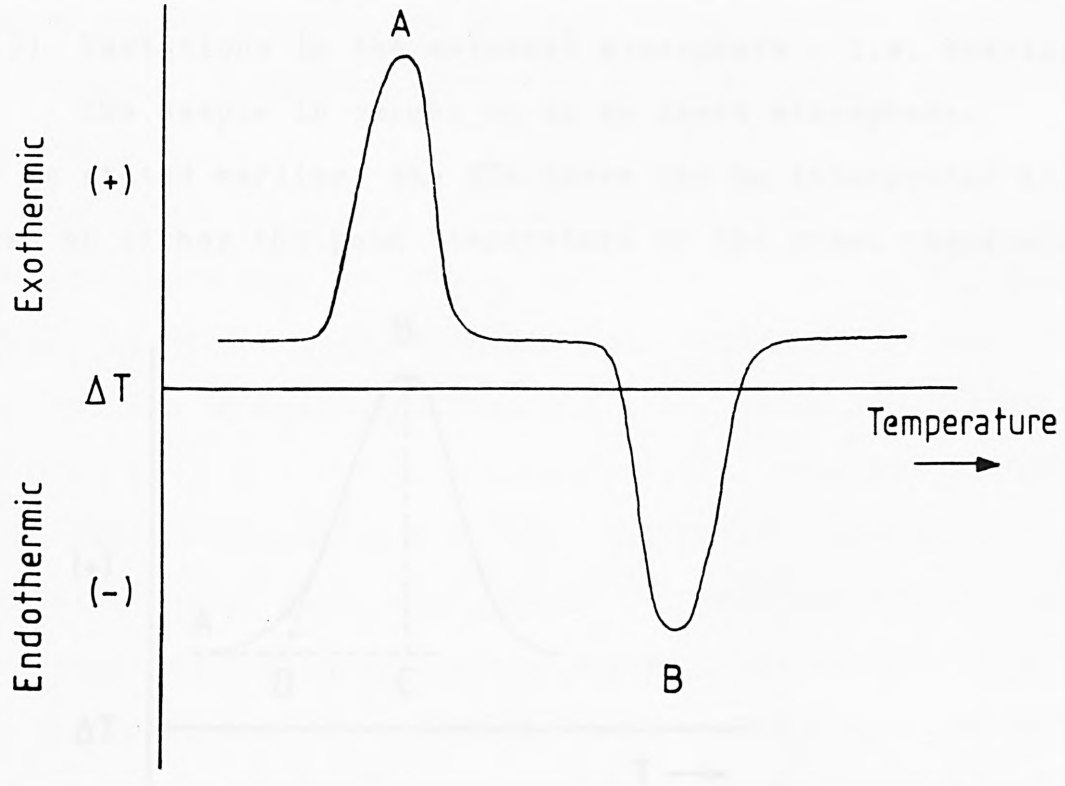

FIGURE 1.(14). Idealised DTA Trace Showing Exothermic (A) and Endothermic (B) Processes.

Figure 1.(14). shows an idealised DTA curve, in which peak A represents the exothermic process and peak B the endothermic process. The temperature at which the process first becomes detectable by DTA, is termed the onset temperature. At this point, the curve deviates from the baseline, it peaks when the rate of heat evolution, as detected by a differential thermocouple, is at a maximum and returns to the baseline when the process being measured is complete. Although the peak temperature is more easily measured than the onset temperature, it tends to vary to a greater extent with experimental conditions, such as the rate of heating. DTA peaks can be affected by a number of factors:

(1) Sample purity- a pure sample will give a sharp DTA peak.

(2) Heating rate.

(3) Packing of the sample in the holder.

(4) Amount of sample used.

(5) Variations in the external atmosphere - i.e. heating the sample in oxygen or in an inert atmosphere.

As stated earlier, the DTA curve can be interpreted in terms of either the peak temperature or the onset temperature.

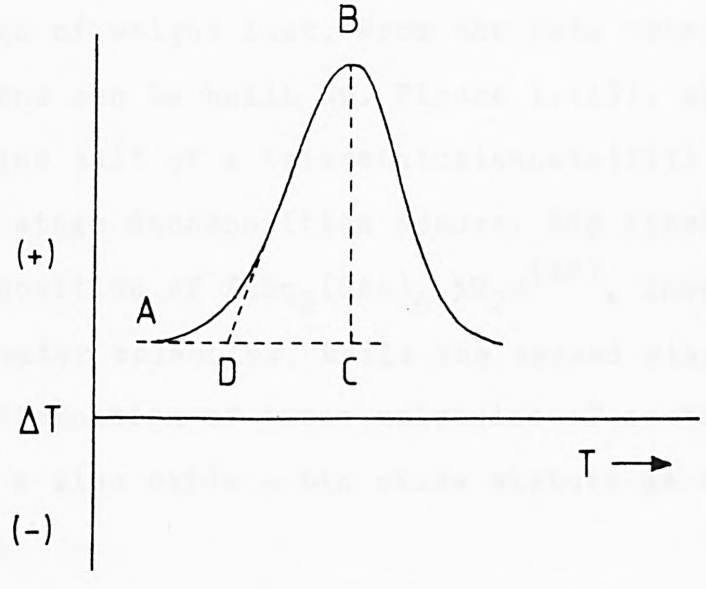

The peak temperature C, is described as the temperature at which the maximum evolution or absorption of heat occurs. The onset temperature D, is the point of intersection of the tangent drawn at the point of greatest slope on the leading edge of the peak (AB), with the extrapolated baseline (AC). Use of the onset temperature, minimises any errors which might arise from changes in the experimental conditions; for this reason, onset rather than peak temperatures are quoted throughout this thesis.

DTA traces were recorded on a Stanton Redcroft STA-780 Thermal Analyser, usually using samples of approximately 10mg of material, at a heating rate of 10°C per minute, with a DTA sensitivity of 100μV, under a nitrogen atmosphere.

1.3.(3). Other Analytical Techniques.

1.3.(3).1. Thermogravimetric Analysis.

The Stanton Redcroft STA-780 Thermal Analyser used to record the DTA traces, has the additional feature of being able to perform thermogravimetric analysis on the sample as the DTA is being recorded.

The sample is heated in a controlled manner and any decompositions that occur are recorded in terms of the percentage of weight lost. From the data obtained, decomposition patterns can be built up. Figure 1.(15). shows the DTA/TG of the zinc salt of a triacetatostannate(III) complex, in which a two stage decomposition occurs. The first stage in the decomposition of $ZnSn_2(OAc)_6.5H_2O$[22], involves the loss of five water molecules, while the second stage results from the elimination of three molecules of acetic anhydride to leave a zinc oxide - tin oxide mixture as the residue.

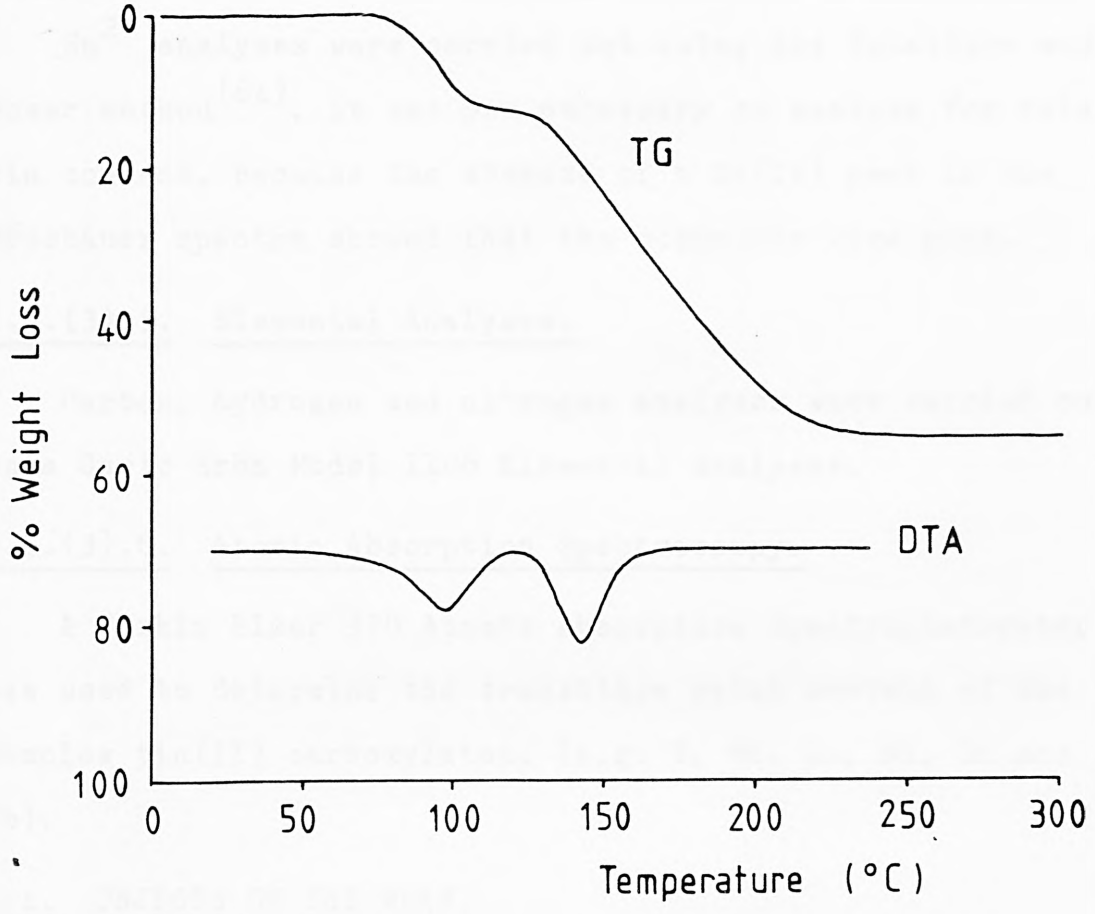

FIGURE 1.(15). DTA/TG of $ZnSn_2(CH_3COO)_6.5H_2O$.

1.3.(3).2. Infrared Spectroscopy.

Infrared spectra were obtained as KBr discs, Nujol mulls or as thin films, on a Perkin Elmer 599 Infrared Spectrophotometer. Peaks are given the following spectral assignments:

s - strong, br - broad, sh - sharp, m - medium,
w - weak, v - very weak.

1.3.(3).3. X-Ray Diffraction Studies.

X-ray powder diffractograms were recorded in the Physics Department, The City University. Diffractogram lines were converted into d-spacings and quoted in Angstroms ($\mathring{A}$), their intensities were expressed as a percentage of the most intense line.

1.3.(3).4. Tin Analysis.

Sn^{2+} analyses were carried out using the Donaldson and Moser method[64], it was not necessary to analyse for total tin content, because the absence of a Sn(IV) peak in the Mössbauer spectra showed that the compounds were pure.

1.3.(3).5. Elemental Analyses.

Carbon, hydrogen and nitrogen analyses were carried out on a Carlo Erba Model 1106 Elemental Analyser.

1.3.(3).6. Atomic Absorption Spectroscopy.

A Perkin Elmer 370 Atomic Absorption Spectrophotometer was used to determine the transition metal content of the complex tin(II) carboxylates, (e.g. K, Mn, Co, Ni, Zn and Pb).

1.4. OBJECTS OF THE WORK.

The work in this thesis has been divided into four main sections:

I - The preparation of some novel tin(II) carboxylates and the reinvestigation of some known ones. The crystal structure determination of two novel compounds was carried out using X-ray crystallography.

II - An in-depth study on the polymerisation of propylene oxide and trioxane and the room temperature curing of a silicone resin.

III - The preparation and characterisation of some di-organotin(IV) oxycarbonates, including a thorough investigation of their thermal decompositions.

IV - Solid state chemistry on systems of the type: $SnX_2 : MS_2$ where X = F, Cl, Br, and M = Sn, Mo.

REFERENCES.

1. W.H. Baur, Acta Cryst., (1956), 9, 515.
2. L. Brockway and F. Wall, J. Amer. Chem. Soc., (1934), 56, 2373.
3. R.K. Ingham, S.D. Rosenberg and H. Gilman, Chem, Rev., (1960), 60, 459.
4. G. Engel, Z. Krist., (1935), 90, 341.
5. M.W. Lister and L.E. Sutton, Trans. Faraday Soc., (1941), 37, 406.
6. 'Organotin Chemistry - New Chemistry and Applications', J.J. Zuckermann, A.C.S. Advances in Chemistry Series No. 157, (1956).
7. 'The Organic Chemistry of Tin', W.P. Neumann, (1967), Wiley and Sons, New York.
8. 'Organotin Compounds', Ed. A.K. Sawyer, Dekker, New York (1971), Vols. 1,2 and 3.
9. A.G.Davies and P.G. Smith, 'Comprehensive Organometallic Chemistry - Synthesis, Reactions and Structures of Organometallic Compounds', (1982), p.579, Ed. G. Wilkinson, F.G. Stone and E.W. Abel, Pergamon Press, New York.
10. W.P. Neumann, 'Proc. 2nd Int. Conf. Ge, Sn, Pb Compounds' Ed. M. Gielen and P.G. Harrison, Rev. Si, Ge, Sn and Pb Compounds, Spec. Issue, (1978), 51.
11. . Liebig, Ann. Pharm., (1836), 17, 75.
12. P.H. Hobson, U.S.P. 2,892,815 / 1959.
13. F. Koch, Ger. 1,272,536 / 1958.
14. W.H. Cook, U.S.P. 4,096,129 / 1978.
15. K. Siminobu, M. Matsumura, H. Morishuta, M. Koyama and N. Kuboto, Japan 70 33,435.
16. W.J. Eldridge, U.S.P. 4,173,692 / 1979.
17. T. Moringa, H. Inata and S. Kawase, Japan Kokai 76 102, 094.
18. Kureha Chem. Ind. Co. Ltd., Japan 7493 / 1960.

19. W.R. Proops and G.W. Fowler, U.S.P. 3,117,099 / 1964.

20. W.R. Proops and G.W. Fowler, U.S.P. 3,201,360 / 1964.

21. W.R. Proops and G.W. Fowler, Brit. Pat. 966,917 / 1964.

22. Z.B. Arifin, Ph.D. Thesis, University of London, (1981).

23. C.O. Hawk and R.W. Hiteshue, Bureau of Mines, Bulletin No. 622, (1965).

24. E.W. Wilson and J.E. Hutchins, U.S.P. 3,194,791 / 1965.

25. H. Suzuki, H. Fujimoto and H. Muyake, Japan Kokai, 75 09,689 / 1975.

26. O. Makimura, M. Yoshimura and M. Sawata, Japan Kokai, 7466,798 / 1974.

27. M. Naito, H. Kitigawa, M. Katayama and K. Yarwochi, Japan 1288 / 1961.

28. J.M. Barton, Brit. Pat. 992,986 / 1965.

29. J.G. Denmou and M. Cenker, Ger. Offen., 2,455,289.

30. R. Dahl, U.S.P. 3,802,988 / 1974.

31. N. Gobbledick, Ger. Offen., 2,019,767 / 1971.

32. E.F. Chandley, A.J. Lowe and G.R. Rossmy, Brit. Pat. 1,048,992 / 1966.

33. J. Sambeth, A. Archipoff and J. Godechot, U.S.P. 3,560, 416 / 1971.

34. S. Cinnamon, S. Frareich and A. Zilkha, Eur. Polym. J., (1980), 16, (2), 147.

35. B.A. Dombrow and G. Fesman, U.S.P. 3,162,616 / 1964.

36. R.A. Aitken and G. Trappe, Brit. Pat. 1,282,422 / 1972.

37. W.H. Cook, U.S.P. 3,716,523 / 1973.

38. J.E. Maier, Ger. Offen., 1,950,559 / 1970.

39. O.W. Smith and J.V. Koleske, U.S.P. 4,119,593 / 1978.

40. G.M. Burnett, A.J. MacArthur and J. Hay, Eur. Polym. J., (1967), 3, (3), 331.

41. C.F. Thompson, Brit. Pat. 1,078,870 / 1967.

42. V.P. Davydova, A.V. Karlin, I.V. Sevastyanove and Zh.N. Kostyakova, Kauch Rezina., (1980), 3, 6.

43. H.A. Vaugh, U.S.P. 3,349,048 / 1967.

44. N.P. Smetankina, N.N. Laskovenko and V.A. Mironov, Vysokomol. Soedin Ser. B., (1974), 16, (3), 1967.

45. M. & T. Chems. Inc., U.S.P. Appl. 955,906 / 1978.

46. G.C. Colovos, T.R. McCellan and K.W. Rausch, Adhes. Age, (1966), 9, (11), 23.

47. B.M. Bulygin and Z.V. Malafeeva, Khim. Prom-st., Ser: Melody Anal. Kontrolya Kach. Prod. Khim. Prom-st., (1979), (8),32.

48. Nippon Oils and Fats Co. Ltd., Jpn. Kokai Tokkyo Koho 80 73,770 / 1980.

49. G.E. Kessler, V.Y. Rochev, R. Stukan and L.M. Romanov, Vysokomol Soedin Ser. B, (1973), 15, (3), 159.

50. G.E. Kessler, V.Y. Rochev, L.M. Romanov and O.P. Kevdin, Vysokomol Soedin Ser. A, (1977), 19, (2), 416.

51. W. Voss and R. Joachim, Brit. Pat. 988,939 / 1965.

52. W. Voss and R. Joachim, Ger. (East) 34,499 / 1965.

53. V.E.B. Filmfabrik Agfa Wolfen, Belg. 611,444 / 1961.

54. S.S. Caldwell, G.T. Cherloff and G.B. Curtis, U.S.P. 2,629,700 / 1953.

55. J.W. Britain and P.G. Gemeinhardt, J. Appl. Pol. Sci., (1960), 4, (11), 207.

56. R.L. Mossbauer, Z. Phys., (1958), 151, 124.

57. O.C. Kistner and A.W. Sunyar, Phys. Rev. Letts., (1960), 4, 229.

58. A.J.F. Boyle, D.St.P.Bunbury, C. Edwards and H.E. Hall, Proc. Phys. Soc. London, (1960), 76, 165.

59. V.S. Shipnel, V.A. Bryakhanov and N.N. Delagin, Zh. Eksp. Theor. Fiz., (1961), 41, 1525, 1767.

60. R.H. Herber and J.J. Spijkerman, J. Chem. Phys., (1965), 43, 4057.

61. M.Sano and R.H. Herber, J. Inorg. Nucl. Chem., (1968), 30, 409.

62. R.S. Preston, S.S. Hama and J. Herberle, Phys. Rev., (1962), 128, 2207.

63. F.W.D. Woodhams, Software and Microsystems, (1982), 1, (4), 108.

64. J.D. Donaldson and W. Moser, Analyst, (1959), 84, 10.

CHAPTER TWO

PREPARATIVE STUDIES

2.1. INTRODUCTION.

In this chapter, the preparation of a number of new tin(II) carboxylates and carboxylatostannates(II) are described. The transition metal complex derivatives of tin(II) formate studied previously by Arifin[1], have been re-examined to establish their exact formulation. The Mössbauer spectra of many of the compounds reported by Filmore[2], have been recorded again, because Filmore's spectra were collected on the basic type of spectrometer available at the time and better instruments and fitting programs are now available.

The compounds prepared were characterised by their analytical, infrared, X-ray diffraction and Mössbauer spectroscopic data and their thermal decompositions were investigated.

2.2. GENERAL PREPARATIVE STUDIES.

It is well known that tin(II) compounds are easily oxidised and hydrolysed and in order to overcome these problems in the synthesis of tin(II) carboxylates, the reactions were carried out in an oxygen-free nitrogen environment and the products dried *in vacuo* over potassium hydroxide pellets. The solid tin(II) carboxylates are stable for several months before they undergo oxidation. They are immediately hydrolysed, even by cold water, giving hydrous tin(II) oxide ($5SnO.2H_2O$).

Although many tin(II) compounds (e.g. sulphate and chloride) may be used as starting materials in the preparation of stannous carboxylates, blue-black stannous oxide was utilised throughout this work. It is preferred since it is stable to oxidation and hydrolysis for indefinite

periods and it is readily prepared.

2.3. PREPARATION OF THE TRANSITION METAL COMPLEXES OF TIN(II) FORMATE.

2.3.(1). Experimemtal.

Blue-black stannous oxide (0.01 mole; 1.4g) was dissolved by refluxing it for one hour under an oxygen-free nitrogen atmosphere, in 50% v/v aqueous formic acid (100ml when M = Mn or Pb; 50ml when M = Co, Ni or Zn). The appropriate metal carbonate (0.01 mole) was then added and the reflux continued for half an hour. The resulting mixture was filtered hot, concentrated to about 20ml on a rotary evaporator and allowed to cool. The crystalline products obtained were washed with ether and dried *in vacuo* over potassium hydroxide pellets.

The compounds prepared were the transition metal (Mn, Co, Ni, Zn) formatostannates(II) and a new complex lead formatostannate(II).

2.3.(2). Elemental Analysis.

The analytical data for the complexes are presented in Table 2.(1). The results are consistent with the following formulae:

$$MSn(HCOO)_4.xH_2O$$

for the transition metal derivatives and

$$PbSn_3(HCOO)_8$$

for the lead formatostannate(II).

The complexes prepared by Arifin[1] were reported to be

$$M_3Sn_4(HCOO)_{14}.8H_2O$$

and the difference in the complex formed is attributed to the different preparative conditions employed.

Complex Tin(II) Formate	% Sn	% C	% H	% M
$MnSn(HCOO)_4.3H_2O$				
Observed	30.3	12.35	2.21	12.8
Calculated	29.1	11.77	2.45	13.5
$CoSn(HCOO)_4.4H_2O$				
Observed	27.0	12.09	1.96	14.1
Calculated	27.6	11.18	2.81	13.7
$NiSn(HCOO)_4.2H_2O$				
Observed	33.3	11.99	1.98	-
Calculated	30.2	12.21	2.06	-
$ZnSn(HCOO)_4.2H_2O$				
Observed	29.3	12.04	2.22	14.6
Calculated	29.7	12.01	2.02	13.3
$PbSn_3(HCOO)_8$				
Observed	38.6	10.39	0.87	22.4
Calculated	39.5	10.18	0.90	19.3

TABLE 2.(1). Analytical Data for Complex Tin(II) Formates.

2.3.(3). Thermal Analysis.

The simultaneous differential thermal analysis (DTA) and thermogravimetric analysis (TG) of the compounds prepared were carried out on a Stanton Redcroft STA-780 Thermal Analyser (see also Chapter 1 Section 1.3.(2).). All the samples decompose without melting, giving grey-

black residues at temperatures above 300°C.

The complex tin(II) formates undergo a three stage decomposition, the first stage (except for the lead salt) at 101 - 140°C corresponds to the loss of water molecules of crystallisation. In each case the final residue is a metal oxide - stannous oxide mixture and the formates do not decompose in a single mechanism, but do so in a number of stages. It appears that the formate groups are lost in two stages, so that the formates which are bound less strongly to the tin are lost first. The formate groups are found to decompose to carbon dioxide and formaldehyde. Figure 2.(1). shows the DTA and TG traces for $MnSn(HCOO)_4.3H_2O$.

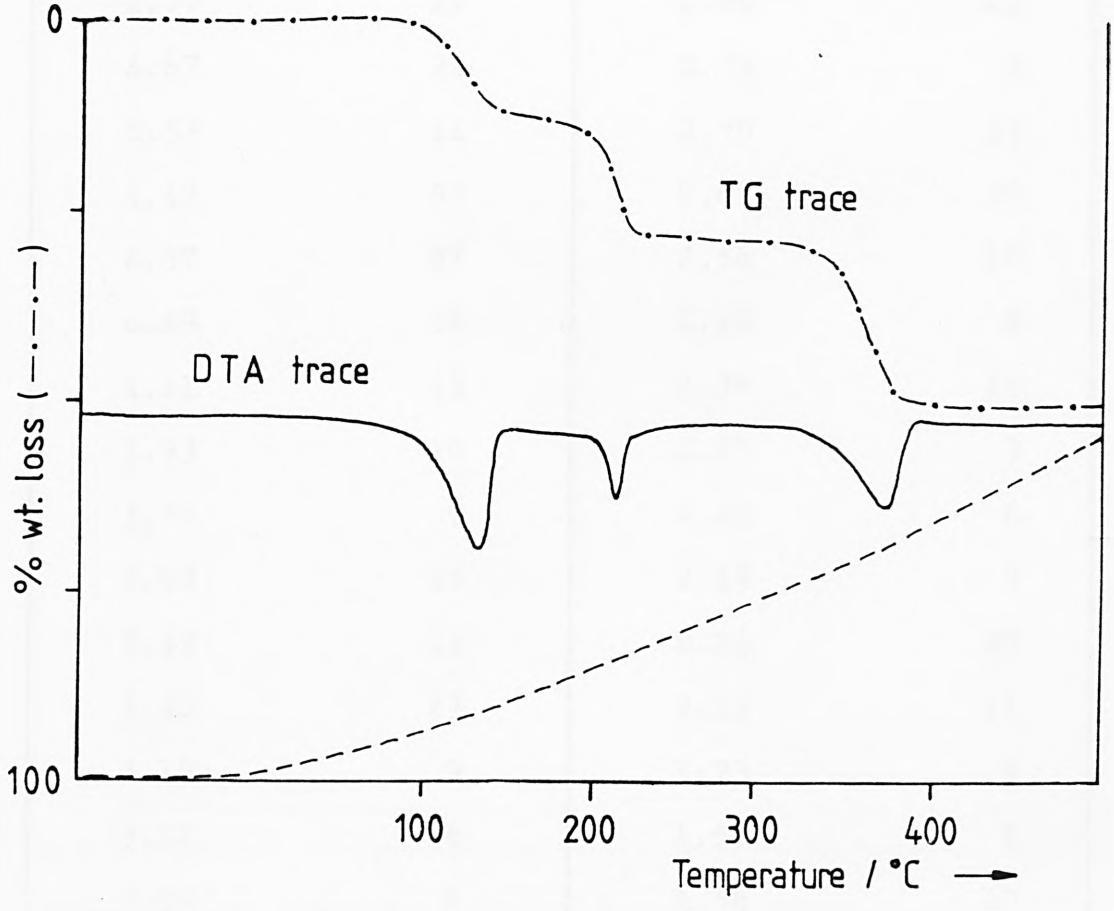

FIGURE 2.(1). Thermal Decomposition of $MnSn(HCOO)_4.3H_2O$ by Simultaneous Differential Thermal Analysis (DTA) and Thermogravimetric (TG) Analysis.

2.3.(4). X-ray Diffraction.

X-ray powder diffractograms were recorded for all the compounds prepared, the data obtained are listed below in Table 2.(2).

TABLE 2.(2). X-ray Powder Diffraction Data for Complex Tin(II) Formates.

$MnSn(HCOO)_4.3H_2O$			
d spacing (Å)	R.I.	d spacing (Å)	R.I.
8.59	94	2.93	9
5.01	100	2.89	9
4.77	21	2.84	21
4.67	24	2.75	9
4.53	14	2.70	19
4.42	50	2.67	20
4.37	97	2.56	10
4.29	56	2.48	8
4.11	13	2.39	10
3.93	10	2.27	3
3.75	9	2.25	6
3.68	16	2.19	9
3.49	14	2.14	29
3.40	23	2.10	11
3.19	9	1.73	9
3.12	6	1.59	5
3.09	6	1.56	10

$NiSn(HCOO)_4.2H_2O$			
d spacing (Å)	R.I.	d spacing (Å)	R.I.
8.67	100	2.64	13
4.90	48	2.57	23
4.55	53	2.50	9
4.31	78	2.48	10
4.13	17	2.39	9
3.95	28	2.30	6
3.69	30	2.18	6
3.40	23	2.15	29
3.21	39	2.05	7
3.11	9	1.97	4
3.04	6	1.92	3
2.94	16	1.91	8
2.90	8	1.80	5
2.87	19	1.74	9
2.81	8	1.70	15
2.77	9	1.60	8
2.73	5		

TABLE 2.(2). (contd.).

$CoSn(HCOO)_4.4H_2O$		$PbSn_3(HCOO)_8$	
d spacing (Å)	R.I.	d spacing (Å)	R.I.
8.59	100	8.59	76
4.90	76	5.25	100
4.58	79	4.35	45
4.29	93	4.29	45
4.11	12	3.65	12
3.92	17	3.39	9
3.68	21	3.27	27
3.58	8	3.19	13
3.52	5	2.99	15
3.40	30	2.84	19
3.35	19	2.72	15
3.19	17	2.60	17
3.07	12	2.47	7
2.83	14	2.38	13
2.76	14	2.36	17
2.65	27	2.14	19
2.59	21	2.09	13
2.14	19	2.00	17
2.11	12	1.94	13
2.o6	14	1.55	37
1.84	12	1.54	35
1.83	12		
1.78	48		

TABLE 2.(2). (contd.).

$ZnSn(HCOO)_4.2H_2O$			
d spacing (Å)	R.I.	d spacing (Å)	R.I.
8.51	71	2.46	12
4.85	89	2.28	5
4.60	18	2.14	17
4.55	25	2.06	7
4.29	100	1.93	4
4.13	6	1.90	5
3.90	5	1.85	15
3.68	8	1.84	18
3.35	36	1.83	33
3.18	7	1.82	30
2.92	8	1.73	6
2.84	11	1.71	5
2.82	11	1.69	2
2.75	4	1.65	2
2.64	96	1.61	5
2.48	10		

TABLE 2.(2). (contd.).

Compound					Assignments
(1)	(2)	(3)	(4)	(5)	
3300 br	3290 br	3330 br	3300 br	-	OH stretch (H_2O)
2870 sh	2890 w	2900 w	2870 w	2850 w	CH stretch
1570 vs	1565 vs	1570 s	1570 s	1535 s	$\nu(CO_2)$ asymm. str.
1360 s	1360 s	1350 s	1370 m	1370 m	$\nu(CO_2)$ sym. str.
-	-	-	1350 m	1335 m	
1275 m	-	-	1275 m	1275 m	
775 sh	780 s	775 sh	775 sh	780 m	$\delta(CO_2)$ sym. def.
565 vw	565 m	550 m	550 w	760	

TABLE 2.(3). Infrared Data for the Complex Tin(II) Formates : (1) $MnSn(HCOO)_4.3H_2O$, (2) $CoSn(HCOO)_4.4H_2O$, (3) $NiSn(HCOO)_4.2H_2O$, (4) $ZnSn(HCOO)_4.2H_2O$, (5) $PbSn_3(HCOO)_8$.

2.3.(5). Infrared Data.

Table 2.(3). contains the infrared data for the complex tin(II) formates, along with their spectral assignments. The following abbreviations are utilised in describing the signal intensities observed:-

br-broad, vs-very strong, s-strong, m-medium, w-weak, vw-very weak, sh-sharp.

2.3.(6). Mössbauer Data.

^{119}Sn Mössbauer spectra of the complex tin(II) formates were recorded. Their spectra consist of quadrupole split tin(II) doublets (Δ = 1.68 - 1.94 mms^{-1}), with isomer shifts in the range 3.28 to 3.31 mms^{-1}.

Compound	δ (mms^{-1})	Δ (mms^{-1})
$MnSn(HCOO)_4.3H_2O$	3.29	1.68
$CoSn(HCOO)_4.4H_2O$	3.31	1.71
$NiSn(HCOO)_4.2H_2O$	3.29	1.68
$ZnSn(HCOO)_4.2H_2O$	3.32	1.81
$PbSn(HCOO)_8$	3.28	1.71
$Sn(HCOO)_2$	3.33	1.69

TABLE 2.(4). Mössbauer Parameters of the Complex Tin(II) Formates.

In Table 2.(4)., the Mössbauer parameters of the compounds prepared in this study are compared with those of stannous formate, so as to demonstrate the change in the parameters

on complexation. The isomer shifts of the complex tin(II) formates are slightly lower (about 3.21-3.32 mms^{-1}) than that of the parent tin(II) formate (δ=3.33 mms^{-1}) and this is consistent with the presence of the triformatostannate-(II) ion, $Sn(HCOO)_3^-$, in the complexes.

2.4. PREPARATION OF LEAD TRIACETATOSTANNATE(II).

2.4.(1). Introduction.

Previous workers[1,2] have prepared both the parent tin(II) acetate, $Sn(CH_3COO)_2$, and the transition metal complexes, $MSn_2(CH_3COO)_6.xH_2O$ (where M = Mn, Cd, when x=0; M = Co, Ni, when x=5; and M = Zn when x=6). The preparation and characterisation of a new lead salt, $PbSn_2(CH_3COO)_6$, is described in this section.

2.4.(2). Experimental.

Blue-black stannous oxide (0.02 mole; 2.7g) was dissolved in 50% v/v aqueous acetic acid (60ml) by refluxing for 1½ hours in an oxygen-free nitrogen atmosphere. Lead carbonate (0.01 mole; 2.7g) was added to the hot solution and refluxing continued for a further half an hour. The resulting solution was filtered hot and concentrated to 30ml on a rotary evaporator. White crystals of $PbSn_2(CH_3COO)_6$ were obtained from the cooled solution. These were filtered off, washed with ether and dried *in vacuo* over potassium hydroxide pellets.

2.4.(3). Characterisation.

The compound was identified by elemental analysis (see Table 2.(5).).

	%Sn	%C	%H	%O	%Pb
Observed	29.9	18.16	2.20	24.46	25.2
Calculated	29.7	18.04	2.27	24.03	25.9

TABLE 2.(5). Elemental Analysis of Lead Triacetatostannate(II).

The DTA/TG traces for $PbSn_2(CH_3COO)_6$ were recorded. A complex three stage decomposition occurs, but an accurate study of the products could not be carried out since the high volatility of stannous acetate[3] causes loss of tin in this system.

The infrared spectrum of the lead complex was recorded as a KBr disc; the data and spectral assignments are in Table 2.(6).

Peak Position (cm^{-1})	Assignment
3140 br	CH str.
1530 s	$\nu(CO_2)$ asym. str.
1460 m	CH str.
1400 m	CH str.
1380 s	$\nu(CO_2)$ sym. str.
1045 w	
1020 w	
940	
725 m	$\delta(CO_2)$ sym. def.
680 w	C-C str.

TABLE 2.(6). Infrared Data for $PbSn_2(CH_3COO)_6$.

Compound	δ (mms^{-1})	Δ (mms^{-1})
$PbSn_2(CH_3COO)_6$	3.13	1.94
$MnSn_2(CH_3COO)_6$	2.69	1.51
$CoSn_2(CH_3COO)_6.5H_2O$	3.07	1.83
$NiSn_2(CH_3COO)_6.5H_2O$	2.94	1.70
$ZnSn_2(CH_3COO)_6.6H_2O$	3.00	1.97
$CdSn_2(CH_3COO)_6$	2.98	1.91
$Sn(CH_3COO)_2$	3.21	1.77

TABLE 2.(7). ^{119}Sn Mössbauer Parameters for Complex Tin(II) Acetates.

Table 2.(7). contains the Mössbauer parameters for lead tin(II) acetate and compares them with those of the known transition metal tin(II) acetates[1]. The isomer shift of the lead derivative is very similar to those of the other complex tin(II) acetates previously studied, and it is likely that all of the compounds including the Pb derivative have similar tin environments. Crystal structure determinations have shown that the tin atoms of the tri-carboxylatostannate(II) ion[4,5] occupy distorted trigonal pyramidal sites, with the lone pair at the apex of the pyramid and therefore, it is probable that the tin atoms in $PbSn_2(CH_3COO)_6$ are similar.

2.5. PREPARATION OF POTASSIUM [HYDROGEN BIS-(MALEATO)] STANNATE(II).

2.5.(1). Introduction.

The crystal structure of tin(II) maleate monohydrate[6] has been determined, but little is known about the tin(II) maleate complexes. In this section, the preparation and

characterisation of the potassium complex derivative is described. The unusual composition of this complex prompted the crystal determination, which is described in Chapter 3, Section 3.3.

2.5.(2). Preparation and Analysis.

Blue-black stannous oxide (0.02 mole; 2.7g) was added to 20% w/v aqueous maleic acid (50ml), the mixture was then refluxed for 1.25 hours in a nitrogen atmosphere, until the stannous oxide had dissolved. Potassium carbonate (0.02 mole; 2.7g) was added and refluxing continued for 0.5 hour. The mixture was filtered whilst hot, to remove any undissolved matter and white crystals appeared almost immediately. The solution was allowed to cool slowly to room temperature and the crystals filtered off and washed with ether. The analytical data for the product are given in Table 2.(8).

Element	Observed %	Calculated %
Sn	31.0	30.7
C	24.80	24.84
H	1.22	1.30
K	8.5	10.1

TABLE 2.(8). Elemental Analysis for Potassium Tin Maleate.

Results indicate that the compound has the following molecular formula:

$$KSn[CH(COO) : CH(COO)][CH(COO) : CHCOOH]$$

2.5.(3). Infrared Data.

The infrared data and spectral assignments are given in Table 2.(9). The formula for this compound is verified by the infrared data, since both a free carboxylate group and one bonded to tin are observed. Typically, bonding of a carboxylate ion to tin shifts the carbonyl stretching frequency to $\sim 1515 cm^{-1}$(7).

Peak Position (cm^{-1})	Assignment
3500 br	OH str. (H_2O)
3350 br	
1715 s	C=O str.
1660 w	C=C
1630 w	C=C
1560 s	$\nu(CO_2)$ asymm. str.
1490 w	-CH=CH-
1390 s	$\nu(CO_2)$ sym. str.
1335 br	ν(C-H)
1310 br	
1210 m	ν(C-O)
1180 m	
980 m	ν(C-O)
910 sh	
860 s	O-H bend
840 s	
705 sh	-CH=CH-
655 s	$\delta(CO_2)$ sym. def.
630 s	
545 s	Sn-O
455 s	$\rho(CO_2)$

TABLE 2.(9). Infrared Data for KSn[CH(COO):CH(COO)]-[CH(COO):CHCOOH].

2.5.(4). X-Ray Powder Diffraction Data.

The X-ray powder diffraction data for this compound appear below in Table 2.(10).

d spacing (Å)	R.I.	d spacing (Å)	R.I.
12.11	97	2.91	25
9.03	12	2.82	12
6.76	12	2.80	14
6.19	100	2.69	8
6.11	83	2.61	3
6.03	53	2.56	4
5.57	17	2.47	10
5.13	13	2.45	56
4.82	25	2.44	60
4.60	5	2.39	11
4.51	6	2.30	7
4.29	9	2.26	11
4.19	7	2.15	4
4.08	74	2.09	13
3.88	7	2.08	7
3.68	15	1.99	5
3.52	46	1.96	6
3.47	15	1.91	2
3.33	23	1.88	2
3.24	9	1.87	3
3.06	12	1.71	5
3.02	6	1.55	4

TABLE 2.(10). X-ray Diffraction Data for the Complex: $KSn[CH(COO) : CH(COO)][CH(COO) : CHCOOH]$.

2.5.(5). Mössbauer Data.

The Mössbauer spectrum of potassium tin maleate was recorded and its parameters compared with those of tin(II) maleate monohydrate, as shown below:

Compound	δ (mms^{-1})	Δ (mms^{-1})
KSn Maleate	3.22	1.65
$SnC_2H_2C_2O_4.H_2O$	3.28	1.72

The crystal structure of stannous maleate monohydrate is known. Each tin atom is at the apex of a distorted square pyramid, the basal plane of which is made up of four oxygen atoms, three from each of three different maleate groups and the fourth from a water of crystallisation, with two short and two slightly longer Sn-O bonds arranged alternatively around the basal plane. As expected, there is a drop in the chemical shift upon complex formation for the potassium complex tin(II) maleate. This suggests that the Sn-O bonds in the potassium salt are shorter than those in the parent compound.

2.6. REINVESTIGATION OF THE MÖSSBAUER PARAMETERS OF SOME TIN(II) CARBOXYLATES AND RELATED COMPOUNDS.

A detailed study of the Mössbauer parameters of some tin(II) carboxylates and diols was carried out earlier by Filmore[2]. Since then however, the Mössbauer spectrometers and fitting programs have been vastly improved. It was therefore decided, to re-record the spectra of some of these compounds and to note the variations obtained, if any.

This section describes the results obtained and in Table 2.(11)., the Mössbauer data are listed.

Small differences in the Mössbauer parameters were observed, but no systematic error trends could be determined.

Compound	Mössbauer Parameters			
	This Work		Filmore[2]	
	δ (mms^{-1})	Δ (mms^{-1})	δ (mms^{-1})	Δ (mms^{-1})
Monocarboxylates				
$Sn(HCOO)_2$	3.33	1.69	3.05	1.56
Sn Octoate	3.22	2.02	-	-
Dicarboxylates				
$Sn(CH_2C_2O_4)$	3.40	1.65	3.46	1.74
$Sn(C_2H_2C_2O_4).H_2O$	3.28	1.72	3.36	1.76
$Sn(EDTA)_2$	3.41	1.54	-	-
Diols				
$SnCl_2$	4.07	0.0	4.07	0.0
$SnCl_2$.Ethylene Glycol	3.47	1.54	3.58	1.27
$SnCl_2$.Propylene Glycol	3.61	1.31	3.48	1.22
$SnCl_2$.Glycerol	3.63	1.42	3.47	1.08
$SnBr_2$	3.96	0.0	3.93	0.0
$SnBr_2$.Ethylene Glycol	3.92	1.18	3.49	0.99
$SnBr_2$.Propylene Glycol	3.62	1.14	3.46	1.07
$SnBr_2$.Glycerol	3.66	1.14	-	-

TABLE 2.(11). Mössbauer Parameters of Some Tin(II) Carboxylates and Related Compounds.

Compound	4-Nearest Sn-O Bond Distances (Å)	Average of 4-Nearest Sn-O Bonds (Å)	80K δ (mms^{-1})
SnC_2O_4	2.23, 2.23, 2.39, 2.39	2.312	3.70
$Na_2Sn(C_2O_4)_2$	2.25, 2.25, 2.36, 2.36	2.301	3.67
$Sn(CH_2C_2O_4)$	2.18, 2.23, 2.26, 2.56	2.308	3.40
$Sn(C_2H_2C_2O_4).H_2O$	2.18, 2.20, 2.31, 2.44	2.281	3.28
$Sn(HCOO)_2$	2.36, 2.36, 2.13, 2.14 2.37, 2.36, 2.20, 2.20	2.260	3.33
$K_2Sn(C_2O_4)_2.H_2O$	2.14, 2.20, 2.30, 2.36	2.250	3.19

TABLE 2.(12). Chemical Shifts, Nearest Sn-O Bond Distances (Å) and Average of Nearest Neighbour Sn-O Bond Distances (Å).

Compound	3-Nearest Sn-O Bond Distances (Å)	Average of 3-Nearest Sn-O Bonds (Å)	80K δ (mms^{-1})
KSn[CH(COO) : CH(COO)] [CH(COO) : CHCOOH]	2.20, 2.20, 2.21	2.203	3.22
$K_2Sn_2(CH_2C_2O_4)_3.H_2O$	2.20, 2.18, 2.18 2.16, 2.21, 2.24	2.194	3.15
$KSn(HCOO)_3$	2.14, 2.17, 2.18	2.163	3.05
$CaSn_2(CH_3COO)_6$	2.14, 2.14, 2.14	2.140	2.80

TABLE 2.(12). (contd.) Chemical Shifts, Nearest Sn-O Bond Distances (Å) and Average of Nearest Neighbour Sn-O Bond Distances (Å).

Since the chemical shifts of tin(II) carboxylates and their complexes can be related to the s-electron density about the tin nucleus, there should be a relationship between the chemical shift and the Sn-O bond distances, which must also provide a measure of the Sn s-electron involvement in bonding.

A trend is seen to exist between the average of nearest Sn-O bond distances and the chemical isomer shift for the tin(II) carboxylates (see Table 2.(12).). There is a decrease in the s-electron density around the tin atom as the average of the nearest Sn-O bond distances decreases. The decrease in chemical isomer shifts indicates a reduction in the s-electron density as the Sn-O bond length decreases and becomes increasingly covalent.

This trend also appears to be part of a wider relationship between tin-ligand bond lengths and Mössbauer parameters described by Grimes[8].

2.7. SUMMARY.

Several tin(II) derivatives of mono- and di-carboxylic acids have been prepared and isolated as pure crystalline derivatives. The complexes are fairly stable to oxidation and can be stored in sealed glass ampoules for long periods. They all decompose without melting to give a variety of decomposition products, including in most cases, tin(II) oxide. They are hydrolysed by water to give hydrous tin(II) oxide. The compounds are characterised by elemental analysis, Mössbauer spectroscopy, X-ray powder diffraction, infrared spectroscopy and thermogravimetric analysis.

The Mössbauer parameters of the tin(II) carboxylates are discussed in terms of their structures. The isomer

shifts and Sn-O bond distances are consistent with the relatively high covalency of the Sn-O bonds. A reduction in the isomer shift is observed upon complex formation and this is consistent with an increase in covalency of the Sn-O bonds, which is confirmed by a shortening of the Sn-O bond distances. The quadrupole splitting parameters for the tin(II) carboxylates are relatively large and are in agreement with the lone-pair distorted environments found for the tin atoms.

REFERENCES.

1. Z.B. Arifin, Ph.D. Thesis, University of London, (1981).

2. E. Filmore, Ph.D. Thesis, University of London, (1972).

3. W. Simpson, Ph.D. Thesis, University of Aberdeen, (1962).

4. A. Jelen and O. Lindqvist, Acta Chem. Scand., (1969), 23, 3071.

5. S.J. Clark, J.D. Donaldson, J.C. Dewan and J. Silver, Acta Cryst.,(1979), B35, 2550.

6. J.C. Dewan, J. Silver, J.A. Andrew, J.D. Donaldson and D.R. Laughlin, J. Chem. Soc. Dalton Trans., (1977), 368.

7. J.D. Donaldson, J.F. Knifton and S.D. Ross, Spectrochim. Acta, (1965), 21, 1043.

8. S.M. Grimes, Ph.D. Thesis, The City University, London, (1982).

CHAPTER THREE

CRYSTAL STRUCTURE DETERMINATIONS

3.1. GENERAL THEORY OF CRYSTAL STRUCTURE DETERMINATION.

3.1.(1). The Structure Factor.

The electrons in the lattice planes of a crystal diffract X-rays in discrete directions according to the Bragg law. By measuring the intensities of these reflections it is possible to deduce the distribution of electron density within the crystallographic unit cell, and hence determine the structure of the crystal.

For the jth atom at coordinates x_j, y_j, z_j, with an atomic scattering factor f_j, the structure factor, F(hkl), may be related to the atomic position by the expression,

$$F(hkl) = \Sigma_j \, f_j(hkl) \exp 2\pi i \, (hx_j + ky_j + lz_j) \qquad \text{Eqn. 3.(1).}$$

the summation being carried out over all atoms. This structure factor is related to the intensity of the reflection (hkl) by:

$$I_{hkl} \propto F_{hkl}^{\,2} \qquad \text{Eqn. 3.(2).}$$

However, equation 3.(1). applies for stationary atoms only. In a real crystal, thermal vibrations[1] cause the atoms to vibrate thus distributing the electron density cloud over a larger volume than that assumed in the ideal stationary case, and so the scattering power of the atom is reduced. To account for thermal vibrations, the structure factor is modified by a function, T(hkl):

$$T(hkl) = \exp -(b_{11}h^2 + b_{22}k^2 + b_{33}l^2 + 2b_{12}hk + 2b_{13}hl + 2b_{23}kl) \qquad \text{Eqn. 3.(3).}$$

where $b_{11} = 2\pi^2 a^{*2} U_{11}$, $b_{22} = 2\pi^2 b^{*2} U_{22}$, etc. U_{11} is the vibration component in the 100 direction parallel to a* with units of $\mathring{A}^2$, b_{ij} are called the anisotropic temperature factors. In the rare case where the temperature factors are

isotropic, T(hkl) is calculated as an average over all directions so that

$$b_{11} = b_{22} = b_{33} \text{ , etc.}$$

Thus, equation 3.(1). becomes,

$$F_T(hkl) = \Sigma_j \, f_j(hkl) \, T_j(hkl) \, \exp 2\pi i(hx_j + ky_j + lz_j)$$

3.1.(2). Data Reduction.

The observed reflection intensities are influenced by the time over which the crystal plane will give diffraction (Lorentz factor), by the polarisation of the X-ray beam, and by absorption of X-rays by the crystal. The measured intensities must therefore be corrected by data reduction to give the modulus of the structure factor.

The Lorentz factor is a correction made to allow for the time spent by each plane in passing through the Bragg condition and depends on the method of recording reflections. For data collection on a diffractometer, the Lorentz correction (L) is $(\sin 2\theta)^{-1}$. The polarisation factor, p, corrects for the partial plane polarisation of the X-ray beam on reflection off the lattice planes and is given by

$$p = \tfrac{1}{2}(1 + \cos^2 2\theta)$$

When a beam of monochromatic X-rays passes through a crystal of thickness, t, the intensity of the transmitted radiation, I, is related to that of the incident radiation, I_o, by

$$I = I_o \exp(-ut)$$

where u is the linear absorption coefficient, this is a constant and may be calculated[2]. If the thickness of the

crystal is less than the optimum thickness, $t_{opt} = 2/u$, then an absorption correction is not necessary and may be neglected in all but the most precise determinations.

Hence the final intensity equation is:

$$I_{obs}(hkl) \alpha Lp\ A(hkl)\ F_T^2(hkl)$$

and

$$\left|F_T(hkl)\right|^2_{obs} = I_{obs}(hkl)\ (Lp)^{-1}\ A^*_{hkl}$$

where $A^*(hkl) = \frac{1}{A(hkl)}$

The structure factor obtained experimentally is on a relative scale, but its phase and absolute values can only be obtained from calculated data in the process of crystal structure determination.

3.1.(3). Fourier Series[3].

The electron density in a crystal, ρ, can be represented by a three-dimensional Fourier series:

$$\rho(x,y,z) = \frac{1}{V} \Sigma_h \Sigma_k \Sigma_l \left|F(hkl)\right| \exp(2\pi i(hx + ky + lz))$$

where x, y, and z are the fractional atomic coordinations of the atoms within the unit cell and

$$F(hkl) = \left|F(hkl)\right| \exp(i\alpha(hkl))$$

As only $\left|F(hkl)\right|$ is measured experimentally, it is necessary to determine the phase angles, $\alpha(hkl)$, before the structure can be solved. In this work, the general method used to solve this problem was to find the positions of the heavy atoms in the cell by a Patterson synthesis and then to assume the sign of $F(hkl)_{obs}$ was the same as that of the calculated structure factor, $F(hkl)_{calc}$, obtained by phasing the reflections on the positions of the heavy atom.

3.1.(4). Patterson Function and the Heavy Atom Method.

In order to overcome the phase problem, Patterson[4] defined a Fourier series using the experimentally obtained $F^2(hkl)$ values that do not involve the phase of the structure factor. The Patterson function represents all interatomic vectors reduced to a common origin. The magnitude of the Patterson peak is proportional to the product of the atomic numbers of the two atoms giving rise to the peak, so that vectors between the heaviest atoms produce the most intense peaks[5]. Thus if one atom has many more electrons than the others contained in the unit cell, the 'Heavy Atom' dominates the magnitude and phases of the structure factors.

If the space group is known, the general positions allow the vectors to be calculated by vector subtraction and correlated with the peaks on the Patterson function. With the heavy atom positions known, the phase of each reflection can be approximated to that due to the heavy atoms so as to obtain an electron density map from which more accurate heavy atom positions and the approximate positions of the lighter atoms can be obtained.

3.1.(5). Difference Fourier.

Since the observed data can never be a complete series, termination errors occur in the Fourier synthesis. Hence in practice, when the heavy atom positions are known a difference Fourier is used to locate the light atom positions. The difference synthesis is found by subtracting the calculated electron densities from those observed. The resultant difference map then shows only the residual electron density.

3.1.(6). Reliability Factor and Weighting.

The atomic positions x, y, z, and the temperature factors B_j (b_{ij} for anisotropic factors) are refined by a method of least squares to obtain the best fit between $F(hkl)_{obs}$ and $F(hkl)_{calc}$. The correctness of the structure is measured in terms of the residual, R, where

$$R = \Sigma_i \left(\frac{|F|_o - |F|_c}{|F|_o} \right)_i$$

which tends to a minimum as a better fit between observed and calculated structure factors over the total number of reflections, i, is achieved. For least squares refinement, it is necessary to weight the input data, to allow for variations in the accuracy of measuring weak and strong reflections. The weighting is achieved using a factor w_i such that,

$$R_w = \left\{ \Sigma_i \; w_i \left(\frac{|F|_o - |F|_c}{|F|_o} \right)_i \right\}^{\frac{1}{2}}$$

When $w_i = 1$, $R_w = R$. An alternative weighting scheme uses weightings that are proportional to the inverse variances of the observations,

$$w_i = (\sigma^2 (|F|_o)_i + g(|F|_o)_i^2)^{-1}$$

3.2. COMPUTER PROGRAMS USED IN X-RAY CRYSTALLOGRAPHY.

3.2.(1). SHELX-76.

SHELX-76[6] is an integrated program for performing crystallographic calculations. These are valid for all space groups and there is no limit on the number of reflections. Its facilities include,

(i) data reduction, including numerical absorption

correction with crystal plots,

(ii) rejection of systematic absences, least-squares determination of inter-batch scale factors, averaging equivalent reflections,

(iii) full matrix, least-squares refinements,

(iv) rigid group location on refinement,

(v) various Fourier syntheses with peaks search,

(vi) structure factor lists.

3.2.(2). POWDER AND POWREF[7].

These programs fit and refine respectively, the data obtained from powder cameras. They may be used separately or as a combined POWDER-POWREF run.

3.2.(3). XRAY-72.

XRAY-72[8] is a manual report for the use of a library of crystallographic programs designed to perform the calculations needed to solve the structure of crystals by diffraction techniques.

3.2.(4). PLUTO.

PLUTO[9] is a program for plotting molecular and crystal structures. The principal features of PLUTO are:

(a) plotting of single molecules or assemblies of molecules.

(b) use of stick or solid ball-and-spoke representations.

(c) variable sizes for atoms and bonds.

(d) automatic labelling to avoid overlap.

(e) stereo or mono views with or without perspective.

(f) flexible control of view direction.

In this work, the crystal structure determination of

two tin(II) dicarboxylate derivatives are described. Previous workers have detailed the structures of tin(II) maleate monohydrate[10] and dipotassium trismalonatodistannate monohydrate[11] and, it is for this reason that the structures of tin(II) malonate and potassium [hydrogenbis-(maleato)]stannate(II) are investigated.

3.3. THE CRYSTAL STRUCTURE DETERMINATION OF POTASSIUM [HYDROGENBIS-(MALEATO)]STANNATE(II).

3.3.(1). Preparation of the Crystals.

Blue-black tin(II) oxide (0.02 mole; 2.7g) was dissolved in a 20% w/v aqueous maleic acid solution (50ml) by refluxing the mixture for 1¼ hours under a nitrogen atmosphere. Potassium carbonate (0.02 mole; 2.7g) was added and the mixture refluxed for a further half an hour. The resultant solution was filtered hot to remove any undissolved matter and cooled to give a white crystalline product, which was filtered , washed with petroleum ether (b.p. 40-60° C) and dried in vacuo over potassium hydroxide. The elemental analysis of this compound is given in Chapter 2.

3.3.(2). Determination of the Space Group and Cell Dimensions.

A small crystal, which had a maximum thickness of 0.23mm, and that showed perfect extinction, was set up along a unique crystal axis using the Precession camera. Zero layer precession and zero, first and second level Weissenberg photographs were obtained and the data in Table 3.(1). derived.

As a result of this data, the crystal was uniquely assigned to the space group P1 or $P\bar{1}$. The space group $P\bar{1}$ (No. 2 in the International Tables for X-ray Crystallo-

Crystal Class	Triclinic
Cell Dimensions ($\mathring{A}$)	a = 7.631 (12) b = 12.305 (3) c = 7.246 (8)
Angles (^{o})	α = 97.02 (6) β = 109.83 (28) γ = 87.48 (7)
Cell Volume ($\mathring{A}$)^3	612.77
Molecular Weight	386.90
Density (measured by the displacement of benzene) gcm^{-3}	2.09
Density (calculated for Z=2) gcm^{-3}	2.10
F(000)	372.00
u	22.63
No systematic absences	

TABLE 3.(1). Crystal Data for KSn[CH(COO):CH(COO)]-[CH(COO):CHCOOH].

graphy) was assumed in the refinement and confirmed in the completed structure.

3.3.(3). Collection of Intensity Data.

Intensity data on crystals of potassium [hydrogen bis-(maleato)]stannate(II) were obtained at the SERC diffractometer service at Queen Mary College, University of London, on an Enraf Nonius CAD4 diffractometer. The output showed that 2148 unique reflections were observed, of which 97 were suppressed because $I < 2\sigma I$. This output was then used in the SHELX program for the structure determination.

3.3.(4). Location of the Tin Atom.

There were no systematic absences in the reflections, this is consistent with the space groups P1 and $P\bar{1}$. Refinement was only successful in the latter case.

The centrosymmetric space group $P\bar{1}$ has the equivalent positions

$$\begin{matrix} x & y & z \\ \bar{x} & \bar{y} & \bar{z} \end{matrix}$$

these positions give peaks in the Patterson vector map at

$$2x \quad 2y \quad 2z$$

The atoms present in the unit cell are Sn, K, O, C and H and the Sn-Sn vector would be expected to give the largest peak in the Patterson map. Apart from the origin peak, the highest peak (358) in the Patterson synthesis at x = 0.2699, y = 0.1996, z = 0.0276, was assigned to the Sn-Sn vector. A five cycles, least-squares full matrix refinement based on the Sn position was carried out and a three-dimensional difference Fourier map phased on this Sn position calculated. The lowest residual (R = 0.37) was obtained with the tin parameters,

x	y	z
0.2740	0.2003	0.0296

3.3.(5). Location of the Light Atoms in the Unit Cell.

3.3.(5).1. Potassium Atom and Oxygen Atoms Directly Bonded to the Tin.

The largest peak in the difference Fourier map based on the tin position was at x = 0.922, y = 0.115, z = 0.281. This peak was assumed to be due to the potassium atom. The difference Fourier map also contained peaks that were

separated from the tin position by distances that were consistent with Sn-O bonds. These peaks were assumed to be oxygen atoms at the following positions:

O1	0.245	0.039	0.111
O2	0.960	0.194	0.954
O3	0.254	0.249	0.324

Refinement of the Sn, K and O1, O2 and O3 coordinates reduced the residual to R = 0.22, and gave the following parameters,

	x	y	z
K	0.9221	0.1152	0.2821
O1	0.2441	0.0387	0.1124
O2	0.9591	0.2004	0.9556
O3	0.2515	0.2482	0.3296

3.3.(5).2. Location of the Remaining Oxygen Atoms and the Carbon Atoms.

Using the positions obtained for the oxygen atoms bonded to tin and knowing that the arrangement of the maleate group is

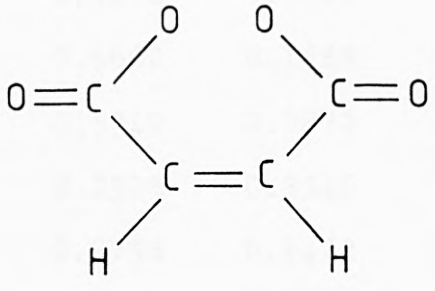

The distances between atoms and the Fourier map peaks gave the following oxygen and carbon atom coordinates:

O4	0.979	0.105	0.679
O5	0.552	0.068	0.210
O6	0.250	0.413	0.243

O7	0.240	0.604	0.408
O8	0.225	0.682	0.685
C1	0.418	0.009	0.207
C2	0.657	0.159	0.687
C3	0.535	0.087	0.696
C4	0.253	0.357	0.372
C5	0.876	0.147	0.776
C6	0.258	0.389	0.571
C7	0.264	0.494	0.662
C8	0.249	0.599	0.582

Refinement of these atomic positions with those for Sn, K, O1, O2, and O3, further reduced the residual to R = 0.077 and gave the following parameters:

	x	y	z
O4	0.9788	0.1045	0.6791
O5	0.5520	0.0681	0.2104
O6	0.2496	0.4127	0.2413
O7	0.2401	0.6046	0.4037
O8	0.2246	0.6818	0.6846
C1	0.4178	0.0093	0.2065
C2	0.6662	0.1588	0.6874
C3	0.5349	0.0872	0.6964
C4	0.2528	0.3510	0.3724
C5	0.8758	0.1472	0.7756
C6	0.2578	0.3894	0.5710
C7	0.2642	0.4944	0.6621
C8	0.2491	0.5987	0.5816

Recalculation of the structure using these atomic positions with anisotropic temperature factors, interlayer

structure factors and weighting of the atoms reduced the residual to R = 0.025.

3.3.(5).3. Location of the Hydrogen Atoms.

The positions of the hydrogen atoms were estimated from the difference Fourier map at this stage to be at: H1 0.391, 0.102, 0.652; H2 0.626, 0.221, 0.613; H3 0.250, 0.325, 0.443; H4 0.270, 0.501, 0.807; H5 0.217, 0.531, 0.324.

These hydrogen atoms were refined to the following positions:-

	x	y	z
H1	0.3977	0.0961	0.6317
H2	0.6220	0.2137	0.6082
H3	0.2639	0.3412	0.6582
H4	0.2803	0.4973	0.7846
H5	0.2341	0.5257	0.3101

Final full matrix, least-squares refinement of all positions and of anisotropic temperature factors for all the atoms, except the hydrogens, gave a final residual of 0.021, which was weighted to R_W = 0.022. The final observed and calculated structure factors are given in Appendix I and the final atomic positions and thermal parameters are listed in Table 3.(2). The bond distances and angles which were obtained using the program SHELX are in Table 3.(3).

3.3.(6). Structural Description and Discussion.

The structure of potassium [hydrogen bis-(maleato)]-stannate(II) consists of potassium ions and discrete dimeric anionic units, $[Sn(CHCOO:CHCOO)(CHCOO:CHCOOH)]^-$, which are hydrogen bonded to each other so that an extended polymeric network is obtained. The asymmetric unit of the anionic

TABLE 3.(2). Atomic Positions and Anisotropic Temperature Factors for KSn(CHCOO:CHCOO)(CHCOO:-CHCOOH) with Estimated Standard Deviations in Parenthesis.

Atomic Positions.

Atoms	x/a	y/b	z/c
Sn	0.2740 (0)	0.2003 (0)	0.0296 (0)
K	0.9229 (1)	0.1142 (0)	0.2805 (1)
O1	0.2433 (2)	0.0385 (1)	0.1152 (3)
O2	0.9590 (3)	0.1954 (1)	0.9573 (2)
O3	0.2588 (3)	0.2483 (2)	0.3284 (3)
O4	0.9808 (3)	0.1053 (2)	0.6807 (3)
O5	0.5560 (3)	0.0704 (2)	0.2127 (3)
O6	0.2532 (5)	0.4147 (2)	0.2473 (4)
O7	0.2402 (6)	0.6048 (2)	0.4031 (6)
O8	0.2306 (6)	0.6815 (2)	0.6869 (6)
C1	0.4200 (3)	0.0113 (2)	0.2053 (3)
C2	0.6687 (4)	0.1571 (2)	0.6910 (4)
C3	0.5392 (4)	0.0897 (2)	0.6985 (4)
C4	0.2572 (4)	0.3514 (2)	0.3693 (4)
C5	0.8844 (4)	0.1491 (2)	0.7799 (3)
C6	0.2631 (5)	0.3908 (3)	0.5742 (5)
C7	0.2572 (6)	0.4926 (3)	0.6586 (6)
C8	0.2411 (6)	0.5999 (3)	0.5818 (7)
H1	0.3977 (48)	0.0961 (27)	0.6317 (45)
H2	0.6220 (79)	0.2137 (48)	0.6082 (80)
H3	0.2639 (131)	0.3412 (84)	0.6582 (139)
H4	0.2803 (84)	0.4973 (51)	0.7846 (83)
H5	0.2341 (87)	0.5257 (61)	0.3101 (93)

TABLE 3.(2). Continued.

Anisotropic Temperature Factors (U_{ij} x 10^{-3})

Atoms	U_{11}	U_{22}	U_{33}
Sn	37.8 (1)	29.0 (4)	35.8 (1)
K	31.9 (3)	29.8 (4)	31.4 (3)
O1	26.8 (8)	25.1 (9)	40.4 (9)
O2	37.4 (9)	33.1 (10)	28.0 (8)
O3	43.7 (10)	26.7 (10)	38.1 (9)
O4	44.2 (10)	40.2 (11)	31.7 (9)
O5	32.6 (10)	56.9 (13)	45.6 (11)
O6	117.9 (23)	35.5 (12)	61.8 (14)
O7	149.7 (32)	27.6 (13)	125.9 (26)
O8	135.6 (32)	36.6 (16)	155.7 (33)
C1	30.2 (12)	33.5 (13)	24.4 (11)
C2	37.1 (14)	29.0 (13)	32.3 (12)
C3	31.2 (13)	38.9 (15)	31.5 (12)
C4	39.1 (14)	26.0 (14)	42.1 (14)
C5	37.1 (13)	23.9 (12)	28.3 (11)
C6	68.4 (21)	34.6 (16)	47.2 (16)
C7	78.4 (24)	39.6 (18)	63.1 (21)
C8	62.7 (21)	29.6 (17)	110.3 (32)
H1	41.4 (80)	-	-
H2	71.9 (179)	-	-
H3	117.4 (370)	-	-
H4	114.7 (207)	-	-
H5	166.5 (217)	-	-

TABLE 3.(2). Continued.

Anisotropic Temperature Factors (U_{ij} x 10^{-3})

Atoms	U_{23}	U_{13}	U_{12}
Sn	3.9 (1)	18.9 (1)	-6.0 (1)
K	2.0 (2)	14.5 (2)	-3.9 (2)
O1	5.3 (7)	12.5 (7)	0.8 (7)
O2	2.5 (7)	12.7 (7)	0.4 (7)
O3	-0.8 (7)	14.1 (8)	-4.3 (8)
O4	3.7 (8)	17.5 (8)	8.0 (8)
O5	2.1 (9)	11.9 (8)	-14.4 (9)
O6	10.0 (11)	45.1 (15)	0.0 (13)
O7	8.6 (14)	85.0 (24)	-0.7 (15)
O8	-29.9 (18)	80.1 (28)	-1.4 (17)
C1	-5.8 (9)	11.9 (9)	-2.4 (10)
C2	6.7 (10)	8.5 (10)	10.3 (11)
C3	0.5 (11)	7.1 (10)	7.8 (11)
C4	0.6 (11)	14.2 (11)	-2.9 (11)
C5	8.7 (9)	13.3 (10)	3.7 (10)
C6	-2.0 (13)	23.2 (15)	-3.2 (14)
C7	-10.5 (16)	32.5 (18)	-0.6 (16)
C8	-11.1 (18)	42.2 (21)	-2.5 (15)

TABLE 3.(3). Bond Distances (Å) and Angles (°) in KSn[CH(COO):CH(COO)][CH(COO):CHCOOH] with Estimated Standard Deviations in Parenthesis.

Coordination to Tin:		
Sn - O(1)	2.199	(2)
Sn - O(2)	2.199	(2)
Sn - O(3)	2.212	(2)
Sn - O(4)	2.866	
Sn - O(5)	2.642	
Sn - O(6)	2.931	
O(1) - Sn - O(2)	79.9	(1)
O(1) - Sn - O(3)	79.7	(1)
O(2) - Sn - O(3)	80.9	(1)
Association to Potassium:		
K - O(1)	3.052	
K - O(2)	2.752	
K - O(3)	2.932	
K - O(4)	2.799	
K - O(5)	2.644	
K - O(8)	2.728	
K - H(1)	3.574	
K - H(2)	3.829	
Bonding in Maleate Group:		
O(1) - C(1)	1.292	(3)
C(1) - O(5)	1.246	(3)
C(1) - C(3)	1.469	(4)
C(3) - C(2)	1.310	(4)
C(3) - H(1)	0.993	(32)
C(2) - H(2)	0.951	(54)

TABLE 3.(3). Continued.

C(2) - C(5)	1.501	(4)
C(5) - O(4)	1.236	(3)
C(5) - O(2)	1.284	(3)
O(3) - H(2)	2.806	
O(4) - H(2)	2.820	
C(1) - O(1) - Sn	102.8	(1)
C(5) - O(2) - Sn	108.3	(1)
O(1) - C(1) - O(5)	120.6	(2)
O(2) - C(5) - O(4)	123.5	(2)
O(2) - C(5) - C(2)	115.9	(2)
O(4) - C(5) - C(2)	120.5	(2)
C(5) - C(2) - C(3)	127.8	(2)
H(2) - C(2) - C(5)	115.5	(34)
H(2) - C(2) - C(3)	116.3	(34)
H(1) - C(3) - C(2)	125.2	(19)
O(1) - C(1) - C(3)	119.7	(2)
O(5) - C(1) - C(3)	119.7	(2)
C(1) - C(3) - C(2)	125.7	(2)
C(1) - C(3) - H(1)	109.0	(19)

Bonding in Protonated Maleate Group:

O(3) - C(4)	1.268	(3)
C(4) - O(6)	1.240	(4)
C(4) - C(6)	1.491	(4)
C(6) - C(7)	1.331	(5)
C(6) - H(3)	0.912	(99)
C(7) - C(8)	1.479	(5)
C(7) - H(4)	0.868	(54)
C(8) - O(8)	1.200	(4)

TABLE 3.(3). Continued.

C(8) - O(7)	1.301	(5)
O(7) - H(5)	1.108	(70)
O(7) - H(2)	2.508	
O(6) - H(5)	1.402	
Sn - O(3) - C(4)	112.0	(2)
O(3) - C(4) - O(6)	122.0	(2)
O(3) - C(4) - C(6)	115.4	(2)
O(6) - C(4) - C(6)	122.6	(3)
C(4) - C(6) - C(7)	129.6	(3)
C(4) - C(6) - H(3)	119.5	(61)
H(3) - C(6) - C(7)	110.8	(61)
C(6) - C(7) - C(8)	131.8	(4)
C(6) - C(7) - H(4)	113.9	(41)
C(8) - C(7) - H(4)	113.9	(41)
C(7) - C(8) - O(8)	119.0	(4)
C(7) - C(8) - O(7)	120.0	(3)
O(7) - C(8) - O(8)	121.0	(4)
C(8) - O(7) - H(5)	116.5	(34)
H(5) - O(6) - C(4)	114.7	(26)

moiety is shown in Figure 3.(1).

Both tin atoms in the asymmetric unit are coordinated through two oxygen atoms of bridging bidentate maleate groups giving rise to a 14-membered ring system and to the oxygen atoms of terminal monodentate monoprotonated maleate moieties. The potassium atoms lie between the layers of the dimaleatodistannate rings. The projections of the unit cell viewed along the X-, Y- and Z- axes are shown in Figures 3.(2) - 3.(6).

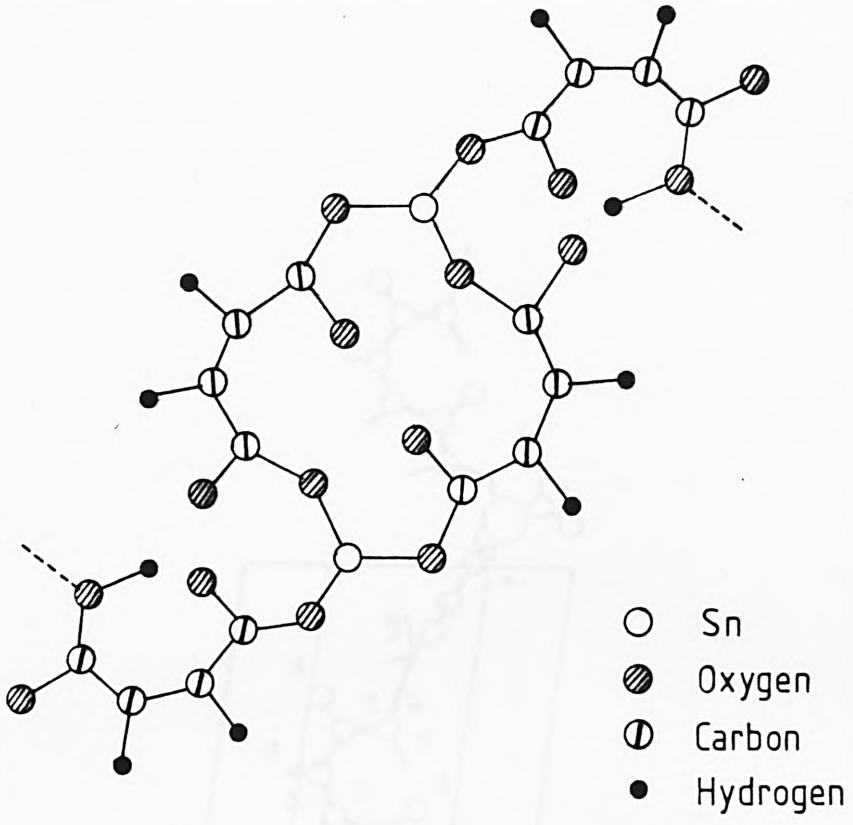

FIGURE 3.(1). Stick Diagram of the Asymmetric Unit in KSn(CHCOO:CHCOO)(CHCOO:CHCOOH).

3.3.(6).1. The Tin Environment.

The environments of the two tin atoms in the asymmetric unit of KSn[CH(COO):CH(COO)][CH(COO):CHCOOH], are identical. The tin atom is coordinated by three oxygen atoms, two of which arise from the bridging maleate groups and give Sn-O bond distances of 2.199 Å. The third Sn-O bond distance is at 2.212 Å and results from coordination to a third, mono-protonated maleate group. The O-Sn-O bond angles are 79.7, 79.9 and 80.9°. Three longer Sn-O contacts to oxygen atoms of neighbouring maleate groups at 2.642, 2.866 and 2.931 Å, complete a distorted octahedral environment around the tin, illustrated in Figure 3.(7).

The distortion about the tin environment is due to the presence of a stereochemically active lone pair of electrons

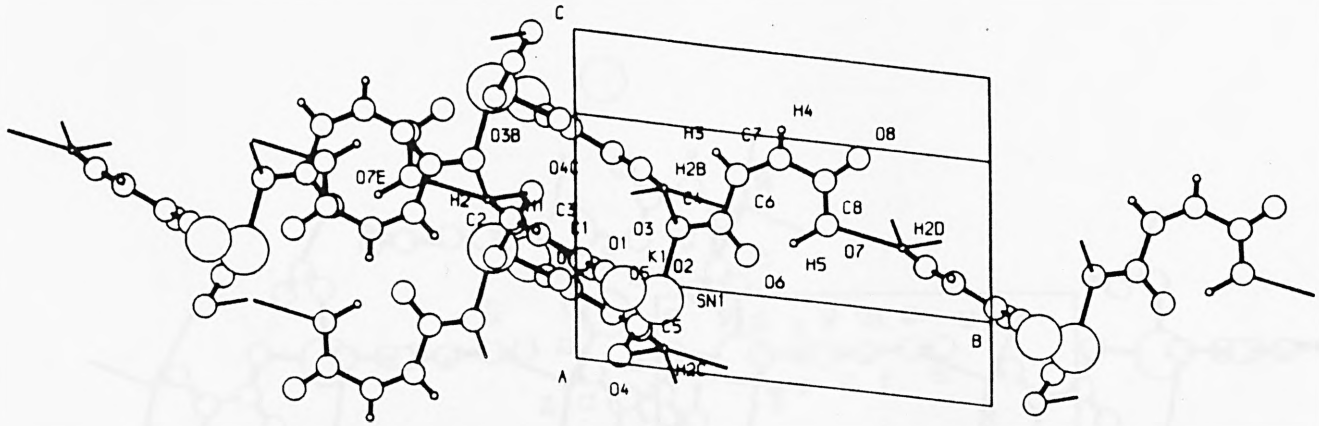

FIGURE 3.(2). Projection of the Unit Cell of KSn[CH(COO):CH(COO)][CH(COO):CHCOOH] Along the X-Axis, Without Crystal Packing.

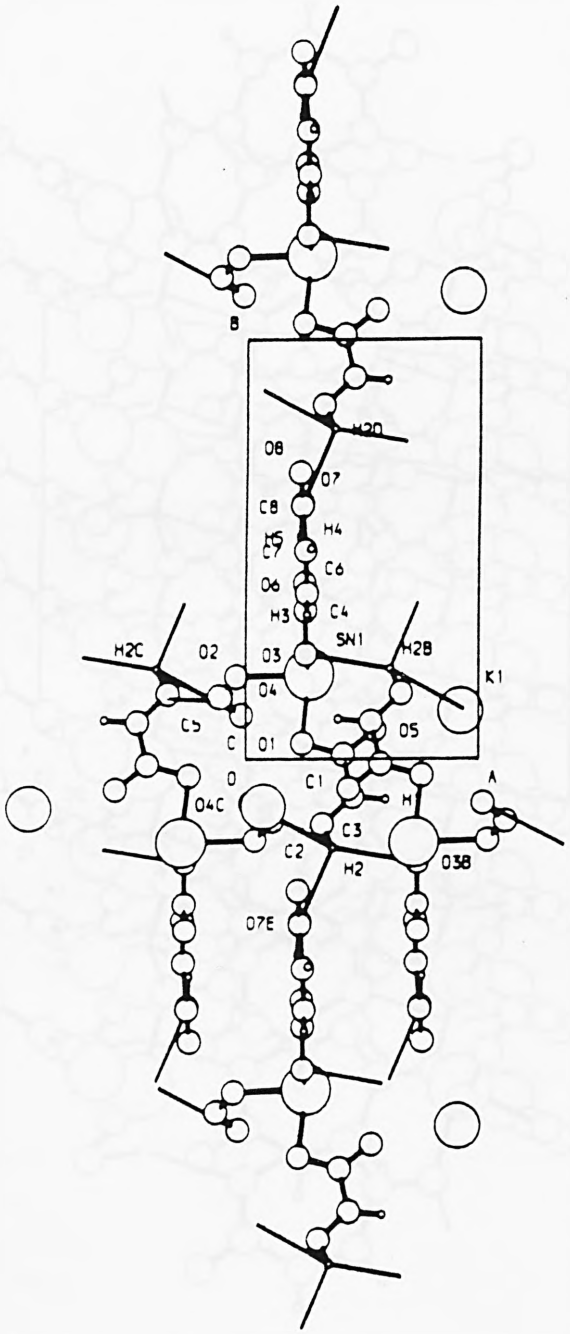

FIGURE 3.(3). Projection of the Unit Cell of KSn[CH(COO):CH(COO)][CH(COO):CHCOOH] Along the Z-Axis, Without Crystal Packing.

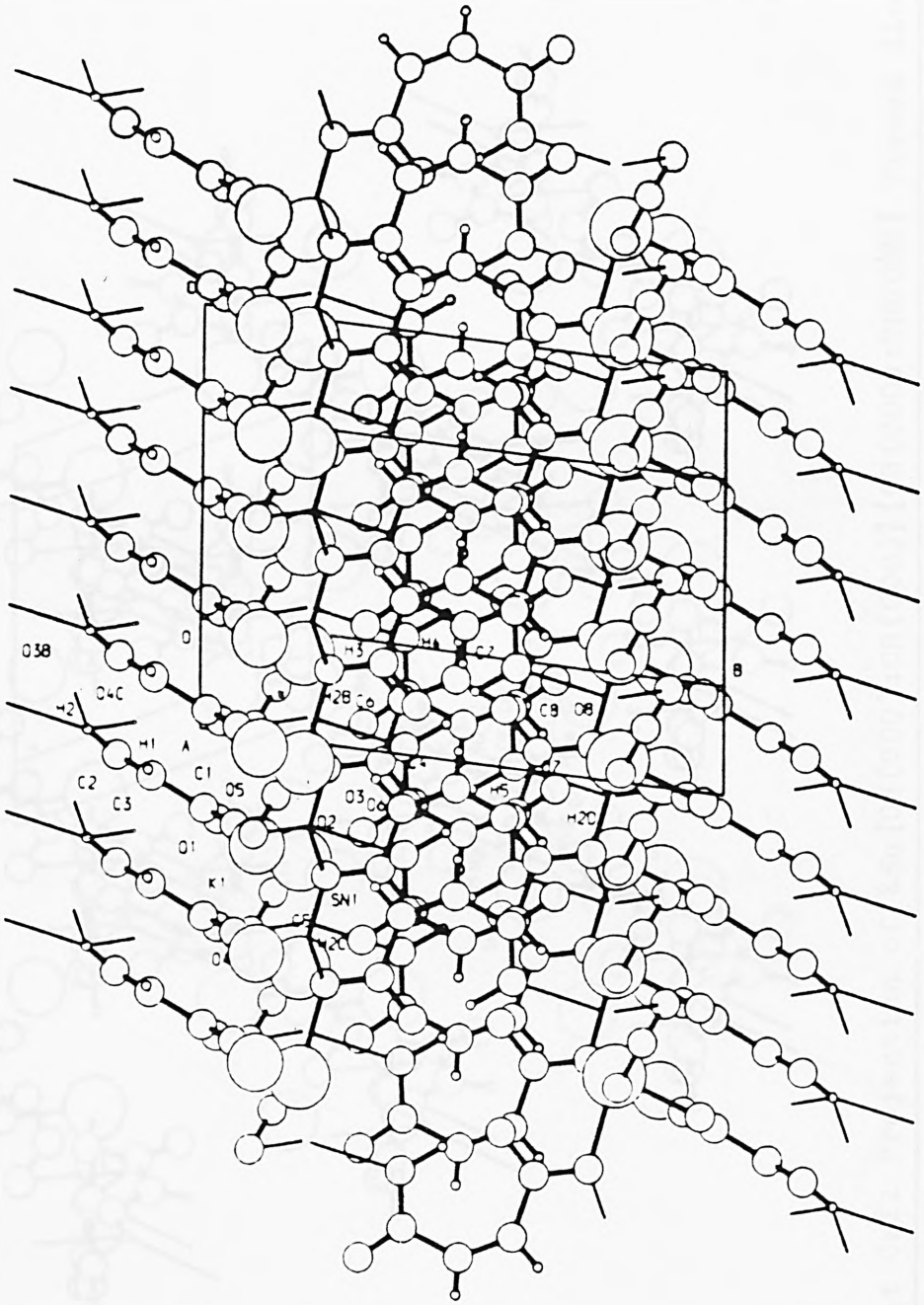

FIGURE 3.(4). Unit Cell Projection of the Compound KSn[CH(COO):CH(COO)][CH(COO):CHCOOH] Viewed Along the X-Axis.

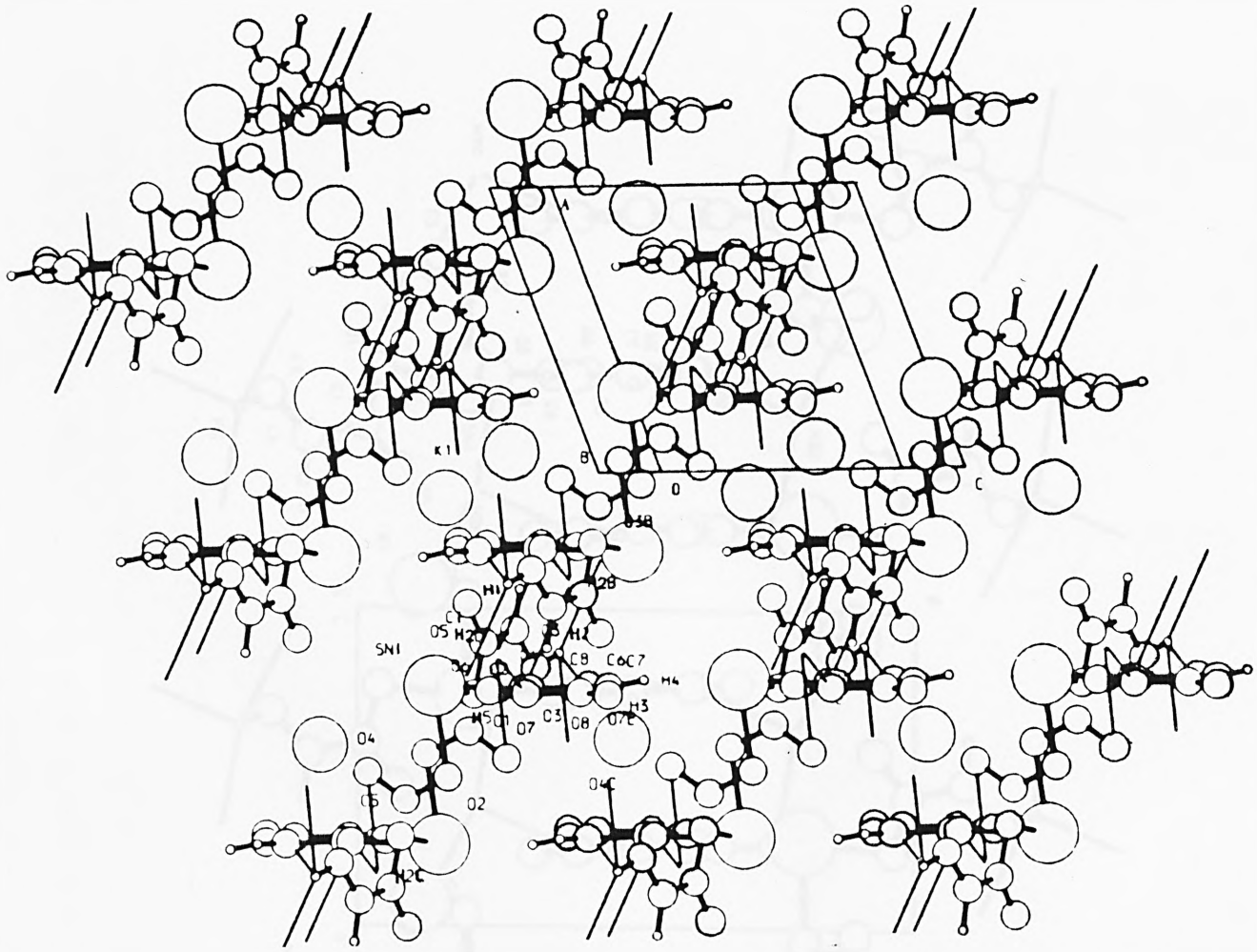

FIGURE 3.(5). Unit Cell Projection of KSn[CH(COO):CH(COO)][CH(COO):CHCOOH] Viewed Along the Y-Axis.

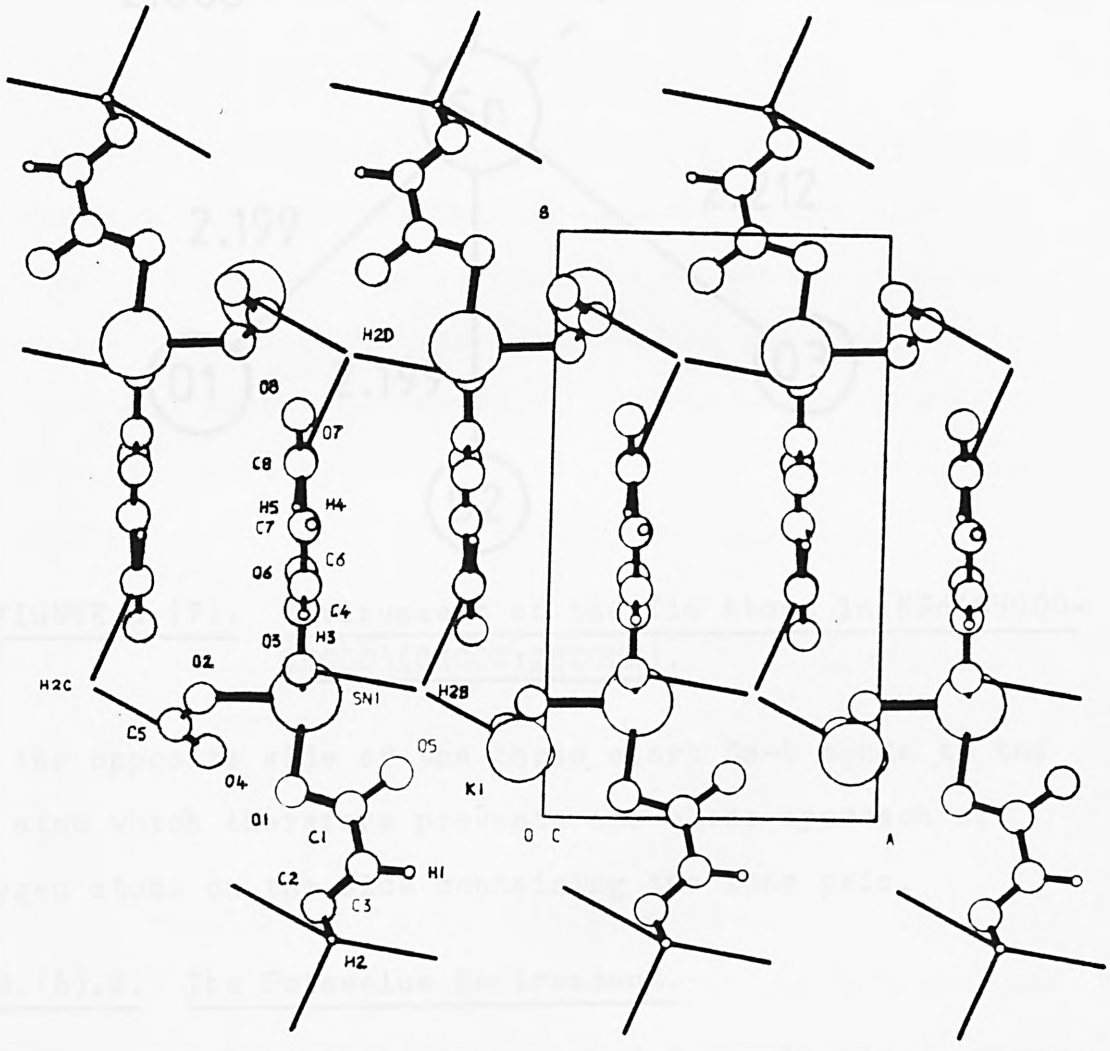

FIGURE 3.(6). Unit Cell Projection of the Compound KSn[CH(COO):CH(COO)][CH(COO):CHCOOH] Viewed Along the Z-Axis.

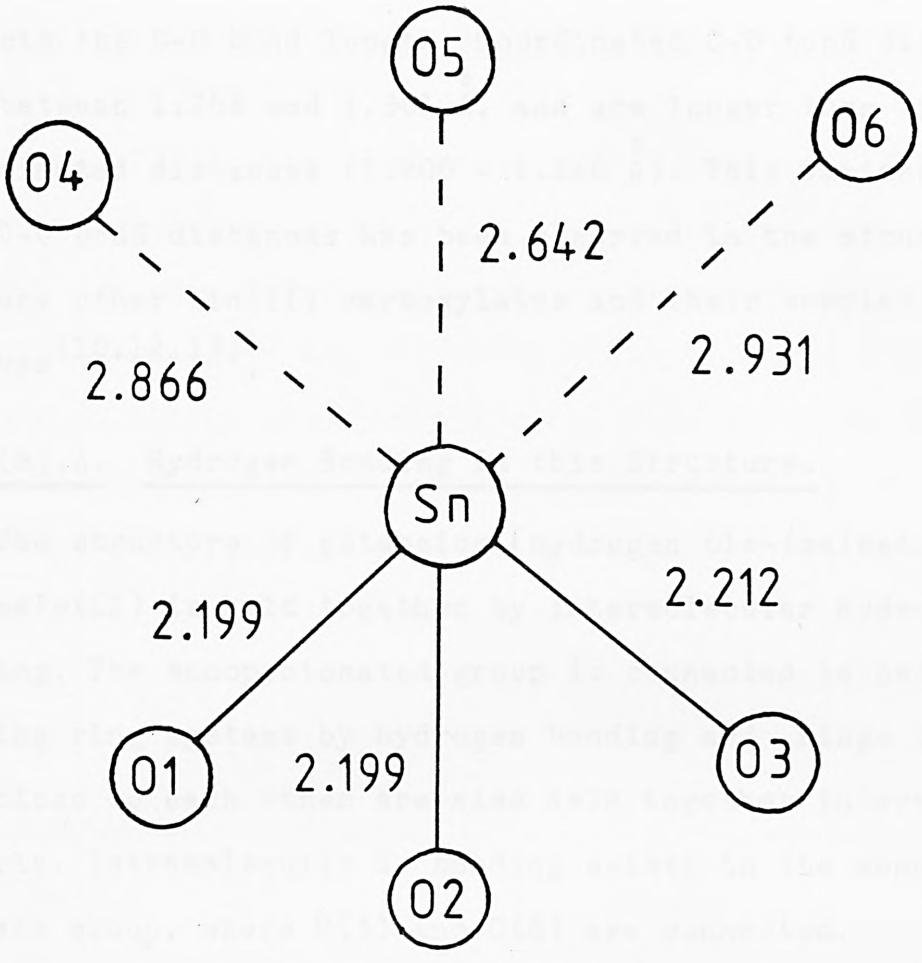

FIGURE 3.(7). Environment of the Tin Atoms in KSn(CHCOO-CHCOO)(CHCOO:CHCOOH).

on the opposite side of the three short Sn-O bonds to the Sn atom which therefore prevents the close approach of oxygen atoms on the side containing the lone pair.

3.3.(6).2. The Potassium Environment.

The potassium cation is surrounded by six oxygen atoms with K-O = 2.644, 2.728, 2.752, 2.799, 2.932 and 3.052 Å, and has two hydrogen atoms at K-H = 3.574 and 3.829 Å.

3.3.(6).3. The Maleate Environment.

The protonated and non-protonated maleate groups are structurally very similar. The bond distances and bond angles are consistent with a regular array of sp^2 hybridised carbon atoms. The coordination of oxygen to tin

affects the C-O bond length. Coordinated C-O bond distances are between 1.268 and 1.301 Å, and are longer than the uncoordinated distances (1.200 - 1.246 Å). This variance in the C-O bond distances has been observed in the structures of many other tin(II) carboxylates and their complex derivatives[10,12,13].

3.3.(6).4. Hydrogen Bonding in this Structure.

The structure of potassium [hydrogen bis-(maleato)]-stannate(II) is held together by intermolecular hydrogen bonding. The monoprotonated group is connected to neighbouring ring systems by hydrogen bonding and rings which lie close to each other are also held together intermolecularly. Intramolecular H- bonding exists in the monoprotomaleate group, where H(5) and O(6) are connected.

3.4. THE CRYSTAL STRUCTURE DETERMINATION OF TIN(II) MALONATE.

3.4.(1). Preparation of the Crystals.

Blue-black tin(II) oxide (0.01 mole; 1.35g) was dissolved by refluxing in a 20% w/v aqueous malonic acid solution (50ml) for 1½ hours under an oxygen-free nitrogen atmosphere. The resulting mixture was filtered hot, to remove any undissolved matter, and the clear solution allowed to cool slowly to room temperature. The white crystalline product that was obtained, over a period of two days, was filtered off, washed with petroleum ether (b.p. 40-60°C) and dried in vacuo over pellets of potassium hydroxide. The compound was analysed as $SnCH_2C_2O_4$: Observed % Sn 54.6, % C 16.34, % H 0.87; Calculated : % Sn 53.77, % C 16.32, % H 0.91.

3.4.(2). Determination of the Space Group and the Cell Dimensions.

Crystals of tin(II) malonate were sent to the S.E.R.C. diffractometer service at Queen Mary College, University of London, for intensity data collection on an Enraf Nonius CAD4 diffractometer and determination of the space group and the cell dimensions. The crystal data for stannous malonate are listed in Table 3.(4). The output showed that 1295 unique reflections were observed, of which 130 weak reflections were suppressed because $I < 2\sigma I$. This output was then used in the SHELX program[6] for structure determination.

Crystal Class	Monoclinic
Cell Dimensions	a = 8.3765 (15) b = 9.6886 (15) c = 5.7896 (8)
Angles (°)	α = 89.95 (10) β = 93.02 (10) γ = 90.00 (10)
Cell Volume $(\mathring{A})^3$	469.86
Molecular Weight	220.73
Density (measured by the displacement of benzene) gcm^{-3}	3.02
Density (calculated for Z=4) gcm^{-3}	3.12
F(000)	408.00
μ	49.51

TABLE 3.(4). The Crystal Data for $SnCH_2C_2O_4$.

The systematic absences are:

hkl no absences - P

0k0 absent for h odd - 2_1

h0l absent for h odd - a

The crystals are uniquely assigned to the space group $P2_1/a$ (a non-standard form of the space group $P2_1/c$, No. 14 in the International Tables for X-ray Crystallography).

This centrosymmetric space group has the following equivalent positions:

x	y	z
-x	-y	-z
$\frac{1}{2}$-x	$\frac{1}{2}$+y	-z
x-$\frac{1}{2}$	-$\frac{1}{2}$-y	z

3.4.(3). Location of the Tin Atom.

The three highest peaks (458, 427 and 252) in the Patterson vector map occurred at the positions: 0.30, 0.50, 0.43; 0.50, 0.25, 0.00; and 0.80, 0.25. 0.44. These were assigned the Sn-Sn vectors 2x-$\frac{1}{2}$, $\frac{1}{2}$, 2z; $\frac{1}{2}$, 2y+$\frac{1}{2}$, 0; and 2x, 2y, 2z, respectively, from four tin atoms in general positions based on x = 0.399, y = 0.124, z = 0.218. A five cycles, least squares full matrix refinement based on the tin position was carried out and a three-dimensional difference Fourier map phased on the tin position calculated. The lowest residual (R = 0.20) was obtained with the tin parameters,

x	y	z
0.3988	0.1299	0.2176

3.4.(4). The Location of the Light Atoms in the Unit Cell.

The atom arrangement in a malonate group is

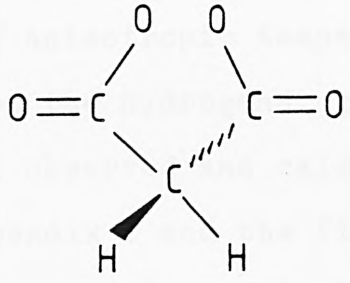

Using this and the expected distances between atoms in a malonate group, the peaks in the Fourier map gave the following oxygen and carbon coordinates:

O1	0.634	0.354	0.143
O2	0.434	0.261	0.926
O3	0.349	0.982	0.920
O4	0.719	0.615	0.614
C1	0.563	0.328	0.948
C2	0.623	0.399	0.745
C3	0.737	0.514	0.761

Refinement of these atomic positions with those of Sn, reduced the residual to R = 0.07 and gave the following parameters:

	x	y	z
O1	0.6333	0.3446	0.1431
O2	0.4345	0.2597	0.9220
O3	0.3444	0.9820	0.9214
O4	0.7180	0.6025	0.6101
C1	0.5626	0.3275	0.9515
C2	0.6280	0.3917	0.7276
C3	0.7355	0.5124	0.7586

The positions of the hydrogen atoms were not located

as they represent less than 2% of the electron density in the structure.

Final full matrix least-squares refinement of all the positions and of anisotropic temperature factors for all of the atoms, except the hydrogens, gave a final residual of 0.041. The final observed and calculated structure factors are given in Appendix I and the final atomic positions and thermal parameters are listed in Tables 3.(4). and 3.(5). The bond distances and angles obtained using the program appear in Table 3.(6).

Atom	x/a	y/b	z/c
Sn	0.3987 (1)	0.1244 (1)	0.2178 (1)
O1	0.6334 (8)	0.3445 (8)	0.1432 (12)
O2	0.4345 (8)	0.2593 (8)	0.9230 (13)
O3	0.3445 (8)	0.9826 (8)	0.9212 (12)
O4	0.7183 (12)	0.6029 (10)	0.6091 (17)
C1	0.5634 (11)	0.3278 (10)	0.9508 (17)
C2	0.6275 (13)	0.3887 (12)	0.7253 (17)
C3	0.7353 (11)	0.5122 (10)	0.7592 (17)

TABLE 3.(4). Atomic Positions for $SnCH_2C_2O_4$ with the Estimated Standard Deviation in Parenthesis.

Atom	U_{11}	U_{22}	U_{33}	U_{23}	U_{13}	U_{12}
Sn	14.1 (3)	20.8 (4)	10.0 (3)	1.7 (3)	0.0 (2)	-2.1 (3)
O1	12.9 (32)	27.7 (41)	14.5 (32)	2.2 (29)	0.2 (26)	-5.1 (29)
O2	14.8 (33)	23.7 (39)	19.9 (35)	7.4 (30)	-1.3 (27)	-10.4 (30)
O3	13.0 (32)	17.3 (35)	20.2 (35)	-7.0 (29)	-5.7 (26)	2.4 (27)
O4	47.2 (56)	35.7 (53)	39.4 (52)	21.5 (43)	-9.1 (43)	-14.4 (44)
C1	13.6 (43)	11.9 (42)	14.6 (43)	1.0 (35)	4.0 (34)	2.2 (36)
C2	23.5 (51)	27.5 (55)	15.9 (45)	5.4 (43)	9.2 (39)	-10.4 (46)
C3	10.8 (41)	15.2 (44)	15.6 (43)	3.9 (36)	1.0 (34)	-1.4 (35)

TABLE 3.(5). Anisotropic Temperature Factors ($U_{ij} \times 10^{-3}$) for $SnCH_2C_2O_4$ with Estimated Standard Deviations in Parenthesis.

TABLE 3.(6). Bond Distances (Å) and Angles (°) in $SnCH_2C_2O_4$ with the Estimated Standard Deviations in Parenthesis.

Coordination to Tin:		
Sn - O(1)	2.949	(7)
Sn - O(1A)	2.261	(7)
Sn - O(2)	2.182	(7)
Sn - O(3)	2.228	(7)
Sn - O(3A)	2.556	(7)
Sn - O(4)	3.011	(7)
O(1A) - Sn - O(2)	86.8	(3)
O(1A) - Sn - O(3)	77.1	(3)
O(2) - Sn - O(3)	78.3	(3)
Coordination in Malonate Group:		
C(1) - O(1)	1.242	(12)
C(1) - O(2)	1.270	(12)
C(3) - O(3)	1.276	(12)
C(3) - O(4)	1.239	(13)
C(2) - C(1)	1.554	(13)
C(3) - C(2)	1.506	(14)
C(1) - O(2) - Sn	111.3	(6)
C(3) - O(3) - Sn	130.6	(9)
O(2) - C(1) - O(1)	122.7	(9)
C(2) - C(1) - O(1)	122.4	(9)
C(2) - C(1) - O(2)	114.9	(9)
C(3) - C(2) - C(1)	115.0	(9)
C(2) - C(3) - O(4)	115.2	(9)

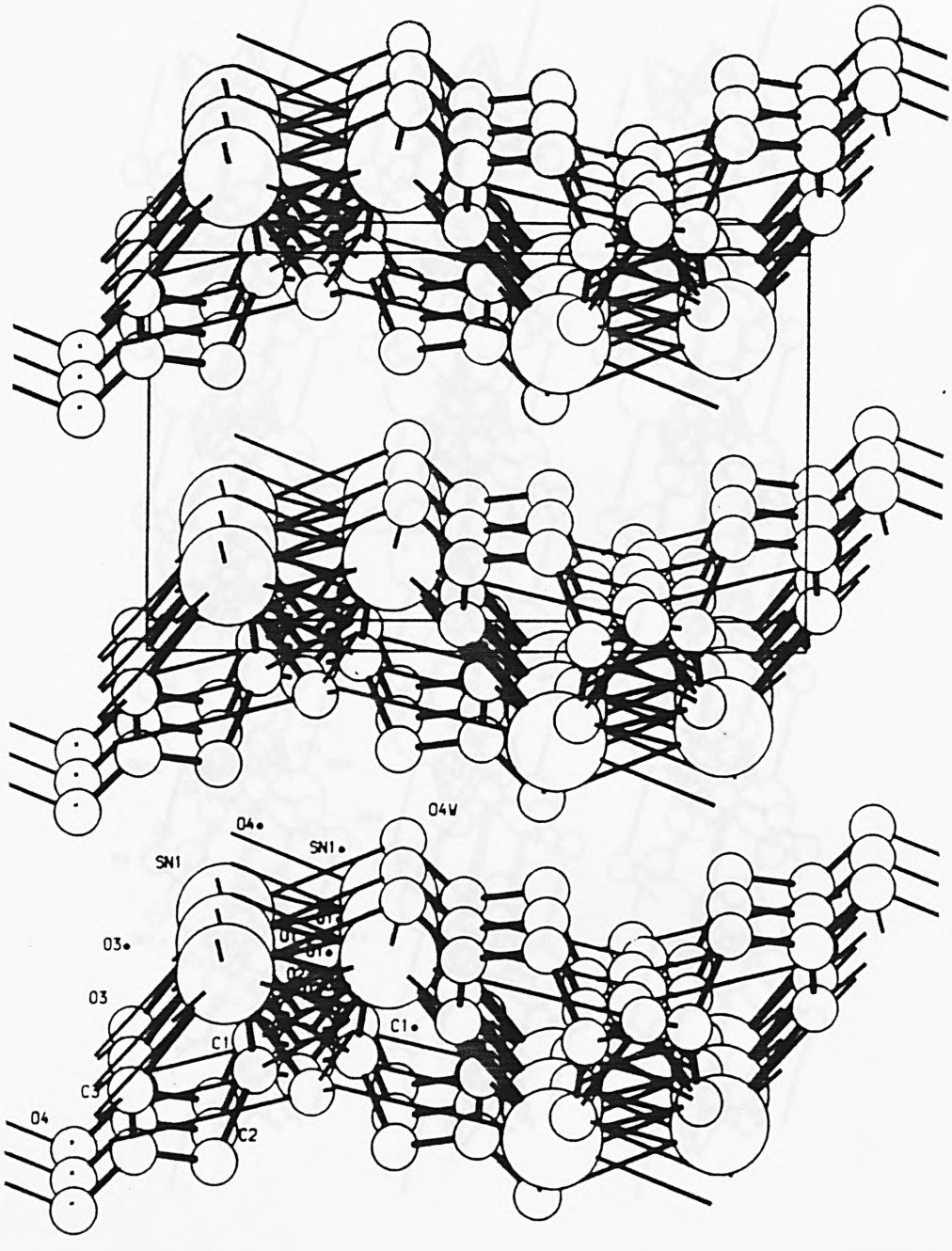

FIGURE 3.(8). Projection of the Unit Cell of Stannous Malonate Viewed Along the X-Axis.

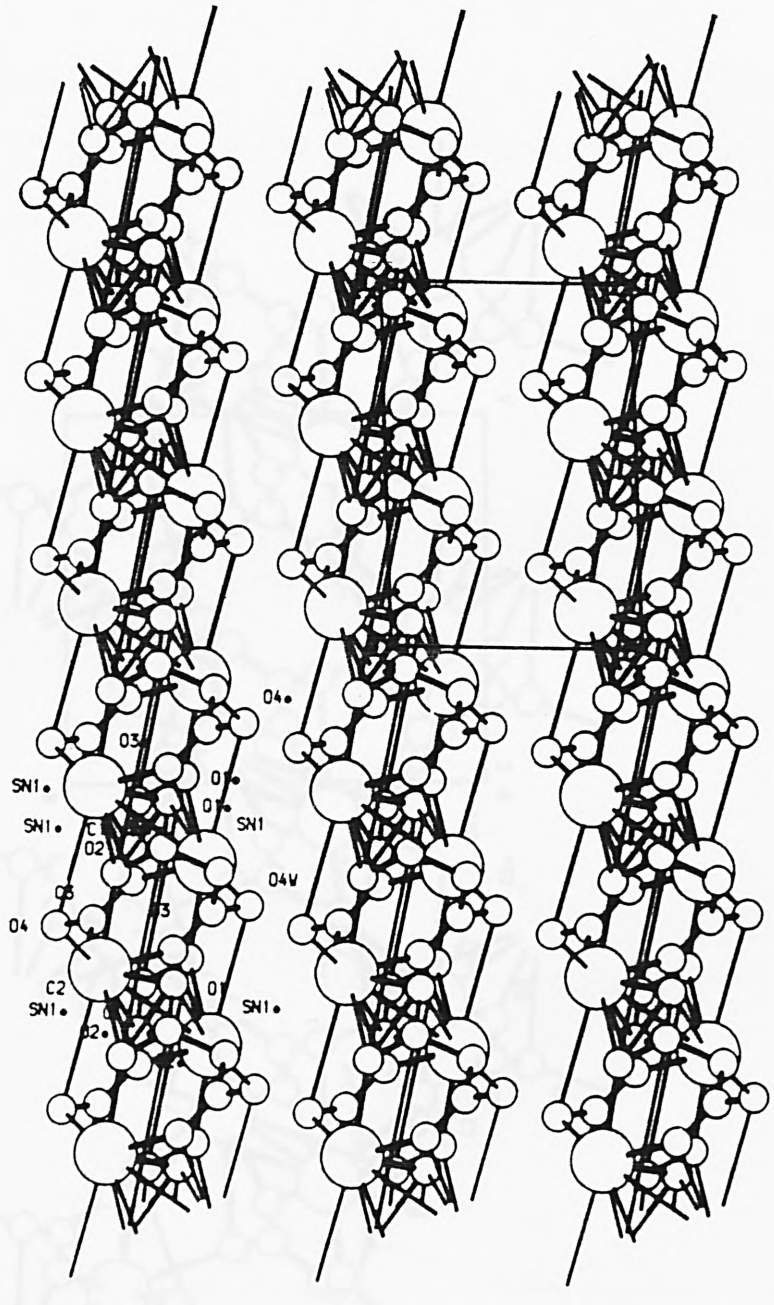

FIGURE 3.(9). Projection of the Unit Cell of Stannous Malonate Viewed Along the Y-Axis.

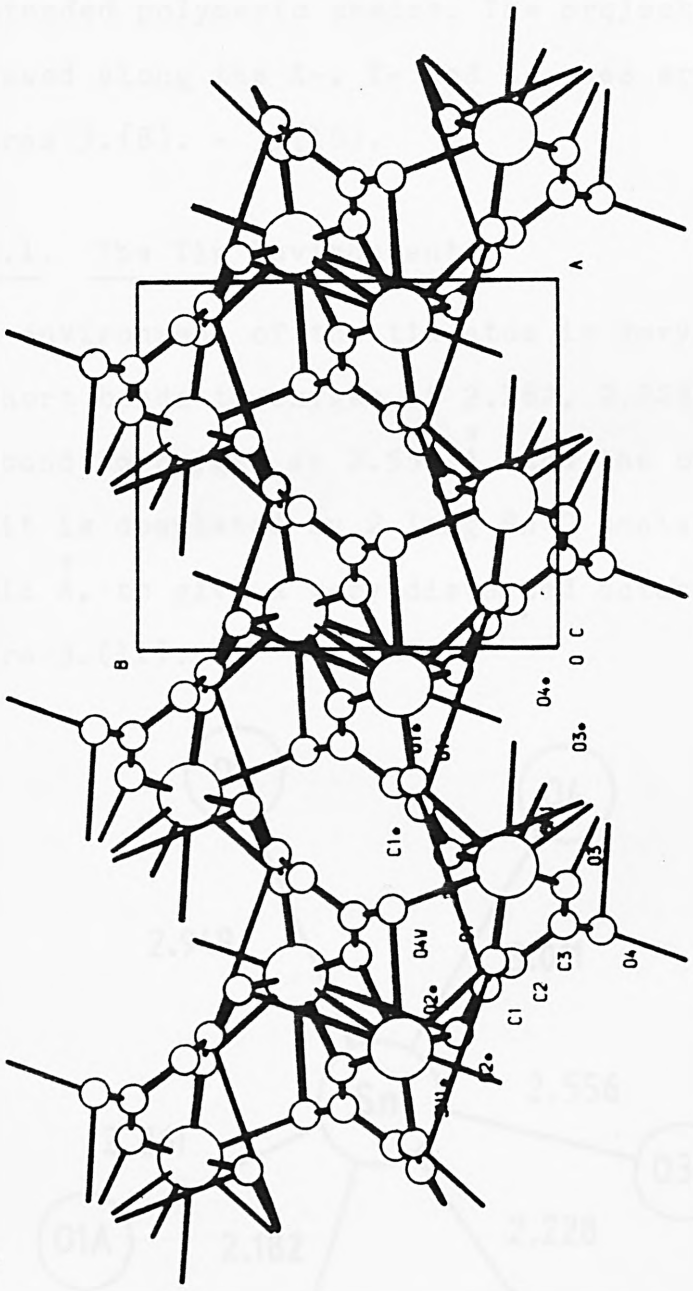

FIGURE 3.(10). Projection of the Unit Cell of Stannous Malonate Viewed Along the Z-Axis.

3.4.(5). Structural Description and Discussion.

The structure of tin(II) malonate consists of a layer network in which each malonate group is bonded to two different tin(II) atoms via two of its oxygen atoms, to form extended polymeric chains. The projections of the unit cell viewed along the X-, Y- and Z- axes are illustrated in Figures 3.(8). - 3.(10).

3.4.(5).1. The Tin Environment.

The environment of the tin atom is very unusual, it has three short bonds to oxygen at 2.182, 2.228 and 2.261 Å, a longer bond to oxygen at 2.556 Å and the coordination around it is completed by 2 long Sn-O contacts at 2.949 and 3.011 Å, to give a very distorted octahedron, as shown in Figure 3.(11).

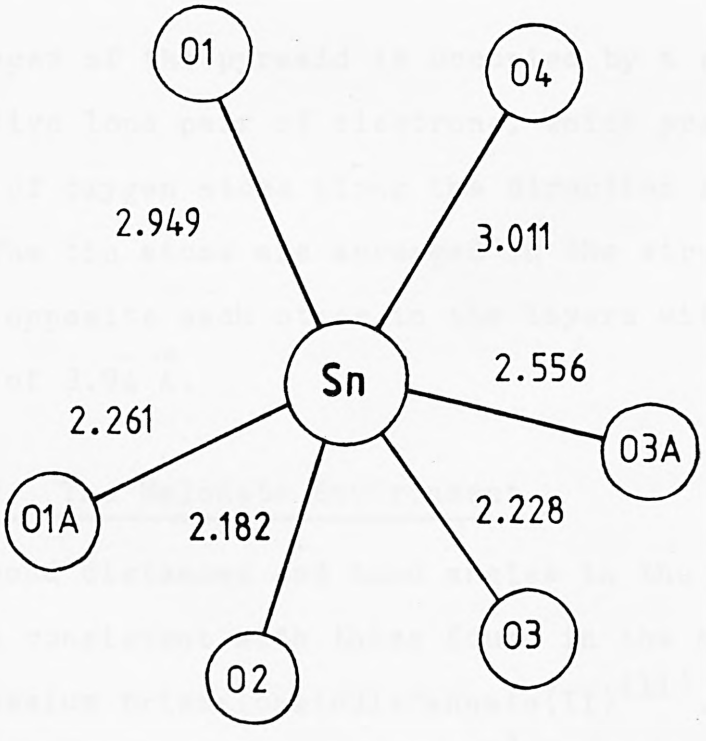

FIGURE 3.(11). The Tin Environment in Stannous Malonate.

The Sn-O bond at 2.556 Å however, is between that

accepted for a true Sn-O bond and a Sn-O contact. Therefore, it is not possible to describe the tin environment as being purely trigonal pyramidal or square pyramidal, the structure is intermediate between the two (c.f. $SnSO_4$.2 thiourea which has a tin environment intermediate between distorted trigonal and square pyramidal[14]). The arrangement of the oxygen atoms about the tin is illustrated in Figure 3.(12).

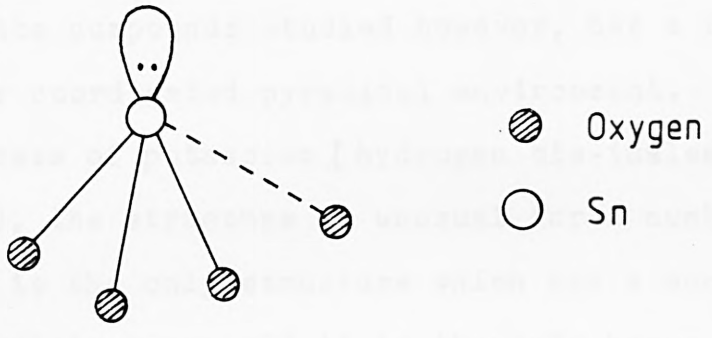

FIGURE 3.(12). Arrangement of Sn-O Bonds in Stannous Malonate.

The apex of the pyramid is occupied by a stereochemically active lone pair of electrons, which prevent the close approach of oxygen atoms along the direction in which it points. The tin atoms are arranged in the structure so that they are opposite each other in the layers with Sn-Sn contacts of 3.94 Å.

3.4.(5).2. The Malonate Environment.

The bond distances and bond angles in the malonate group are consistent with those found in the malonate ion in dipotassium trismalonatodistannate(II)[11]. The C-O bond distances are 1.270 and 1.276 Å when the oxygens are bonded to tin and are 1.242 and 1.239 Å for the uncoordinated oxygens.

3.5. SUMMARY - THE CRYSTAL STRUCTURES OF TIN(II) CARBOXYLATES AND THEIR COMPLEX DERIVATIVES.

In this work, the crystal structures of two materials were studied. It had been expected from the literature review[11-20] that the tin(II) compounds with dicarboxylate acid groups would be in distorted four coordinated environments arising from chelating or bridging carboxylates. Neither of the compounds studied however, has a clearly defined four coordinated pyramidal environment.

In the case of potassium [hydrogen bis-(maleato)]-stannate(II), the structure is unusual for a number of reasons: it is the only structure which has a monoprotonated carboxylate group and it is the only known complex tin(II) carboxylate where the ratio of Sn:K ions is 1:1. The similarity in the structure of the maleate and malonate ligands, enables comparisons to be drawn between this structure and the one solved by Arifin[11], for dipotassium trismalonatodistannate(II) monohydrate. Both these complexes have the unusual features listed below:

(a) Distannate ring systems with the coordination about tin completed by a third ligand group, and

(b) A distorted trigonal pyramidal environment about the tin. Maleate and malonate ligands are dicarboxylic acid derivatives and therefore, a four-pyramidal arrangement is expected.

Arifin attributed the trigonal pyramidal environment around the tin in the malonate complex to the polymeric nature of the $Sn(CH_2C_2O_4)_3^{2n-}_n$ anions. In the maleate complex, the $[Sn(CHCOO{:}CHCOO)(CHCOO{:}CHCOOH)]^-$ anionic units obtained, are discrete and unlike the malonate structure,

this type of chelating is unable to extend. There are three short Sn-O bond distances of 2.199, 2.199 and 2.212 Å, as none of the other oxygen atoms is close enough to the tin to form a bond, a trigonal pyramidal environment about the tin is obtained. This is the preferred arrangement for most tin compounds. The apparent polymeric nature of the structure arises from hydrogen bonding.

In the case of tin(II) malonate, an environment in between that of three and four coordination is obtained. The structure consists of three short Sn-O bonds (2.182, 2.228 and 2.261 Å) and a fourth Sn-O bond distance at 2.556 Å which is neither short enough to be typical of the longer four-pyramidal nearest neighbour Sn-O bonds, nor far enough away from the tin to be regarded as totally non-bonding. This gives a trigonal pyramidal arrangement. Evidence for this type of structure has been provided by Nicholson[14] who used this arrangement to explain the structure of $SnSO_4$.2 thiourea.

REFERENCES.

1. M.J. Beurger, "Crystal Structure Analysis", (1969), Wiley, New York. p. 231.
2. "International Tables for X-ray Crystallography", (1962), Kynoch Press, Birmingham.
3. G.H. Stout and L.H. Jensen, "X-ray Structure Determination", (1968), Macmillan, London.
4. A.L. Patterson, Phys. Rev., (1934), 46, 372; Z. Krist., (1935), 90, 517.
5. H. Lipson and W. Cochran, "The Crystalline State", vol.3, (1966), Bell.
6. G.M. Sheldrick, "Program for Crystal Structure Determination", (1975), University of Cambridge.
7. J.D. Donaldson and D.C. Puxley, Chem. Commun., (1972), 289.
8. "The X-ray System Version of June 1972", Technical Report TR-192 of the Computer Science Centre, University of Maryland, U.S.A.
9. W.S.D. Motherwell, "PLUTO: Plotting Molecular and Crystal Structures", (1979), University of Cambridge.
10. J.C. Dewan, J. Silver, J.A. Andrew, J.D. Donaldson and D.R. Laughlin, J. Chem. Soc., Dalton Trans., (1977), 368.
11. Z. Arifin, Ph.D. Thesis, (1981), University of London.
12. S.J. Clark, J.D. Donaldson, J.C. Dewan and J. Silver, Acta Cryst. B, (1979), B35, 2550.
13. J.D. Donaldson, M.J. Donaghue and C.H. Smith, Acta Cryst. B, (1976), B32, 2098.
14. D. Nicholson, Ph.D. Thesis, (1972), University of London.
15. A. Jelen and O. Lindqvist, Acta Chem. Scand., (1969), 23, 3071.
16. J.C. Dewan, J. Silver, J.D. Donaldson and M.J.K. Thomas, J. Chem. Soc., Dalton Trans., (1977), 2319.

17. J.C. Dewan, J. Silver and J.D. Donaldson, Unpublished Work.

18. P.G. Harrison and E.W. Thornton, J. Chem. Soc., Dalton Trans., (1978), 1274.

19. A.D. Christie, R.A. Howie and W. Moser, Inorg. Chim. Acta Letts., (1976), 36, L447.

20. J.C. Dewan, J. Silver, J.D. Donaldson and R.M.A. Grimsey, Unpublished Work.

CHAPTER FOUR

POLYMERISATION STUDIES

CHAPTER FOUR

POLYMERISATION STUDIES

4.1. INTRODUCTION.

4.1.(1). Polymerisation Reactions.

Polymerisation reactions can be classified into two groups known as (i) addition and (ii) condensation polymerisations. In general, addition polymerisation involves a chain reaction, with a very fast reaction rate, in which the chain propagator can be either a free radical or an ion. In condensation polymerisation, a reaction occurs between two polyfunctional molecules to give one longer polyfunctional molecule, accompanied by the elimination of a small molecule such as water. An example is provided by the reaction between ethylene glycol and terephthalic acid, as shown below:

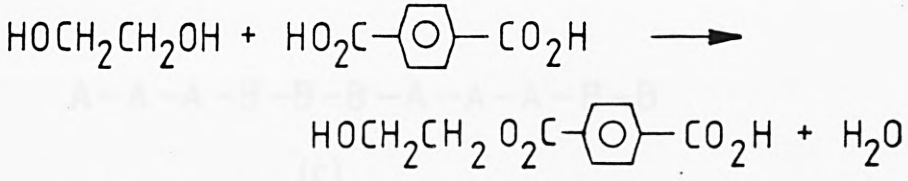

Further reaction can occur until one of the reactants is used up, thus producing a linear polymer. Branched and cross-linked polymers can be formed in both types of polymerisation however, using more complex monomeric units.

The term copolymer refers to a polymer made by polymerising two or more suitable monomers together. Four different types of copolymer exist, depending upon the arrangement of the monomeric units within the polymer structure:

(a) Random copolymer - the different repeating units are distributed randomly throughout the polymer chain,

(b) Alternating copolymer - the different units are alternated within the polymer chain,

(c) Block copolymer - blocks of one repeating unit alternate with blocks of another type,

(d) Graft copolymer - blocks of one type of repeating unit are attached (grafted) onto the backbone of a linear polymer containing another type of repeating unit.

The different types of copolymer are illustrated diagrammatically in Figure 4.(1). below.

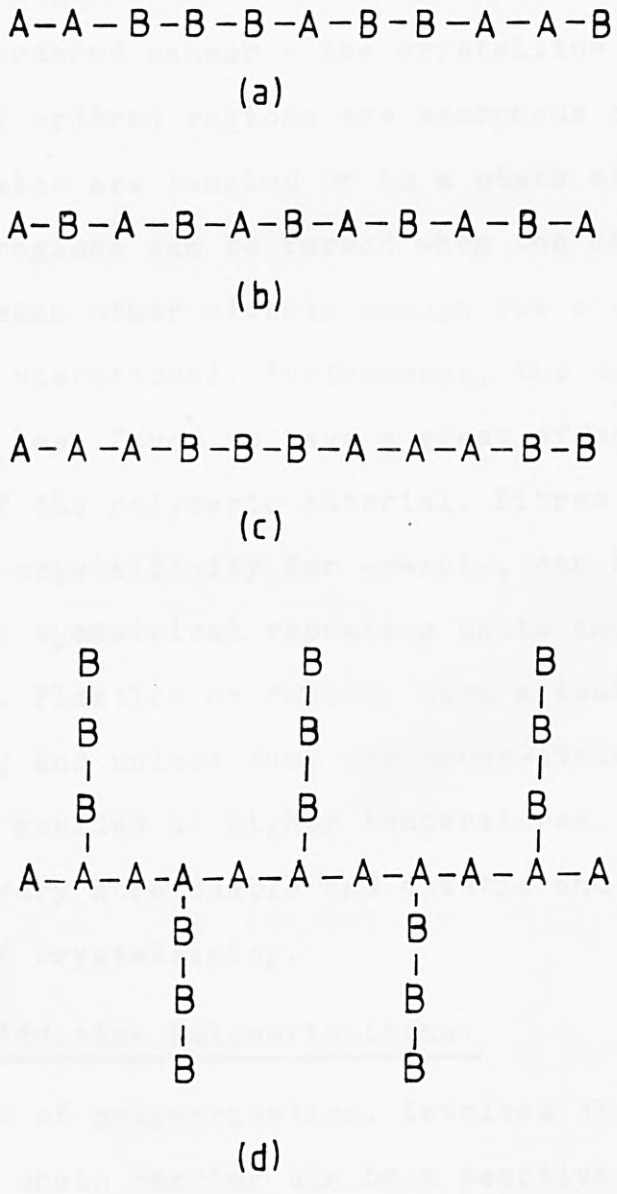

FIGURE 4.(1). Diagrammatic Representation of (a) Random, (b) Alternating, (c) Block and (d) Graft Copolymers, Where A and B Represent the Different Monomeric Repeating Units.

Chain growth during polymerisation is governed by random events, therefore, polymer chains within the same polymeric material will have different lengths and hence different relative molecular masses. As a consequence of this, any experimental determination of the molecular weight of a polymer, will only give an average value.

X-ray studies have shown that within a bulk polymer, there may be regions in which the polymer chains are arranged in a highly ordered manner - the crystalline areas, and between these ordered regions are amorphous sections, in which the chains are tangled or in a state of disorder. The crystalline regions can be formed when the chains are able to approach each other closely enough for strong interchain forces to be operational. Furthermore, the degree of crystallinity has been found to have a great effect upon the properties of the polymeric material. Fibres of high tensile strength and crystallinity for example, can be formed from polymers with symmetrical repeating units and high interchain forces. Plastics or resins, have a smaller degree of crystallinity and unless they are cross-linked, may be softened and moulded at higher temperatures. Elastomers, or rubbers are very stretchable and elastic and have a very low degree of crystallinity.

4.1.(1).1. Addition Polymerisations.

This type of polymerisation, involves chain reactions, in which the chain carrier can be a reactive species which contains either a free radical or an ion. Each chain reaction has three distinct processes:

(a) Initiation (b) Chain propagation (c) Termination

(i) Free Radical Polymerisation.

This is the most common type of addition polymerisation. Initiation involves the decomposition of the initiator by thermal or photochemical means, followed by the addition of a monomer molecule to one of the resulting radicals. If R$^{\cdot}$ represents the free radical formed from the initiator I and the monomer is CH_2=CHX, then the initiation process can be represented by stages (1) and (2) below:

$$(1)\quad I \longrightarrow 2R^{\cdot}$$

$$(2)\quad R^{\cdot} + CH_2{=}CHX \longrightarrow R{-}CH_2{-}\dot{C}HX$$

Propagation, is the subsequent further addition of monomeric units to the free radical complex, as in step (3):

$$(3)\quad R{-}CH_2{-}\dot{C}HX + CH_2{=}CHX \longrightarrow R{-}CH_2{-}CHX{-}CH_2{-}\dot{C}HX$$

and so on to form high molecular weight polymers. Termination can then occur either by a combination process as in step (4),

$$(4)\quad \sim CH_2{-}\dot{C}HX + \dot{C}HX{-}CH_2 \sim \longrightarrow \sim CH_2{-}CHX{-}CHX{-}CH_2 \sim$$

or by a disproportionation process as in step (5), in which

$$(5)\quad \sim CH_2{-}\dot{C}HX + \dot{C}HX{-}CH_2 \sim \longrightarrow \sim CH_2{-}CH_2X + CHX{=}CH \sim$$

the transfer of a hydrogen atom from one radical to another, produces two inactive polymer molecules.

Usually the propagation and termination steps are very

fast, but the rate and degree of polymerisation can be controlled by the use of retarders and inhibitors, which react with the radicals as soon as they are produced. With the inhibitors, polymerisation cannot proceed until all of the inhibitor has been used up, but once this has occurred, the rate of polymerisation approaches that of the normal uninhibited process. The retarders are less reactive than the inhibitors and compete with the monomer for the radical species, thus reducing the rate and degree of polymerisation.

(ii) Cationic Polymerisation.

In this type of polymerisation, the chain carriers are carbonium ions (C^+ ions). Typical catalysts are Lewis acids (electron pair acceptors) and Friedel-Crafts catalysts - such as $AlCl_3$, $AlBr_3$, BF_3, $TiCl_4$, $SnCl_4$, H_2SO_4 and other strong acids. Unlike free radical polymerisations, which generally occur at elevated temperatures, cationic polymerisations proceed best at low temperatures. Furthermore, the nature of the solvent is important as well. Since the ionic mechanisms involve charged species, their stability is influenced by solvent polarity, whereas the free radical polymerisations usually involve neutral radical species.

Acid catalysed polymerisations can be represented by the following scheme:

Initiation -

$$HA + CH_2{=}CHX \longrightarrow CH_3{-}C^{\oplus}\begin{matrix}H\\X\end{matrix} + A^{\ominus}$$

Propagation -

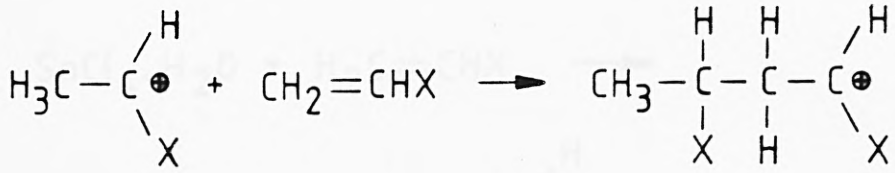

which is repeated to produce the polymer chain.

Termination - this can occur in three ways:

(1) combination of the carbonium ion and the associated anion,

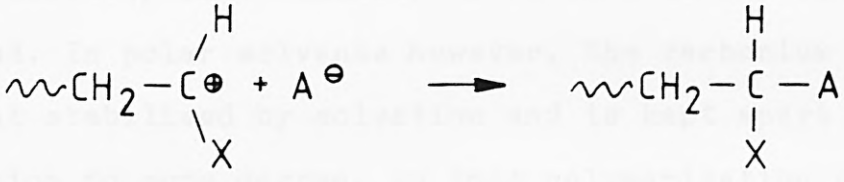

(2) rearrangement of the ion pair to give unsaturation in the polymer and regenerate the original acid or complex,

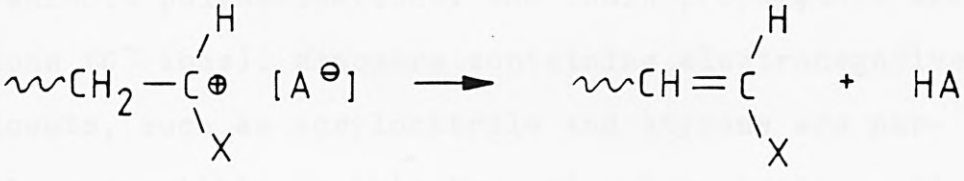

(3) termination via chain transfer to the monomer,

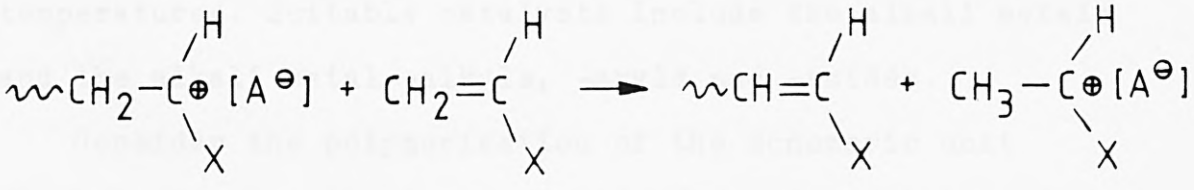

Proton transfer in the initiation stage cannot occur in the case of the Friedel-Crafts catalysts, since they contain no hydrogen atoms and for this reason, it is necessary to have a cocatalyst, usually water, present before the polymerisation can proceed.

Solvent effects in this type of polymerisation are very marked. In non-polar solvents, the carbonium ion can react

$$SnCl_4 + H_2O \longrightarrow SnCl_4.H_2O$$

$$SnCl_4.H_2O + H_2C{=}CHX \longrightarrow$$

$$H_3C{-}\overset{\displaystyle H}{\underset{\displaystyle X}{C^{\oplus}}} + [SnCl_4OH]^{\ominus}$$

with its counter ion, giving a reaction similar to that of normal electrophilic addition of HA to a double bonded compound. In polar solvents however, the carbonium ion is somewhat stabilised by solvation and is kept apart from the counterion to some degree, so that polymerisation can occur in the normal way.

(iii) Anionic Polymerisation.

In anionic polymerisations, the chain propagators are carbanions (C^- ions). Monomers containing electronegative substituents, such as acrylonitrile and styrene are particularly susceptible to this type of polymerisation. Like cationic polymerisations, the reactions proceed at low temperatures. Suitable catalysts include the alkali metals and the alkali metal -alkyls, -aryls and -amides.

Consider the polymerisation of the monomeric unit $CH_2{=}CHX$, by the alkali metal amide KNH_2. In certain solvents the potassium amide is strongly ionised and the initiation process can be represented by the equation below:

$$H_2N^{\ominus} + H_2C{=}\overset{\displaystyle H}{\underset{\displaystyle X}{C}} \longrightarrow H_2N{-}\overset{\displaystyle H}{\underset{\displaystyle H}{C}}{-}\overset{\displaystyle H}{\underset{\displaystyle X}{C}}{:}^{\ominus}$$

Propagation then occurs by the addition of further monomer molecules to the carbanion, as shown,

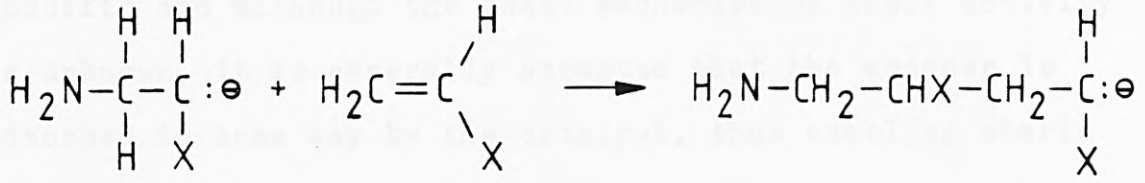

In this type of polymerisation, provided that inert solvents and pure reactants are used, the polymerisation should stop when all the available monomeric units have been used up. Even then, the carbanions are not destroyed and if more monomer were added, the polymerisation would recommence. These polymers are known as 'living' polymers. If however, traces of impurities, such as water, carbon dioxide, alcohols and other materials are present, then termination will occur as indicated below.

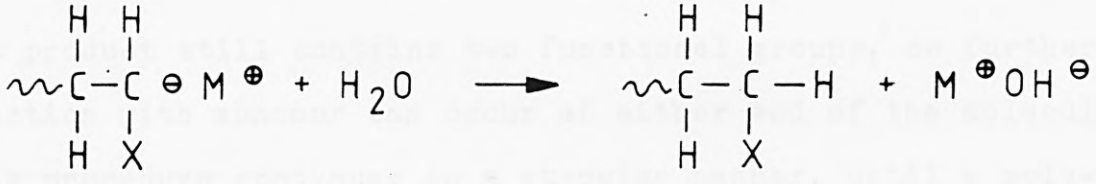

Another important type of catalyst is the Ziegler-Natta catalyst. These are mixed catalyst systems, using an alkyl or aryl compound of a group I-III element and a halide of a transition metal. For example, an n-hexane solution of triethylaluminium, $Al(C_2H_5)_3$, with titanium tetrachloride, $TiCl_4$, produces a brown-black precipitate which catalyses the polymerisation of ethene at low temperatures. Prior to the use of this catalyst, polyethylene was produced using free radicals at pressures between 1000 and 3000 atmospheres and at temperatures up to 250°C. The free radical method resulted in a branched polymer, whereas the use of Ziegler-

Natta catalysts gave essentially linear polymers. Polymerisation reactions using Ziegler-Natta catalysts are stereospecific and although the exact mechanism of their activity is unknown, it is generally accepted that the monomer is adsorbed in some way by the catalyst, thus enabling steric control of the propagation stages of the polymerisation.

4.1.(1).2. Condensation Polymerisations.

Condensation polymerisation involves the reaction between two polyfunctional molecules, to form a larger polyfunctional molecule with the elimination of water or another small molecule. For example, in the reaction of terephthalic acid with ethylene glycol,

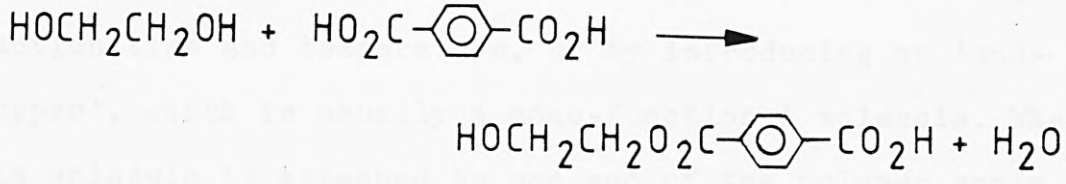

The product still contains two functional groups, so further reaction with monomer can occur at either end of the molecule. This procedure continues in a stepwise manner, until a polymer is produced, whose molecular weight increases steadily during the reaction, therefore reaction times are long if high molecular weight polymers are required. If the small molecule is removed as it is eliminated, this will help to promote the polymerisation, as it will reduce the possibility of unfavourable side reactions.

If the monomer contains three functional groups, then the formation of branched structures is likely. As the reaction continues and the size of the branched molecules increases, there is an increased probability that condensation can occur in such a way as to link one polymer chain to another - this process is known as cross-linking.

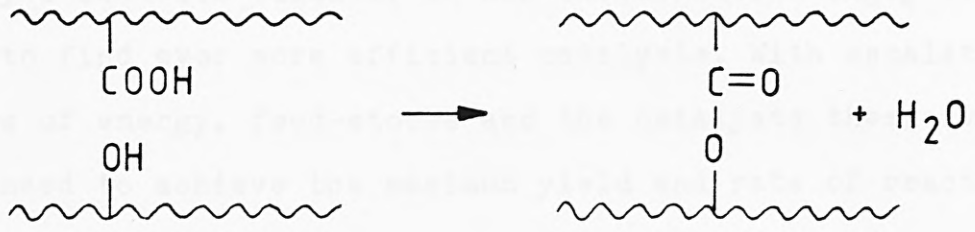

Cross-linking affects the properties of the polymer, generally, they become stronger materials and are far more resistant to chemical and mechanical forces.

In theory, as condensation polymerisation does not have a terminating stage, the reaction can continue until one or other of the functional groups are depleted. In practise though, the polymerisation can be stopped by controlling the reaction time and temperature, or by introducing an 'end-stopper', which is usually a mono-functional molecule. When this molecule is attached to one end of the polymer chain, no further reaction can occur.

4.1.(1).3. Copolymerisation.

A vast range of polymers can be prepared by polymerising an appropriate mixture of monomers; examples include vinyl chloride - vinyl acetate and phenylethene - buta-1,3-diene copolymers. Depending upon the monomers used, the polymerisations will be of the addition or condensation types and will be controlled by the conditions imposed by these types of polymerisation.

4.1.(2). Scope of the Work.

The role of catalysts in enhancing chemical reactions has long been established, often they cause specificity in a reaction, thus limiting unwanted side-products, or they

can increase the rate of otherwise very slow reactions. In today's economic climate, it has become increasingly important to find ever more efficient catalysts. With escalating costs of energy, feed-stocks and the catalysts themselves, the need to achieve the maximum yield and rate of reaction is paramount.

A review of the literature (Chapter 1. Section 1.(2).), reveals that tin(II) carboxylates have been widely tested as polymerisation catalysts. In spite of this however, very little information has been presented in the literature on the mode of action of the tin moiety and its fate during the polymerisation reactions. The main aims of this work therefore, were to study the reactions of tin(II) carboxylates and tin(II) halides with various monomers and to compare their efficiencies with known catalysts for the systems.

Throughout the course of this work, three polymer systems have been investigated:

(1) the polymerisation of propylene oxide, which will be shown to have an anionic or a cationic mechanism, depending upon the catalyst used,

(2) the polymerisation of trioxane using a cationic mechanism to give a polyether,

(3) the room temperature curing of a commercially available silicone resin.

The polymers obtained were characterised by differential thermal analysis, infrared, NMR and Mössbauer spectroscopy and their molecular weights determined by viscometry. The study of the silicone resin was limited to an investigation of the reaction times required to cause a hard cure of the resin, when using a vast range of catalysts and solvents and to determine the effect of temperature, catalyst con-

centration and solvent concentration upon the cure times.

The analytical techniques used to characterise the polymers are described in Chapter 1. Section 1.(3). The determination of the molecular weights of the polymers obtained, is discussed below.

4.1.(3). Determination of Polymeric Molecular Weight by Viscometry.

Solution viscosity is basically a measure of the size or extension in space of polymer molecules. It is empirically related to molecular weight for the linear polymer molecules. The ease of measurement and the usefulness of the viscosity molecular weight correlation are so great, that viscosity measurements prove to be an extremely valuable tool for the molecular weight characterisation of polymers.

As a result of the random nature of the processes involved in the polymerisations, polymers in their purest form, even when synthesised from rigorously purified monomers have a range of molecular weights. Therefore, the polymer sample cannot be characterised by a single molecular weight determination and viscosity measurements simply give the average molecular weight of the polymer.

In dilute solutions, the following viscosity related quantities are found to apply:

(1) Relative viscosity, η_{rel},

defined as the ratio of the solution flow time (t) to the flow time of the pure solvent (t_o)

$$\eta_{rel} = \frac{t}{t_o}$$

(2) Specific viscosity, η_{sp},

defined as the relative increment in viscosity of

the solution over the viscosity of the solvent.

$$\eta_{sp} = \frac{\eta - \eta_o}{\eta_o}$$

$$= \eta_{rel} - 1$$

(3) Reduced specific viscosity, η_{red},

this is the specific viscosity expressed in terms of per unit concentration (c).

$$\eta_{red} = \frac{\eta_{sp}}{c}$$

$$= \frac{\eta_{rel} - 1}{c}$$

(4) Inherent viscosity, η_{inh},

defined as

$$\eta_{inh} = \frac{\ln(\eta_{rel})}{c}$$

The intrinsic viscosity, $[\eta]$, is the inherent viscosity extrapolated to zero.

$$[\eta] = \lim_{c \to o} \eta_{inh}$$

In practise, the intrinsic viscosity is obtained by measuring the relative viscosity, η_{rel}, at several concentrations. These sample concentrations should not be too high because of additional effects which may arise from intermolecular forces and chain entanglement. If the inherent viscosity is plotted against the concentration (g/100ml), then the intrinsic viscosity is given by the viscosity at zero concentration, as shown in Figure 4.(2).

The average molecular weight M, of the polymer is given by the Mark-Houwick-Sakurada equation:

$$[\eta] = kM^a$$

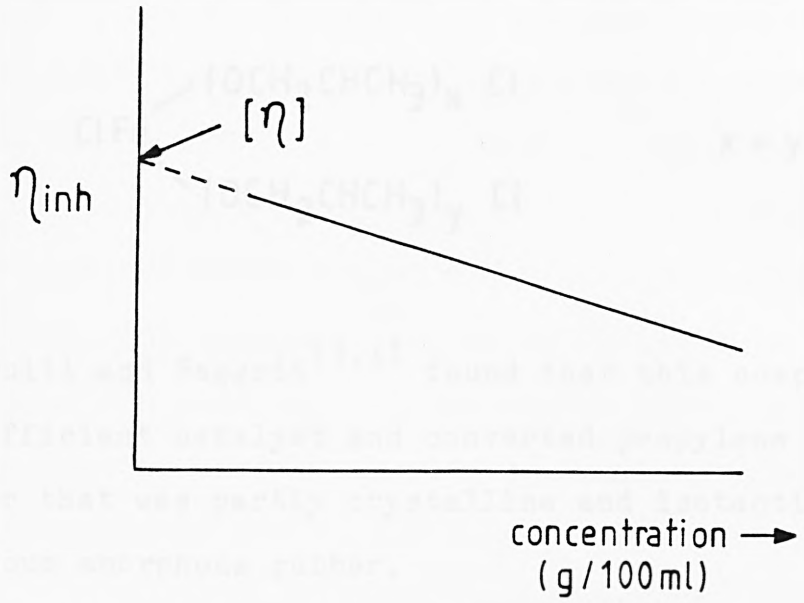

FIGURE 4.(2). Plot of Inherent Viscosity Against Concentration, Extrapolated Back to Zero, to Show the Intrinsic Viscosity, [η].

where k and a are constants for a given temperature in a given solvent. Extensive tables of k and a constants are available in the literature.

4.2. THE POLYMERISATION OF PROPYLENE OXIDE.

4.2.(1). Introduction.

Propylene oxide is an epoxide which forms a polyether on polymerisation. The first reports of its 'polymerisation' appeared in 1927[1], when Levene and Walti found that an acid catalyst produced a cyclic dimer, whereas treatment with a base, resulted in larger molecules, such as tetramers. Molecular weights of 2000 were obtained by Fife and Roberts[2], from the treatment of the monomer with sodium hydroxide or alkoxide, in the presence of alcohols at temperatures of 100 - 200°C and at high pressures. In 1955, Pruitt and Baggett[3,4], developed a ferric chloride - propylene oxide complex catalyst which acts as a Lewis acid and to which Colclough[5] assigned the following structure:

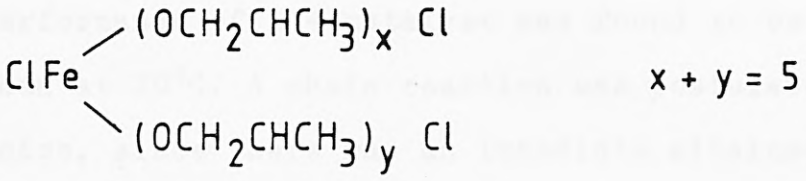

Pruitt and Baggett[3,4] found that this complex was a very efficient catalyst and converted propylene oxide to a polymer that was partly crystalline and isotactic and partly a viscous amorphous rubber.

Extensive work on the polymerisation of propylene oxide was carried out by Price and his co-workers, when using powdered potassium hydroxide as catalyst at room temperature and atmospheric pressure[6,7]. They obtained 33% polymeris-

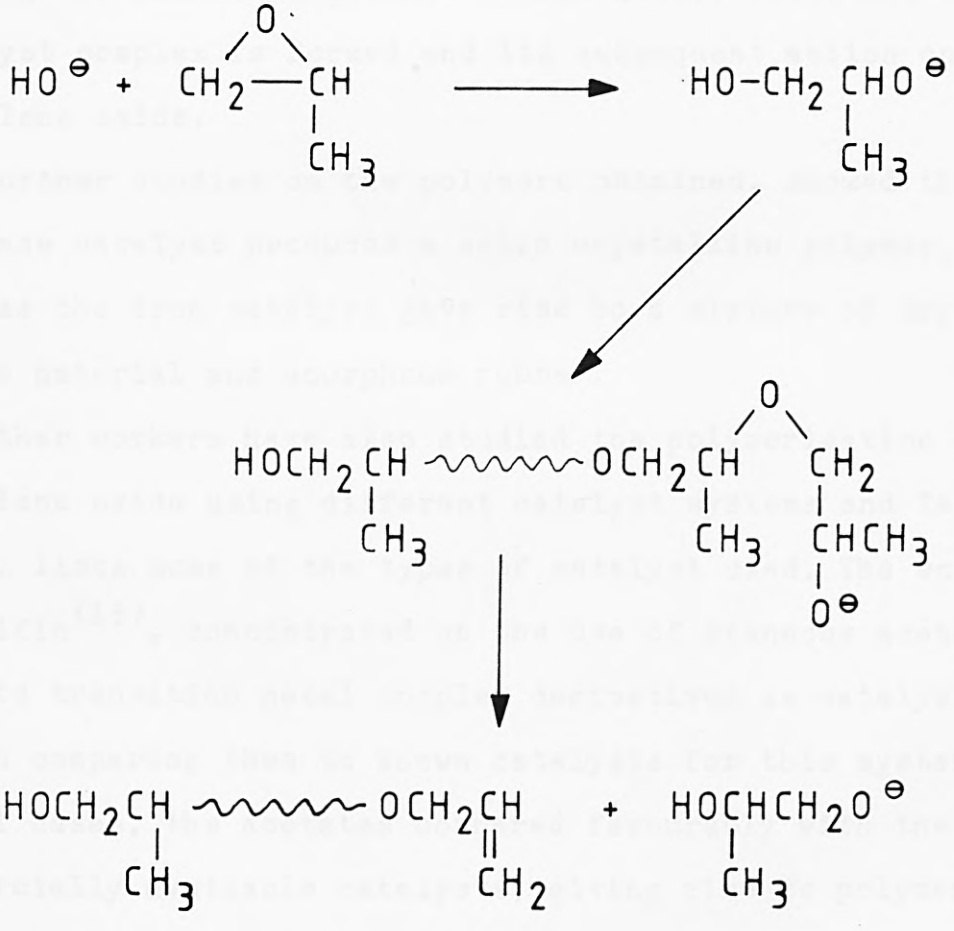

SCHEME 4.(1). Mechanism for the Basic Polymerisation of Propylene Oxide.

ation in 51 hours. The yield of polymer increased with time and the performance of the catalyst was found to be better at 33°C than at 20°C. A chain reaction was postulated for the mechanism, since there was an immediate attainment of a fairly high molecular weight and a relatively small increase thereafter. The suggested mechanism is shown in Scheme 4.(1).

Price[7,8] also studied the acidic catalysis of propylene oxide using the ferric chloride - propylene oxide complex first prepared by Pruitt and Baggett. This catalyst increased both the yield of the polymerisation and the average molecular weight of the polymer produced. In this case, a co-ordinate propagation mechanism was proposed, in which the metal acts as a Lewis acid and coordinates with the oxygen atom on the monomer molecule. Scheme 4.(2). shows how the catalyst complex is formed and its subsequent action on the propylene oxide.

Further studies on the polymers obtained, showed that the base catalyst produced a solid crystalline polymer, whereas the iron catalyst gave rise to a mixture of crystalline material and amorphous rubber.

Other workers have also studied the polymerisation of propylene oxide using different catalyst systems and Table 4.(1). lists some of the types of catalyst used. The work of Arifin[15], concentrated on the use of stannous acetate and its transition metal complex derivatives as catalysts and on comparing them to known catalysts for this system. In all cases, the acetates compared favourably with the commercially available catalysts, giving rise to polymers of similar properties and molecular weights. It was found that the polymerisations were affected by temperature, the catalyst concentration and reaction time, with the optimum

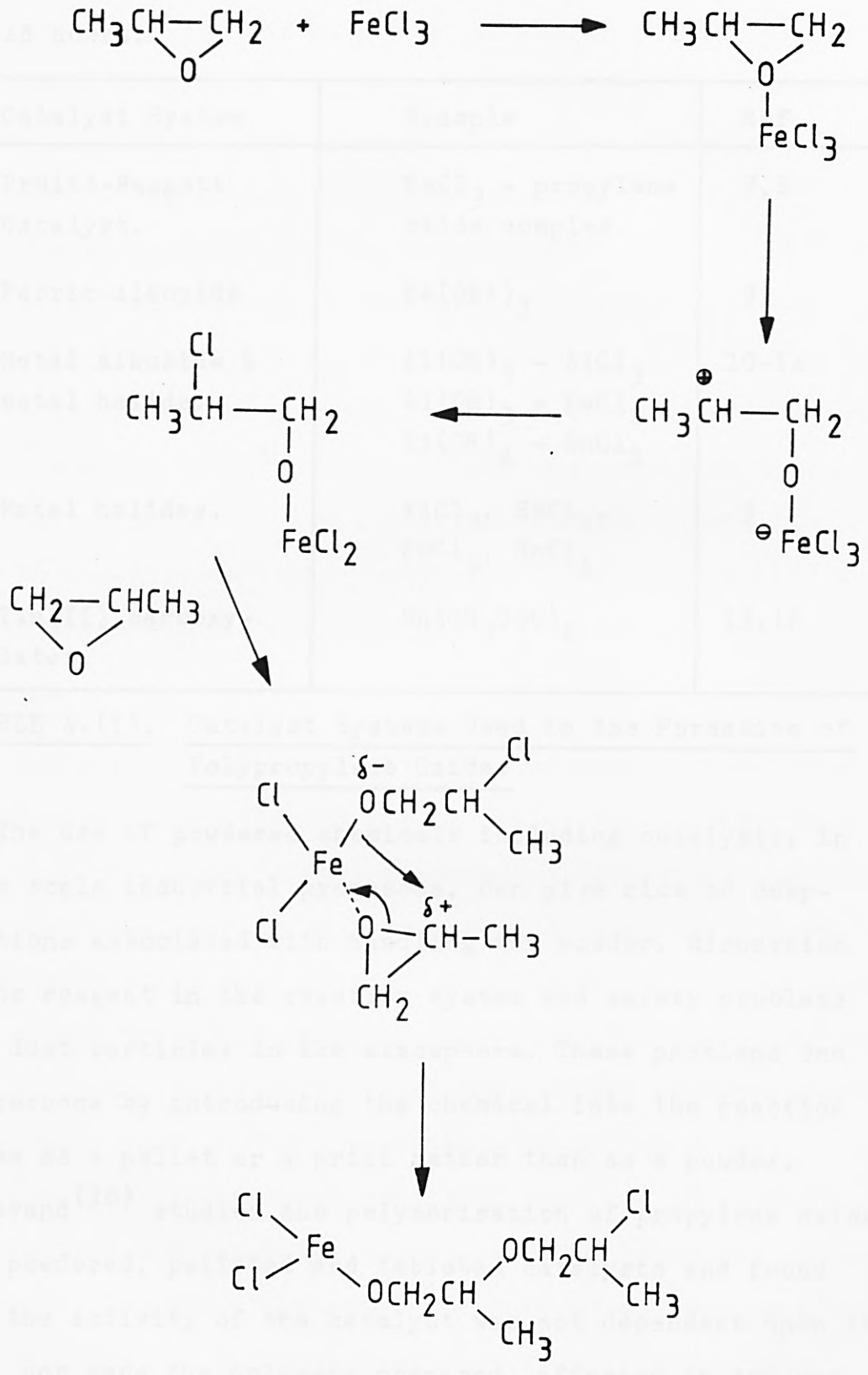

SCHEME 4.(2). Mechanism for the Acidic Polymerisation of Propylene Oxide.

conditions consisting of the use of 1 wt.% catalyst, at 100°C for 48 hours.

Catalyst System	Example	Ref
Pruitt-Baggett Catalyst.	$FeCl_3$ - propylene oxide complex.	7,8
Ferric alkoxide	$Fe(OEt)_3$	9
Metal alkoxide & metal halide.	$Al(OR)_3$ - $AlCl_3$ $Al(OR)_3$ - $FeCl_2$ $Ti(OR)_4$ - $ZnCl_2$	10-14
Metal halides.	$AlCl_3$, $SbCl_5$, $FeCl_3$, $SnCl_4$	5
Tin(II) carboxylates.	$Sn(CH_3COO)_2$	15,16

TABLE 4.(1). Catalyst Systems Used in the Formation of Polypropylene Oxide.

The use of powdered chemicals including catalysts, in large scale industrial processes, can give rise to complications associated with handling the powder, dispersion of the reagent in the reaction system and safety problems from dust particles in the atmosphere. These problems can be overcome by introducing the chemical into the reaction system as a pellet or a prill rather than as a powder. Donbavand[16] studied the polymerisation of propylene oxide with powdered, pelleted and tableted catalysts and found that the activity of the catalyst was not dependent upon its form, nor were the polymers prepared, affected in any way. Another important finding by Donbavand, was that the binding agents used in certain pellets and tablets, did not affect the polymerisation, if it proceeded by a homogeneous mechanism.

Recent industrial applications of polypropylene oxide have included its use as a high molecular weight 'monomer' in the production of polyether polyols, which can then be used to prepare polyurethanes[17] and its use as an additive to stabilise coal-water-oil fuel mixtures[18].

The aims of the project are twofold:

(1) to find a catalyst that performs better than the compounds cited in the literature,

(2) to follow the polymerisation reaction with time and analyse the polymers obtained and postulate a mechanism for the reaction. If the mechanism is fully understood, it may be possible to design catalysts which will be able to achieve maximum yields and produce good quality polymers.

4.2.(2). Experimental.

The polymerisation reactions on propylene oxide (10ml; 0.143 moles) were carried out in sealed ampoules at 100°C for 48 hours, using 1 wt.% catalyst (0.1g). The contents of the opened ampoules were then stored in a desiccator at room temperature over potassium hydroxide pellets, to allow any excess propylene oxide to evaporate off. The crude polymers obtained, were white in colour, ranged in consistency from soft, tacky solids, to firm, waxy solids.

The crude polymer was separated into its crystalline (isotactic) and amorphous (atactic) forms. This was achieved by dissolving the polymer in an excess of acetone, refluxing the solution for at least half an hour and cooling the solution to -30°C, to precipitate the crystalline polymer, which was then filtered off and dried. The atactic moiety was then obtained by evaporation of the filtrate. The crystalline polymer was obtained as a white, brittle solid

and the amorphous moiety as a yellow, tacky liquid. This process of separating the crude polymer into crystalline and amorphous fractions is also said to result in the hydrolysis of any inorganic material present[10].

The nature of the polypropylene oxide polymers prepared in this work, were studied by Mössbauer, infrared, ^{1}H nmr and ^{13}C nmr spectroscopies and their thermal properties obtained by simultaneous thermogravimetric and differential thermal analysis. The molecular weights of the polymers were determined by viscosity measurements.

Compounds which were tested for their catalytic activity include some tin(II) carboxylates, complex tin(II) carboxylates and tin(II) halides. Details of the preparations of these compounds appear in Chapter 2.

4.2.(3). Results and Discussions.

4.2.(3).1. Polymer Yield.

After thorough drying in a desiccator for 3 days, the polymers obtained were weighed, to determine the yield. The efficiency of the catalysts used was evaluated by comparing the yields of the polymer prepared in this project, with the yields reported in the literature for other catalysts.

The data in Table 4.(2)., compare the yields of polypropylene oxide obtained using the tin(II) compounds and with the standard ferric chloride - propylene oxide complex and potassium hydroxide catalysts. The standard catalysts are very efficient for the polymerisation of propylene oxide, but to achieve high yields, either high catalyst concentrations or extended reaction times have to be used. Under similar conditions, some tin(II) compounds compare favourably with the standard catalysts.

Catalyst	Conditions	Yield (wt.%)
$Sn(CHOO)_2$	*	9.7
	1 wt.% catalyst 100°C / 114 hrs.	28.4
$Sn(CH_3COO)_2$	*	11.2
Sn Octoate	*	21.2
	1 wt.% catalyst 100°C / 114 hrs.	70.1
SnC_2O_4	*	0.0
Sn Malonate	*	0.0
Sn Maleate	*	0.0
$PbSn_2(CH_3COO)_6$	*	3.4
	1 wt.% catalyst 100°C / 114 hrs.	5.0
$KSn(CH_2ClCOO)_3$	*	1.4
SnF_2	*	0.0
$SnCl_2$	*	45.2
$SnBr_2$	*	31.9
SnI_2	*	22.6
	1 wt.% catalyst RT / 1 month.	17.8
$KSnCl_3$	*	18.2
SnClF	*	19.6
$FeCl_3$-PO	4 wt.% catalyst 100°C / 24 hrs.	80.0 (19)
$FeCl_3$-PO	1 wt.% catalyst 80°C / 265 hrs.	45.0 (7)
KOH	8.4 wt.% catalyst RT / 3 days.	62.0 (19)

* Unless otherwise stated, the conditions employed for the polymerisation are: 1 wt.% catalyst / 100°C / 48 hrs.

TABLE 4.(2). Yield of Polypropylene Oxide Produced for Different Catalyst Systems.

The polymer yields with the tin(II) monocarboxylates, increase with increasing alkyl chain length, from 28.4 wt.% for stannous formate, to 70.1 wt.% for stannous octoate. In general, the use of tri-monocarboxylatostannate(II) complexes instead of the tin(II) monocarboxylates, leads to lower yields, although yields of between 35-99 wt.% polymer were obtained by Arifin[15], for the manganese and cobalt tri-acetatostannate(II) derivatives. These values are however somewhat inflated, since very high catalyst concentrations (upto 10 wt.%) were used.

It is interesting to note, that the stannous dicarboxylates are completely inactive in this polymerisation system. It is possible, that this is related to the structure of the compounds, since the monocarboxylate species tend to have trigonal pyramidal tin coordination, whereas the dicarboxylates are normally polymeric with square pyramidal tin environments, with bidentate bridging dicarboxylate groups. The tin(II) halides, except stannous fluoride, are all exceptionally good catalysts - they give excellent yields (11.5-45.2 wt.%) with 1.0 wt.% catalyst, after a 48 hour polymerisation.

4.2.(3).2. Polymer Separation.

It is possible to separate the crude polymer into its crystalline and amorphous fractions, by the procedure outlined in Section 4.2.(2). Weighed portions of selected polymers, obtained after a 48 hour polymerisation, were separated and the relative yields of the resulting fractions then determined. These yields are recorded in Table 4.(3)., along with the results obtained with standard catalytic systems reported in the literature. Studies[20,21] on the tacticity

of the crystalline and amorphous fractions of polypropylene oxide have shown that the crystalline part of the polymer is >95% isotactic and the amorphous moiety is essentially atactic.

Catalyst	% Crystalline Fraction	% Amorphous Fraction	Ref
$Sn(CHOO)_2$	44.4	55.6	
$Sn(CH_3COO)_2$	26.6	73.4	
Sn Octoate	39.8	60.2	
$SnCl_2$	37.8	62.2	
$SnBr_2$	23.6	76.4	
SnI_2	21.2	78.8	
$KSnCl_3$	31.5	68.5	
SnClF	21.2	78.8	
$FeCl_3$-PO	13.5	86.5	19
KOH	0.0	100.0	16
$ZnEt_2$-H_2O	21.1	78.9	19

TABLE 4.(3). Effect of Catalyst on the Relative Amounts of Crystalline and Amorphous Fractions Formed in the Polymerisation of Propylene Oxide.

Figure 4.(3). shows the different stereochemical polymer types, (i) isotactic (ii) syndiotactic and (iii) atactic.

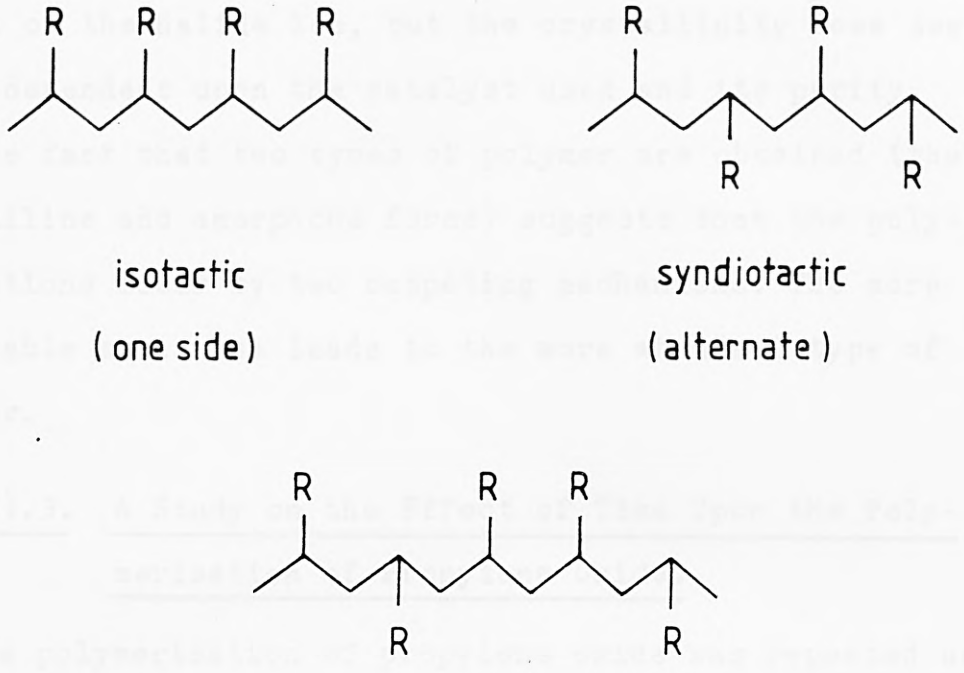

FIGURE 4.(3). Basic Stereochemical Polymer Types.

Thus, the ability of the catalyst to produce crystalline polymers is a reflection of their specificity in promoting the reaction. Crystallinity in the polymer is advantageous in some applications, because the polymer chains can approach close to each other and arrange themselves to allow inter-chain bonding to come into operation and to increase the strength in the polymer.

The data in Table 4.(3). show that potassium hydroxide is a non-specific catalyst; it has no control over the tacticity of the resulting polymer, which is 100% amorphous. Tin(II) compounds produce greater amounts of crystalline polymer (ranging from 21.2% to 71.0%) than any of the

catalysts reported in the literature. There is no obvious trend in crystallinity with respect to the alkyl chain length or the halide ion, but the crystallinity does seem to be dependent upon the catalyst used and its purity.

The fact that two types of polymer are obtained (the crystalline and amorphous forms) suggests that the polymerisations occur by two competing mechanisms. The more favourable mechanism leads to the more abundant type of polymer.

4.2.(3).3. A Study on the Effect of Time Upon the Polymerisation of Propylene Oxide.

The polymerisation of propylene oxide was repeated using 1.0 wt.% stannous acetate at 100°C, but reaction times of 6, 12, 18, 24, 42, 48 and 67 hours. The yields of the resulting polymers were calculated and percentages of the crystalline and amorphous fractions determined.

Time (hours)	Polymer Yield (wt.%)
6	3.41
12	5.19
18	5.61
24	6.23
42	9.50
48	11.23
67	20.85

TABLE 4.(4). The Effect of Time Upon the Polymer Yield.

Table 4.(4). and Figure 4.(4). show the effect of an increase in the polymerisation time upon the yield of the

crude polymer. As one would expect, there is a steady increase in the polymer yield with increase in reaction time, i.e. more of the monomer is used up as the polymerisation proceeds. Initially, there is a fairly high yield of polymer, in the middle stages of the reaction, a reasonably constant yield of between 5.19 and 6.23 wt.% is obtained and with longer reaction times, the yield increases dramatically. As

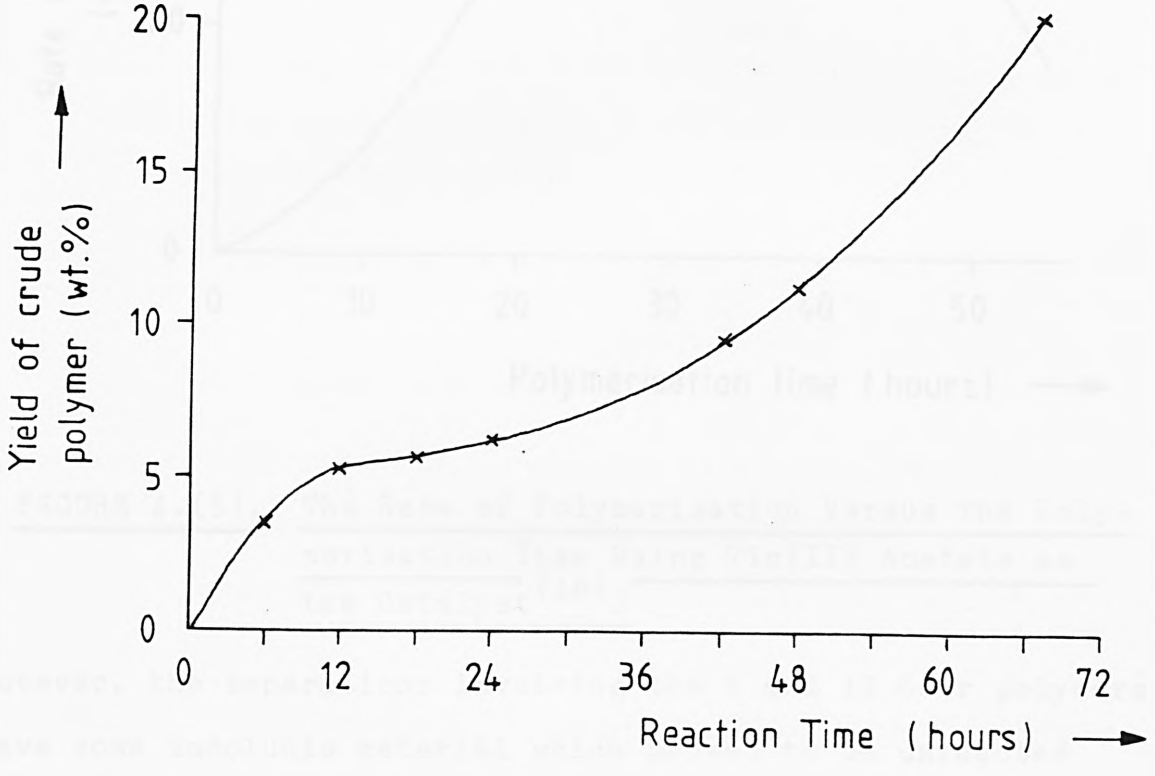

FIGURE 4.(4). Graph Showing the Increase in the Yield of Crude Polymer With Reaction Time.

this is an addition polymerisation reaction, this rapid rate of production should continue until most of the monomer is used up. This is shown most effectively in Figure 4.(5)., which illustrates the results obtained by Donbavand[16], using 1.0 wt.% powdered tin(II) acetate.

A weighed amount of each of the crude polymers was separated into their crystalline and amorphous fractions.

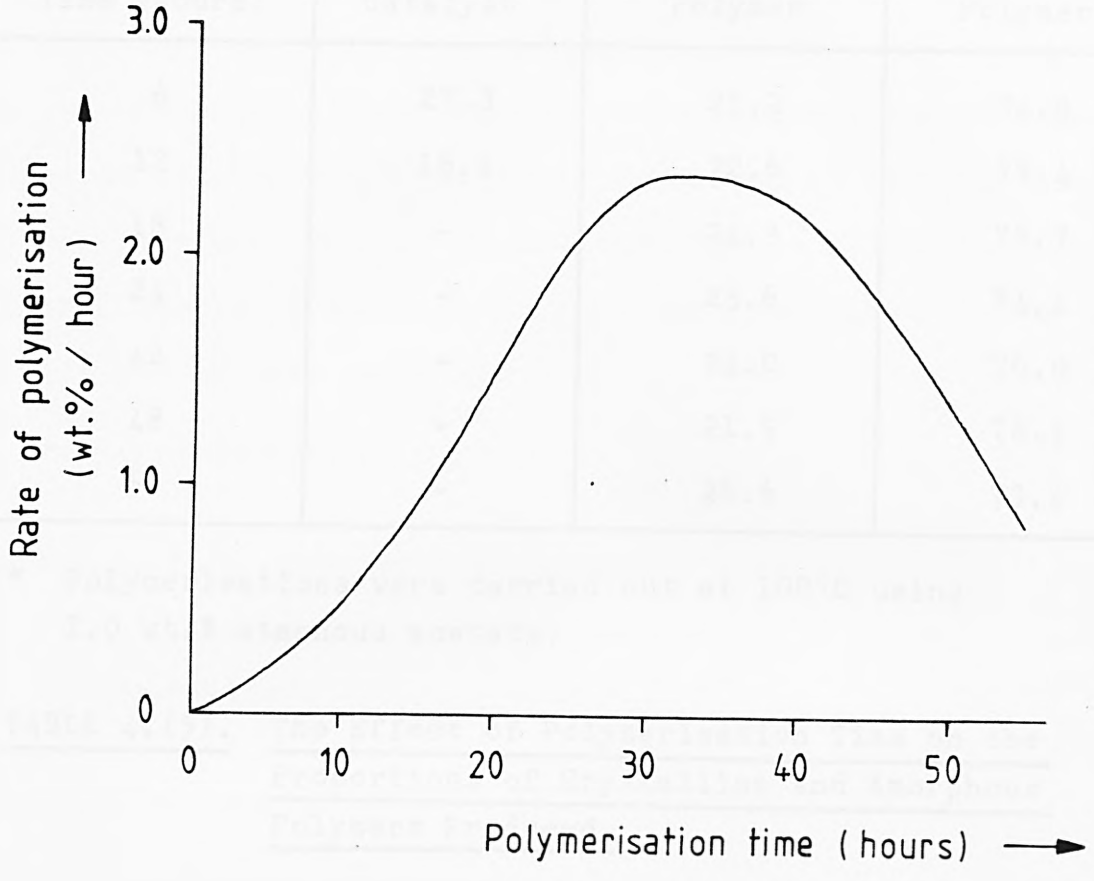

FIGURE 4.(5). The Rate of Polymerisation Versus the Polymerisation Time Using Tin(II) Acetate as the Catalyst[16].

However, the separations involving the 6 and 12 hour polymers gave some insoluble material which proved to be unreacted catalyst. This solid was filtered off, weighed, and expressed as a percentage of the amount of the catalyst used in the reaction. The separation procedure was then continued in the normal way, but the weights of the two fractions were corrected to account for the unreacted stannous acetate, before percentage crystalline and amorphous polymers were calculated. Table 4.(5). lists the results obtained for all the polymers.

From the results, it can be seen that, essentially the same proportions of crystalline and amorphous polymers are

Polymerisation Time (hours)	% Unreacted Catalyst	% Crystalline Polymer	% Amorphous Polymer
6	27.3	25.2	74.8
12	16.1	22.6	77.4
18	-	24.3	75.7
24	-	25.6	74.4
42	-	24.0	76.0
48	-	21.9	78.1
67	-	26.6	73.4

* Polymerisations were carried out at 100°C using 1.0 wt.% stannous acetate.

TABLE 4.(5). The Effect of Polymerisation Time on the Proportions of Crystalline and Amorphous Polymers Produced.

obtained regardless of the reaction time used. This means that the ability to form a crystalline polymer is a property of the catalyst itself and its purity and is not a function of polymerisation reaction time. This means that the active sites required to form a certain type of polymer are established fairly early in the polymerisation procedure and that increasing the reaction time will only increase the chain lengths of polymers growing from these sites. Most of the catalyst is incorporated into the polymer within six hours; in twelve hours, there is only about 16.1% of unreacted catalyst and after 18 hours, all of the catalyst has reacted to form the active sites necessary to promote chain growth.

4.2.(3).4. Molecular Weight Determination.

The molecular weights of selected polymers were deter-

mined by viscosity measurements in benzene solution, using an Ubbelohde viscometer (the flow time for pure benzene is 70-72 seconds at 25°C) with 0.02-0.50 g/100ml at 25 ±0.05°C. The relationship between viscosity measurements and molecular weight is well established and is described in Section 4.1.(3) The relative and inherent viscosities can be obtained, either directly or indirectly, from the flow times of the solvent and polymer solutions:

$$\text{relative viscosity, } \eta_r = \frac{t}{t_o}$$

where t_o = flow time for pure benzene.

t = flow time for polymer solution.

$$\text{inherent viscosity, } \eta_{inh} = \frac{\ln(\eta_r)}{c}$$

where c = concentration of polymer in g/100ml solvent.

By varying the concentrations of the polymer solutions, a range of inherent viscosities can be obtained. A plot of inherent viscosity versus concentration, extrapolated back to zero concentration, gives the intrinsic viscosity of the polymer.

i.e. $\eta_{int} = \lim_{c \to o} \eta_{inh}$

From the intrinsic viscosity an estimate of the average molecular weight may be obtained using the Mark-Houwink-Sakuradu equation, using the constant quoted by Price and Miller[11].

$$\eta_{int} = (1.4 \times 10^{-4}) M^{0.8}$$

where M = average molecular weight.

The viscosity measurements obtained for polypropylene oxide, using stannous octoate, $SnCl_2$, $SnBr_2$, SnI_2 and $Sn(CH_3COO)_2$ (18, 42 and 48 hour polymerisations) are shown

Catalyst	Concentration of Polymer (g/100ml)	η_{rel}	η_{inh}
Sn Octoate	0.060	1.125	1.957
	0.073	1.163	2.061
	0.144	1.184	1.713
	0.242	1.445	1.518
$SnCl_2$	0.085	1.194	2.086
	0.168	1.304	1.586
	0.214	1.434	1.687
	0.331	1.460	1.140
$SnBr_2$	0.024	1.020	0.211
	0.150	1.030	0.195
	0.250	1.055	0.215
	0.315	1.042	0.131
	0.350	1.038	0.107
SnI_2	0.035	1.004	0.101
	0.118	1.010	0.083
	0.159	1.010	0.065
	0.213	1.012	0.055
$Sn(CH_3COO)_2$ -(18 hours)	0.046	1.079	1.185
	0.084	1.096	1.095
	0.146	1.150	0.955
	0.198	1.187	0.866
$Sn(CH_3COO)_2$ -(42 hours)	0.050	1.069	1.330
	0.082	1.107	1.250
	0.173	1.197	1.037
	0.245	1.431	0.864
$Sn(CH_3COO)_2$ -(48 hours)	0.053	1.088	1.593
	0.102	1.171	1.547
	0.147	1.246	1.495
	0.212	1.365	1.447

TABLE 4.(6). Viscosity Measurements For Polypropylene Oxide Obtained Using Various Catalysts.

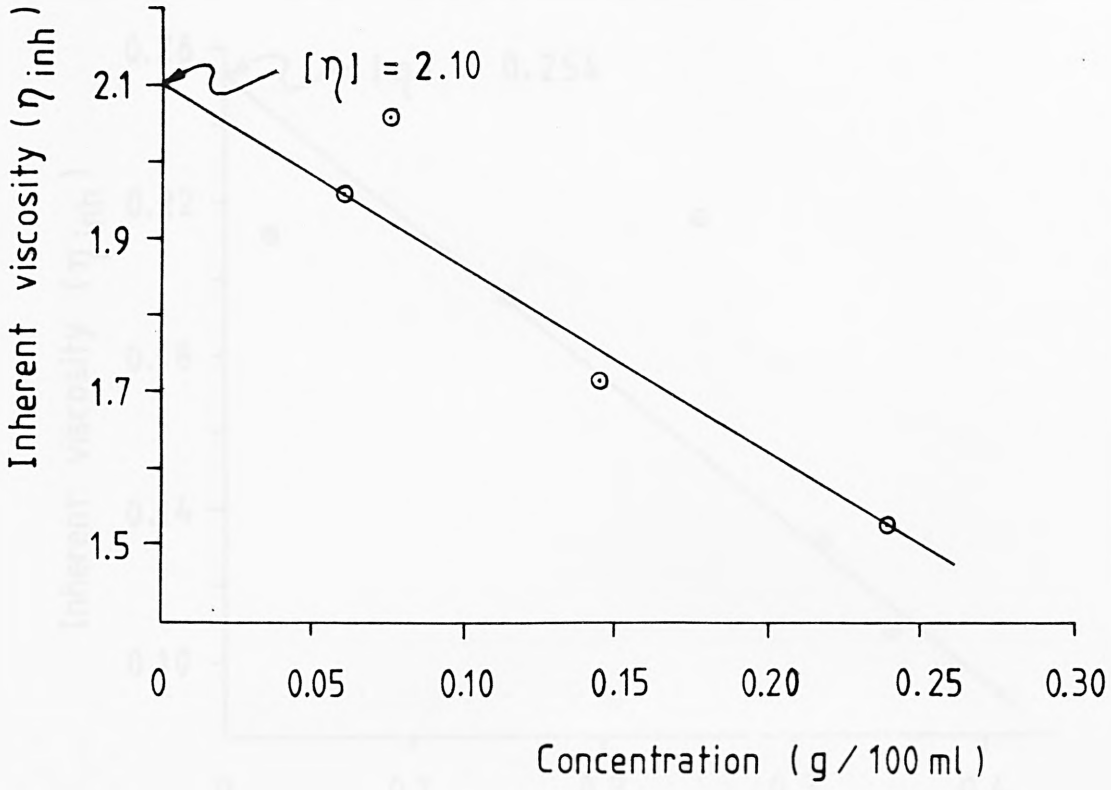

FIGURE 4.(6). Plot of Inherent Viscosity Versus Concentration, for Stannous Octoate.

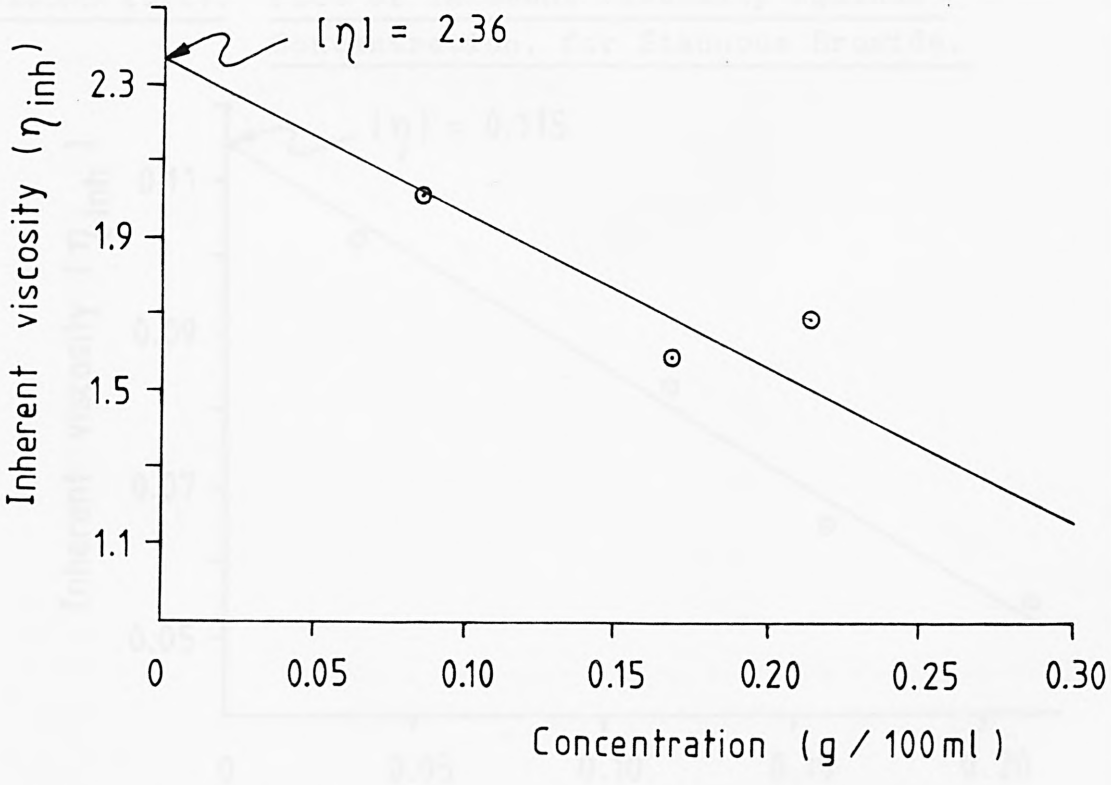

FIGURE 4.(7). Plot of Inherent Viscosity Versus Concentration, for Stannous Chloride.

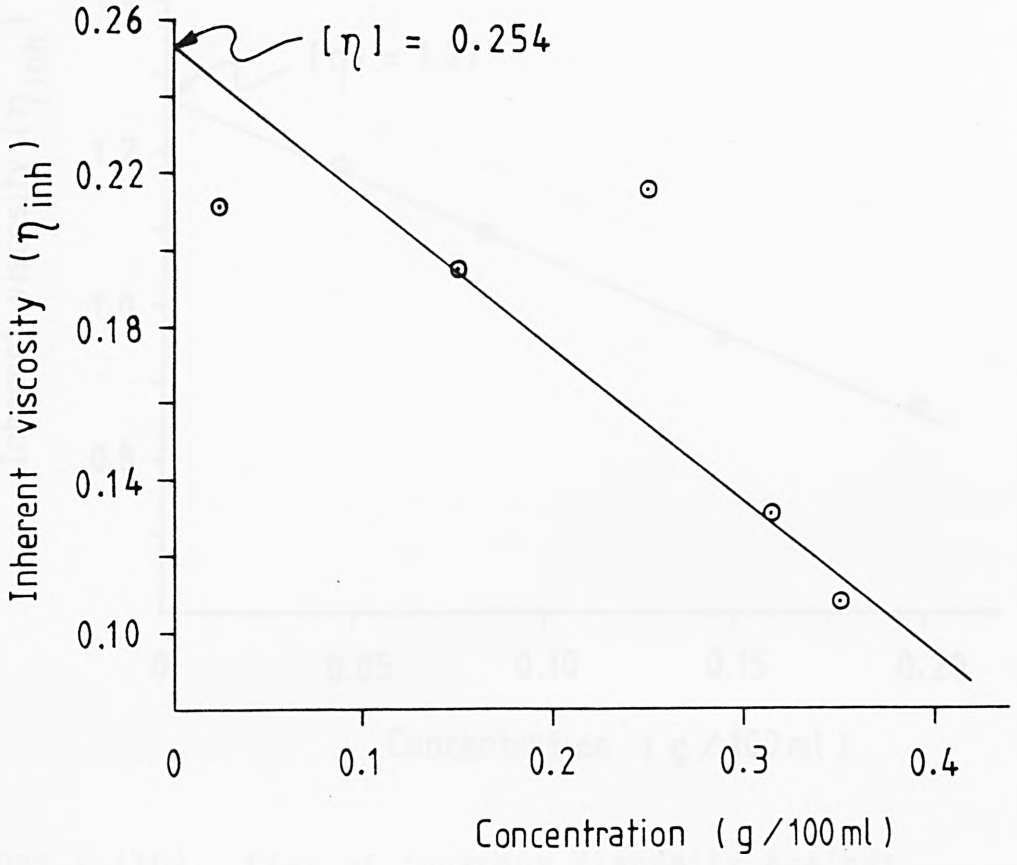

FIGURE 4.(8). Plot of Inherent Viscosity Against Concentration, for Stannous Bromide.

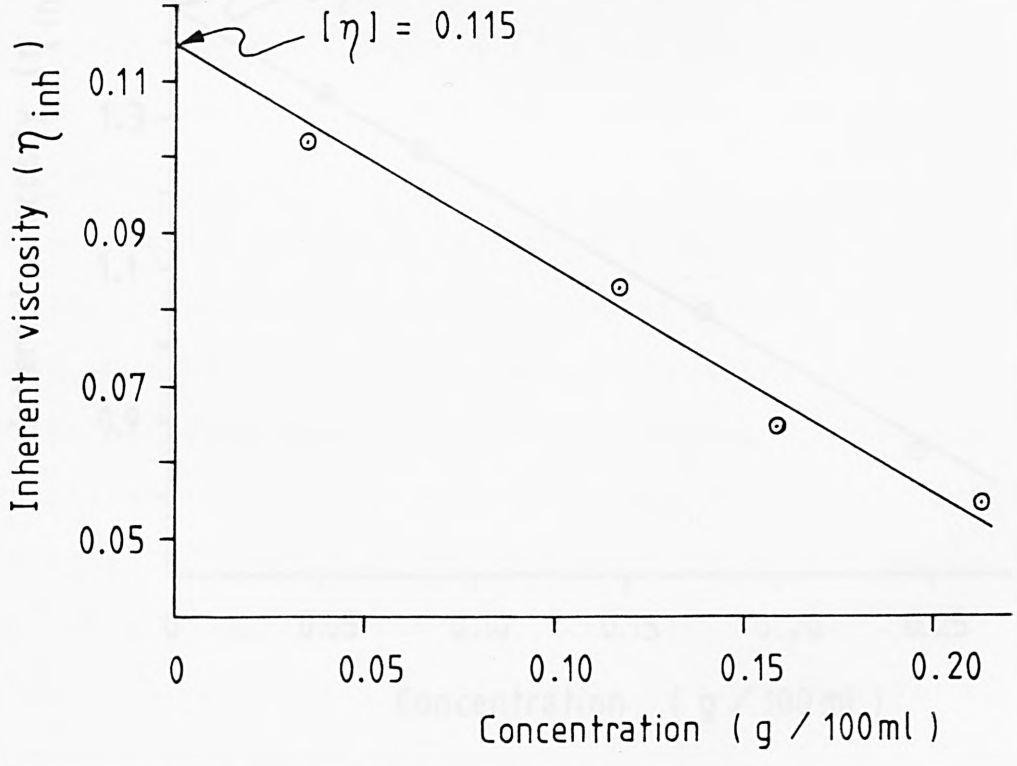

FIGURE 4.(9). Plot of Inherent Viscosity Against Concentration, for Stannous Iodide.

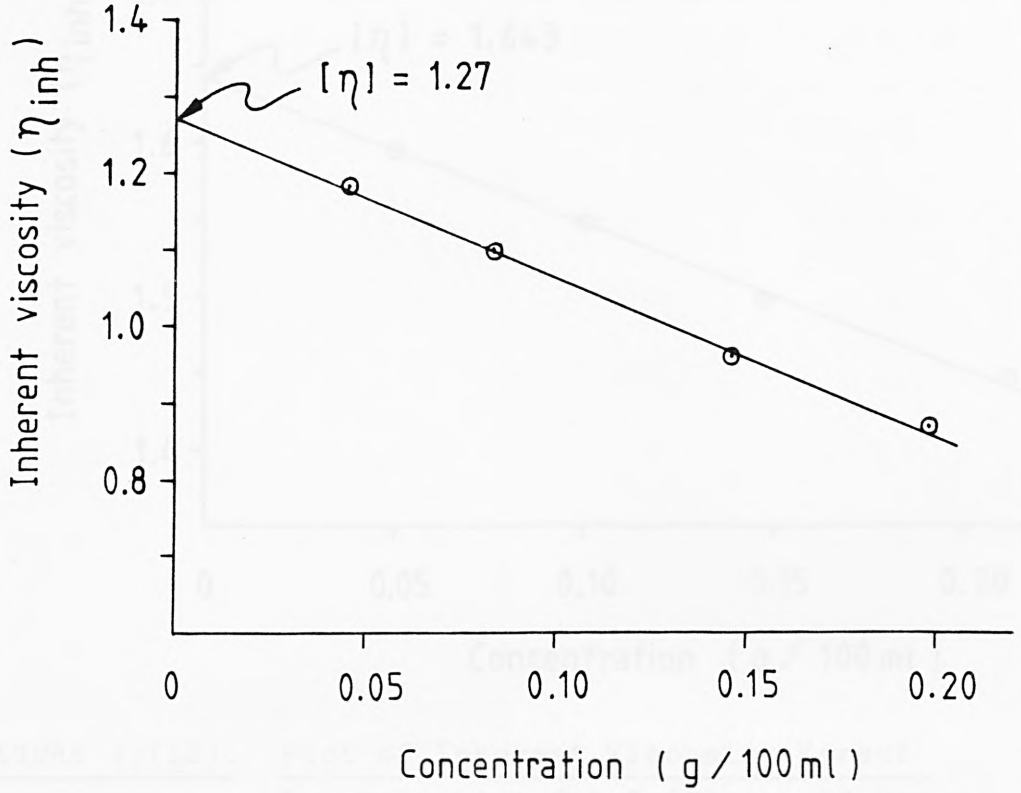

FIGURE 4.(10). Plot of Inherent Viscosity Against Concentration for $Sn(OAc)_2$, 18 Hours.

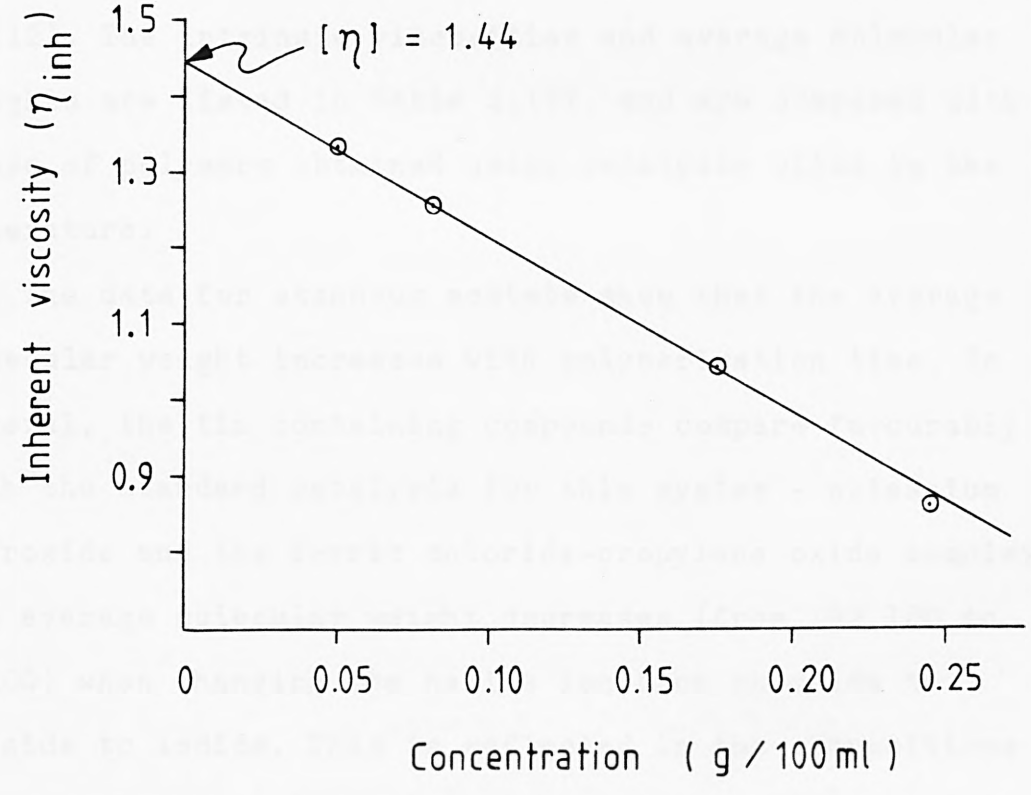

FIGURE 4.(11). Plot of Inherent Viscosity Against Concentration for $Sn(OAc)_2$, 42 Hours.

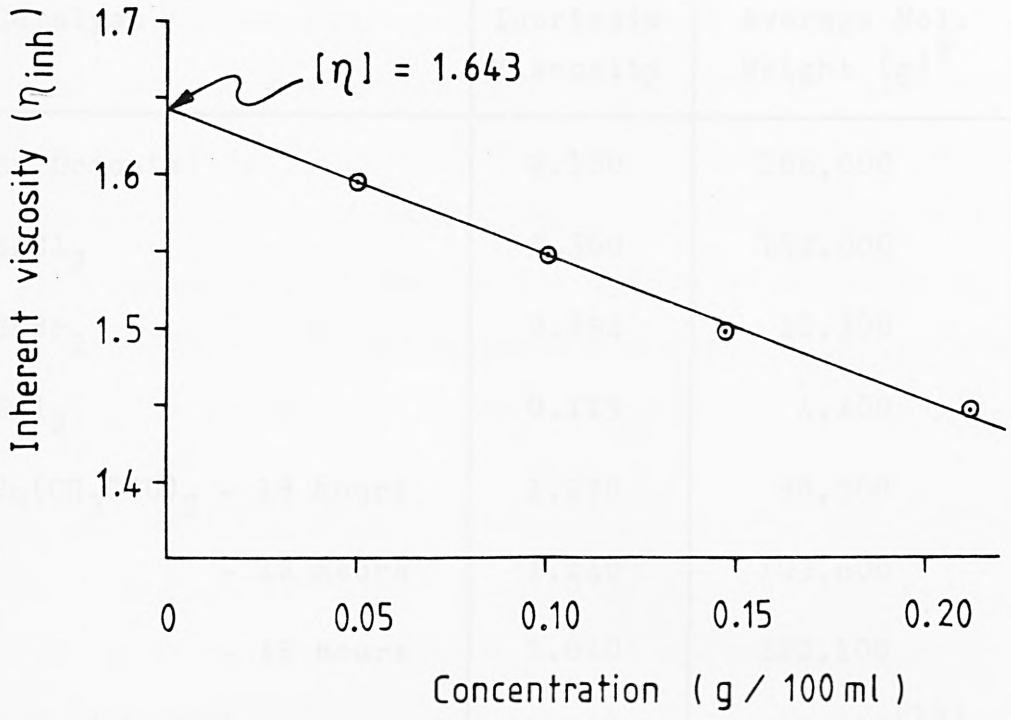

FIGURE 4.(12). Plot of Inherent Viscosity Versus Concentration for $Sn(OAc)_2$, 48 Hours.

in Table 4.(6). and the subsequent plots yielding the intrinsic viscosity values are shown in Figures 4.(6) to 4.(12). The intrinsic viscosities and average molecular weights are listed in Table 4.(7). and are compared with those of polymers obtained using catalysts cited in the literature.

The data for stannous acetate show that the average molecular weight increases with polymerisation time. In general, the tin containing compounds compare favourably with the standard catalysts for this system - potassium hydroxide and the ferric chloride-propylene oxide complex. The average molecular weight decreases (from 192,100 to 4,400) when changing the halide ion from chloride to bromide to iodide. This is reflected in the compositions of the polymers, since stannous chloride produces a firm, solid polymer, whereas stannous bromide and iodide give

Catalyst	Intrinsic Viscosity	Average Mol. Weight (g)*
Sn Octoate	2.100	166,000
$SnCl_2$	2.360	192,000
$SnBr_2$	0.254	11,300
SnI_2	0.115	4,400
$Sn(CH_3COO)_2$ - 18 hours	1.270	88,500
- 42 hours	1.440	103,600
- 48 hours	1.640	122,100
$MnSn_2(CH_3COO)_6$	1.380	98,000[15]
$CoSn_2(CH_3COO)_6.5H_2O$	0.250	11,000[15]
$ZnSn_2(CH_3COO)_6.6H_2O$	0.230	11,000[15]
$CdSn_2(CH_3COO)_6$	0.410	22,000[15]
KOH	0.142	5,700[16]
$FeCl_3$ - PO	0.260	12,000[19]
$ZnEt_2.H_2O$	2.530	244,000[19]
$MgCl_2.OEt$	12.000	1,466,000[10]

* $\eta_{int} = (1.4 \times 10^{-4}) M^{0.8}$

TABLE 4.(7). Effect of the Catalyst Used Upon the Average Molecular Weight.

very soft, tacky solids. Both tin(II) octoate and tin(II) acetate catalysts produce high molecular weight polymers (166,000g and 122,100g respectively) that compare favourably with those obtained using most of the catalysts reported in the literature for this system. Comparison of stannous acetate with the complex tin(II) acetates show

that the normal compound produces polymers of higher molecular weight. The manganese complex however, is reported to yield an average molecular weight of 98,000[15], but this is somewhat unusual, since the other complexes (Co, Zn and Cd), give polymers with fairly low molecular weights. It seems likely that both the manganese and tin moieties are active species in the use of $Mn(Sn(CH_3COO)_3)_2$, as catalyst.

4.2.(3).5. Infrared Spectroscopy of Polypropylene Oxide.

The thin film infra-red spectra of all the polymers prepared in this work were recorded on a Perkin-Elmer 599 spectrophotometer. All the spectra obtained are identical, regardless of the catalyst used and are identical to the spectra that have been published in the literature[22]. Figures 4.(13). and 4.(14). show the infra-red spectra of the crude polymers produced using (a) a carboxylate and (b) a halide catalyst respectively. Their data appear in Table 4.(8)., along with the spectral assignments given by Kawasaki et al.[23]. The extra peak observed in Figure 4.(13) at 1735cm^{-1}, is assigned to the carbonyl stretching mode in the carboxylate group of the catalyst. This means that the carboxylate is present as the free ion, since the coordination to tin shifts the ν_s(C=O) stretching frequency to about 1515cm^{-1}.

The infrared spectra of the crystalline and amorphous fractions were also recorded and similar spectra obtained, regardless of whether a carboxylate or a halide catalyst was used. A comparison of the carbonyl stretching region in Figure 4.(15)., shows that the carboxylate ion is absent in the crystalline polymer, but is present in the amorphous moiety. The carbonyl peak is considerably enhanced in the

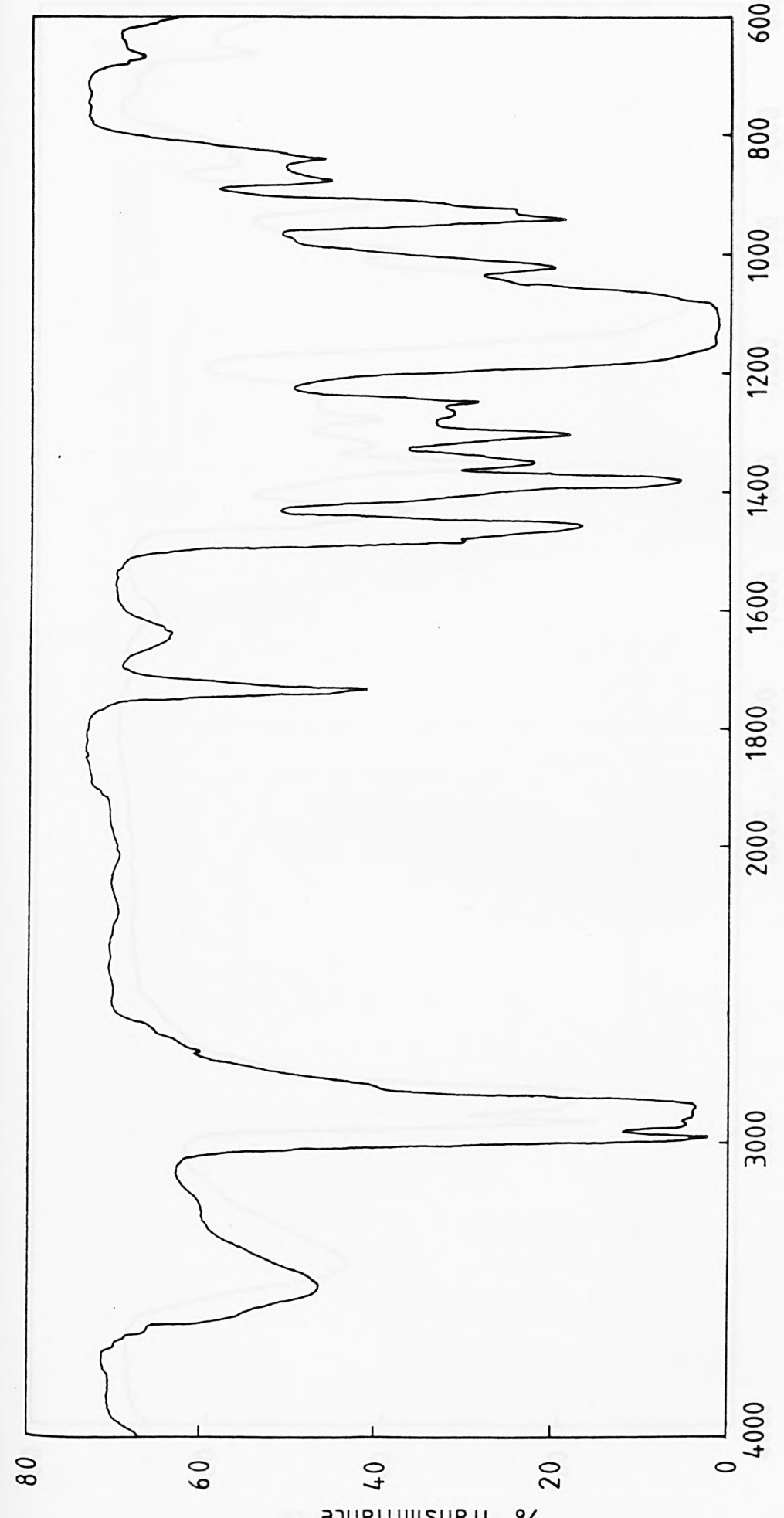

FIGURE 4.(13). Infrared Spectrum of Polypropylene Oxide Prepared Using a Stannous Carboxylate Catalyst.

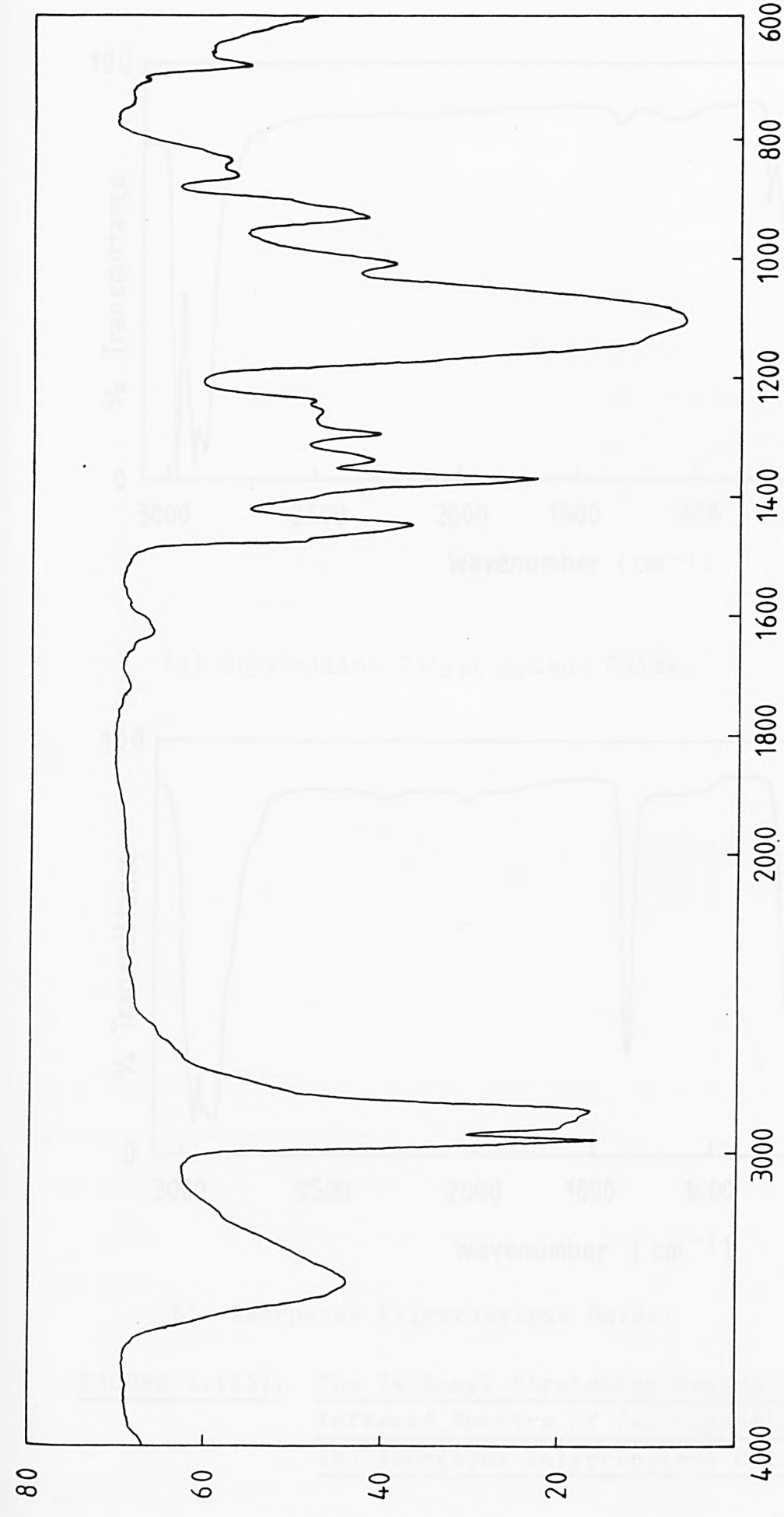

FIGURE 4.(14). Infrared Spectrum of Polypropylene Oxide Prepared Using a Tin(II) Halide Catalyst.

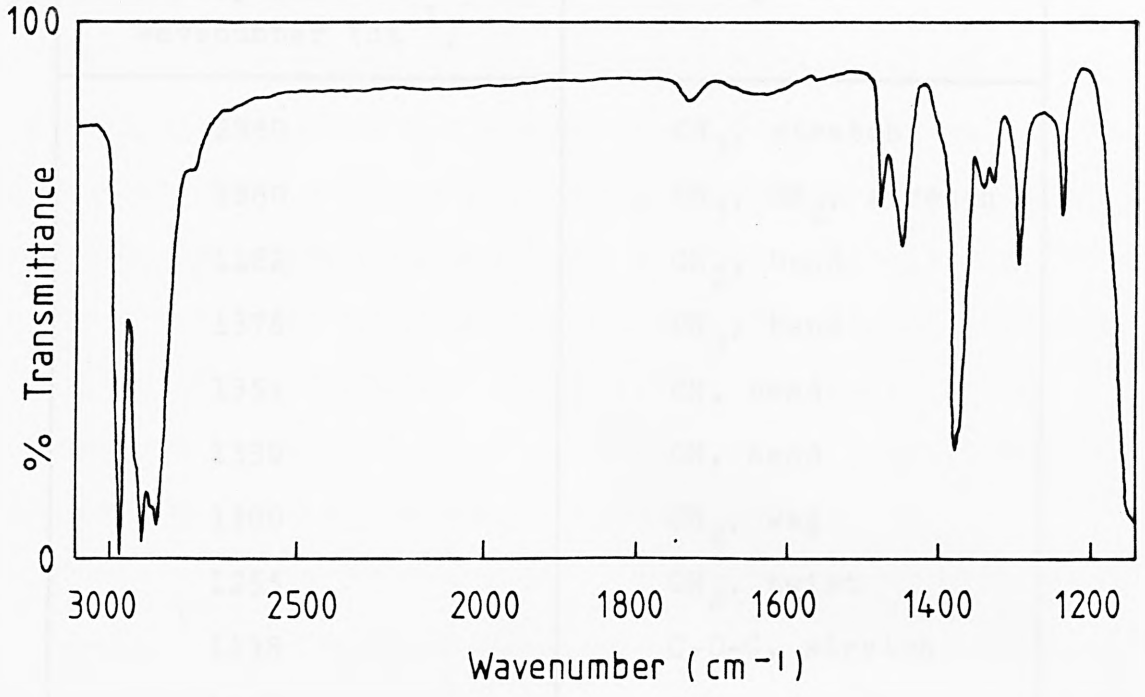

(a) Crystalline Polypropylene Oxide.

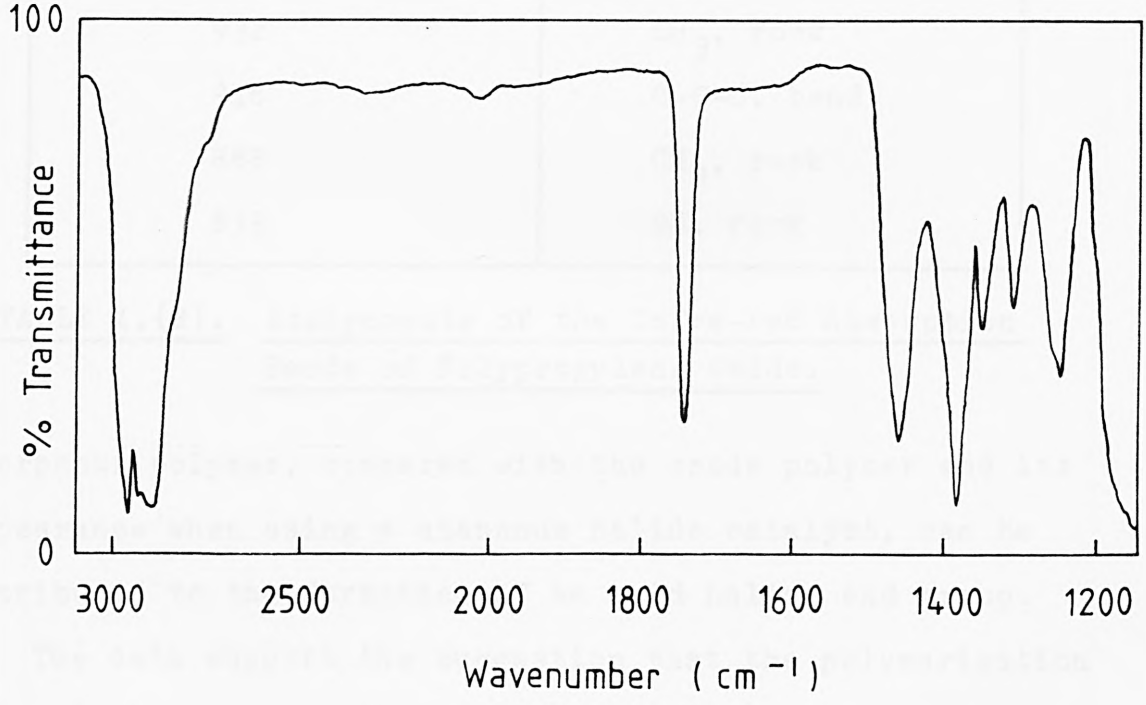

(b) Amorphous Polypropylene Oxide.

FIGURE 4.(15). The Carbonyl Stretching Region in the Infrared Spectra of (a) Crystalline and (b) Amorphous Polypropylene Oxide.

Absorption Band Wavenumber (cm^{-1})	Assignment
2980	CH_3, stretch
2860	CH_3, CH_2, stretch
1482	CH_2, bend
1378	CH_3, bend
1354	CH, bend
1330	CH, bend
1300	CH_2, wag
1255	CH_2, twist
1138	C-O-C, stretch
1100	C-C, stretch
1038	CH_3, rock
1012	CH_3, rock
932	CH_3, rock
918	C-O-C, bend
868	CH_2, rock
833	CH, rock

TABLE 4.(8). Assignments of the Infra-red Absorption Bands of Polypropylene Oxide.

amorphous polymer, compared with the crude polymer and its appearance when using a stannous halide catalyst, can be attributed to the formation of an acid halide end group.

The data support the suggestion that the polymerisation proceeds by two competing mechanisms. The formation of the crystalline polymer must involve the tin moiety of the catalyst and the amorphous polymer must include the bonding of the carboxylate or halide molecules, probably as end groups. Further evidence for this will be provided when the Mössbauer results are discussed in Section 4.2.(3).7.

4.2.(3).6. Differential Thermal Analysis.

The melting points of the polymers were obtained from the analysis of their DTA traces. From Table 4.(9)., it can be seen that the melting point is independent of the catalyst used and the polymerisation time, but that the melting point of the crystalline polymer, is considerably higher than that of the amorphous fraction. The polymers decompose in the temperature range 315° - 360°C, losing their organic components, to leave a residue of tin(II) oxide.

Catalyst	Melting Point (°C)
$Sn(CH_3COO)_2$	58
Sn Octoate	55
$PbSn_2(CH_3COO)_6$	67
$KSn(CH_2ClCOO)_3$	51
$SnCl_2$	58
$SnBr_2$	50
SnI_2	54
$KSnCl_3$	58
SnClF	60
Sn Octoate (crystalline)	54
$Sn(CH_3COO)_2$ (crystalline)	53
$SnCl_2$ (crystalline)	58
SnI_2 (amorphous)	27
$Sn(CH_3COO)_2$ (amorphous)	30
$Sn(CH_3COO)_2$ - 6 hours	51
- 12 hours	57
- 18 hours	54
- 24 hours	58

TABLE 4.(9). Melting Points of Polypropylene Oxide Obtained Using Various Catalysts.

4.2.(3).7. Mössbauer Spectroscopy.

The ^{119}Sn Mössbauer spectra of the crude polymers obtained after 48 hour polymerisations, were recorded at 80K. Table 4.(10). lists the results obtained for all of the catalyst systems tested.

Compound	Mössbauer Data of Compound δ (mm/s)	Δ (mm/s)	Mössbauer Data of Polymer δ (mm/s)
$SnCl_2$	4.07	0.0	0.03
$SnBr_2$	3.93	0.0	-0.04
SnI_2	3.85	0.0	0.06
$SnCl_4$	0.85	0.0	0.02
SnClF	3.68	1.10	0.02
$KSnCl_3$	3.70	0.89	0.13
$Sn(CHOO)_2$	3.05	1.56	0.02
$Sn(CH_3COO)_2$	3.21	1.77	0.03
$PbSn_2(CH_3COO)_6$	3.13	1.94	0.10
$MnSn_2(CH_3COO)_6$	2.69	1.51	0.06
$CoSn_2(CH_3COO)_6.5H_2O$	3.07	1.83	0.06
$NiSn_2(CH_3COO)_6.5H_2O$	2.94	1.70	0.06
$ZnSn_2(CH_3COO)_6.6H_2O$	3.00	1.97	0.06
$CdSn_2(CH_3COO)_6$	2.98	1.91	-0.04
$KSn(CH_2ClCOO)_3$	2.84	1.97	0.08
Sn Octoate	3.22	2.02	0.10

TABLE 4.(10). Mössbauer Data for the Tin Containing Catalysts and Their Polymers.

Figure 4.(16). shows the Mössbauer spectra of stannous acetate and of the polymer it produces.

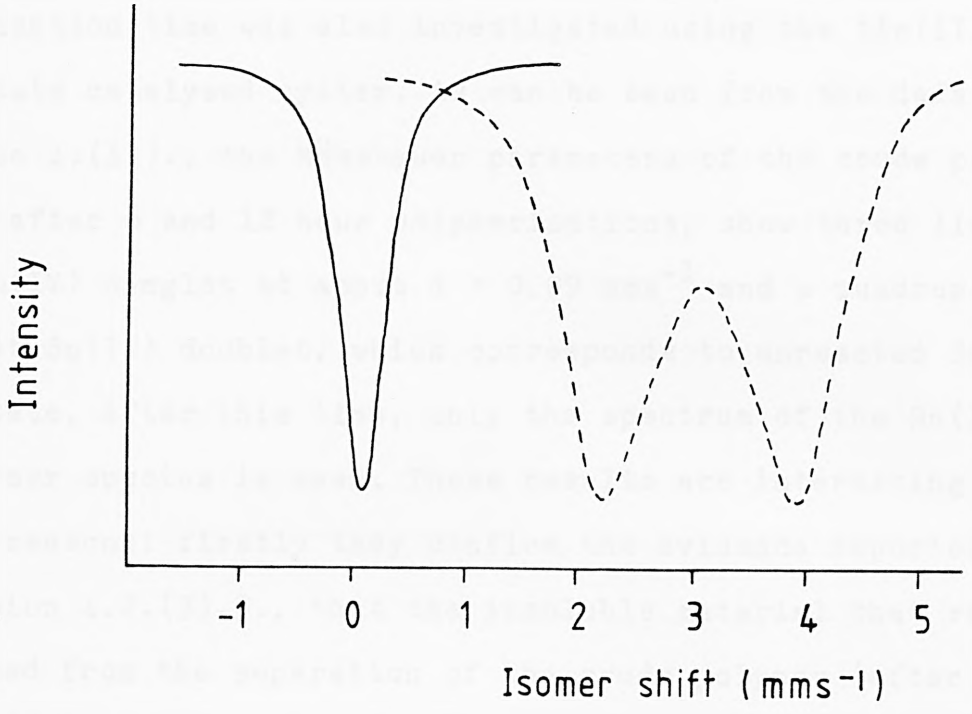

FIGURE 4.(16). Mössbauer Spectra of --- Stannous Octoate and —— the Polymer it Produces.

The Mössbauer spectra of the normal tin(II) halides, show a Sn(II) singlet with a large isomer shift (δ = 3.85-4.07 mms^{-1}), whereas those for the complex tin(II) halides are quadrupole split doublets with similar isomer shifts and Δ = 0.89 - 1.29 mms^{-1}. The normal and complex tin(II) carboxylates, both show quadrupole split doublets with $\delta \sim 3.00$ mms^{-1} and a large quadrupole splitting of 1.70 - 2.02 mms^{-1}. The Mössbauer spectra of the polymers obtained using these compounds as catalysts, consist of a singlet in the tin(IV) region of the spectrum, that has an isomer shift in the range -0.04 to 0.13 mms^{-1}. Thus, as a result of initiating the polymerisation of propylene oxide, the tin is oxidised and the isomer shift of the Sn(IV) species

produced, is consistent with the tin atom being surrounded octahedrally by six oxygen atoms.

The change in the Mössbauer parameters with the polymerisation time was also investigated using the tin(II) acetate catalysed system. As can be seen from the data in Table 4.(11)., the Mössbauer parameters of the crude polymer after 6 and 12 hour polymerisations, show three lines; a Sn(IV) singlet at about δ = 0.09 mms^{-1} and a quadrupole split Sn(II) doublet, which corresponds to unreacted Sn(II) acetate. After this time, only the spectrum of the Sn(IV) polymer species is seen. These results are interesting for two reasons: firstly they confirm the evidence reported in Section 4.2.(3).3., that the insoluble material that resulted from the separation of the crude polymer (after 6 and 12 hour polymerisations), was unreacted catalyst.

Polymerisation Time (hours)	Sn(II) Species δ (mm/s)	Sn(II) Species Δ (mm/s)	Sn(IV) Species δ (mm/s)
6	2.89	1.33	0.108
12	3.09	1.84	0.092
18	-	-	0.084
24	-	-	0.087
48	-	-	0.028

TABLE 4.(11). Effect of Polymerisation Time on the Mössbauer Parameters.

Secondly, the results show that the catalyst is not affected by refluxing with the monomer for extended periods of time and that the tin(IV) species must arise from a reaction

between the tin moiety of the catalyst and the monomer.

The fate of the tin moiety in both the crystalline and amorphous polymers was also studied and the results are shown in Table 4.(12). The crystalline polymers contain a tin(IV) species, with an isomer shift of between 0.02 and 0.15 mms^{-1}. This shows that the tin species is not removed from the polymer by the separation procedure and that it must be strongly bound to the polymer. The amorphous polymers give very weak Mössbauer resonances, suggesting that the tin part of the catalyst plays only a minor role in the formation of the amorphous polymer.

Catalyst	Crystalline Polymer δ (mm/s)	Amorphous Polymer δ (mm/s)*
$SnCl_2$	0.03	(0.01)
SnI_2	0.02	(-0.18)
$Sn(CHOO)_2$	0.02	-
$Sn(CH_3COO)_2$ - 6 hours	0.15	(0.02)
- 24 hours	0.10	(-0.07)
- 48 hours	0.05	(-0.06)
- 67 hours	0.05	-
Sn Octoate	0.03	-

* Brackets denote very weak spectra, with large errors involved in the computer fitting.

TABLE 4.(12). Comparison of Mössbauer Data for Different Forms of Polypropylene Oxide.

Thus, the Mössbauer and infrared data seem to suggest

that a tin containing moiety from the tin(II) carboxylate or halide is responsible for the catalytic formation of the crystalline polymer and that the anionic moiety of the catalyst, favours the formation of the amorphous polymer. Possible mechanisms for the polymerisation of propylene oxide, based upon these results, are outlined in Section 4.2.(4).

4.2.(3).8. Nuclear Magnetic Resonance Spectroscopy (NMR).

^{1}H Nmr Spectra.

Nmr spectroscopy is a technique which records transitions between the energy levels of magnetic nuclei in an external magnetic field. It involves the absorption of electromagnetic radiation in the radio frequency region, by a sample placed in an external magnetic field. A plot of the absorption against the external magnetic field gives the nmr spectrum.

In proton (^{1}H) nmr, a precessing or spinning proton can have two orientations when placed in an external magnetic field, and can align itself parallel to the field or opposed to it, i.e.

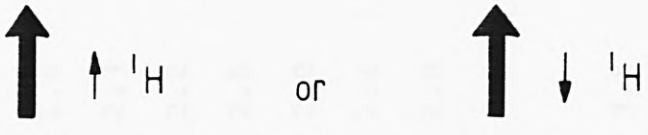

The precessional frequency of all protons is not the same. The precise value for any one proton, depends upon its chemical environment and the difference in the absorption position of a given proton from the absorption position of a reference proton, which is known as the chemical shift δ. Table 4.(13). lists the shifts of some methyl (CH_3), methylene (CH_2) and methine (CH) protons in different chemical environments. The values may vary, if inductive or steric

Methyl protons		Methylene protons		Methine protons	
Proton	δ	Proton	δ	Proton	δ
CH_3-C	0.9	-C-CH_2-C	1.4	C-CH-C	1.5
CH_3-C-C=C	1.1	-C-CH_2-C-C=C	1.7	-C-CH-C-O	2.0
CH_3-C-O	1.3	-C-CH_2-C-O	1.9	-C-CH-C-O	2.0
CH_3-C=C	1.6	-C-CH_2-C=C	2.3		
CH_3-Ar	2.3	-C-CH_2-Ar	2.7	-CH-Ar	3.0
CH_3-CO-R	2.2	-C-CH_2-CO-R	2.4	-C-CH-CO-R	2.7
CH_3-CO-Ar	2.6			-C-CH-CO-Ar	3.3
CH_3-CO-O-R	2.0	-C-CH_2-CO-O-R	2.2		
CH_3-CO-O-Ar	2.4				
CH_3-CO-N-R	2.0	-C-CH_2-CO-N-R	2.2		
CH_3-O-R	3.3	-C-CH_2-O-R	3.4	-C-CH-O-R	3.7
		-C-CH_2-O-H	3.6	-C-CH-O-H	3.9
CH_3-O-C=C	3.8				
CH_3-O-Ar	3.8	-C-CH_2-O-Ar	4.3		
CH_3-O-CO-R	3.7	-C-CH_2-O-CO-R	4.1	-C-CH-O-CO-R	4.8

TABLE 4.(13). Chemical Shifts (δ) of Methyl, Methylene and Methine Protons in ppm. Units.

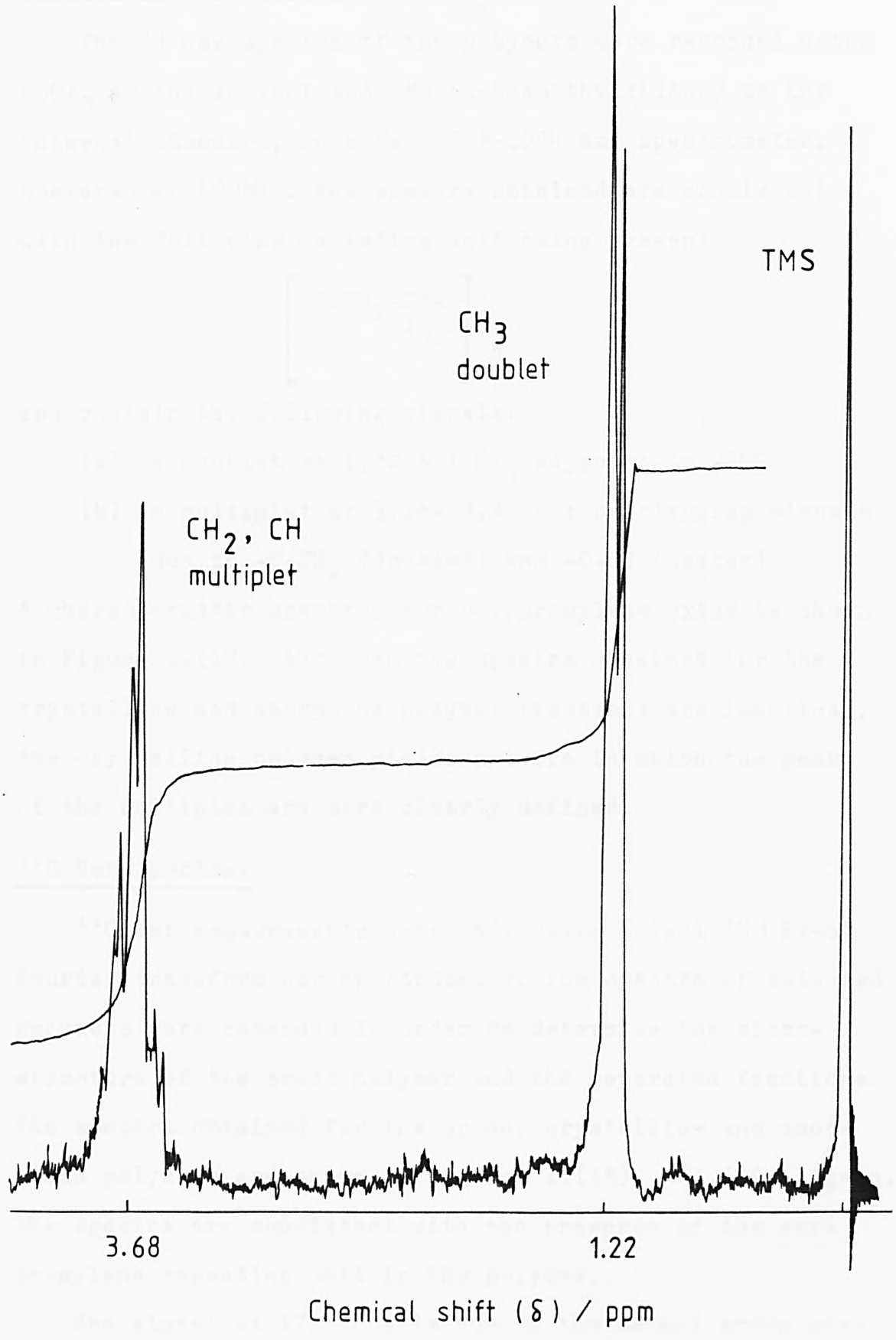

FIGURE 4.(17). ^{1}H Nmr Spectrum of Polypropylene Oxide.

effects are in operation.

The ^{1}H nmr spectra of the polymers were recorded using $CDCl_3$ as the solvent and TMS (tetramethylsilane) as the internal standard, on a Jeol JNM-100H Nmr spectrometer, operated at 100MHz. The spectra obtained are consistent with the following repeating unit being present

$$\left[-O-CH_2-\underset{\displaystyle CH_3}{\underset{|}{CH}}- \right]_n$$

and contain the following signals:

(a) a doublet at 1.22 δ : CH_3 adjacent to -CHO

(b) a multiplet at 3.46- 3.86 δ : overlapping signals due to $-O-CH_2$ (doublet) and -O-CH (sextet)

A characteristic spectrum for polypropylene oxide is shown in Figure 4.(17). Although the spectra obtained for the crystalline and amorphous polymer fractions are identical, the crystalline polymer yields spectra in which the peaks of the multiplet are more clearly defined.

^{13}C Nmr Spectra.

^{13}C nmr measurements were made using a Jeol JNM FX-60 Fourier transform nmr spectrometer. The spectra of selected polymers were recorded in order to determine the microstructure of the crude polymer and the separated fractions. The spectra obtained for the crude, crystalline and amorphous polymers are shown in Figures 4.(18). - 4.(20). Again, the spectra are consistent with the presence of the oxypropylene repeating unit in the polymer.

The signal at 17.6 ppm is due to the methyl group next to the secondary carbon atom and the multiplet in the range 73.0 - 79.2 δ arises from overlapping signals due to $-O-CH_2$ and -CH-O-.

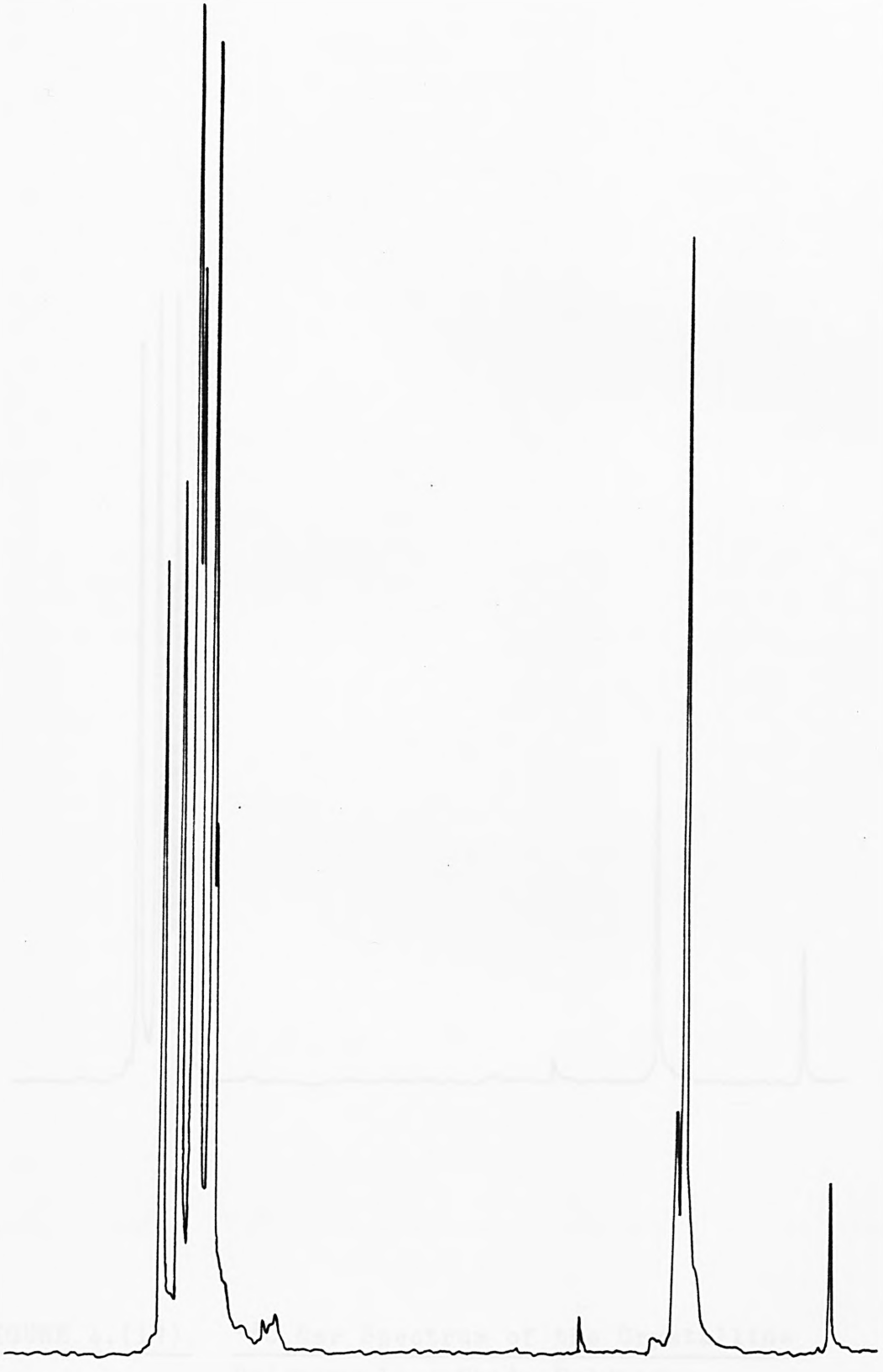

FIGURE 4.(18). ^{13}C Nmr Spectrum of the Crude Polypropylene Oxide Polymer.

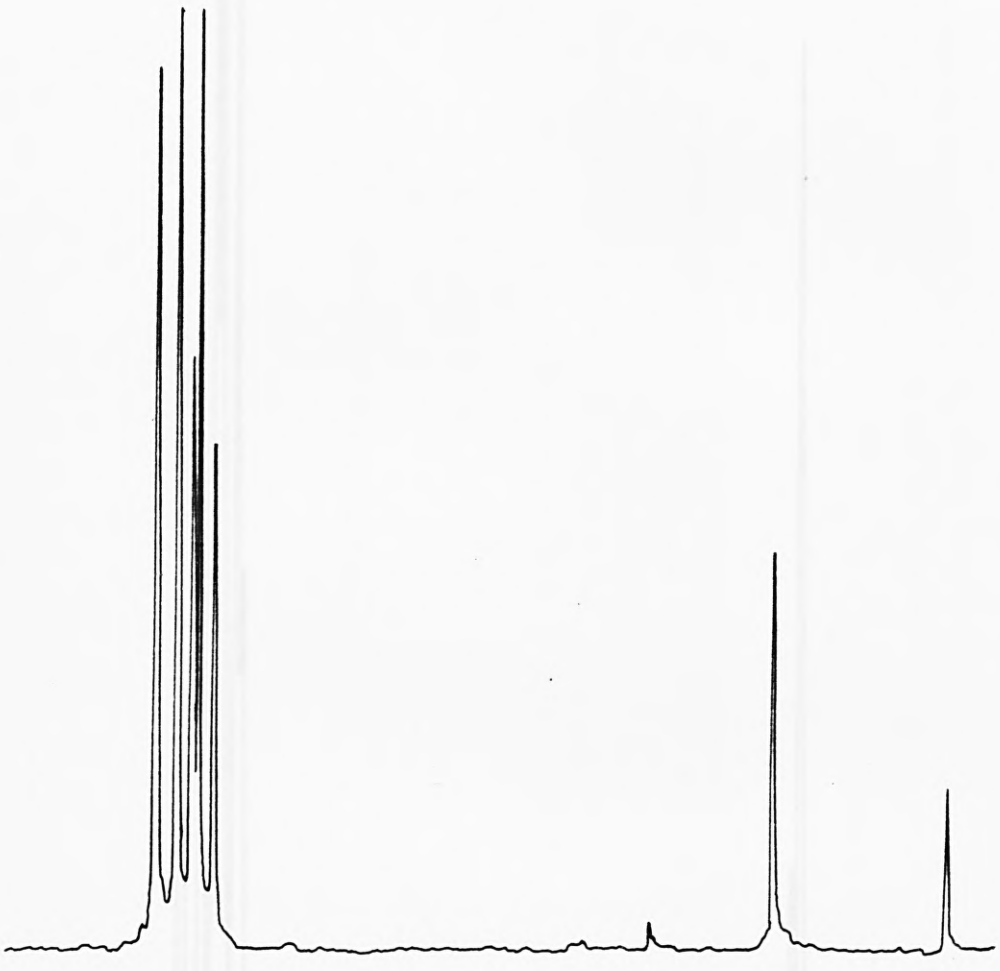

FIGURE 4.(19). ^{13}C Nmr Spectrum of the Crystalline Polypropylene Oxide Polymer.

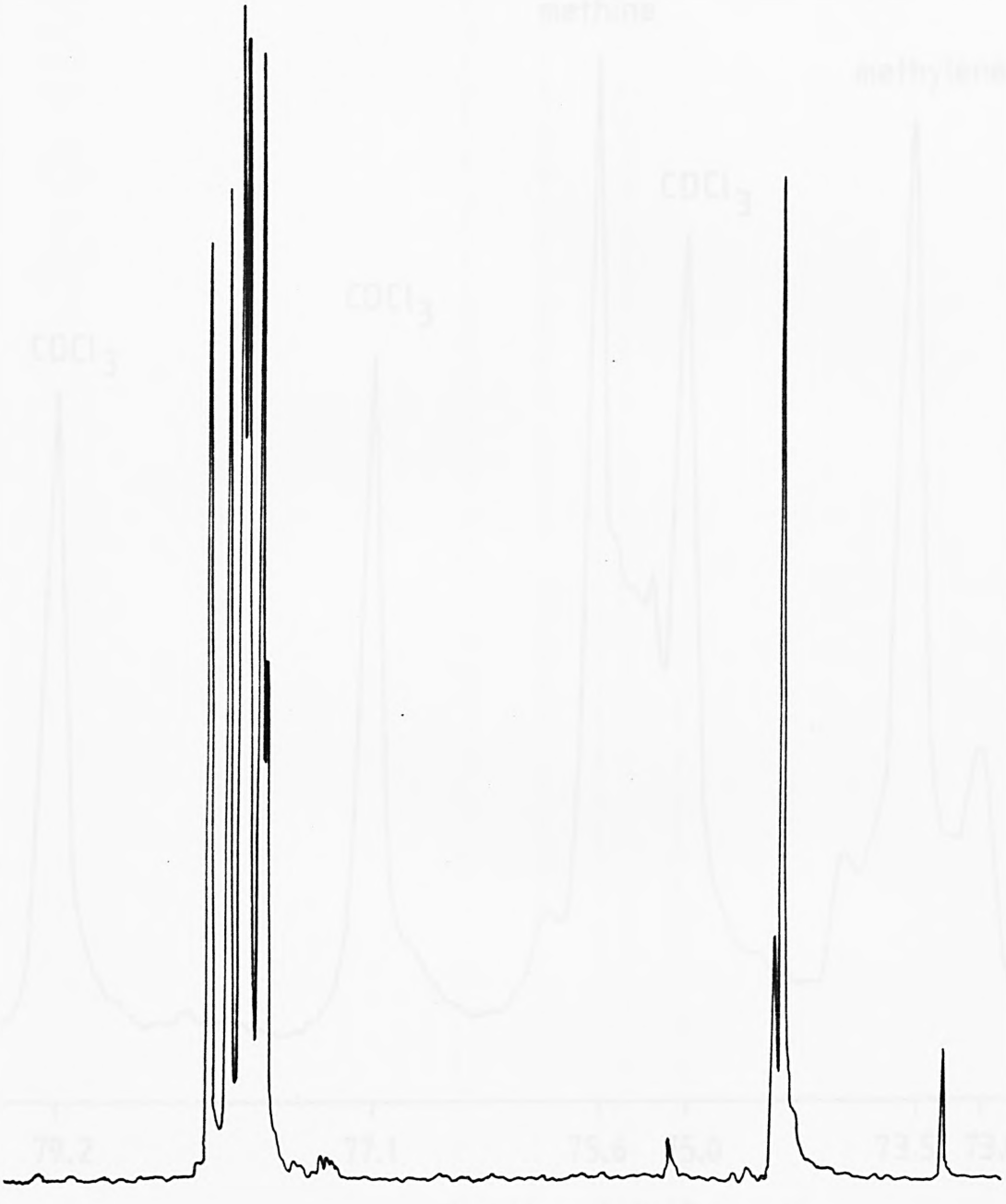

FIGURE 4.(20). ^{13}C Nmr Spectrum of the Amorphous Polypropylene Oxide Polymer.

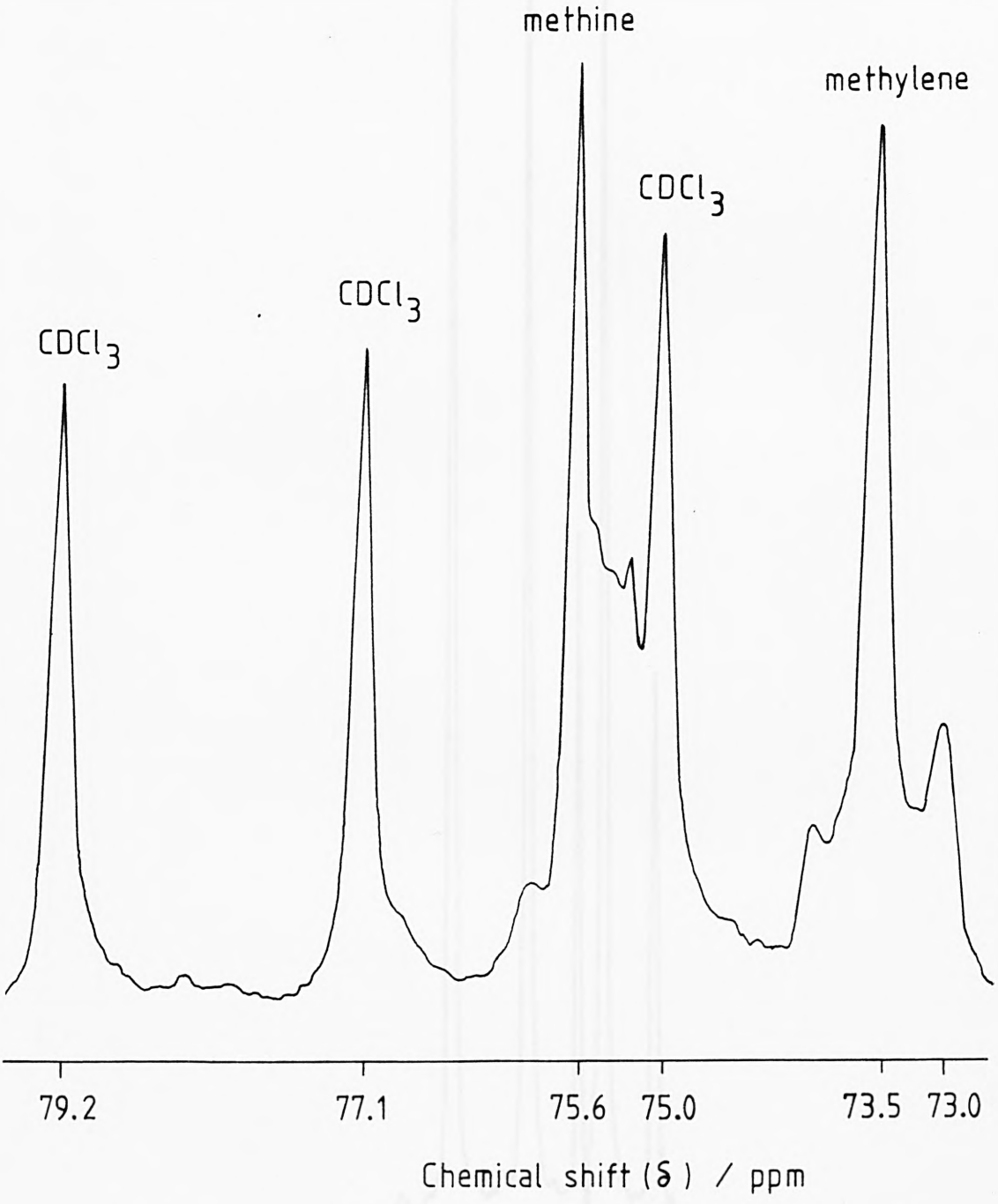

FIGURE 4.(21).(a). Expanded ^{13}C Nmr Spectrum of the Methylene and Methine Carbons of Crude Polypropylene Oxide.

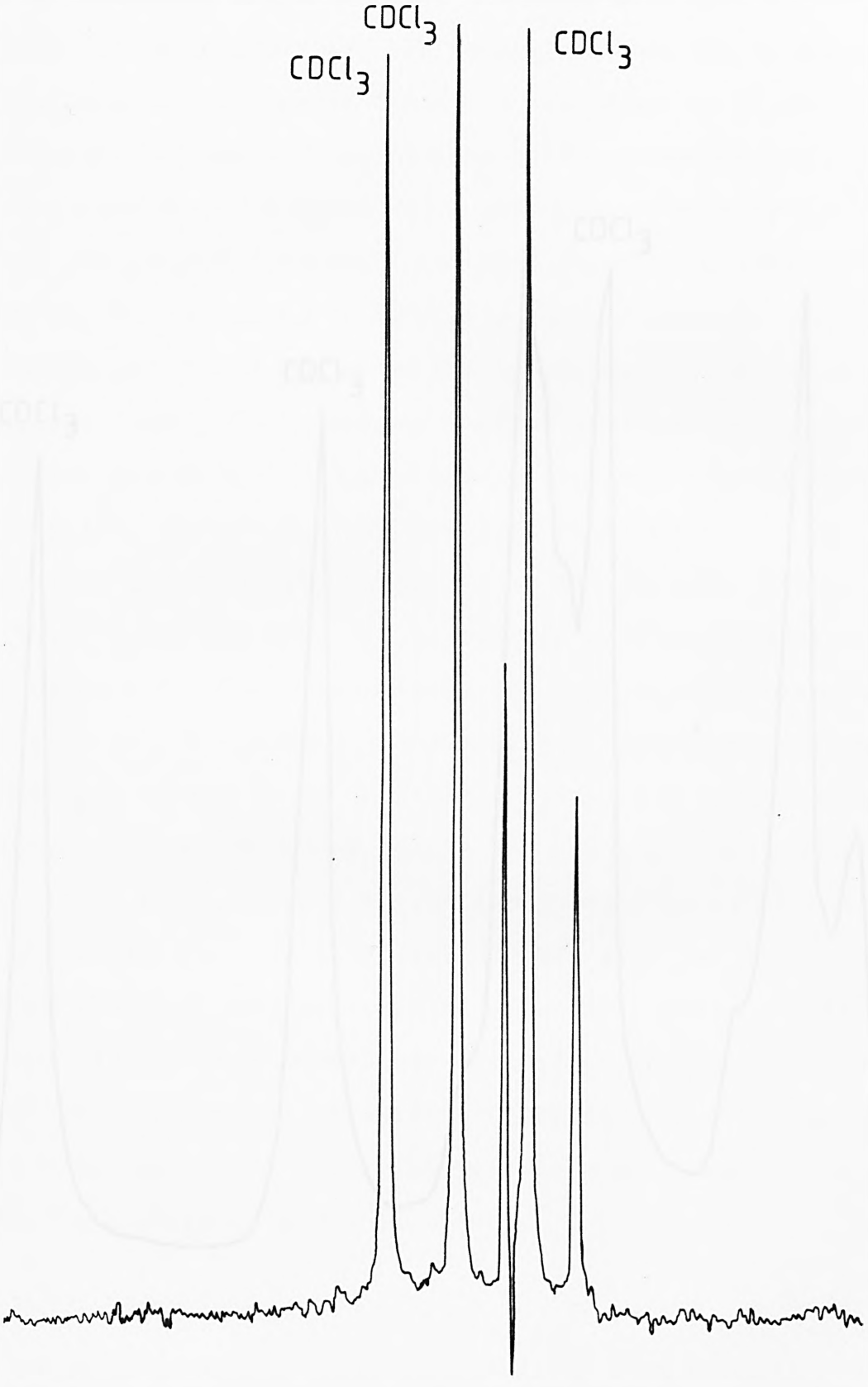

FIGURE 4.(21).(b). Expanded ^{13}C Nmr Spectrum of the Methylene and Methine Carbons of Crystalline Polypropylene Oxide.

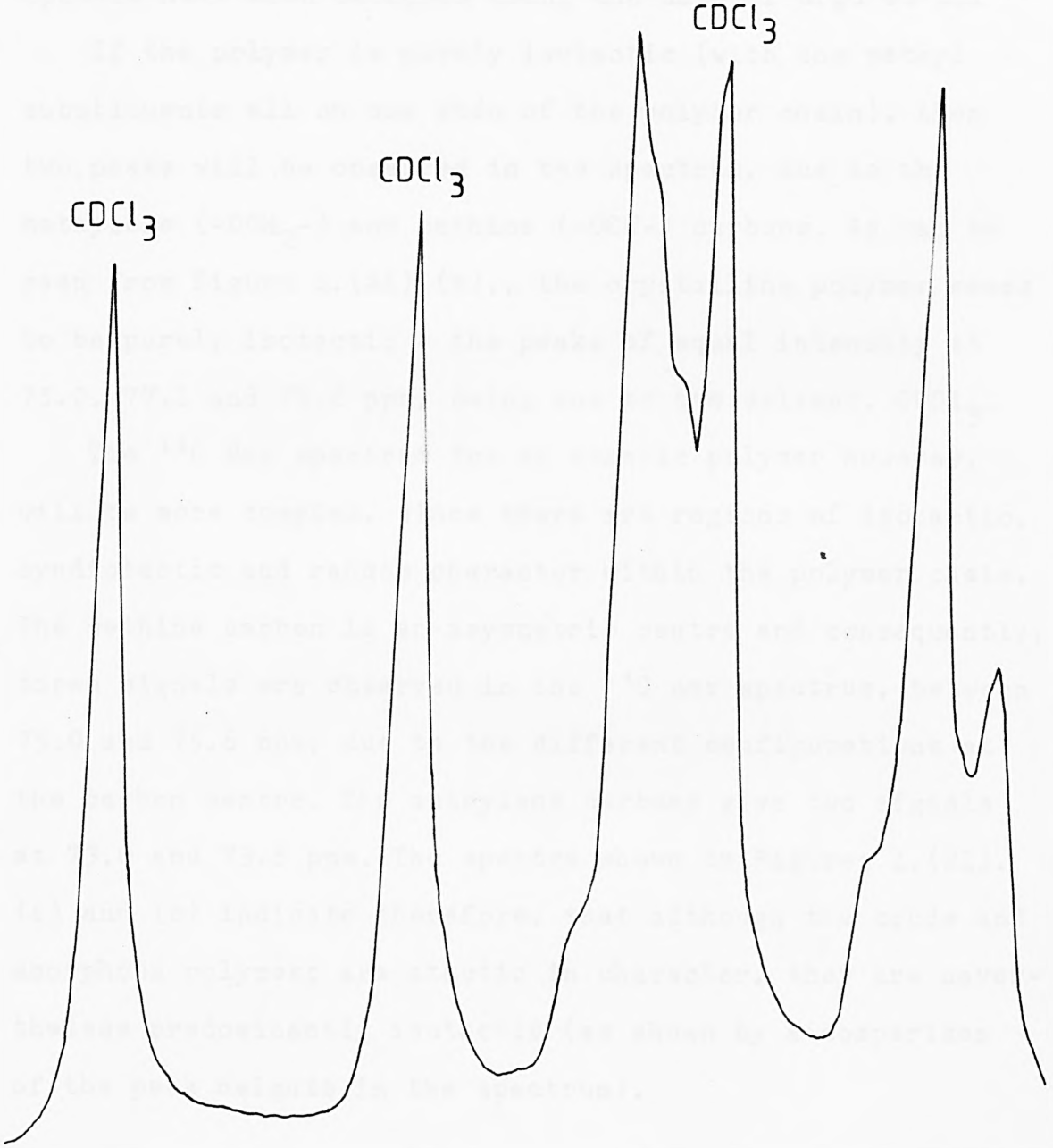

FIGURE 4.(21).(c). Expanded ^{13}C Nmr Spectrum of the Methylene and Methine Carbons of Amorphous Polypropylene Oxide.

By expanding the multiplet, the fine structure on the signals can be studied and the expansions for the crude, crystalline and amorphous fractions are shown in Figures 4.(21).(a), (b) and (c) respectively. The peaks in the spectra have been assigned using the data of Urgu et al.[24].

If the polymer is purely isotactic (with the methyl substituents all on one side of the polymer chain), then two peaks will be observed in the spectrum, due to the methylene ($-OCH_2-$) and methine (-OCH-) carbons. As can be seen from Figure 4.(21).(b)., the crystalline polymer seems to be purely isotactic - the peaks of equal intensity at 75.0. 77.1 and 79.2 ppm, being due to the solvent, $CDCl_3$.

The ^{13}C Nmr spectrum for an atactic polymer however, will be more complex, since there are regions of isotactic, syndiotactic and random character within the polymer chain. The methine carbon is an asymmetric centre and consequently, three signals are observed in the ^{13}C nmr spectrum, between 75.0 and 75.6 ppm, due to the different configurations at the carbon centre. The methylene carbons give two signals at 73.0 and 73.5 ppm. The spectra shown in Figures 4.(21). (a) and (c) indicate therefore, that although the crude and amorphous polymers are atactic in character, they are nevertheless predominantly isotactic (as shown by a comparison of the peak heights in the spectrum).

4.2.(4). Summary.

The polymerisation of propylene oxide with a variety of Sn(II) catalysts was studied and the results obtained, compared with those achieved using $FeCl_3$ and KOH, the catalysts cited in the literature[3,4,6,8]. In most cases, the tin(II) compounds performed well in comparison with the

standards, yielding polymers after relatively short polymerisation times, with large molecular weights and high proportions of crystalline polymer. Nmr studies confirm the presence of the oxypropylene repeating unit in the polymer chain and infrared and Mössbauer spectroscopy studies lead to the conclusion that a tin containing moiety of the catalyst, favours the formation of the crystalline polymer, whilst the anion associated with the tin compound favours the formation of the amorphous fraction.

Possible mechanisms for the formation of polypropylene oxide are outlined below:-

(I)

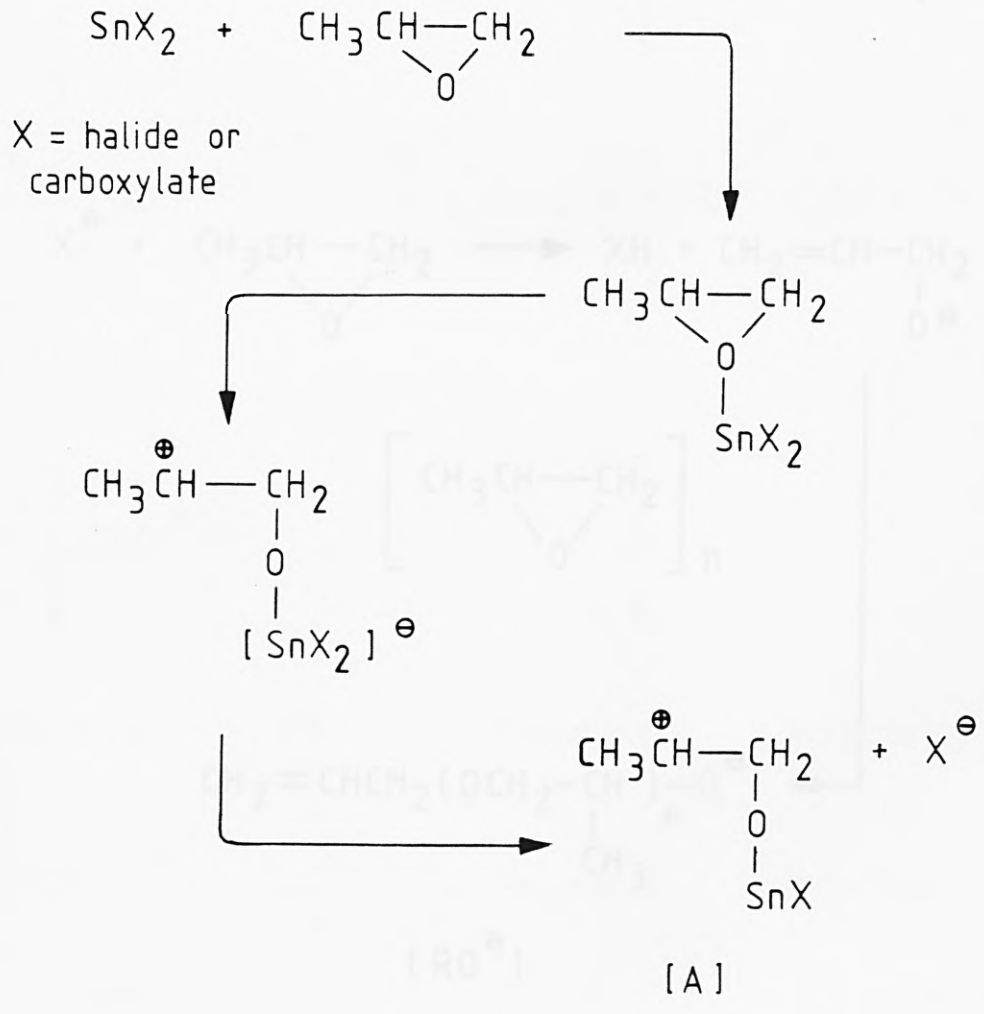

[A]

(II)

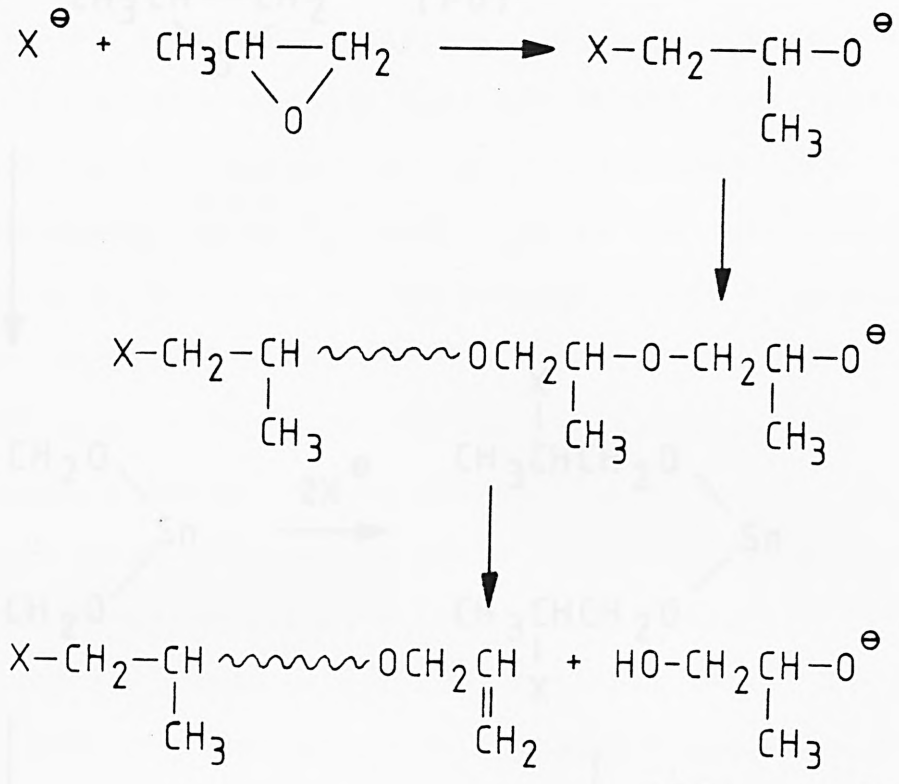

(III)

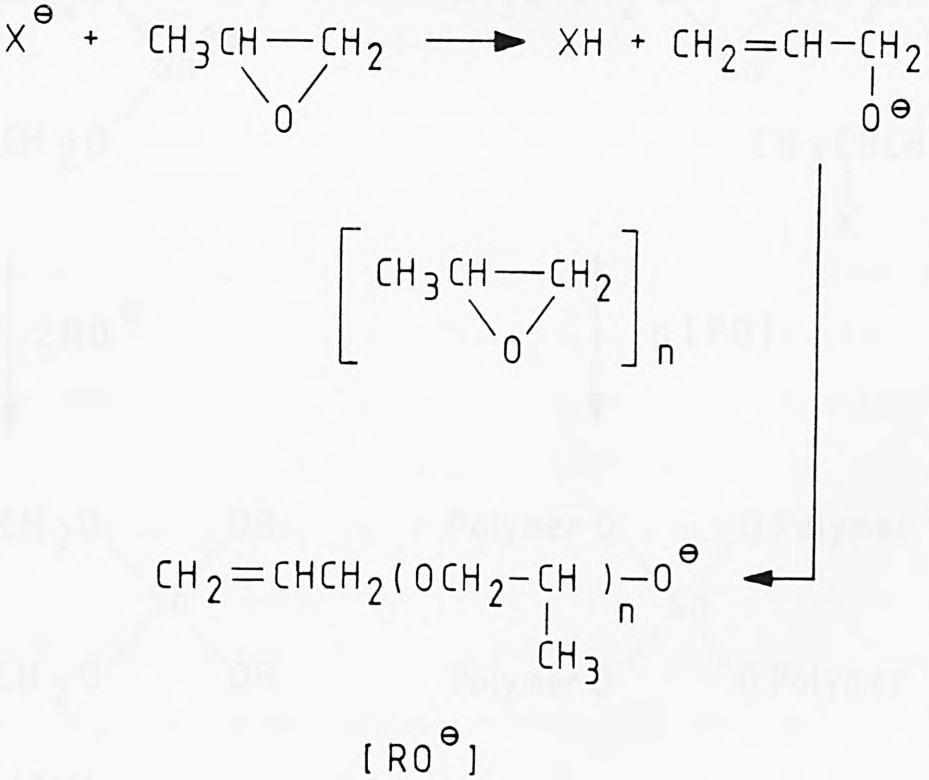

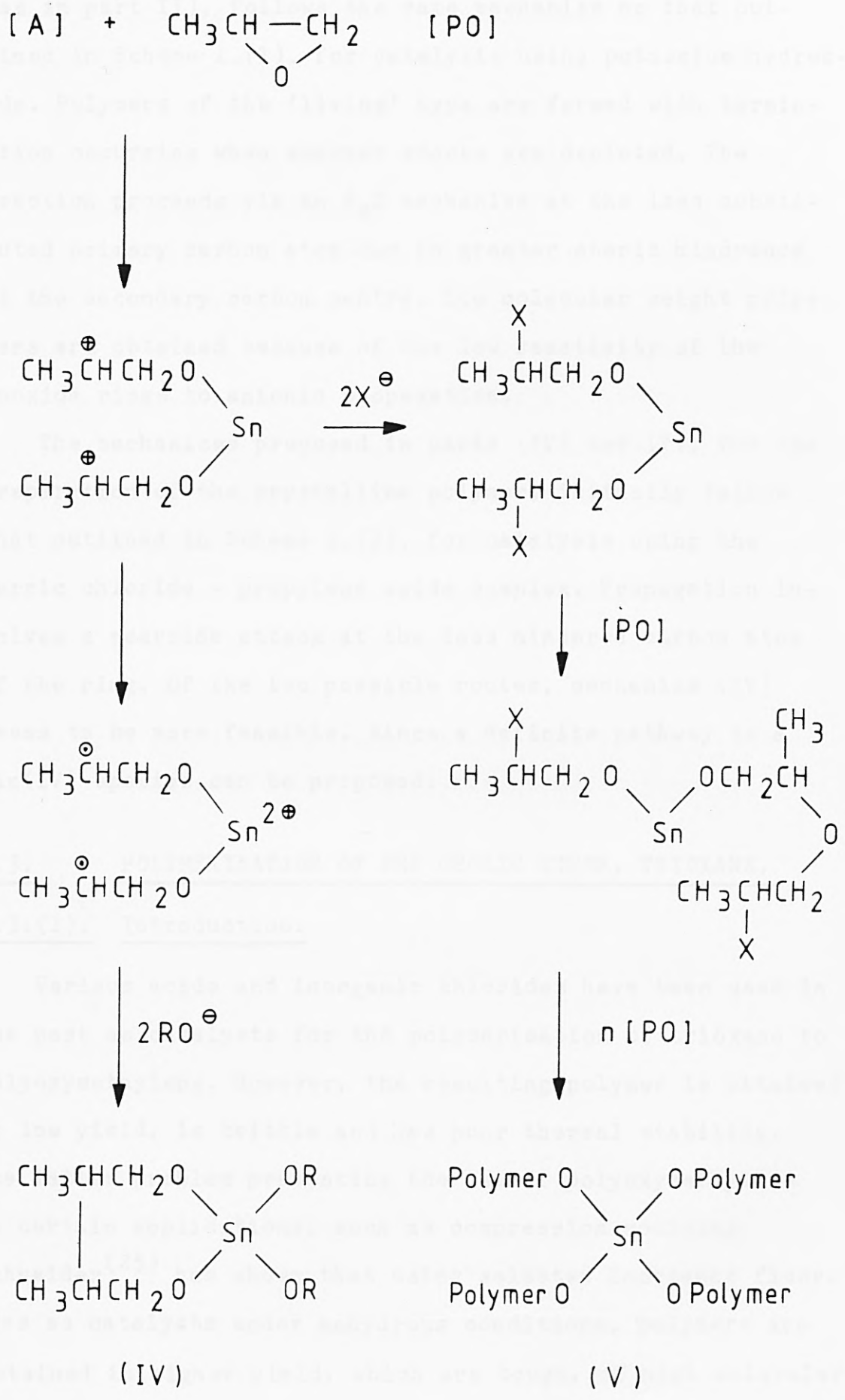
[A] + CH3CH—CH2 [PO]
O
CH3CHCH2O
Sn
2X⊖
X
[PO]
2RO⊖
n [PO]
Polymer O
O Polymer
(IV)
(V)

The formation of the amorphous polymer by the anion X^- (as in part II), follows the same mechanism as that outlined in Scheme 4.(1). for catalysis using potassium hydroxide. Polymers of the 'living' type are formed with termination occurring when monomer stocks are depleted. The reaction proceeds via an S_N2 mechanism at the less substituted primary carbon atom due to greater steric hindrance at the secondary carbon centre. Low molecular weight polymers are obtained because of the low reactivity of the epoxide rings to anionic propagation.

The mechanisms proposed in parts (IV) and (V), for the preparation of the crystalline polymer, initially follow that outlined in Scheme 4.(2). for catalysis using the ferric chloride - propylene oxide complex. Propagation involves a rearside attack at the less hindered carbon atom of the ring. Of the two possible routes, mechanism (IV) seems to be more feasible, since a definite pathway to a tin(IV) species can be proposed.

4.3. POLYMERISATION OF THE CYCLIC ETHER, TRIOXANE.

4.3.(1). Introduction.

Various acids and inorganic chlorides have been used in the past as catalysts for the polymerisation of trioxane to polyoxymethylene. However, the resulting polymer is obtained in low yield, is brittle and has poor thermal stability. The latter problem preventing the use of polyoxymethylene in certain applications, such as compression moulding. Schneider[25] has shown that using selected inorganic fluorides as catalysts under anhydrous conditions, polymers are obtained in higher yield, which are tough, of high molecular

weight and capable of being oriented and compression moulded. These inorganic fluoride catalysts include, SbF_3, BiF_3, NiF_2, AlF_3, TiF_4, MnF_2, HgF_2, AgF_2, ZnF_2, PF_5 and HF. Of these, the trivalent metal fluorides are particularly good catalysts. Antimony trifluoride is preferred, since it gives the highest quality polymers.

More recently, the polymerisation of trioxane has been carried out in the presence of a catalyst complex[26], which consists of a metal carboxylate and an organic acid halide. Typically, zinc acetate, cadmium acetate, ferric acetate and zinc benzoate are used with acetyl chloride. The polymerisation can be carried out over a range of temperatures, but the preferred temperature is 125°C. These reactions are also best carried out under anhydrous conditions, since the presence of a small amount of water, decreases the molecular weight of the polymer produced.

In both cases, the polymerisation proceeds by a cationic reaction mechanism, based upon Friedel-Crafts type catalysis.

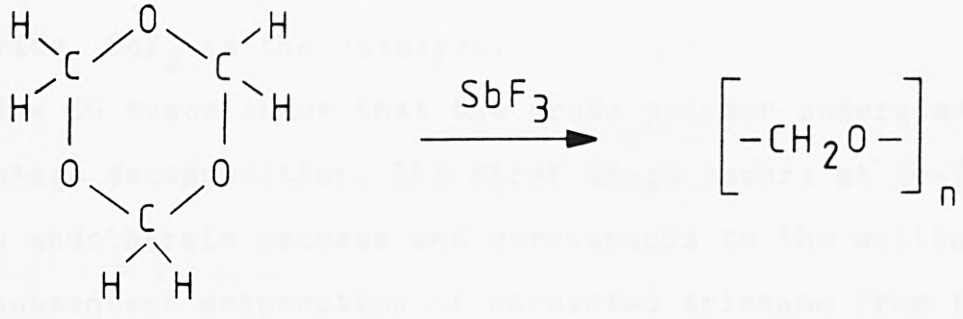

The aims of this work are to investigate the use of tin(II) halides and carboxylates in promoting the polymerisation of trioxane and to investigate the factors which affect the polymerisation.

4.3.(2). Experimental.

Trioxane (5.0g) recrystallised from methylene chloride (CH_2Cl_2), was placed in an ampoule with the tin(II) catalyst (0.05g) and where appropriate, acetyl chloride (0.2ml) was added. The ampoule was sealed and placed in an oven at 125°C for the duration of the experiment. Polyoxymethylene was obtained as a white solid powdery mass. The contents of the ampoules were characterised by simultaneous DTA/TG and by their X-ray diffraction, ^{119}Sn Mössbauer, infrared and ^{1}H nmr data. Yields of polymer were derived from the TG traces as a function of the percentage polymerisation. Compounds tested for their catalytic activity included the stannous carboxylates and halides.

4.3.(3). Results and Discussion.

4.3.(3).1. Thermal Analysis.

The simultaneous DTA and TG traces of the polymers were recorded on a Stanton Redcroft STA-780 Thermal Analyser. Figure 4.(22). shows the trace obtained when using stannous fluoride, SnF_2 as the catalyst.

The TG trace shows that the crude polymer undergoes a two stage decomposition. The first stage occurs at 46-78°C in an endothermic process and corresponds to the melting and subsequent evaporation of unreacted trioxane from the polymer mixture. The endothermic peak at 103°C, is due to the decomposition of the polyoxymethylene produced. From the trace, it can be deduced that about 72% of the polymer mixture consists of trioxane, i.e. the yield of polymer is about 28%.

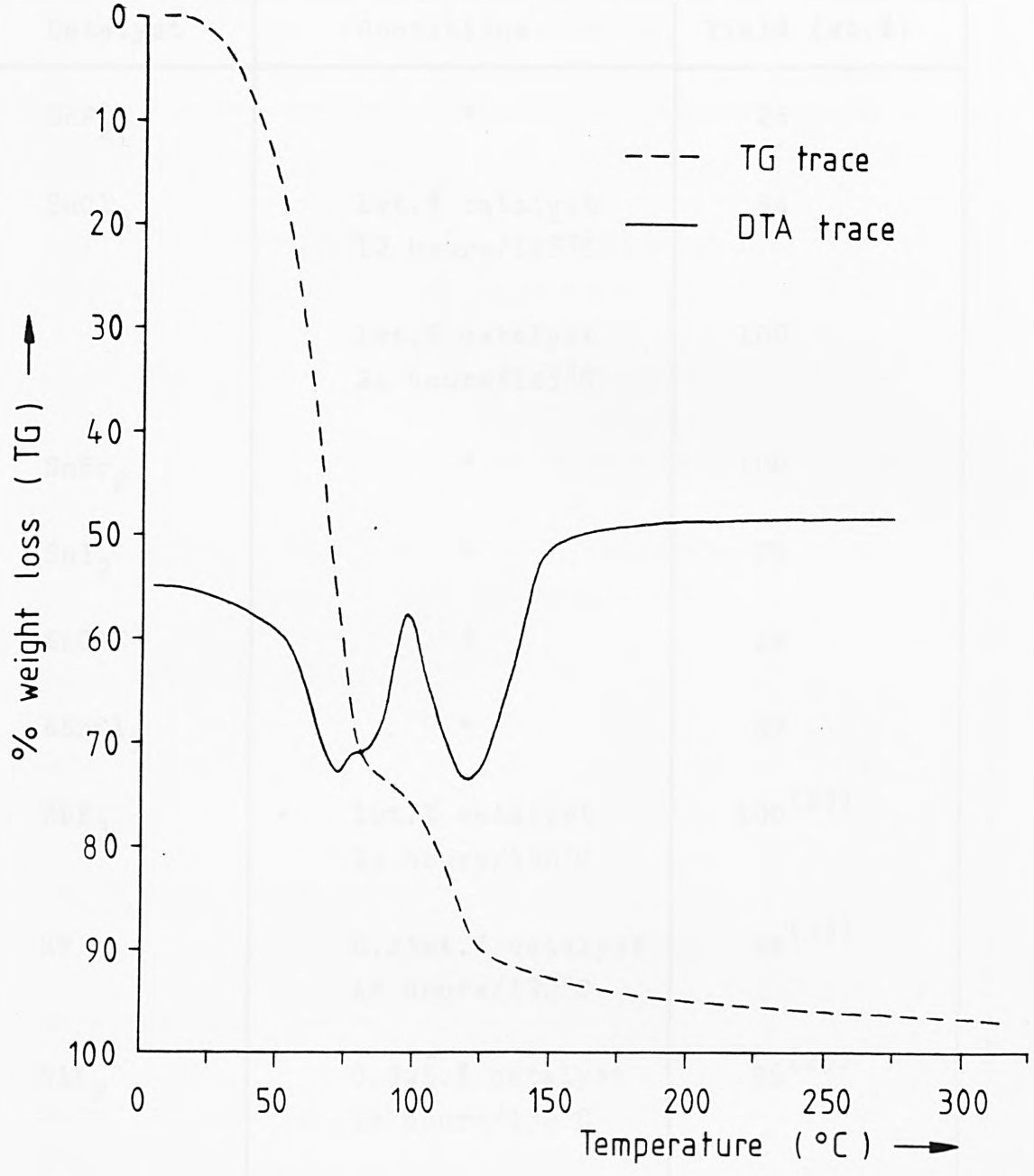

FIGURE 4.(22). DTA/TG Trace of Polyoxymethylene Obtained Using an SnF_2 Catalyst.

4.3.(3).2. Polymer Yield.

Tables 4.(14). and 4.(15). list the yields of polymer obtained from thermogravimetry. The results are expressed as a weight percentage of the total expected product weight from the polymerisation reactions, using a variety of tin (II) catalysts. The tables also contain the data obtained by Schneider[25] and Barton[26] for comparison.

Catalyst	Conditions	Yield (wt.%)
SnF_2	*	28
$SnCl_2$	1wt.% catalyst 12 hours/125°C	94
	1wt.% catalyst 24 hours/125°C	100
$SnBr_2$	*	100
SnI_2	*	75
SnClF	*	48
$KSnCl_3$	*	67
SbF_3	1wt.% catalyst 24 hours/130°C	100[25]
HF	0.25wt.% catalyst 48 hours/130°C	98[25]
NiF_2	0.5wt.% catalyst 48 hours/130°C	96[25]
MnF_2	1wt.% catalyst 48 hours/130°C	60[25]
ZnF_2	1wt.% catalyst 48 hours/130°C	97[25]

* Unless otherwise stated, conditions employed in the polymerisations are: 1wt.% catalyst, 48 hours/125°C.

TABLE 4.(14). Polymer Yields Obtained Using Inorganic Fluoride Catalysts.

Catalyst	Conditions	Yield (wt.%)
$Sn(CHOO)_2$	*	0
$Sn(CHOO)_2 + CH_3COCl$	1wt.% catalyst 4 hours/125°C	53
$Sn(CH_3COO)_2$	1wt.% catalyst 2wt.% catalyst 5wt.% catalyst	0 0 0
$Sn(CH_3COO)_2 + CH_3COCl$	1wt.% catalyst 4 hours/125°C	40
$CoSn_2(CH_3COO)_6.5H_2O$	*	0
$CoSn_2(CH_3COO)_6.5H_2O + CH_3COCl$	1wt.% catalyst 4 hours/125°C	82
$Co(CH_3COO)_2 + CH_3COCl$	1wt.% catalyst 22 hours/40°C	16[26]
$MnSn_2(CH_3COO)_6.6H_2O$	*	0
$MnSn_2(CH_3COO)_6.6H_2O + CH_3COCl$	1wt.% catalyst 4 hours/125°C	90
$NiSn_2(CH_3COO)_6.5H_2O$	*	0
$NiSn_2(CH_3COO)_6.5H_2O + CH_3COCl$	1wt.% catalyst 4 hours/125°C	87
$Ni(CH_3COO)_2 + CH_3COCl$	1wt.% catalyst 22 hours/40°C	12[26]
$ZnSn_2(CH_3COO)_6.6H_2O$	*	0
$ZnSn_2(CH_3COO)_6.6H_2O + CH_3COCl$	1wt.% catalyst 4 hours/125°C	100

(Table 4.(15). continued over)

Catalyst	Conditions	Yield (wt.%)
$Zn(CHOO)_2$ + CH_3COCl	1wt.% catalyst 21 hours/40°C	60[26]
$PbSn_2(CH_3COO)_6$	*	0
$PbSn_2(CH_3COO)_6$ + CH_3COCl	1wt.% catalyst 4 hours/40°C	75
SnC_2O_4	*	0
SnC_2O_4 + CH_3COCl	1wt.% catalyst 21 hours/40°C	91[26]
Sn Octoate	*	12
CH_3COCl	0.2ml catalyst 12 hours/125°C	74

* In each case unless otherwise stated, conditions used for the polymerisations were as follows:- 1wt.% catalyst at 125°C for 24 hours and where appropriate, with 0.2ml acetyl chloride added.

TABLE 4.(15). Polymer Yields Obtained Using Carboxylate Catalysts.

Antimony trifluoride was considered to be the most efficient catalyst for this system by Schneider[25]. He found that 100% polymerisation was obtained using 1wt.% catalyst in a 7 hour reaction at 125°C. The tin(II) halides studied in this present work, are found to have a comparable activity or to be slightly less active than antimony trifluoride. Stannous chloride and bromide give 100% polymerisations, SnI_2, SnClF and $KSnCl_3$ are less efficient, giving between 48% and 75% polymerisation. Tin(II) fluoride

was found to be the least active of all the halides (cf. results obtained for the polypropylene oxide system, in Section 4.2.(3).1.).

Both the normal salts and the transition metal complex derivatives of the tin(II) carboxylates, are found to be inactive in this system, even when the catalyst concentration is increased to 5wt.% (see Table 4.(15).). A dramatic increase in the activity of the carboxylates is however noted when a small amount ($\leqslant 2\%$) of acetyl chloride is added to the reaction mixture containing 1wt.% catalyst. Polymer yields of between 40wt.% and 100wt.% are obtained. It is interesting to note, that these high polymer yields in the mixed tin(II) carboxylate - acetyl chloride system are obtained after only 4 hours. Use of acetyl chloride alone as a catalyst, results in a 74% polymerisation after 12 hours. The activities of the catalysts follow the order,

$$\begin{matrix}\text{Sn(II) carboxylate} \\ + \\ \text{Acetyl chloride}\end{matrix} \quad >> \quad \begin{matrix}\text{Acetyl} \\ \text{chloride}\end{matrix} \quad >>> \quad \begin{matrix}\text{Stannous} \\ \text{carboxylate}\end{matrix} \quad = 0$$

and provide evidence for the operation of a synergistic effect, which makes the acetyl chloride / stannous carboxylate mixture more efficient than either component of the mixture separately.

A comparison of the polymer yields obtained for cobalt acetate and nickel acetate[26] with the corresponding transition metal tricarboxylatostannates(II), shows that the presence of tin in the catalyst, increases the activity considerably. The yields of 16 and 12wt.% polymerisation respectively, achieved with Co and Ni acetates, increase to 82 and 87wt.% respectively, for $CoSn_2(CH_3COO)_6.5H_2O$ and $NiSn_2(CH_3COO)_6.6H_2O$.

4.3.(3).3. X-Ray Powder Diffraction Studies.

The X-ray powder diffraction data (Table 4.(16).) for both trioxane and the polyoxymethylene products, were obtained using 11.64cm cameras and CuK_{α} radiation. The X-ray diffractograms are reproduced in Figure 4.(23).

Trioxane		Polyoxymethylene	
2θ	I	2θ	I
8.0	15.7	8.0	12.0
9.4	13.8	9.5	12.4
16.9	8.4		
18.6	100.0		
20.2	13.4		
		22.8	100.0
23.7	91.0		
30.5	4.2		
32.9	67.8		
		34.8	41.5
36.0	6.7		
38.0	73.5		
		40.1	3.9
41.2	14.8		
44.5	17.1		
45.4	7.1	45.5	2.3
		48.0	14.5
49.6	5.6		
51.0	5.8		
53.4	9.8	53.8	6.4

TABLE 4.(16). X-Ray Powder Diffraction Data for Trioxane and Polyoxymethylene.

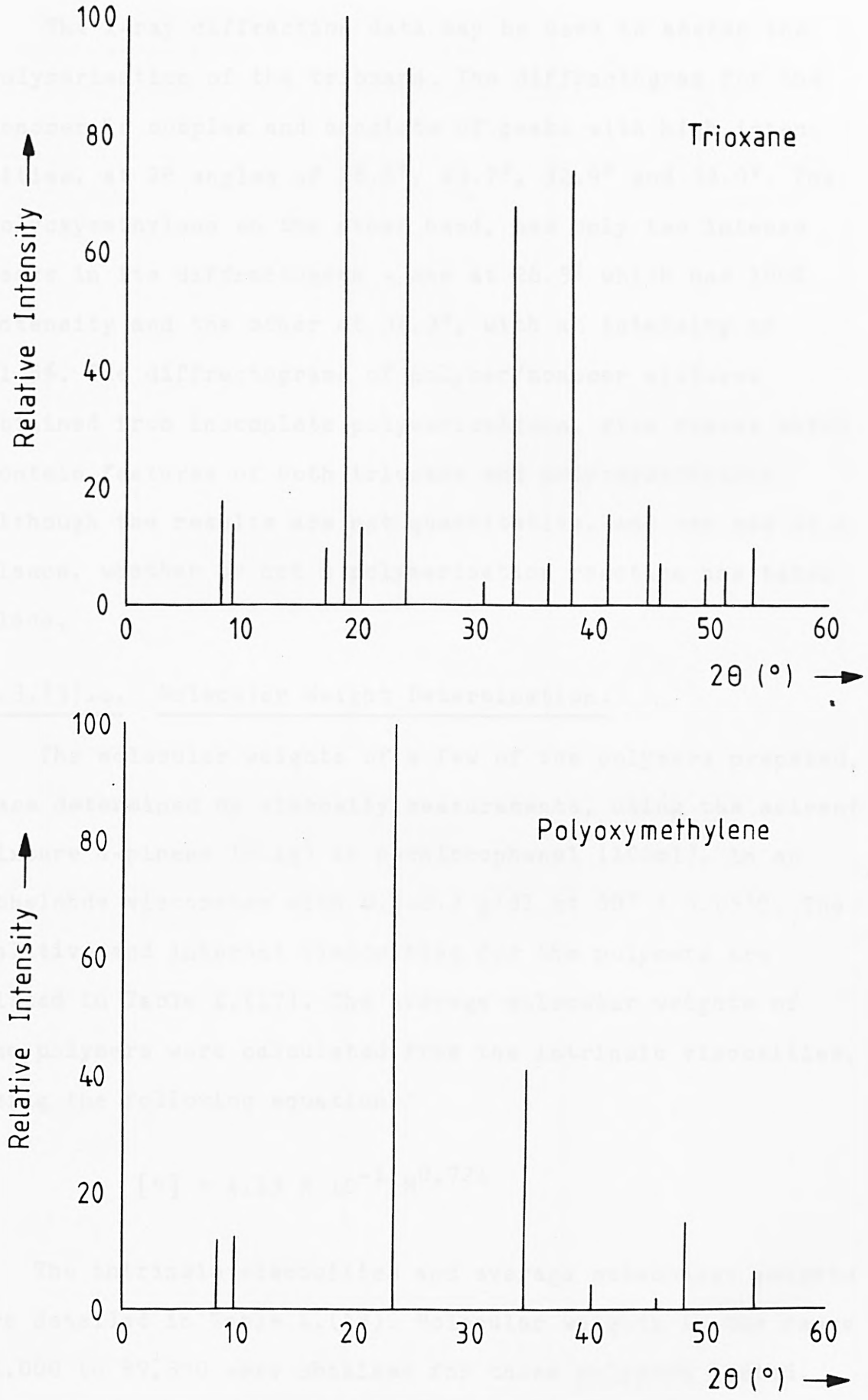

FIGURE 4.(23). X-Ray Diffractograms for Trioxane and Polyoxymethylene.

The X-ray diffraction data may be used to assess the polymerisation of the trioxane. The diffractogram for the monomer is complex and consists of peaks with high intensities, at 2θ angles of 18.6°, 23.7°, 32.9° and 38.0°. The polyoxymethylene on the other hand, has only two intense peaks in its diffractogram - one at 26.5° which has 100% intensity and the other at 34.3°, with an intensity of 41.5%. The diffractograms of polymer/monomer mixtures obtained from incomplete polymerisations, give traces which contain features of both trioxane and polyoxymethylene. Although the results are not quantitative, one can see at a glance, whether or not a polymerisation reaction has taken place.

4.3.(3).4. Molecular Weight Determination.

The molecular weights of a few of the polymers prepared, were determined by viscosity measurements, using the solvent mixture α-pinene (0.4g) in p-chlorophenol (100ml), in an Ubbelohde viscometer with 0.2-0.3 g/dl at 60° ± 0.05°C. The relative and inherent viscosities for the polymers are listed in Table 4.(17). The average molecular weights of the polymers were calculated from the intrinsic viscosities, using the following equation:

$$[\eta] = 4.13 \times 10^{-4} M^{0.724}$$

The intrinsic viscosities and average molecualar weights are detailed in Table 4.(18). Molecular weights in the range 71,000 to 87,300 were obtained for those polymers tested. Molecular weights for polyoxymethylene cited in the literature, vary between 30,000 and 130,000[27,28].

Polymerisation Catalyst	Polymer Concn. (g/100ml)	η_{rel}	η_{inh}
CH_3COCl	0.3358	1.011	1.102
	0.2849	1.005	1.261
	0.2655	1.003	1.329
$Sn(CH_3COO)_2$ + CH_3COCl	0.2240	1.010	1.510
	0.2522	1.016	1.390
	0.2350	1.013	1.460
$NiSn_2(CH_3COO)_6.5H_2O$ + CH_3COCl	0.2498	1.018	1.405
	0.2450	1.014	1.420
	0.2390	1.011	1.435

TABLE 4.(17). Relative and Inherent Viscosities for Polyoxymethylene.

Polymerisation Catalyst	Intrinsic Viscosity	Average Mol. Wt.
CH_3COCl	1.35	71,500
$Sn(CH_3COO)_2$ + CH_3COCl	1.56	87,300
$NiSn_2(CH_3COO)_6.5H_2O$ + CH_3COCl	1.49	81,900

TABLE 4.(18). Intrinsic Viscosities and Average Molecular Weights for Polyoxymethylene.

4.3.(3).5. Infrared Analysis.

The infrared spectra of the polyoxymethylene samples prepared, were obtained as KBr discs. All of the polymers gave identical spectra, regardless of the catalyst system used. The infrared data are shown in Table 4.(19)., with spectral assignments according to Novak[29] and Tadokoro[30].

Absorption Frequency (cm^{-1})	Assignment
2980 2920	-CH stretch
1470	$-CH_2$ bending
1435 1385	$-CH_2$ wagging
1240	C-O and CH_2 rocking
1140-1090	C-O stretch
990-900	C-O stretch and $-CH_2$ rocking
633	C-O bending
458	C-O bending

TABLE 4.(19). Infrared Data and Spectral Assignment for Polyoxymethylene.

4.3.(3).6. Mössbauer Spectroscopy.

The Mössbauer spectra of some of the polymers prepared, were recorded. Table 4.(20). lists the parameters obtained

and compares them with those of the pure catalyst.

Catalyst	δ (mm/s)	Δ (mm/s)	Polymer δ (mm/s)
SnF_2	3.60	1.80	-0.02
$SnCl_2$	4.07	0.0	-0.05
$SnBr_2$	3.93	0.0	0.13
SnI_2	3.85	0.0	-0.03
SnClF	3.68	1.10	-0.08
$KSnCl_3$	3.71	0.77	0.06
SnC_2O_4 (+ CH_3COCl)	3.70	1.54	0.09
$Sn(CH_3COO)_2$ (+ CH_3COCl)	3.21	1.77	0.09
$MnSn_2(CH_3COO)_6.5H_2O$ (+ CH_3COCl)	2.69	1.51	-0.04

TABLE 4.(20). Mössbauer Parameters of Tin(II) Compounds and of the Polymers Obtained Using them as Catalysts.

Without exception, the Mössbauer spectra of the polymers show a single Sn(IV) peak, with an isomer shift (-0.08 to 0.13 mm/s), which is characteristic of tin octahedrally surrounded by six oxygen atoms.

4.3.(4). Mechanisms for the Formation of Polyoxymethylene.

A mechanism can be postulated which involves the cationic polymerisation of trioxane. This mechanism is analagous to that which occurs during the tin catalysed polymerisation of propylene oxide.

The mechanism of the polymerisation must involve an initiation stage, a propagation step and a termination reaction. Three different types of catalyst were used in this study:- (i) acetyl chloride, (ii) tin(II) halides and (iii) a stannous carboxylate / acetyl chloride complex. The initiation stage varies according to the catalyst involved and arises from the following reactions-

I : Acetyl chloride.

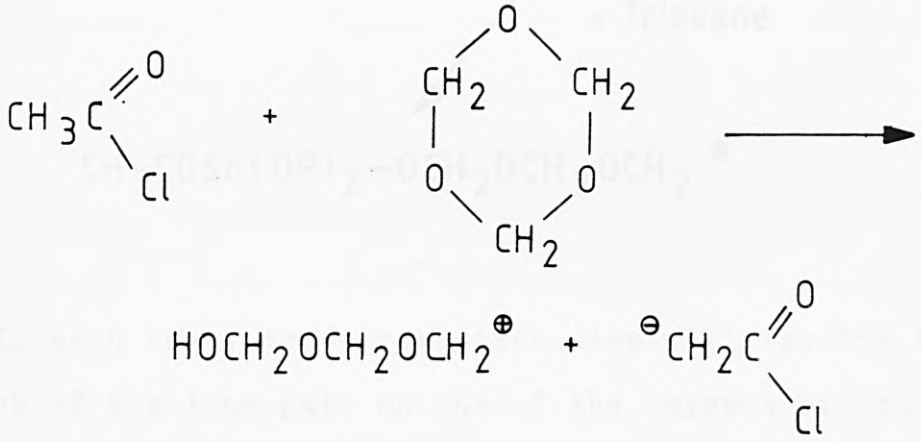

this is the classic type of cationic polymerisation, which involves the abstraction of a proton from the catalyst.

II : Tin(II) Halide.

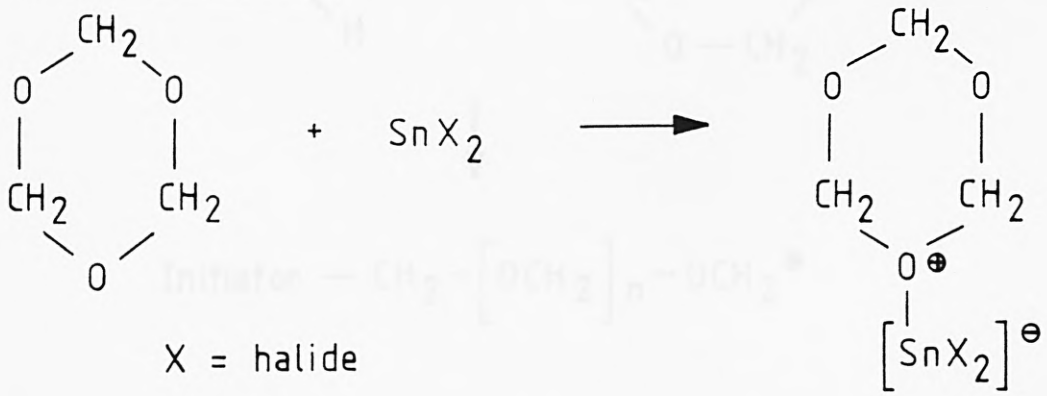

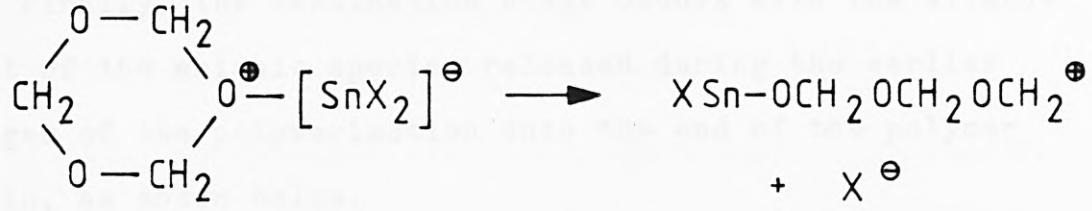

III : Stannous Carboxylate - Acetyl Chloride.

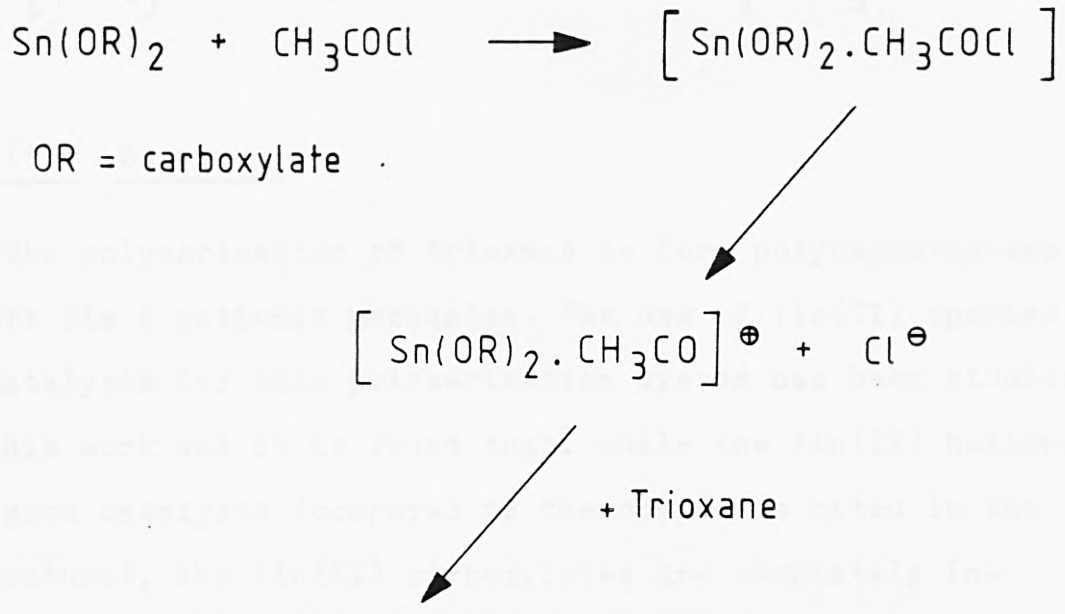

In each case, the propagation step will involve the attack of the lone pair on one of the oxygens of the trioxane onto the carbonium ion (C^+),

i.e.

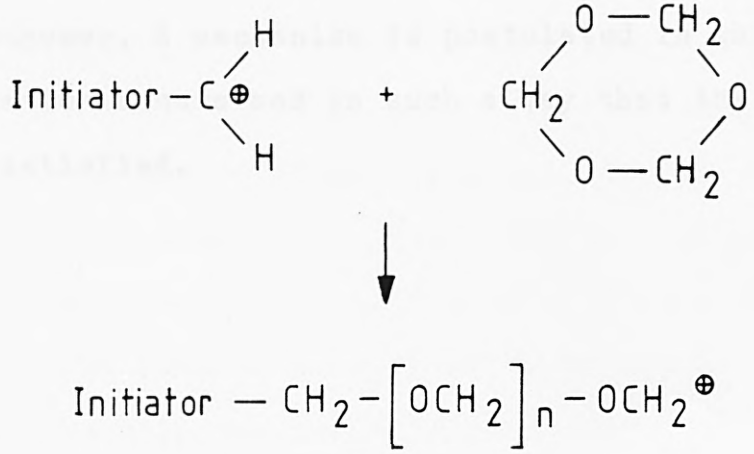

Finally, the termination stage occurs with the attachment of the anionic species released during the earlier stages of the polymerisation onto the end of the polymer chain, as shown below.

$$-\left[OCH_2\right]_n - OCH_2^{\oplus} + X^{\ominus} \longrightarrow -\left[OCH_2\right]_n OCH_2X$$

4.3.(5). Summary.

The polymerisation of trioxane to form polyoxymethylene occurs via a cationic mechanism. The use of tin(II) species as catalysts for this polymerisation system has been studied in this work and it is found that, while the tin(II) halides are good catalysts (compared to the compounds cited in the literature), the tin(II) carboxylates are completely inactive in catalysing the polymerisation of trioxane.

However, the activity of the carboxylates can be greatly enhanced if a small amount of acetyl chloride is added. This is probably due to the formation of a stannous carboxylate-acetyl chloride complex catalyst. The Sn(IV) peak in the Mössbauer spectra of the polymer, at about 0 mm/s, was attributed to a reaction occurring between the tin catalyst and the monomer. A mechanism is postulated in which cationic polymerisation occurs and in such a way that the Mössbauer data are satisfied.

4.4. THE CURING OF A SILICONE RESIN.

4.4.(1). Introduction.

A class of polymers of considerable commercial importance is based on a linear, cyclic or crosslinked arrangement of alternating silicon and oxygen atoms, where the silicon is substituted with organic groups or hydrogen. They are called organopolysiloxanes or simply silicone polymers and can be formulated as shown below:-

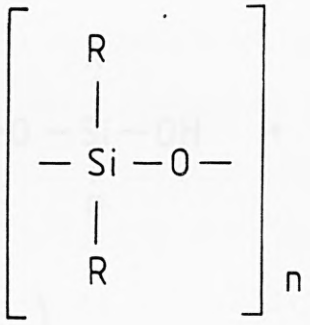

* The organic groups (R), can be alkyl, alkoxy or polyalkoxysiloxy groupings of varying sizes.

The usual procedure for preparing silicone polymers is to hydrolyse, either singly or in an appropriate combination compounds of the type:- R_3SiCl, R_2SiCl_2, $RSiCl_3$ and $SiCl_4$, depending upon the kind of product required. The intermediates in the reaction are believed to be the corresponding silanols (e.g. R_3SiOH) which condense very rapidly, with the elimination of water, to form the -Si-O-Si- link. Scheme 4.(3). shows an idealised route for two and three dimensional silicone polymer formation. In the case of trialkylchlorosilane, hydrolysis leads to a dimer, since this compound is only monofunctional. For this reason, R_3SiCl is often used as a terminator, to regulate the chain lengths of the silicone polymers produced.

Two dimensional polymer

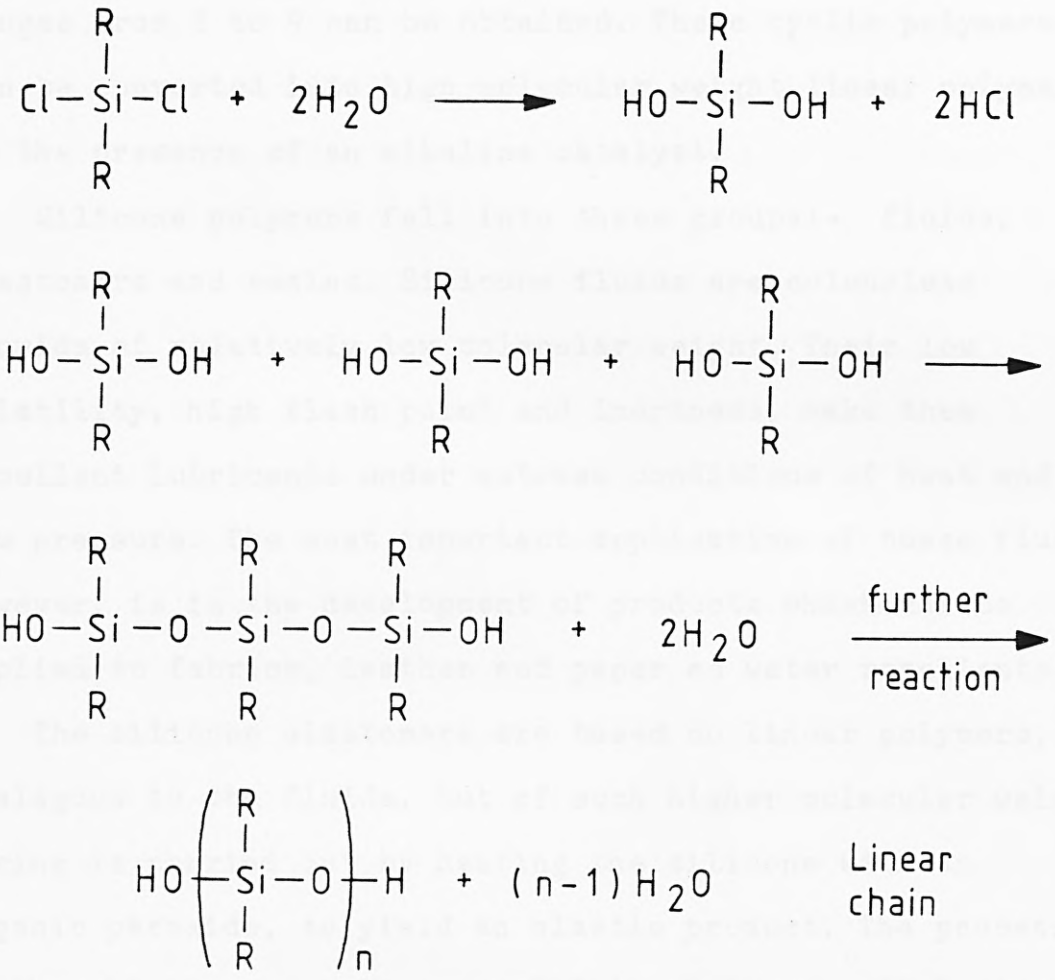

Three dimensional polymer

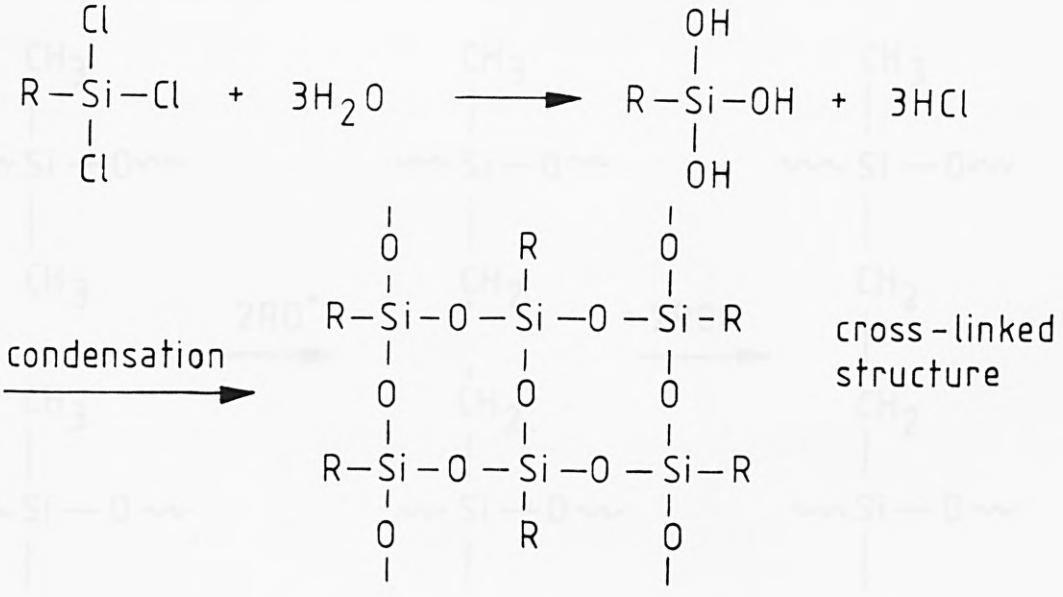

SCHEME 4.(3). Preparation of Two and Three Dimensional Silicone Polymers.

In addition to linear polymers, cyclic forms where n ranges from 3 to 9 can be obtained. These cyclic polymers can be converted into high molecular weight linear polymers in the presence of an alkaline catalyst.

Silicone polymers fall into three groups:- fluids, elastomers and resins. Silicone fluids are colourless liquids of relatively low molecular weight. Their low volatility, high flash point and inertness, make them excellent lubricants under extreme conditions of heat and low pressure. The most important application of these fluids however, is in the development of products which can be applied to fabrics, leather and paper as water repellents.

The silicone elastomers are based on linear polymers, analagous to the fluids, but of much higher molecular weight. Curing is carried out by heating the silicone with an organic peroxide, to yield an elastic product. The process is thought to occur via cross-linking between methyl groups of adjacent polymer chains, forming -Si-CH_2-CH_2-Si- links.

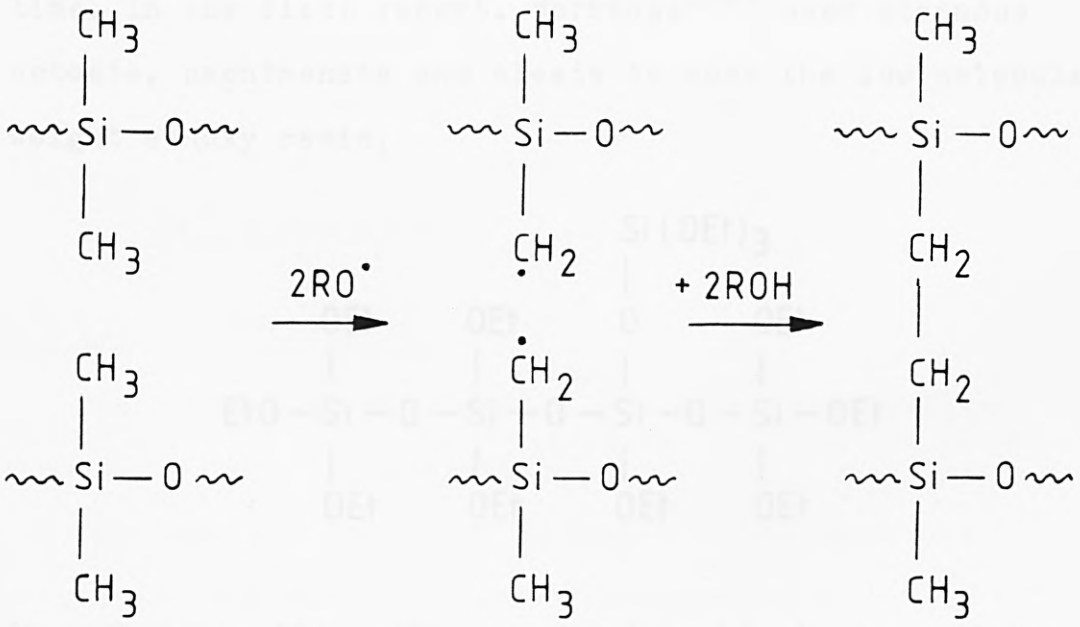

Silicone elastomers show remarkable stability at high temperatures, whilst retaining their elastic properties at low temperatures. They are also resistant to many chemicals, oils and weathering, but generally have poor resistance to hydrocarbon solvents.

Silicone resins have a three-dimensional branched chain structure. They are usually prepared by the hydrolysis of mixtures of the di- and tri-chlorosilanes and the degree of cross-linking is governed by the molar ratio of these two compounds (the greater the proportion of the trichloro-derivative, the greater the amount of cross-linking). Resins can vary in composition from very flexible materials, to hard, brittle glassy materials. As with the fluids, resins are highly water repellent, and their resistance to many organic solvents is poor.

4.4.(2). Scope of This Work.

A review of the literature shows that the use of tin(II) carboxylates as curing catalysts has been known for some time. In the first report, Berridge[31] used stannous octoate, naphthenate and oleate to cure the low molecular weight ethoxy resin,

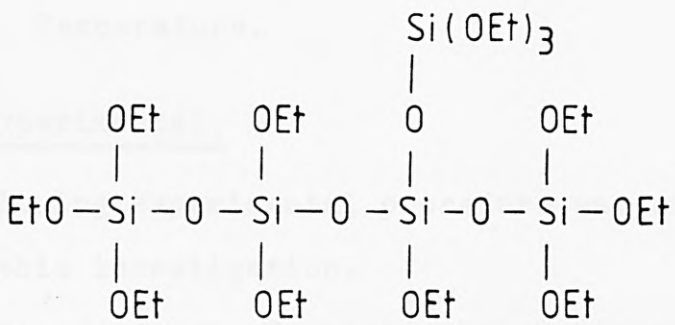

In each case, the resin was cured in 15 minutes and increasing the catalyst concentration, apparently did not

decrease the cure time. The activity of stannous octoate was compared with those of other metal octoates (e.g. Pb, Sb, Fe and Ti) and without exception, the tin catalyst performed far better.

Stannous octoate was also used to cure dimethylpolysiloxane fluids[32], 2 wt.% catalyst cured the fluid in 30 minutes, producing an elastomer which can be stretched or deformed, but which reverts to its original cured shape. The cure of this fluid has also been catalysed by higher tin(II) carboxylates[33]: stannous neodecanoate also gave a 30 minute cure, but required 10 wt.% catalyst to do so, while the use of stannous ricinoleate was accompanied by discolouration in the cured resin.

The results of this section of the thesis are from an investigation of the factors affecting the cure of a given silicone resin. The resin studied was a diorganopolysiloxane, but its exact composition was unknown, since the size and nature of the organic components was not revealed.

The parameters which were studied were as follows:

(a) The catalyst used.

(b) The catalyst concentration.

(c) The solvent used.

(d) Temperature.

4.4.(3). Experimental.

The following experimental procedure was utilised throughout this investigation.

The required amount of catalyst was weighed out accurately and dissolved in an appropriate quantity of solvent. When stannous octoate was used as the catalyst, the solvent acted as a dilutent. The catalyst mixture was

then added to the resin (5g), stirred for about 2-3 minutes and the time taken to obtain a hard cure noted. The uncured resin was a free-flowing, viscous gum which was grey in colour. On curing, a very hard, amorphous rubber was formed. The cured material was water repellent, resistant to acid and organic solvent attack and was thermally stable upto 600°C. The cure was assessed as being the point at which the resin would peel cleanly off the reaction vessel. At this stage, the resultant rubber could not be deformed or indented with applied pressure.

4.4.(4). Variation of the Catalyst Used.

The catalytic activity of a number of tin(II) compounds was tested. The results obtained are shown in Table 4.(21). along with the catalyst concentration and solvent utilised. All results were obtained at room temperature.

The tin(II) monocarboxylates were found to be fairly efficient catalysts in the curing of the silicone resin, although there was no obvious relationship between the cure time and the alkyl chain length. In general, the cure time increased dramatically when the tin compound was complexed and used as an alkali metal or transition metal derivative. The cure time for stannous acetate of 12 minutes for example is increased to between 3 and 6 hours when triacetato-stannate(II) complexes are used.

By far the most efficient catalyst studied was stannous octoate, a hard cure being obtained in 2 minutes using 0.025g catalyst. Unfortunately, with such a fast cure time, proper dispersion of the catalyst into the resin could not be attained and for this reason, methods of reducing the cure time for this particular catalyst were sought.

TABLE 4.(21). Effect of Catalyst on the Cure Time.

Catalyst	Conditions	Cure Time
$Sn(HCOO)_2$	0.1g in 1.0ml ethylene glycol	Overnight
$Zn_4Sn_3(HCOO)_{14}.8H_2O$	0.5g in 1.0ml propylene glycol	30 mins.
$Sn(CH_3COO)_2$	0.25g in 0.2ml propylene glycol	12 mins.
$NaSn(CH_3COO)_3$	0.25g in 0.5ml propylene glycol	6 hours
$KSn(CH_3COO)_3$	0.25g in 0.5ml propylene glycol	6 hours
$MnSn_2(CH_3COO)_6$	0.1g in 0.5ml propylene glycol	6 hours
$CoSn_2(CH_3COO)_6$	0.1g in 0.5ml propylene glycol	5 hrs.40 mins
$ZnSn_2(CH_3COO)_6.6H_2O$	0.5g in 0.5ml propylene glycol	3 hours
$Sn(CH_3CH_2COO)_2$	0.3g in 0.5ml propylene glycol	40 mins.
$Sn(CH_3CH_2COO)_2.$ CH_3CH_2COOH	0.1g in 0.5ml propylene glycol	1 hr.20 mins.
Sn Hexanoate	0.2g in 0.5ml propylene glycol	30 mins.
Sn Octoate	0.025g in 0.25ml propylene glycol	2 mins.
Sn Hexanoate / Sn Octoate	0.06g + 0.03g in 0.3ml propylene glycol	30 mins.

TABLE 4.(21). (contd.)

Catalyst	Conditions	Cure Time
Sn Octoate / Mn Octoate	0.02g + 0.06g in 0.5ml propylene glycol	30 mins.
Sn Propylene-glycolate	0.05g in 1.0ml propylene glycol	Overnight
SnC_2O_4	0.025g in 1.0ml propylene glycol	No cure
Sn Malonate	0.1g in 1.0ml propylene glycol	No cure
Sn Maleate	0.1g in 1.0ml propylene glycol	No cure
SnO	0.5g in 1.0ml propylene glycol	No cure
$SnCl_2$	0.5g in 0.5ml propylene glycol	3.5 hours
$SnBr_2$	0.5g in 0.5ml propylene glycol	Overnight

* All cures were carried out using 5.0g silicone resin.

Two ways of doing this were considered:-

(i) mixing stannous octoate with stannous hexanoate

(ii) mixing stannous octoate with manganous octoate

Mixtures of tin(II) octoate with stannous hexanoate and manganous octoate in the ratios 1:2 and 1:3 respectively, give a cure in 30 minutes. For efficient industrial usage, 10 minute cures are reported to be ideal and this could be achieved with an Sn(II) octoate : Sn(II) hexanoate ratio of 1:0.6

To obtain a good cure the resin and catalyst must be efficiently mixed and problems can arise because of the volumes of solvent required to dissolve some catalysts - the resin is unable to accomodate large volumes of solvent. In general, unless the catalyst mixture was very viscous, 0.75ml was the maximum volume of material that could be properly mixed (by stirring) into 5g of resin.

It was interesting to note that the tin(II) dicarboxylates and tin(II) oxide were totally inactive in this system and that the activity of the stannous halides was low.

4.4.(5). The Effect of the Catalyst Concentration on the Cure Time.

Table 4.(22). shows the results obtained using different concentrations of catalyst to cure the resin, without exception, increasing the catalyst concentraion, decreases the cure time.

The performance of any catalyst may therefore be increased by increasing its concentration, provided that the solubility factors are not affected.

4.4.(6). The Effect of Varying the Solvent Used.

In this section, the effect of different solvents is described. Throughout this work, the solvents utilised were the glycols: ethylene glycol, propylene glycol and glycerol which all have viscosities similar to that of the resin. Table 4.(23). shows a selection of the results obtained.

It was found that the cure time is completely independent of the solvent used. This could be advantageous, since all the catalysts utilised (except stannous octoate) were solids and had to be dissolved in a suitable solvent prior

TABLE 4.(22). Effect of Catalyst Concentration on the Cure Time.

Catalyst	Concentration	Cure Time
$Zn_4Sn_3(HCOO)_2.8H_2O$	0.25g in 1.0ml propylene glycol	1 hour
	0.5g in 1.0ml propylene glycol	30 mins.
$Sn(CH_3COO)_2$	0.1g in 0.5ml propylene glycol	55 mins.
	0.2g in 0.5ml propylene glycol	20 mins.
	0.25g in 0.5ml propylene glycol	12 mins.
$NaSn(CH_3COO)_3$	0.25g in 0.5ml propylene glycol	6 hours
	0.5g in 0.5ml propylene glycol	2.5 hours
$CoSn_2(CH_3COO)_6$	0.05g in 0.5ml propylene glycol	>8 hours
	0.1g in 0.5ml propylene glycol	5.5 hours
	0.25g in 0.5ml propylene glycol	4 hours
$ZnSn_2(CH_3COO)_6$	0.25g in 0.5ml propylene glycol	7 hours
	0.5g in 0.5ml propylene glycol	3 hours

TABLE 4.(22). (contd.)

Catalyst	Conditions	Cure Time
$Sn(CH_3CH_2COO)_2$	0.2g in 0.5ml propylene glycol	55 mins.
	0.3g in 0.5ml propylene glycol	45 mins.
	0.6g in 0.5ml propylene glycol	30 mins.
Sn Hexanoate	0.2g in 0.5ml propylene glycol	1 hour
	0.5g in 0.5ml propylene glycol	35 mins.
	0.75g in 0.5ml propylene glycol	15 mins.
Sn Hexanoate / Sn Octoate	0.06g + 0.03g in 0.3ml propylene glycol	30 mins.
	0.06g + 0.06g in 0.3ml propylene glycol	20 mins.
	0.06g + 0.10g in 0.2ml propylene glycol	10 mins.

* All cures were carried out using 5.0g silicone resin.

TABLE 4.(23). Effect of Solvent on Cure Time.

Catalyst	Solvent	Cure Time
Sn Octoate (0.025g)	0.25ml ethylene glycol	2.5 mins.
	propylene glycol	2 mins.
	glycerol	2 mins.
	xylene	2 mins.
$Sn(CH_3COO)_2$ (0.25g)	0.50ml ethylene glycol	12 mins.
	propylene glycol	15 mins.
	glycerol	10 mins.
$KSn(CH_3COO)_3$ (0.25g)	0.50ml ethylene glycol	6 hours
	propylene glycol	7.25 hours
	glycerol	8.5 hours

* All cures were carried out using 5.0g silicone resin

to use. Knowing that solvent effects are negligible, means that the choice of the solvent can be based upon solubility, viscosity and economy.

Preliminary work using a parent acid solution of the tin(II) carboxylate has shown that similar cure times are also obtained.

4.4.(7). Effects of Temperature on the Cure Time.

Since the resins are often used in relatively low temperature applications, the effect of temperature on the curing of the silicone resin was assessed. The low temperature work was carried out at 2°C, with tin(II) octoate

the most efficient catalyst tested in this study. Table 4.(24). lists the results obtained and Figure 4.(24). displays them in a graphical form.

Whereas at room temperature, 0.025g stannous octoate caused a hard cure in 2 minutes, at 2°C, this amount of catalyst required more than 24 hours to effect a cure.

Stannous Octoate Concentration (g/0.4ml)	Cure Time
0.025	>24 hours
0.050	>12 hours
0.075	3 hours
0.100	80 mins.
0.200	55 mins.
0.300	40 mins.
0.400	25 mins.
0.500	20 mins.
0.700	10 mins.

* All cures were carried out using 5.0g silicone resin.

TABLE 4.(24). Effect of Reducing the Temperature to 2°C Upon the Cure Time, Using Stannous Octoate as the Catalyst.

Increasing the catalyst concentration caused an exponential decrease in the cure time (as shown in Figure 4.(24).), until at 0.7g tin(II) octoate, a 10 minute cure was obtained.

Thus, decreasing the temperature from room temperature to 2°C, caused a 30 fold decrease in the activity of the catalyst.

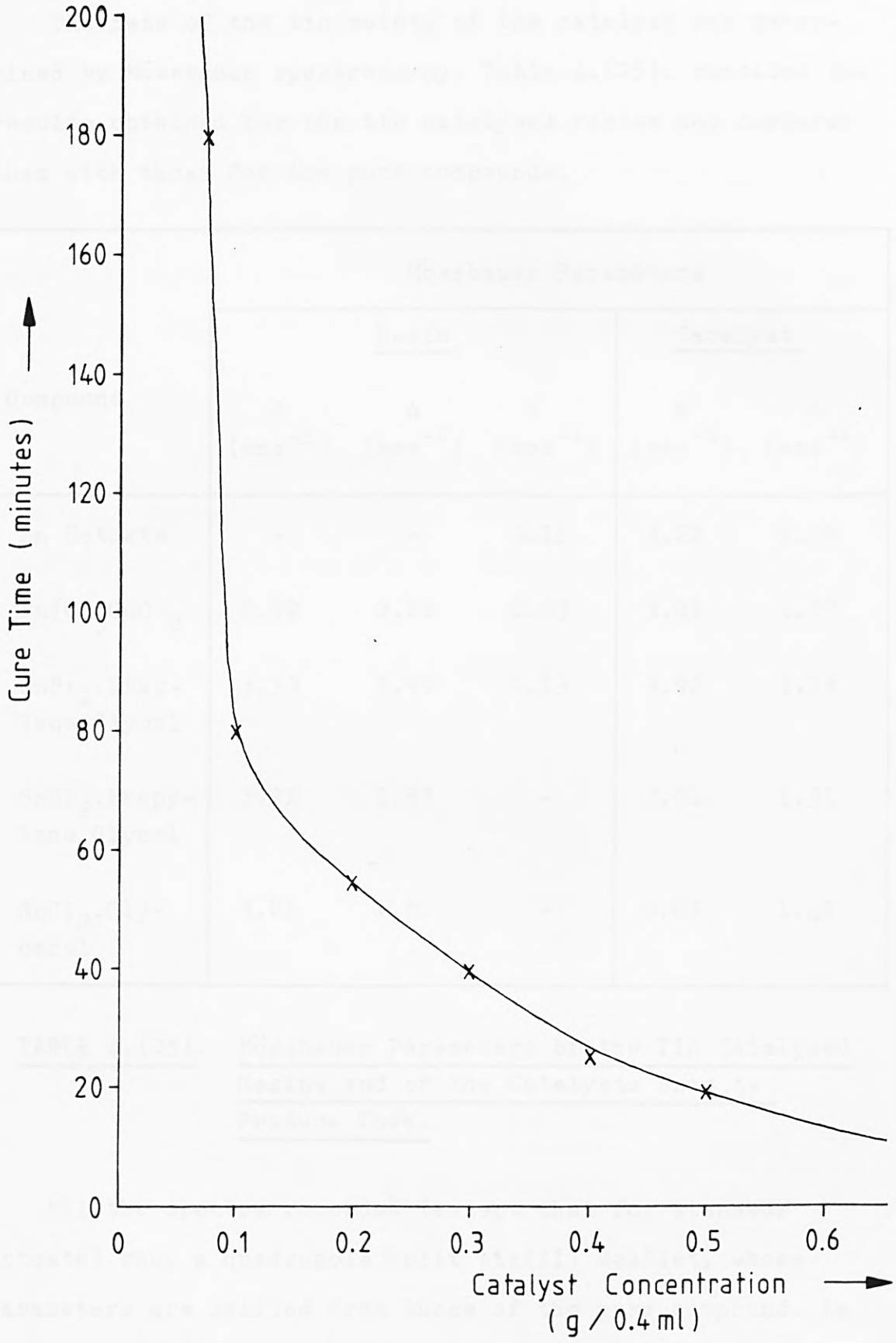

FIGURE 4.(24). Graph Showing the Decrease in Cure Time With Increase in Catalyst Concentration.

4.4.(8). Mössbauer Spectroscopy.

The fate of the tin moiety of the catalyst was determined by Mössbauer spectroscopy. Table 4.(25). contains the results obtained for the tin catalysed resins and compares them with those for the pure compounds.

Compound	Mössbauer Parameters				
	Resin			Catalyst	
	δ (mms^{-1})	Δ (mms^{-1})	δ (mms^{-1})	δ (mms^{-1})	Δ (mms^{-1})
Sn Octoate	-	-	0.11	3.22	2.02
$Sn(CH_3COO)_2$	2.92	2.12	0.03	3.21	1.77
$SnBr_2$.Ethylene Glycol	3.13	1.90	0.13	3.92	1.18
$SnCl_2$.Propylene Glycol	3.22	1.87	-	3.61	1.31
$SnCl_2$.Glycerol	3.21	1.82	-	3.63	1.42

TABLE 4.(25). Mössbauer Parameters of the Tin Catalysed Resins and of the Catalysts Used to Produce Them.

All the spectra recorded (except that for stannous octoate) show a quadrupole split tin(II) doublet, whose parameters are shifted from those of the pure compound. In each case, the isomer shift has decreased. This indicates that the s-electron density about the tin nucleus has decreased, giving more covalent type bonding in the Sn-O

bonds. The quadrupole splitting in the spectra has increased and this implies that there is an increase in the disorder of the environment about the tin nucleus.

The spectra also show a Sn(IV) peak at 0.03-0.13mms^{-1}, which is characteristic of tin octahedrally surrounded by six oxygens. This type of environment is explained in the mechanism shown in the following section. The tin(IV) peak was not observed when $SnCl_2$ was used as the catalyst.

4.4.(9). Mechanism.

Two possible mechanisms can be postulated for the tin catalysed curing of a silicone resin. The mechanisms are dependent upon the composition of the resin, so that the condensation reaction occurs between silanol and alkoxysilane groups or silanol and silane groups. Scheme 4.(4). shows the two possible mechanisms.

Silanol - alkoxysilane curing.

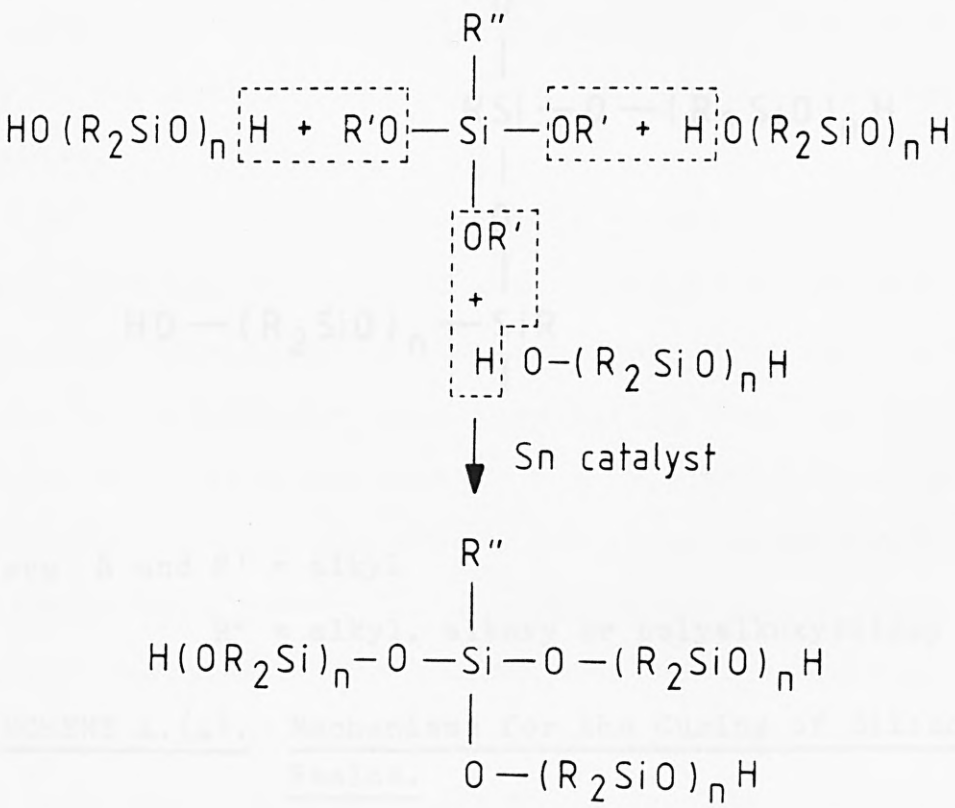

Silanol - silane curing.

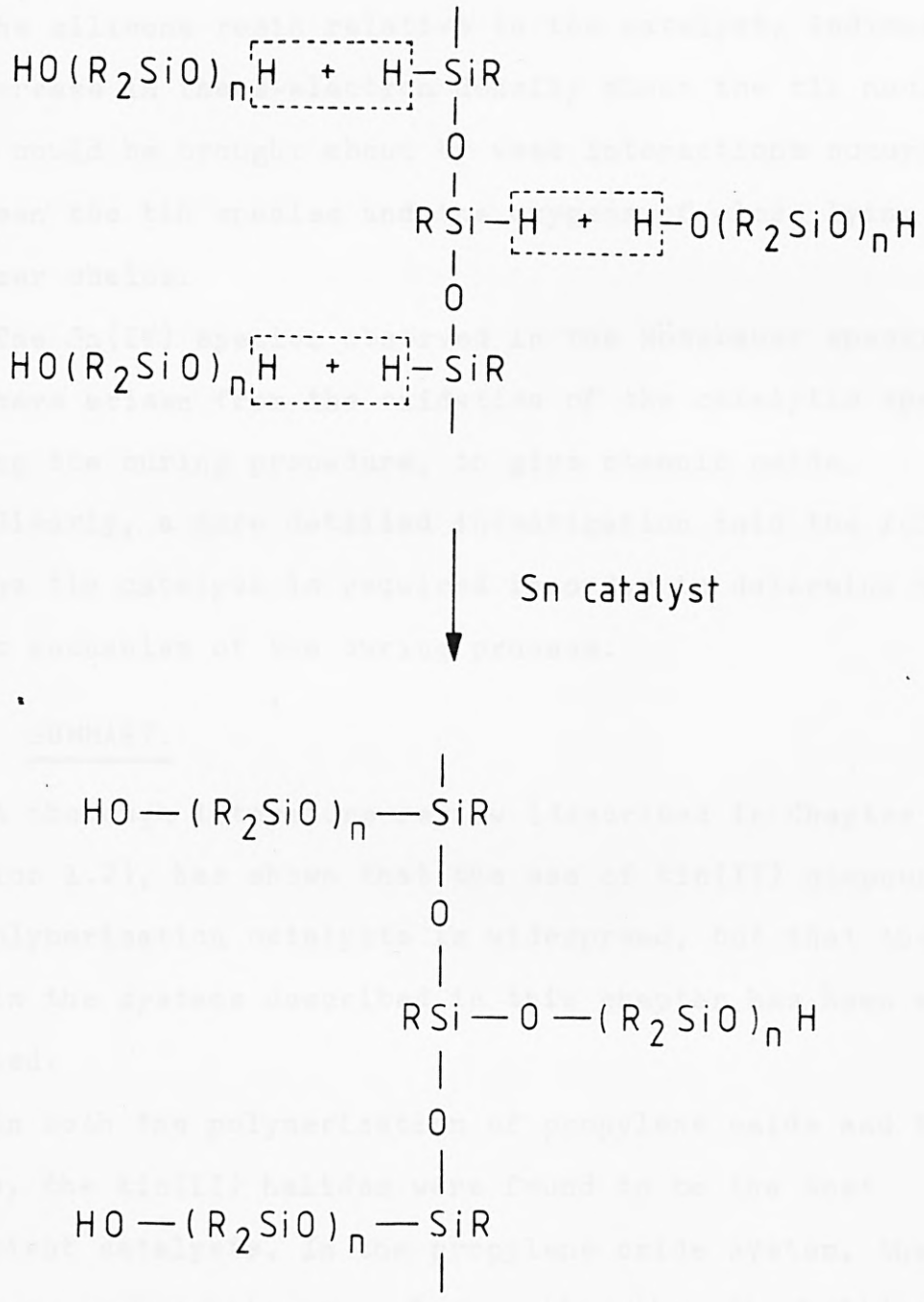

where R and R' = alkyl

R" = alkyl, alkoxy or polyalkoxysiloxy

SCHEME 4.(4). Mechanisms for the Curing of Silicone Resins.

Since the exact composition of the silicone resin is unknown, difficulties arise in postulating a mechanism for its room temperature cure. The decrease in the isomer shift of the silicone resin relative to the catalyst, indicates a decrease in the s-electron density about the tin nucleus. This could be brought about by weak interactions occurring between the tin species and the oxygens of close lying polymer chains.

The Sn(IV) species observed in the Mössbauer spectra may have arisen from the oxidation of the catalytic species during the curing procedure, to give stannic oxide.

Clearly, a more detailed investigation into the role of the tin catalyst is required in order to determine the exact mechanism of the curing process.

4.5. SUMMARY.

A thorough literature review (described in Chapter 1 Section 1.2), has shown that the use of tin(II) compounds as polymerisation catalysts is widespread, but that their use in the systems described in this chapter has been more limited.

In both the polymerisation of propylene oxide and trioxane, the tin(II) halides were found to be the most efficient catalysts. In the propylene oxide system, the stannous carboxylates were less active than the halides, but of comparable activity to the catalysts cited in the literature (ferric chloride - propylene oxide complex and potassium hydroxide). The tin(II) carboxylates were completely inactive in the polymerisation of trioxane, until a small amount of acetyl chloride was added, which caused the activity to increase dramatically. The opposite effect

is observed in the cure of the silicone resin, where the carboxylates are far more efficient than the halides.

Each system was characterised fully and the factors affecting the polymerisation determined, leading to the postulation of reaction mechanisms.

The aim of this project has been to show that tin(II) species are efficient polymerisation catalysts. In the systems studied, this aim has been achieved and this work could be extended to include many other polymerisation systems. It would be interesting to study systems which are commercially known, such as the polyurethane and the polyester systems, so that the exact mechanism of the catalyst's action can be determined.

REFERENCES.

1. P.A. Levene and A.Watti, J. Biol. Chem., (1927), 75, 325.
2. H.R. Fife and F.H. Roberts, U.S.P. 2,448,664 / 1944.
3. M.E. Pruitt and J.M. Baggett, U.S.P. 2,706,181 / 1955.
4. M.E. Pruitt and J.M. Baggett, U.S.P. 2,706,182 / 1955.
5. R.O. Colclough, G. Gee and W.C.E. Higgenson, J. Polymer Sci., (1959), 34, 171.
6. L.E. St. Pierre and C.C. Price, J. Amer. Chem. Soc., (1956), 78, 3432.
7. C.C. Price and M. Osgan, J. Amer. Chem. Soc., (1956), 78, 4787.
8. C.C. Price, M. Osgan, R.E. Hughes and C. Shambelan, J. Amer. Chem. Soc., (1956), 78, 690.
9. A.B. Borkovec, U.S.P. 2,284,454 / 1938.
10. M. Osgan and C.C. Price, J. Polymer Sci., (1959), 34, 153.
11. R.A. Miller and C.C. Price, J. Polymer Sci., (1959), 34, 161.
12. P.E. Ebert and C.C. Price, J. Polymer Sci., (1960), 46, 555.
13. D.Y.W. Adden and F.H. Newth, Brit. Pat., 945,151 / 1959.
14. D.Y.W. Adden and F.H. Newth, Brit. Pat., 945,154 / 1959.
15. Z.B. Arifin, Ph.D. Thesis, University of London, (1981).
16. J. Donbavand, Ph.D. Thesis, The City University, London, (1982).
17. S. Loeschau, J.Winkler, B. Guettes et al., Ger.(East), 147,469 / 1981.
18. A. Naka and S. Honjo, Jpn. Kokai Tokkyo Koho, 79 65, 708.

19. R. Spector, Ph.D. Thesis, University of Pennsylvania, (1965).

20. H. Toni, N. Ogumi and S. Watanabe, Polymer Letters, (1968), 6, 577.

21. T. Hirono, P. Hau Khanh and T. Tsumuta, Die Makromol. Chem., (1972), 153, 331.

22. D.O. Hummel, "Infrared Spectra of Polymers", (1966), Interscience Publishers, London, p. 132.

23. A. Kawasaki, J. Furakawa, T. Tsuruta, T. Saregusa, G. Kakogawa and R. Sakata, Polymer, (1960), 1, 315.

24. T. Urgu, H. Shimazu and K. Matsuzaki, Polymer Letters, (1973), 11, 275.

25. A.K. Schneider, U.S.P. 2,795,571 / 1957.

26. J.M. Barton, Brit. Pat., 992,986 / 1965.

27. F.M. Berardinelli, T.J. Dolce and C. Walling, J. Appl. Polymer Sci., (1965), 9, 1419.

28. C.D. Kennedy, W.R. Sorenson and G.G. McClaglin, Polymer Preprints, p. 665, 150th Amer. Chem. Soc. Meeting, Atlantic City, September, (1965).

29. A. Novak and E. Whalley, Trans. Faraday Soc., (1959), 55, 1484.

30. H. Tadokoro, J. Chem. Phys., (1961), 35, 369.

31. C.A. Berridge, U.S.P. 2,843,555 / 1958.

32. F.A. Smith, U.S.P. 3,109,826 / 1963.

33. R.A. Smith, U.S.P. 3,931,047 / 1976.

CHAPTER FIVE

AN INVESTIGATION OF THE SPECTROSCOPIC AND THERMAL PROPERTIES OF DIORGANOTIN(IV) OXY-CARBONATES

5.1. PREPARATION AND SPECTROSCOPIC STUDIES OF DIORGANOTIN(IV) OXYCARBONATES.

5.1.(1). Introduction.

Although the bis-(triorganotin) carbonates of the type $(R_3SnO)_2C{:}O$, have been well characterised and studied extensively spectroscopically[1-4], there have been very few investigations into the properties of the corresponding diorganotin derivatives. The preparation of dimethyl tin carbonate, Me_2SnCO_3, by the reaction of dimethyl tin dichloride with silver carbonate in methanol[5] or with potassium carbonate in water[6] has been reported in the literature, but later studies have shown[7], that this product is likely to be the oxycarbonate, $(Me_2Sn)_2OCO_3$. Goel et al.[7] also claimed the synthesis of diphenyl oxycarbonate, $(Ph_2Sn)_2OCO_3$, by the reaction of diphenyltin dichloride with caesium carbonate in methanol solution at ambient temperature. Mössbauer spectroscopic studies in the present work however, show that the diphenyl derivative obtained by Goel was impure.

Interest in diorganotin oxycarbonates has recently arisen because of their possible involvement as intermediates in the environmental degradation[8] of bis-(tributyltin) carbonate in wood[9] and their possible use as light stabilisers for rigid P.V.C.[10]

In this work, the syntheses of the diphenyl- and the dimethyltin oxycarbonates are reinvestigated and a series of four new dialkyltin oxycarbonates, $(R_2Sn)_2OCO_3$, prepared. The structures of these compounds in the solid state are discussed in terms of their ^{119}Sn Mössbauer and infrared spectral data. The thermal properties of the diorganotin

oxycarbonates are also investigated and mechanisms for their thermal decomposition pathways are suggested as a result of detailed studies carried out on the products of their decomposition.

5.1.(2). Experimental.

5.1.(2).1. Preparation of $(R_2Sn)_2OCO_3$, where R= Me or Et.

Equimolar (0.005 mole) aqueous solutions of the dialkyl tin dichloride and potassium carbonate were mixed at room temperature, with stirring. The products which precipitated immediately, were filtered off, washed with water and then dried at room temperature, to give fine white free-flowing powders.

5.1.(2).2. Preparation of the Monohydrate Derivatives $(R_2Sn)_2OCO_3.H_2O$, where R= Pr, Bu or Oct.

Because of the low solubility of the higher dialkyltin dichlorides in water, the diorganotin oxycarbonates were prepared in a methanol solution, using caesium carbonate as the source of carbonate ion.

In a typical synthesis, the appropriate diorganotin dichloride (0.005 mole) in methanol was added dropwise to a stirred methanolic solution of an equimolar quantity of caesium carbonate (0.005 mole) at room temperature. The white precipitate which formed immediately, was filtered off and transferred to a beaker of distilled water. The white precipitate was stirred vigorously in the water for 30 minutes, to remove the caesium chloride which was co-precipitated with the diorganotin oxycarbonate during the reaction. The purified product was filtered off and allowed to dry in air, at room temperature.

5.1.(2).3. The Preparation of Diphenyltin Oxycarbonate.

Diphenyl dichloride also has low solubility in water, so the oxycarbonate was prepared in a methanol solution, as described in the previous section. The diphenyltin derivative however, unlike those described in Section 5.1.(2).2. is anhydrous.

5.1.(3). Results.

The analytical data for the products are given below in Table 5.(1). Sn(IV) analyses were carried out by the Analytical Department of the International Tin Research Institute.

R	n	Analysis : Observed (Calculated) (%)		
		C	H	Sn
Me	0	15.66 (16.04)	3.21 (3.21)	64.1 (63.6)
Et	0	24.52 (25.12)	4.68 (4.65)	55.0 (55.4)
Pr	1	31.12 (30.95)	5.90 (5.95)	48.5 (47.2)
Bu	1	36.58 (36.43)	6.85 (6.79)	43.5 (42.5)
Oct	1	50.87 (50.51)	8.86 (8.93)	31.2 (30.4)
Ph	0	47.10 (48.23)	3.53 (3.21)	37.6 (38.3)

TABLE 5.(1). Analytical Data for Diorganotin Oxycarbonates, $(R_2Sn)_2OCO_3.nH_2O$.

Compound	80K		295K		$\nu_{as}(CO)$ (cm^{-1})
	δ (mms^{-1})	Δ (mms^{-1})	δ (mms^{-1})	Δ (mms^{-1})	
$(Me_2Sn)_2OCO_3$	1.12	3.24	1.01	2.98	1510
			1.10	3.24[a]	1510[a]
$(Et_2Sn)_2OCO_3$	1.23	3.32	1.46	3.03	1495
$(Pr_2Sn)_2OCO_3.H_2O$	1.20	3.06	b	b	1510
$(Bu_2Sn)_2OCO_3.H_2O$	1.20	3.02	b	b	1510
$(Oct_2Sn)_2OCO_3.H_2O$	1.24	3.14	b	b	1505
$(Ph_2Sn)_2OCO_3$	0.93	1.97	1.02	2.29	1514
			0.97	2.29[a]	1510[a]
			1.16	3.93[a]	

[a] Ref.7. [b] very weak spectra obtained

TABLE 5.(2). ^{119}Sn Mössbauer Parameters at 80K and Room Temperature and Asymmetric Carbonyl Stretching Frequencies for Diorganotin Oxycarbonates.

The infrared spectra of the oxycarbonates were obtained as potassium bromide discs. The asymmetric carbonyl stretching frequencies for the compounds are listed in Table 5.(2). along with their ^{119}Sn Mössbauer isomer shift and quadrupole splitting parameters.

5.1.(4). Discussion.

The diorganotin oxycarbonates are high melting, insoluble materials which display room temperature Mössbauer spectra. These properties are indicative of polymeric structures in the solid state. The asymmetric carbonyl stretching frequencies in the i.r. spectra of the compounds are in the range 1495 - 1515cm^{-1} and this implies that the carbonate is coordinated to the tin.

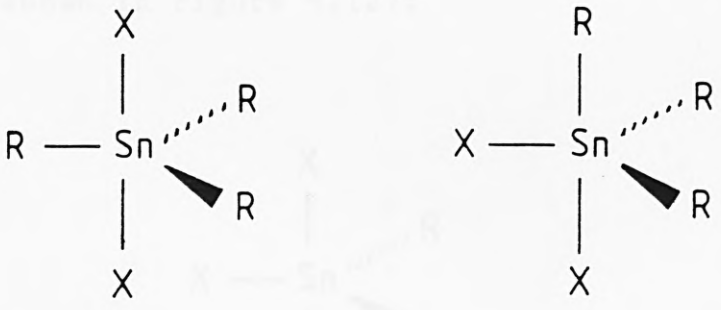

trans - isomer	cis - isomer
Δ = 3.00-4.00 mms^{-1}	Δ = 1.70-2.40 mms^{-1}
e.g.	
$Me_3SnCl_2^-$	$Ph_3SnOCPh{=}CHCOPh$
Δ = 3.23 mms^{-1}	Δ = 2.25 mms^{-1}

FIGURE 5.(1). Quadrupole Splitting Values for Trigonal Bipyramidal Cis- and Trans- R_3SnX_2 Compounds.

Penta-coordination occurs widely among organotin(IV) compounds, most frequently with a trigonal bipyramidal environment about tin. In polymeric species of the type R_3SnX_2, cis- and trans- isomers can be distinguished between by the magnitude of the ^{119}Sn Mössbauer quadrupole splittings, as shown in Figure 5.(1). Typically, cis- isomers give Δ values in the range 1.70 - 2.40mms^{-1} and the trans- structures gives much higher Δ values (3.00 - 4.00mms^{-1})[11]. Therefore, a higher quadrupole splitting value is obtained in structures where the organic groups lie in the trigonal plane and the more electronegative substituents occupy axial positions. Similarly, diorganotin complexes, also exist as five-coordinate trigonal bipyramids[11] and their Δ values of 3.00 to 3.50 mms^{-1} suggest that the organic groups are located in equatorial positions in the trigonal plane, as shown in Figure 5.(2).

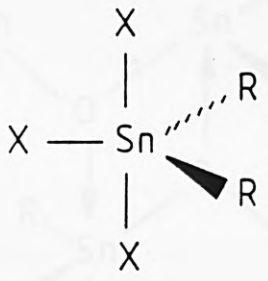

$Me_2SnCl_3^-$	Δ = 3.30
Me_2SnCl_2.sal	Δ = 3.32
$Me_2Sn(OH)NO_3$	Δ = 3.52

FIGURE 5.(2). Typical ^{119}Sn Mössbauer Quadrupole Splitting Values for Trigonal Bipyramidal Cis- R_2SnX_3 Complexes.

The similarity of the ^{119}Sn Mössbauer parameters for the dialkyltin oxycarbonates (δ = 1.12 - 1.24 mms^{-1}) suggests that they all adopt the same structure in the solid state, and the quadrupole splitting values ranging between 3.02 and 3.32 mms^{-1} imply a trigonal bipyramidal geometry about the tin atom with the two alkyl groups occupying equatorial positions. A possible structure for the diorganotin oxycarbonates is illustrated in Figure 5.(3)., the compounds are polymeric with intermolecularly bridging carbonate groups and four membered Sn_2O_2 rings. This structure was first proposed by Goel et al. for the dimethyl derivative[7].

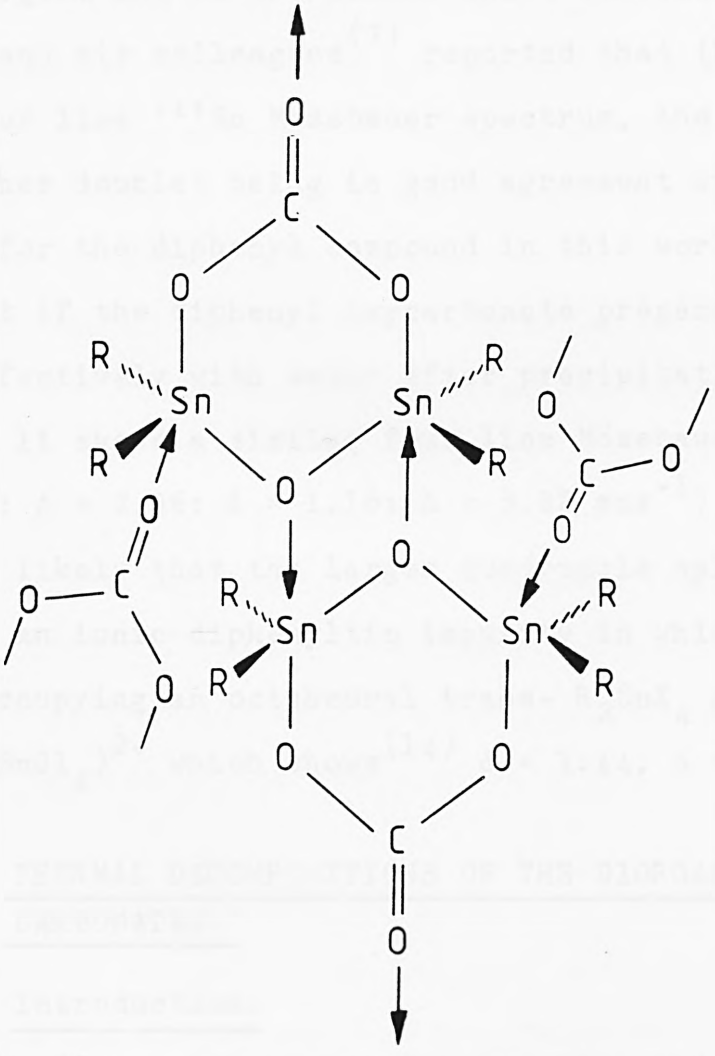

FIGURE 5.(3). Proposed Structure for the Diorganotin Oxycarbonates.

Although the ^{119}Sn Mössbauer parameters for diphenyltin oxycarbonate (δ = 1.02; Δ = 2.29 mms^{-1}) are lower than those for the dialkyltin derivatives, its structure consists of equatorial phenyl groups and trigonal bipyramidal coordination at the tin, as shown in Figure 5.(3). Previous workers[12,13] have shown that the reduction in the values of the Mössbauer parameters arises from the π-electron back donation from the π molecular orbitals of the phenyl groups (lying parallel to the threefold axis) to the orbitals involved in the bonds forming the X-Sn-X axis. As a consequence, the s-electrons on the tin are shielded to a greater degree and so the isomer shift decreases.

Goel and his colleagues[7] reported that $(Ph_2Sn)_2OCO_3$ gave a four line ^{119}Sn Mössbauer spectrum, the parameters of the inner doublet being in good agreement with the values recorded for the diphenyl compound in this work. It was found that if the diphenyl oxycarbonate prepared, was not washed effectively with water after precipitation from methanol, it shows a similar four line Mössbauer spectrum (δ = 1.00; Δ = 2.26: δ = 1.16; Δ = 3.82 mms^{-1}) and it is therefore likely that the larger quadrupole split doublet is due to an ionic diphenyltin impurity in which the tin atom is occupying an octahedral trans- R_2SnX_4 geometry, e.g. $(Ph_2SnCl_4)^{2-}$ which shows[14] δ = 1.44, Δ = 3.80 mms^{-1}.

5.2. THERMAL DECOMPOSITIONS OF THE DIORGANOTIN OXYCARBONATES.

5.2.(1). Introduction.

All the diorganotin oxycarbonates prepared were analysed by simultaneous differential thermal analysis (DTA) and thermogravimetric analysis (TG). The resultant traces show

that the compounds undergo multistage decompositions in the temperature range 140° - 380°C. Unfortunately, it proved difficult to determine the exact mechanisms of the decompositions by consideration of the percentage lost in each stage, and so it was necessary to repeat the decompositions on a much larger scale, trapping out and isolating the decomposition products and residues obtained. A schematic representation of the apparatus[15] used to study the decomposition of up to 5g of sample is shown in Figure 5.(4).

The sample was heated at a constant rate by a Variostat at 120V, and was kept at a certain temperature by a Eurotherm. Nitrogen was continuously flushed through the system to avoid oxidation of the decomposition products and residues. The nitrogen flow also has the effect of carrying over the products to be collected either in the side arm or in the cold finger.

In all cases, the decomposition products and residues obtained, were characterised where appropriate by carbon and hydrogen analyses, ^{119}Sn Mössbauer and infrared spectroscopy and by X-ray powder diffraction. In the case of the diphenyltin oxycarbonate, the decomposition products were identified by running a comparative TLC plate (silica gel - butanol : acetic acid : water elutant) against authentic samples of the anticipated by-products.

5.2.(2). Dimethyltin Oxycarbonate.

The DTA/TG traces of $(Me_2Sn)_2OCO_3$ show that the compound undergoes a two stage, endothermic decomposition: the first stage at 197°C, resulted in the loss of 11% which corresponds to the loss of carbon dioxide, the second stage occurred at 328°C with a loss of 38%, to leave a

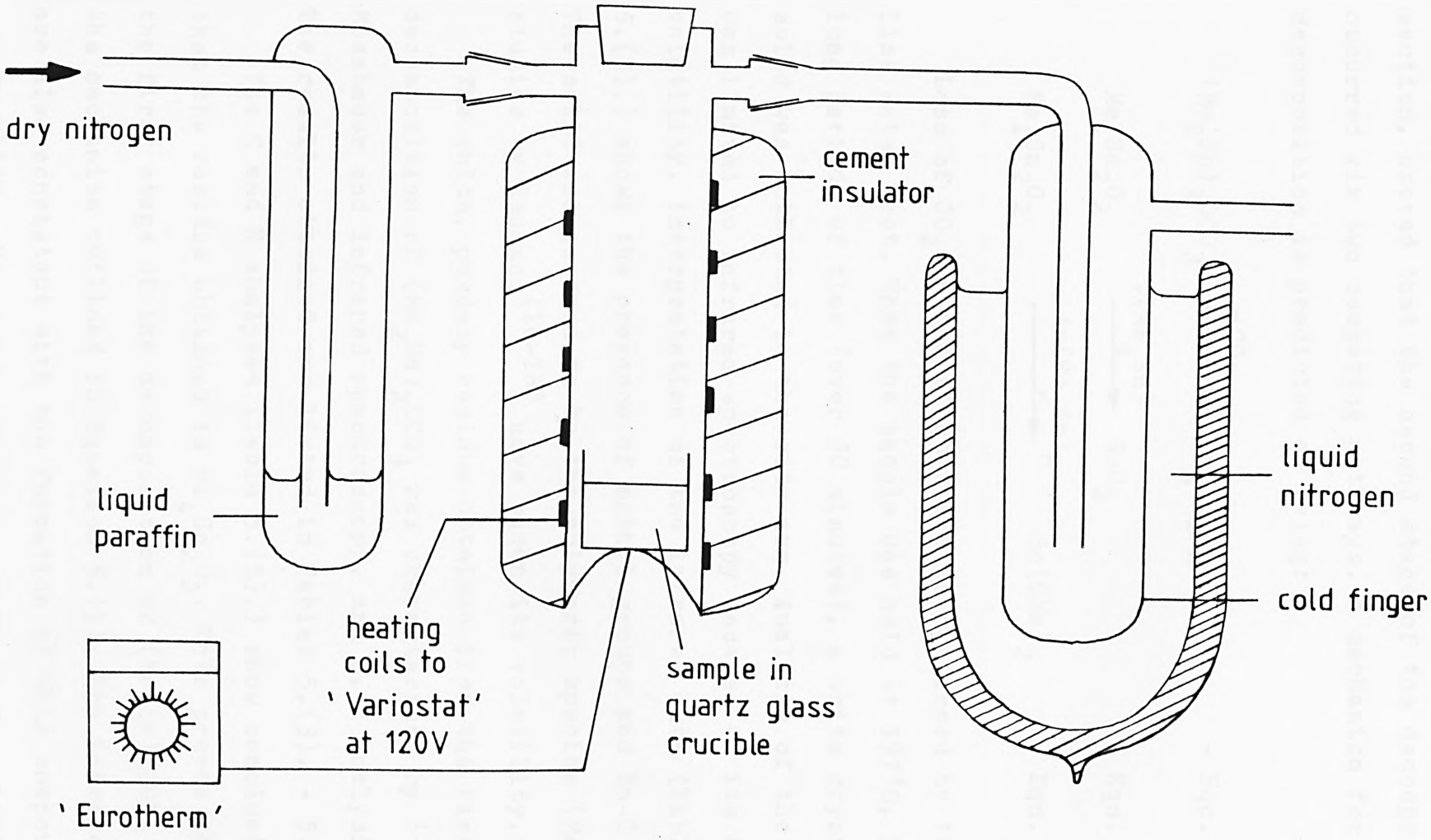

FIGURE 5.(4). Schematic Representation of the Apparatus Used for the Thermal Decomposition of the Diorganotin Oxycarbonates.

residue of 51%. The more accurate decomposition of this compound using the apparatus described in the previous section, proved that the second stage of the decomposition occurred via two competing pathways. A mechanism for the decomposition is predicted as being:

$$(Me_2Sn)_2OCO_3 \xrightarrow{-CO_2} Me_4Sn_2O_2 \qquad \text{- Eqn. 5.(1).}$$

$$Me_4Sn_2O_2 \xrightarrow{-(Me_4Sn)} SnO_2 \qquad \text{- Eqn. 5.(2).}$$

$$Me_4Sn_2O_2 \xrightarrow{-1/n(Me_2Sn)_n} Sn(OMe)_2 \qquad \text{- Eqn. 5.(3).}$$

Loss of CO_2 in the first stage is confirmed by the lime water test. When the sample was held at 197°C, for long periods of time (over 30 minutes), a white crystalline solid was collected in the side arm. Analysis of the solid was limited to infrared spectroscopy because of its high volatility. Interpretation of the infrared data (Table 5.(3).) shows the presence of methyl groups and Sn-C bonds. The solid was assumed to be the polymeric species $(Me_2Sn)_n$, studies by Neumann[16-18] have shown its volatility.

The white, powdery residue obtained from the first stage decomposition of $(Me_2Sn)_2OCO_3$ was characterised by ^{119}Sn Mössbauer and infrared spectroscopy, and C, H analysis. The results obtained are listed in Tables 5.(3). - 5.(5).

The C and H analyses (Table 5.(5).) show conclusively that the residue obtained is $Me_4Sn_2O_2$. This proves that the first stage of the decomposition of $(Me_2Sn)_2OCO_3$ follows the mechanism outlined in Equation 5.(1). The infrared data are also consistent with the formation of this compound.

The ^{119}Sn Mössbauer parameters of $Me_4Sn_2O_2$, obtained at 80K, are compared to those of the polymeric species

1st Stage Product			1st Stage Residue			Final Residue		
$(Me_2Sn)_n$			$Me_4Sn_2O_2$			10% $Sn(OMe)_2$ + 90% SnO_2		
3000 2850	m	ν_{as}(C-H)	3000 2920	m	ν_{as}(C-H)	2980 2920	vw	ν_{as}(C-H)
-			-			1630	m	
1400	w	CH_3 def.	1390	w	CH_3 def.	1400	vw	CH_3 def.
1200	w	$(CH_3)_2$	1180	s	$(CH_3)_2$	-		
795	vs	C-H rock	770	s	C-H rock	-		
560 510	s m	Sn-C	575 530	s w	ν_{as}(Sn-O) ν(Sn-C)	575	vs	ν_{as}(Sn-O)
-			460	s	Sn-O-Sn bend	-		
			295	m				

TABLE 5.(3). Infrared Data for the Decomposition Product and Residues of $(Me_2Sn)_2OCO_3$.

Compound	Mössbauer Parameters δ (mms^{-1})	Δ (mms^{-1})
$(Me_2Sn)_2OCO_3$	1.12	3.24
$Me_4Sn_2O_2$	0.90	2.15
$(Me_2SnO)_n$	0.82	2.13[19]
$Sn(OMe)_2 + SnO_2$	2.94	1.92
	0.16	-
$Sn(OMe)_2$	2.92	1.92[24]

TABLE 5.(4). ^{119}Sn Mössbauer Data for $(Me_2Sn)_2OCO_3$ and the Compounds Obtained from its Decomposition.

Compound	% C	% H
1st stage residue	12.18	3.05
Required for : $Me_4Sn_2O_2$	12.59	3.46
Final residue	1.41	0.34
Required for : 90% SnO_2 + 10% $Sn(OMe)_2$	1.56	0.39

TABLE 5.(5). Carbon and Hydrogen Analyses for the Decomposition Residues of $(Me_2Sn)_2OCO_3$.

dimethyltin oxide[19]. The structure of $(Me_2SnO)_n$ consists of a four membered ring structure of Sn_2O_2[20], which is held together in a reticulated network, as shown below,

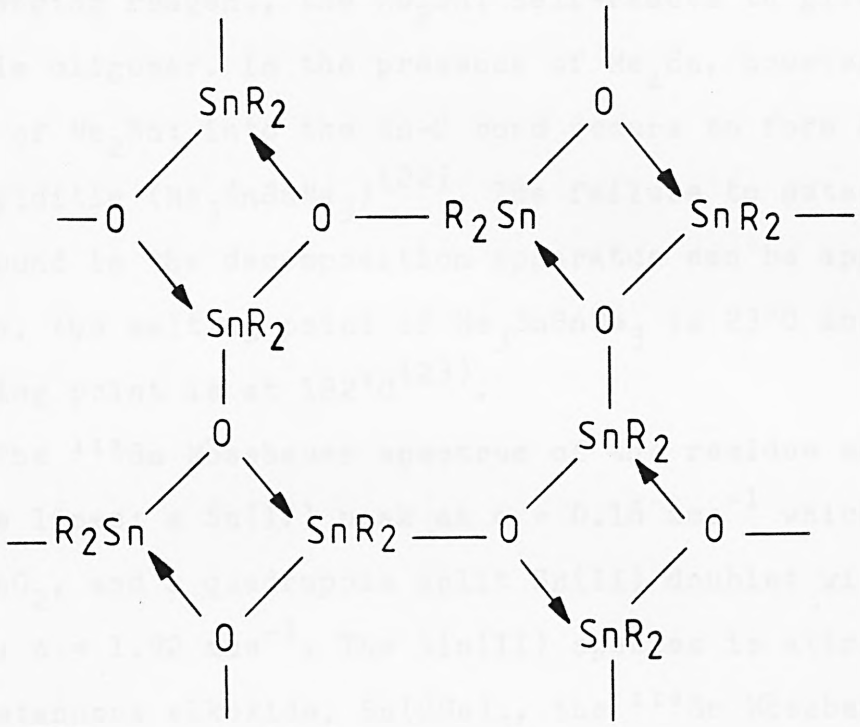

Although the chemical analyses, ^{119}Sn Mössbauer and infrared data for the first decomposition product of $(Me_2Sn)_2OCO_3$ are identical with those of the dimethyltin oxide polymer, the two materials differ in their thermal behaviour. The product obtained from the decomposition is less stable decomposing at 328°C, while $(Me_2SnO)_n$ degrades at 385°C. The difference probably arises because of the effect of the in situ preparation of the compound by the thermal decomposition route which effects the detail of the structure.

The final stage of the decomposition of dimethyltin oxycarbonate occurs at 328°C, by the two mechanisms outlined in Equations 5.(2). and 5.(3). A decomposition product was not detected and the green-brown residue obtained was washed with benzene to remove any uncombusted carbon.

Under the conditions present in the decomposition apparatus, the decomposition products dimethyltin and tetramethyltin, can react together. In the absence of a scavenging reagent, the Me_2Sn: self-reacts to give a fairly stable oligomer. In the presence of Me_4Sn, however, insertion of Me_2Sn: into the Sn-C bond occurs to form hexamethylditin ($Me_3SnSnMe_3$)[22]. The failure to detect this compound in the decomposition apparatus can be appreciated since, the melting point of $Me_3SnSnMe_3$ is 23°C and its boiling point is at 182°C[23].

The ^{119}Sn Mössbauer spectrum of the residue shows three lines: a Sn(IV) peak at δ = 0.16 mms^{-1} which is due to SnO_2, and a quadrupole split Sn(II) doublet with δ = 2.94; Δ = 1.92 mms^{-1}. The tin(II) species is attributed to the stannous alkoxide, $Sn(OMe)_2$, the ^{119}Sn Mössbauer parameters of an authentic sample[24] being δ = 2.92; Δ = 1.92 mms^{-1}. Although the C and H contents of the residue are low at 1.41% and 0.34%, respectively, they cannot be discounted as background impurities and are consistent with the formation of a mixture of 90% SnO_2 and 10% $Sn(OMe)_2$. The composition of the residue is reflected in its infrared spectrum (Table 5.(3).) which shows a very strong absorption due to Sn-O and only weak absorptions for C-H.

5.2.(3). The Thermal Decomposition of Diphenyltin Oxycarbonate.

The accurate thermal decomposition of $(Ph_2Sn)_2OCO_3$ up to a temperature of 600°C, monitored by DTA/TG analysis showed that a three stage endothermic decomposition occurred, in which the first stage involved the loss of carbon dioxide at 145°C. Although the second and third

stages occurred at 297° and 369°C, respectively, the stages were indistinct and it was not subsequently possible to separate these products on the decomposition apparatus.

The white powder, obtained after the loss of carbon dioxide, was analysed for its carbon and hydrogen content, and was characterised by infrared and ^{119}Sn Mössbauer spectroscopy. The data in Tables 5.(6). and 5.(7). show that the white powder is the polymeric species diphenyltin oxide: both the infrared and Mössbauer data of the white powder are identical to that of $(Ph_2SnO)_n$.

Absorption (cm^{-1})	Assignment
3075 m	ν_{as} (C-H)
3050 m	
1485 m	C-C str.
1435 s	
1080 m	C-H in plane bend
1000 w	
725 vs	C-H out of plane
695 vs	bend for Ph
580 s	Sn-O + Sn-C
480 m	O-Sn-O bend
430 s	
330 s	

TABLE 5.(6). Infrared Data of the First Stage Decomposition Residue of $(Ph_2Sn)_2OCO_3$.

	1st Stage Residue	$(Ph_2SnO)_n$
% C	49.75	49.89
% H	3.27	3.49
δ (mms^{-1})	0.87	0.88
Δ (mms^{-1})	1.86	1.73

TABLE 5.(7). Carbon and Hydrogen Analyses and ^{119}Sn Mössbauer Data for the First Stage Decomposition Residue of $(Ph_2Sn)_2OCO_3$ and of $(Ph_2SnO)_n$.

The diphenyltin oxide obtained from the decomposition of $(Ph_2Sn)_2OCO_3$, undergoes a two stage decomposition at 297° - 369°C, to give two solids which were collected from different parts of the side arm of the decomposition apparatus. Both solids were a mixture of yellow platelets and white needles, but the product (1) which travelled furthest along the apparatus had a greater proportion of the platelets than did product (2). Table 5.(8). lists the results obtained when these products were characterised using comparative thin layer chromatography (silica gel - butanol: acetic acid: water elutant)[25]. The R_f values measured were compared with those of the starting materials and authentic samples of biphenyl and tetraphenyltin, to show that both side products were a combination of Ph_2 and Ph_4Sn. Carbon and hydrogen analyses show (Table 5.(9).) that side product (1) contains 85% biphenyl and 15% tetraphenyltin and side product (2) contains 15% Ph_2 and 85% Ph_4Sn.

The comparative TLC of the final decomposition residue

Compound	R_f Value
Biphenyl	1
Ph_4Sn	0
$(Ph_2Sn)_2OCO_3$	No Spot
$(Ph_2SnO)_n$	No Spot
Side Product (1)	
Major Component	1
Minor Component	0
Side Product (2)	
Major Component	0
Minor Component	1
Final Decomposition Residue (Faint Spot)	0

TABLE 5.(8). Characterisation of Side Products (1) and (2) by Comparative TLC.

	% C	% H
Side Product (1)	84.84	6.61
Required for : 85% Ph_2 + 15% Ph_4Sn	84.94	5.94
Side Product (2)	70.96	4.81
Required for : 85% Ph_4Sn + 15% Ph_2	69.05	4.83

TABLE 5.(9). Carbon and Hydrogen Analyses for Side Products (1) and (2).

of $(Ph_2Sn)_2OCO_3$ (Table 5.(8).) has shown that the residue contains a small amount of tetraphenyltin. The carbon and hydrogen analyses in Table 5.(10)., are consistent with the residue being a mixture of 82.5% stannic oxide and 17.5%

	% C	% H
Final Residue	24.46	1.80
Required for : 82.5% SnO_2 + 17.5% Ph_4Sn	25.34	1.77
	δ	Δ
Final Residue	1.42	0
	-0.03	0
Ph_4Sn	1.22	0
SnO_2	0	0

TABLE 5.(10). Carbon and Hydrogen Analyses and ^{119}Sn Mössbauer Parameters for the Final Decomposition Residue of $(Ph_2Sn)_2OCO_3$.

tetraphenyltin. Table 5.(10). also contains the ^{119}Sn Mössbauer parameters of the final residue. The data for the two Sn(IV) singlets obtained agree with the presence of SnO_2 and Ph_4Sn. A very broad and weak infrared spectrum is recorded for the residue, the data (listed in Table 5.(11).) show that the main features are the peaks in the

Absorption (cm^{-1})	Assignment
3020 vw	C-H asym str.
1405 vw	
1050 vw	
735 w	C-H out of plane
705 m	bend for Ph
600 sh	Sn-O + Sn-C
490 br	Sn-O-Sn bend

TABLE 5.(11). The Infrared Data of the Final Decomposition Residue of $(Ph_2Sn)_2OCO_3$.

range 490 - 675 cm^{-1} due to the Sn-O and Sn-C asymmetric stretching modes.

Therefore, the mechanism of the thermal decomposition of diphenyltin oxycarbonate can be outlined as follows:-

$$(Ph_2Sn)_2OCO_3 \xrightarrow{-CO_2} (Ph_2SnO)_n \downarrow$$

$$Ph_2 + Ph_4Sn + SnO_2$$

5.2.(4). The Thermal Decomposition of the Higher Dialkyltin Oxycarbonates.

The higher dialkyltin oxycarbonates decompose thermally in three or four stages to give a stannous oxide - stannic oxide residue mixture. Identification of the intermediate products and residues proved difficult and is limited, in this section, to a brief description of their infrared spectra and carbon and hydrogen analyses. The decomposition stages were not discrete and so pure intermediates could not be obtained.

5.2.(4).1. $(Et_2Sn)_2OCO_3$.

The first stage occurred at 147°C with loss of 10% which corresponds to the loss of carbon dioxide. The infrared and C, H analyses of the white solid residue are detailed in Tables 5.(12). and 5.(13).

$$(Et_2Sn)_2OCO_3 \xrightarrow{-CO_2} (Et_2SnO)_2$$

A loss of 20% is obtained at 232°C to leave a yellow powdery residue. A further 40% is lost at 268°C and this corresponds to the loss of the polymeric species $(Et_2Sn)_n$. The carbon and hydrogen analyses and infrared data of these species and of the final residue (a black, glassy

Compound	% C	% H
1st stage residue $(Et_2SnO)_2$	19.95 (24.92)	4.04 (5.23)
2nd stage product	61.25	4.67
2nd stage residue	14.69	2.98
3rd stage product $(Et_2Sn)_n$	28.93 (27.17)	6.24 (5.70)
Final residue	0.10	0.12

TABLE 5.(12). Carbon and Hydrogen Analyses for the Thermal Decomposition Products and Residues of $(Et_2Sn)_2OCO_3$.

solid) are also listed in Tables 5.(12). and 5.(13).

The ^{119}Sn Mössbauer spectrum of the final solid residue shows a quadrupole split tin(II) doublet with δ = 2.87; Δ = 1.97 mms^{-1} and a tin(IV) singlet with δ = -0.07 mms^{-1}. The Sn(IV) species is assigned to stannic oxide and the Sn(II) species is attributed to the presence of stannous oxide.

The difference in the chemical analyses of the first stage decomposition residue and diethyltin oxide is accounted for by the effects of the *in situ* preparation of the residue by the thermal decomposition pathway.

5.2.(4).2. $(Pr_2Sn)_2OCO_3.H_2O$.

This compound decomposes thermally in four stages. The first two stages at 120° and 211°C, corresponds to the loss of a molecule of water and a molecule of carbon dioxide, respectively, to leave a white powdery solid. These losses result in the formation of $(Pr_2SnO)_n$, as shown by the

$(Et_2SnO)_n$	2nd stage residue	Assignment	Final residue	Assignment
2960 m	2960 m		-	-
2940 m	2940 m	ν_{as}(C-H) in Et.	-	-
2875 m	2875 m		-	-
1455 w	1460 m	C-H bend	-	-
1380 w	1380 m		-	-
1240 w	1240 w		-	-
1180 w	1180 w		-	-
1030 w	1020 m	C-H out of plane bend	-	-
965 w	965 m		-	-
680 m	680 s,br		-	-
560 s	610 s	Sn-O + Sn-C	620 m	Sn-O str.
530 s	540 s		500 br	Sn-O-Sn bend.
470 m	430 s	Sn-O-Sn bend	-	-

TABLE 5.(13). Infrared Data of the Thermal Decomposition Residues of $(Et_2Sn)_2OCO_3$.

carbon and hydrogen analyses given below,

Residue	%C = 31.06	$(Pr_2SnO)_n$	%C = 32.63
	%H = 6.00		%H = 6.38

and the infrared data listed in Table 5.(14).

Peak Position (cm^{-1})	Assignment
2960 s	ν_{as} (C-H)
2870 m	ν_{as} (C-H)
1455 m	C-C bend
1417 m	C-H bend
1375 m	
1325 w	
1060 m	C-H bend (out of plane)
985 m	
660 m	Sn-O
565 s	Sn-O, Sn-C
400 s,br	Sn-O-Sn bend

TABLE 5.(14). Infrared Data of $(Pr_2SnO)_n$.

The final two decomposition stages occur between 275° and 308°C, but it was not possible to distinguish between them. The final decomposition residue (a grey-green solid) was found to be a mixture of stannous oxide and stannic oxide, the absence of organic moieties being proved by the infrared spectrum of the residue. The ^{119}Sn Mössbauer spectrum of the residue shows a tin(IV) singlet at a value of δ = -0.1mms^{-1} (SnO_2) and a quadrupole split tin(II) doublet with parameters of δ = 2.63mms^{-1} and Δ = 1.63mms^{-1} (SnO).

5.2.(4).3. $(Bu_2Sn)_2OCO_3.H_2O$.

The first stage thermal decomposition of the dibutyl-derivative occurred at 125°C and resulted in the loss of a molecule of water to leave a white waxy solid as the residue. The analysis of this residue confirms the formation of $(Bu_2Sn)_2OCO_3$ (Tables 5.(15). and 5.(16).).

	% C	% H
First Decomposition Residue: $(Bu_2Sn)_2OCO_3$	37.07 (37.68)	7.00 (6.70)
Second Decomposition Residue	12.66	2.54
Final Decomposition Residue	0.72	0.02

TABLE 5.(15). Carbon and Hydrogen Analyses of the Decomposition Residues of $(Bu_2Sn)_2OCO_3.H_2O$.

At 230°C, the second stage of the decomposition is observed. A colourless liquid is evolved whose carbon and hydrogen content could not be obtained because of its high volatility. The infrared spectrum of the neat liquid was recorded and the data are in Table 5.(16)., further characterisation of this species was not possible. Carbon dioxide is also lost during the second stage and this is proved by the lime water test.

The yellow solid residue obtained after the second stage decomposition was analysed for its carbon and hydrogen content (Table 5.(15).) and its infrared and ^{119}Sn Mössbauer spectra recorded - the results are contained in Tables 5.(16). and 5.(17). Although the Mössbauer parameters show the presence of stannous oxide and stannic

$(Bu_2Sn)_2OCO_3$	Second Stage Product	Second Stage Residue	Final Residue	Assignment
2960 m	2960 vs	2960 s		
2940 m	2940 vs	2940 s		ν_{as} (C-H)
2860 m	2860 s	2860 m		
1630 w				CO_2^-
1460 m	1460 s	1470 s		
1420 w	1420 m	1420 w		C-H bend
1380 m	1380 s	1380 m		
1290 w	1295 m	1295 w		
1190 w	1180 m	1180 w		
1080 w	1075 s	1075 m		C-H
1010 w	1020 m			
875 m	875 s	870 m		
670 m	670 s			
600 w	595 s	590 s	600 m	Sn-O
555 m	510 s	530 s	540 m	Sn-C
460 w		440 s	430 s	Sn-O-Sn bend

TABLE 5.(16). Infrared Spectral Data of the Decomposition Product and Residues from $(Bu_2Sn)_2OCO_3 \cdot H_2O$.

	δ (mms^{-1})	Δ (mms^{-1})
Second Stage	2.78	2.12
Residue	0.01	-
Final	2.93	1.70
Residue	-0.14	-

TABLE 5.(17). ^{119}Sn Mössbauer Data for the Decomposition Residues of $(Bu_2Sn)_2OCO_3.H_2O$.

oxide, both the infrared spectrum and the carbon and hydrogen analyses indicate that organic groups are present in this residue. The C and H contents are consistent with the presence of 10% Bu_4Sn, 10% SnO and 80% SnO_2. The peak in the Mössbauer spectrum for tetrabutyltin overlaps one of the peaks of the quadrupole split tin(II) doublet, which accounts for the asymmetry observed in the doublet.

The third stage of the decomposition occurs at 312°C and although there is no visible decomposition product, it is assumed that Bu_4Sn is lost in this stage. Previous workers[26] have shown that the thermal decomposition of tetrabutyltin occurs at 275°C, the difference in the decomposition temperatures can be attributed to the *in situ* preparation of Bu_4Sn in the decomposition apparatus. The C and H analyses of the final residue (a brown-grey powder) show that there is a very small percentage of organic matter present, probably as an impurity. The ^{119}Sn Mössbauer data are consistent with the residue being a mixture of stannous oxide and stannic oxide.

The following scheme can be outlined for the decomposition of dibutyltin oxycarbonate monohydrate:

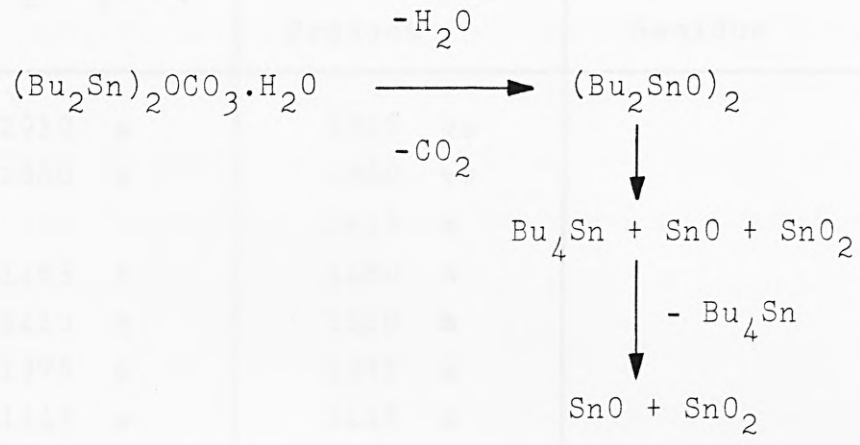

5.2.(4).4. $(Oct_2Sn)_2OCO_3.H_2O$.

Dioctyltin oxycarbonate monohydrate melts at 73°C and then, loses its molecule of water at 118°C to leave a white, waxy solid. The analysis of this solid shows that it is $(Oct_2Sn)_2OCO_3$. Tables 5.(18). and 5.(19). contain the C and H analyses and the infrared data for the decomposition residues of $(Oct_2Sn)_2OCO_3.H_2O$, respectively.

	% C	% H
$(Oct_2Sn)_2OCO_3$	50.56 (51.73)	8.95 (8.95)
Final Residue	0.71	<0.03

TABLE 5.(18). Carbon and Hydrogen Analyses for the Decomposition Residues of $(Oct_2Sn)_2OCO_3.H_2O$.

The next two stages in the thermal decomposition of the dioctyl derivative occur at 254° and 309°, but these stages can not be distinguished. The decomposition product from these two stages was collected as a colourless liquid and the infrared data of the product obtained (see Table 5.(19).). This product proved far too volatile for carbon and hydrogen analyses. The infrared peak at 1615 cm^{-1} is

$(Oct_2Sn)_2OCO_3$	Second Stage Product	Final Residue
2910 s	2920 vs	
2860 s	2860 vs	
	1615 m	
1465 s	1460 s	
1410 m	1410 m	
1375 m	1395 s	
1145 m	1145 m	
1040 m	1070 m	
980 m	1010 m	
910 w	910 w	
825 m	835 w	
720 s	720 m	
680 s	670 m	
595 s	600 m	620 m
550 s	500 m	500 m
450 s		450 m

TABLE 5.(19). Infrared Data of the Species Obtained from the Thermal Decmposition of $(Oct_2Sn)_2OCO_3.H_2O$.

assigned to the C=C stretching frequency and so, a proportion of this residue is assumed to be oct-1-ene. (The decomposition of dioctyltin oxide to oct-1-ene at 295°C has been shown by Reichle[27]).

The final residue which is brown in colour, is shown to have a negligible content of carbon and hydrogen. Its ^{119}Sn Mössbauer spectrum shows a quadrupole split Sn(II) doublet with δ = 2.76 and Δ = 1.94 mms^{-1} and a tin(IV) singlet at δ = -0.01 mms^{-1}, which is consistent with the residue being a mixture of SnO and SnO_2.

5.2.(5). Summary.

The thermal decompositions of the diorganotin oxycarbonates occur via complex mechanisms. In each case the major solid component of the residue is stannic oxide. The dimethyltin derivative contains stannous methoxide as its minor constituent and evidence for this is provided by the carbon and hydrogen analyses and ^{119}Sn Mössbauer parameters. These analytical tools show that the diphenyltin- and higher dialkyltin- derivatives give stannous oxide as the minor component of their final solid decomposition residue.

In all cases, the final decomposition residue undergoes an exothermic phase transition in the temperature range 419° to 491°C. This temperature range is higher than the maximum temperature attainable on the decomposition apparatus used in this present work and for this reason no detailed studies on this phase transition were carried out.

REFERENCES.

1. B.Y.K. Ho and J.J. Zuckerman, Inorg. Chem., (1973), 12, 1552.
2. A.J. Bloodworth, A.G. Davies and S.C. Vasishtha, J. Chem. Soc. (C), (1967), 1309.
3. K. Sisido and S. Kojima, J. Org. Chem., (1964), 29, 907.
4. H. Sato, Bull. Chem. Soc. Jap., (1967), 40, 410.
5. H.C. Clark and R.G. Goel, J. Organometal. Chem., (1967), 7, 263.
6. N.W.G. Debye, D.E. Fenton and J.J. Zuckerman, J. Inorg. Nucl. Chem., (1972), 34, 352.
7. R.G. Goel, H.S. Prasad, G.M. Bancroft and T.K. Sham, Can. J. Chem., (1976), 54, 711.
8. B.G. Henshaw, R.A. Laidlow, R.J. Orsler, J.K Carey and J.G. Savory, Recd. BWPA Ann. Conven., Cambridge, (1978), p.19.
9. P.J. Smith, A.J. Crowe, D.W. Allen, J.S. Brooks and R. Formstone, Chem. Ind., (1977), 874.
10. G. Ayrey and R.C. Poller, Dev. Polym. Stab., (1980), 2, 1.
11. A.G. Davies and P.J. Smith, in 'Comprehensive Organometallic Chemistry', (Ed. G. Wilkinson), (1982), 2, p.519. Pergamon, Oxford.
12. J.N.R. Ruddick and J.R. Sams, J. Organometal. Chem., (1973), 60, 223.
13. R.H. Herber and R. Barbieri, Gazz. Chim. Hal., (1971), 101, 149.
14. B.W. Fitzsimmons, N.J. Seeley and A.W. Smith, J. Chem. Soc. (A), (1969), 143.
15. Decomposition apparatus designed and built by Dr. A.F. Holding, The City University, London, (1982).
16. W.P. Neumann, Rev. Silicon, Germanium, Tin, Lead Compd., (1978), 81.

17. U. Schröer and W.P. Neumann, Angew. Chem., Int. Ed. Engl., (1975), 14, 246.

18. C. Grugel, W.P. Neumann and P. Seifert, Tetrahedron Letts., (1977), 2205.

19. R.V. Parrish and C.E. Johnston, J. Chem. Soc. (A), (1971), 1906.

20. Ref. 11, p.575.

21. M.Hornby, S.M. Grimes, J.D. Donaldson and A.F. Holding, unpublished results.

22. Ref. 11, p.597.

23. 'Organotin Compounds', Ed. A.K. Sawyer, (1971), Dekker, New York, Vol. 3.

24. L. Dudycz, A. Kotlicki and D. Shugar, Carbohydrate Res., (1981), 91, 31.

25. Y. Tanaka and T. Morikawa, Japan Analyst, (1964), 13, (8), 753.

26. G.G. Devyatykh, Izv. Akad. Nauk. SSR, Ser. Khim., (1972), 11, 2472.

27. W.T. Reichle, J. Polymer Sci., (1961), 49, 521.

CHAPTER SIX

THE SOLID STATE PROPERTIES OF SOME TIN(II) COMPOUNDS

6.1. INTRODUCTION.

The stereochemistry of most p-block elements in their lower oxidation states is dominated by the presence of filled non-bonding lone pair orbitals. The environments of these elements in most compounds are lone-pair distorted[1-3]. There are however, a number of compounds that are coloured and show metallic or semi-conducting properties and in which these elements occupy regular octahedral sites[4-8]. An important compound in the studies of undistorted ns^2 species is $CsSnBr_3$, which is a black solid and acts as a pseudo metallic conductor over a wide temperature range[4,9]. Its X-ray and ^{119}Sn Mössbauer data are consistent with it having an undistorted cubic perovskite structure. It has been suggested[10,11] that these properties arise from the population of solid state bands by the ns^2 electrons, as shown in Figure 6.(1).

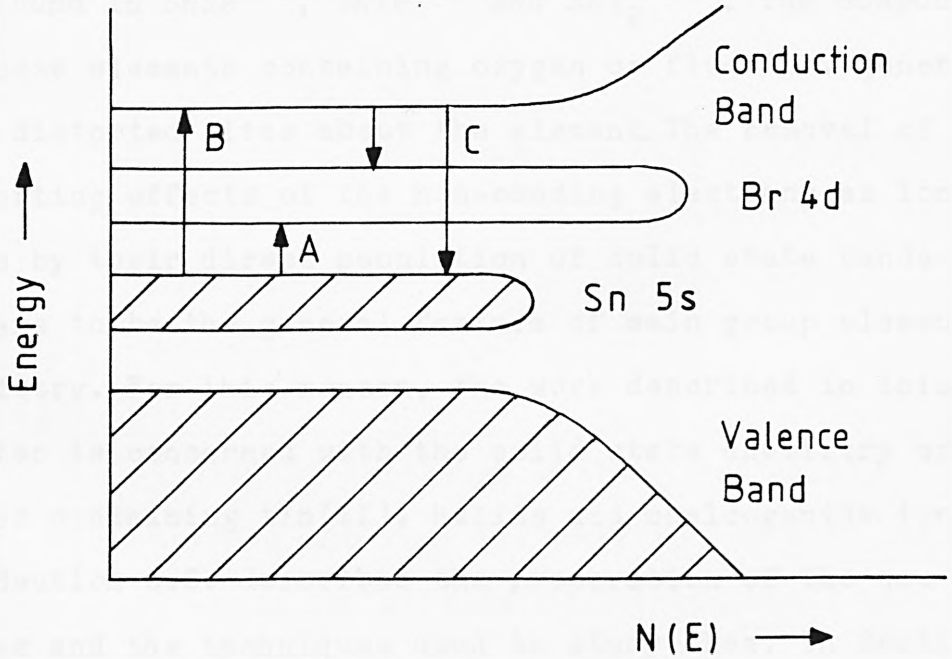

FIGURE 6.(1). Suggested Band Structure for $CsSnBr_3$ Showing Thermal Population (A), Optical Absorption (B) and Emission (C).

The acceptor bands are formed by the overlap of the empty bromine 4d orbitals and are populated by the filled tin 5s orbitals. The donation of the s electron density to the solid state bands by process A, accounts for the relatively low ^{119}Sn Mössbauer isomer shift (δ = 3.97 mms^{-1}) and high electrical conductivity obtained for $CsSnBr_3$. The presence of the next highest energy band allows optical transitions to occur between the $5s^2$ level and the conduction band. This gives rise to the optical absorption edge shown in process B and the two photoemission bands in process C.

High symmetry environments in compounds of the lower oxidation states of most p-block elements are found only in their heavier halide and chalcogenide derivatives, and where these anions are in close contact. Besides $CsSnBr_3$ and related halides, regular octahedral Sn(II) environments are found in SnSe[1], SnTe[1] and SnI_2[12]. The compounds of these elements containing oxygen or fluorine, generally have distorted sites about the element. The removal of the distorting effects of the non-bonding electrons as lone pairs by their direct population of solid state bands appears to be the general feature of main group element chemistry. For this reason, the work described in this chapter is concerned with the solid state chemistry of phases containing tin(II), halide and chalcogenide ions.

Section 6.2. describes the preparation of the new phases and the techniques used to study them. In Section 6.3., the results obtained from the reaction of tin(II) fluoride and the tetravalent metal sulphide, MoS_2, are outlined. The systems SnX_2:SnS_2 (where X = F,Cl or Br) are considered in Section 6.4.

6.2. EXPERIMENTAL.

6.2.(1). Preparation of the Cooled Melts.

All the cooled melts from both systems were prepared in the same way. Varying proportions of the two parent components were ground together and heated under nitrogen until the high melting component dissolves in the low melting compound. The solution melt is allowed to cool under nitrogen and is then characterised by the following techniques:

(i) Differential Thermal Analysis (DTA) -
A plot of the melting point of each melt against its composition gives a phase diagram and permits the identification of the new phases.

(ii) X-Ray Diffraction -
Is used to confirm the information from the phase diagrams on the existence of distinct new phases.

(iii) ^{119}Sn Mössbauer Spectroscopy -
This technique is used to give information on the way in which the outer electrons of the tin atoms are being used in bonding or in band to band effects.

(iv) Electrical Conductivity -
Is used to determine whether the solids obtained show any evidence for direct population of empty state bands by the tin non-bonding electrons.

(v) Optical Properties -
Are used to provide evidence for transitions between the filled Sn 5s electrons and empty solid state bands.

6.2.(2). Analytical Techniques.

Details of DTA, ^{119}Sn Mössbauer spectroscopy and X-ray powder diffraction appear in Chapter 1. To carry out electrical conductivity measurements, the cooled melts are ground into fine powders and are pressed into cylindrical discs using a Beckmann 00-25 Press. A Keithley 616 Digital Electrometer is used to record the electrical resistivity of the sample and the conductivity, σ, is obtained by applying the following equation:

$$\sigma = \frac{1}{A \times R}$$

where 1 = thickness of the pellet, A = the area of the pellet and R = the resistivity of the pellet.

The optical properties of the samples are studied using a Perkin-Elmer Diffuse Reflectance U/V Spectrophotometer. The samples are supported on the underside of a quartz glass slide positioned over an aluminised mirror assembly. The range of wavelengths that were scanned was 200 - 750 nm (6.21 - 1.65 eV).

6.3. THE SnF_2 : MoS_2 SYSTEM.

Cooled melts are prepared with compositions ranging from 97.5 mole % SnF_2 : 2.5 mole % MoS_2 to 35 mole % SnF_2 : 65 mole % MoS_2. The DTA traces of these melts and of the parent compounds are recorded and a graph of the melting point against the composition is constructed to yield the phase diagram for this system, illustrated in Figure 6.(2). The new phases are shown by the maxima; as the parent compound, tin(II) fluoride, is doped with MoS_2 impurities the melting point decreases until it reaches the eutectic

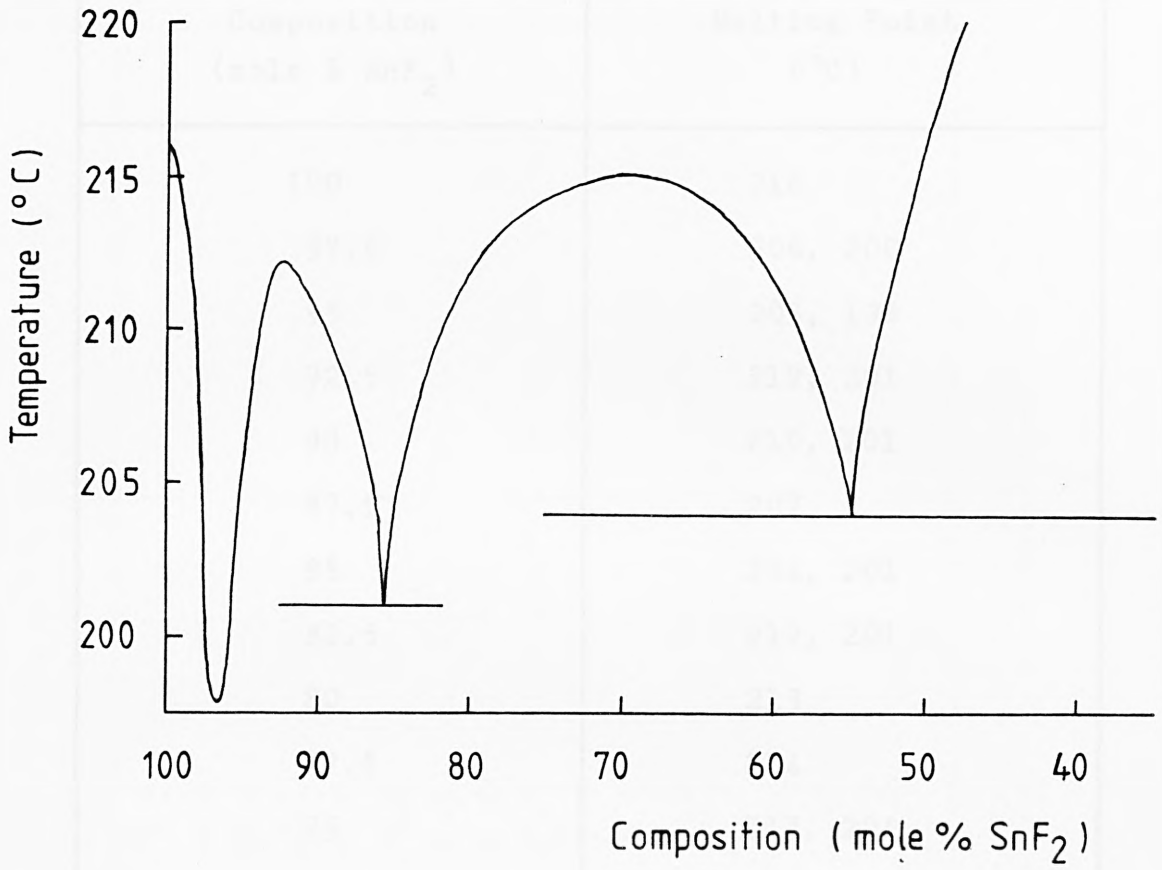

FIGURE 6.(2). The Phase Diagram for the SnF_2 : MoS_2 System.

temperature. Beyond the eutectic composition the system behaves as a new compound doped with MoS_2, the melting point rises to a maximum at the pure new compound composition. Similar data can be obtained from the cooling cycles. The data illustrated in Figure 6.(2). are listed in Table 6.(1).

From the graph, it can be seen that two new phases are formed: one at 92.5 mole % SnF_2 and the other at 70 mole % SnF_2. Three eutectic temperatures are observed at 198°, 201° and 204°C, with compositions of approximately 97, 86 and 55 mole % SnF_2, respectively.

Any new phase formed will have a distinct X-ray powder diffractogram, different to those of the parent compounds. The X-ray data for SnF_2, MoS_2 and the new compounds are in

Composition (mole % SnF_2)	Melting Point (°C)
100	216
97.5	206, 200
95	205, 198
92.5	212, 201
90	210, 201
87.5	207
85	204, 201
82.5	212, 201
80	213
77.5	214
75	213, 204
72.5	215, 203
70	215, 204
67.5	215, 204
65	212, 204
62.5	215, 204
60	213, 204
55	204
35	204

TABLE 6.(1). The Melting Points for the SnF_2 : MoS_2 System.

Table 6.(2). and Figure 6.(3). The patterns for all other compositions in the system are superpositions of the patterns of the appropriate parent compounds and new phases. The X-ray data therefore confirms the existence of the 92.5 mole % SnF_2 : 7.5 mole % MoS_2 phase.

Molybdenum(IV) sulphide is a good semiconductor with

SnF_2		MoS_2		92.5 % SnF_2		70 % SnF_2	
2θ	R.I.	2θ	R.I.	2θ	R.I.	2θ	R.I.
8.3	33	14.1	100	8.2	21	8.3	10
9.3	33	28.9	2	9.4	22	9.4	12
14.1	29	32.6	12	16.3	24	14.3	100
25.0	100	33.4	5	27.8	100	25.0	15
26.2	33	35.8	5	29.3	64	26.3	12
27.8	50	39.5	40	29.5	74	27.7	15
28.1	71	44.1	12	36.8	15	32.6	19
35.5	17	49.8	22	38.0	9	33.4	10
43.8	24	58.3	7	41.5	7	34.8	5
45.6	12	60.2	11	44.7	4	35.8	7
46.3	5			46.0	9	36.6	7
46.8	26			47.1	34	39.5	40
49.1	6			47.7	40	44.1	10
51.3	32			49.6	15	49.8	20
				51.9	26	58.3	11
				58.3	11	60.3	12
				60.2	12		

TABLE 6.(2). X-Ray Powder Diffraction Data for SnF_2, MoS_2 and their New Phases.

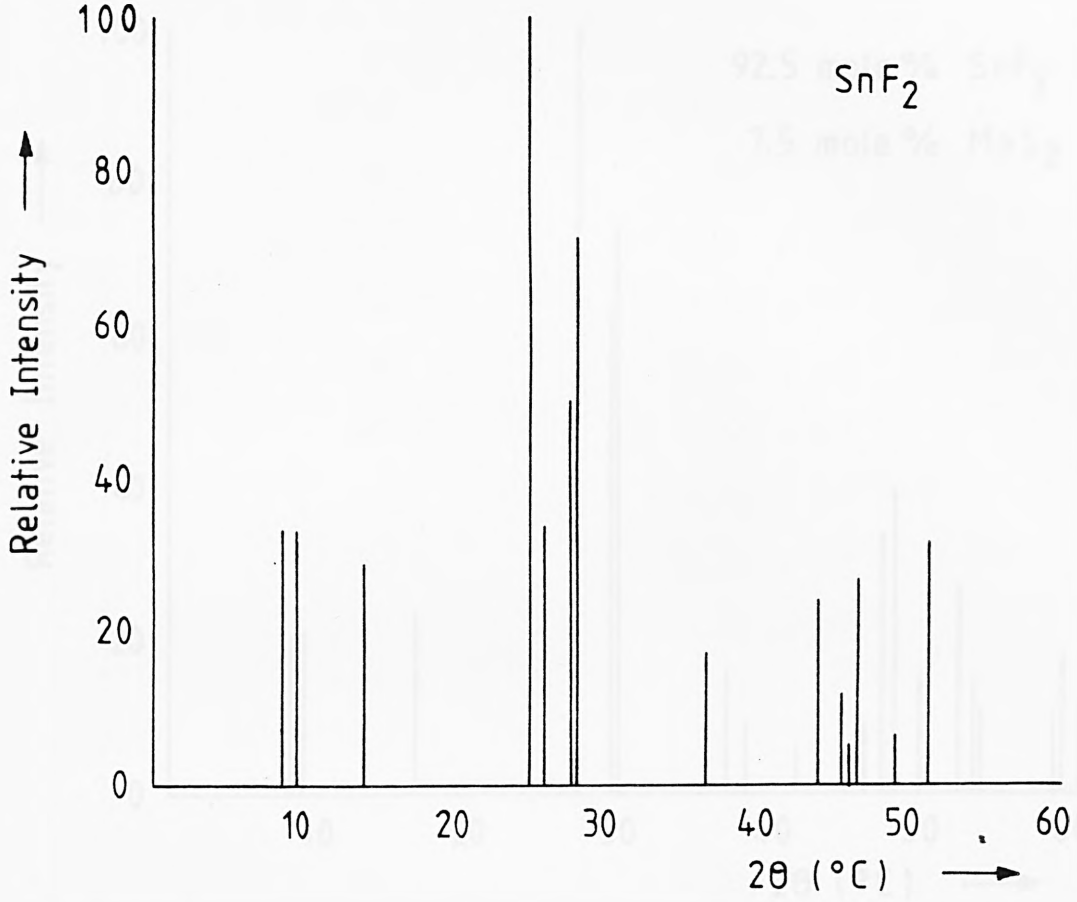
100
80
60
40
20
0
Relative Intensity
SnF_2
10
20
30
40
50
60
2θ (°C)

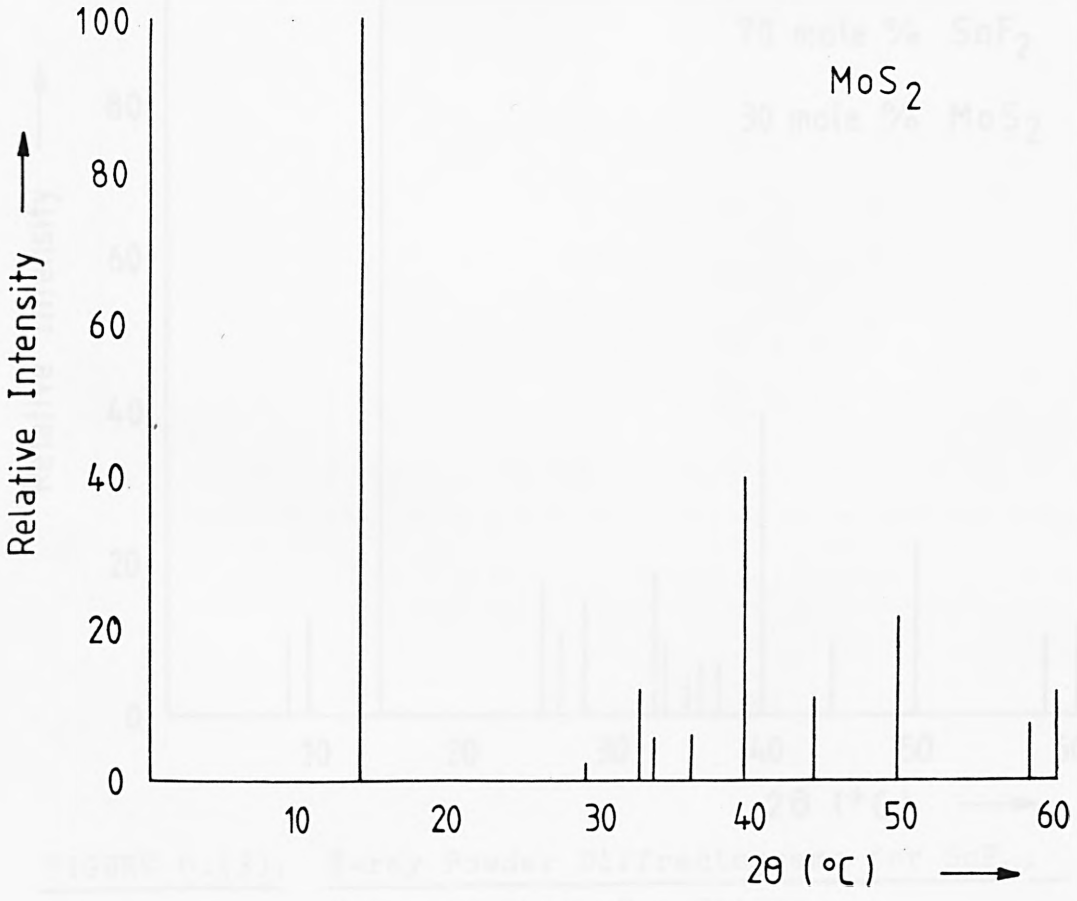
100
80
60
40
20
0
Relative Intensity
MoS_2
10
20
30
40
50
60
2θ (°C)

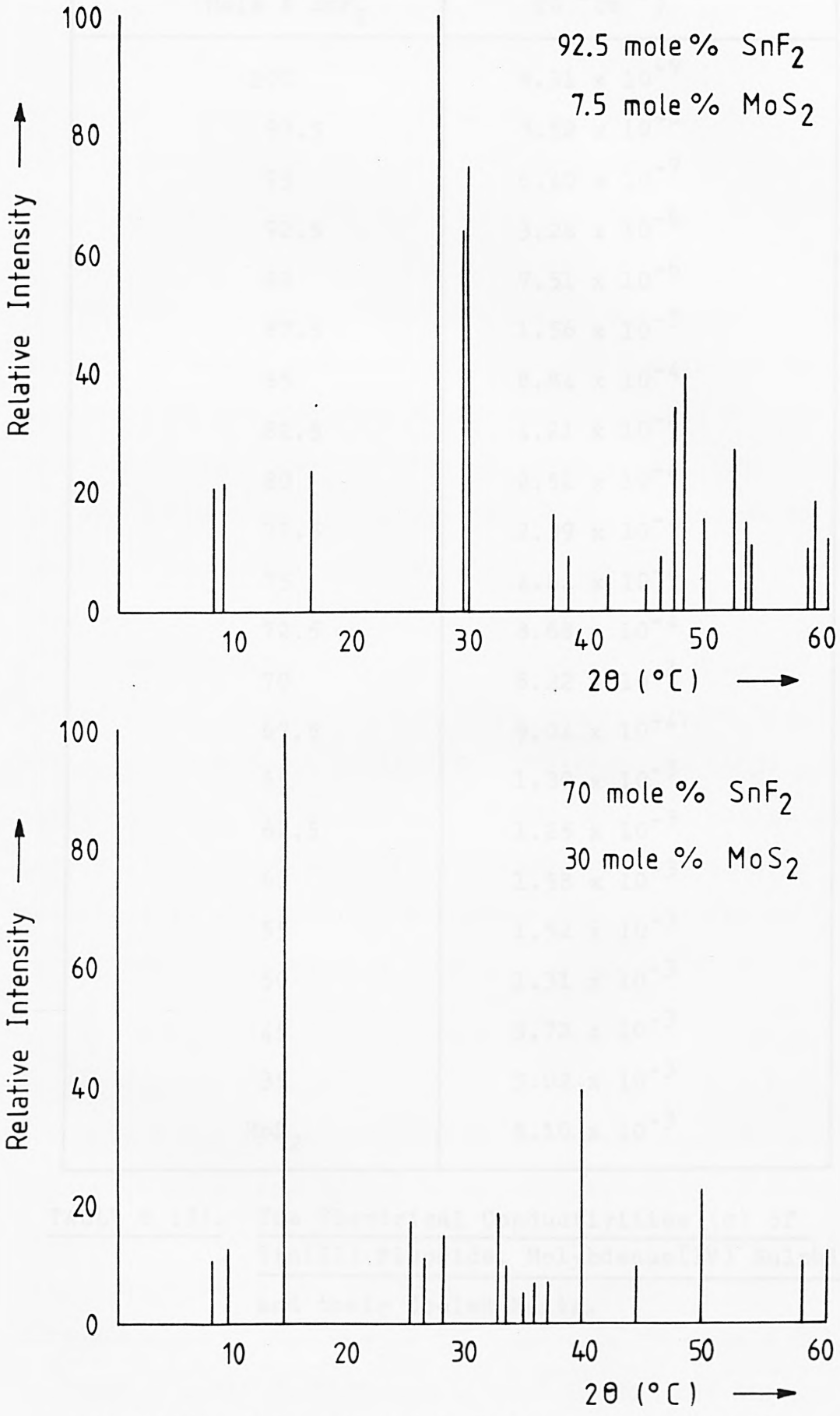

FIGURE 6.(3). X-ray Powder Diffractograms for SnF_2, MoS_2 and their New Phases.

Composition Mole % SnF_2	σ ($\Omega^{-1}cm^{-1}$)
100	8.31×10^{-9}
97.5	3.52×10^{-8}
95	6.40×10^{-7}
92.5	3.28×10^{-6}
90	7.51×10^{-6}
87.5	1.56×10^{-5}
85	8.84×10^{-4}
82.5	4.21×10^{-4}
80	2.52×10^{-4}
77.5	2.39×10^{-4}
75	4.84×10^{-4}
72.5	8.68×10^{-4}
70	8.22×10^{-4}
67.5	9.04×10^{-4}
65	1.30×10^{-3}
62.5	1.25×10^{-3}
60	1.58×10^{-3}
55	1.52×10^{-3}
50	1.31×10^{-3}
45	3.72×10^{-3}
35	3.02×10^{-3}
MoS_2	5.10×10^{-3}

TABLE 6.(3). The Electrical Conductivities (σ) of Tin(II) Fluoride, Molybdenum(IV) Sulphide and their Cooled Melts.

a conductivity of $5.10 \times 10^{-3}\ \Omega^{-1}cm^{-1}$, whilst that of stannous fluoride is $8.31 \times 10^{-9}\ \Omega^{-1}cm^{-1}$. As the proportion of MoS_2 in the cooled melts increases, the conductivity increases until at 45 mole % SnF_2 it approaches that of MoS_2. There is no visible difference in the increasing trend when the new phases are reached (Table 6.(3).).

The diffuse reflectance spectra of the cooled melts provide no useful information about the hopping of the 5s electrons of the tin into the conduction band. MoS_2 shows four absorption bands in its spectrum at 343, 430, 600 and 655 nm, respectively. The spectra of the cooled melts also contain these peaks and they occur at very similar wavelengths.

^{119}Sn Mössbauer spectra are obtained for selected cooled melts, their parameters are compared with those of stannous fluoride in Table 6.(4). Essentially there are no differences in the parameters of SnF_2 and the melts, which implies that molybdenum(IV) sulphide does not cause a reduction in the band gap to enable the 5s electrons to 'hop' into the conduction bands.

The SnF_2 : MoS_2 system described in this section, yields two new phases. The first at 92.5 mole % SnF_2 : 7.5 mole % MoS_2 is identified in the phase diagram and its existence is proved by its X-ray diffractogram. Evidence from other techniques imply that the tin environment is hardly changed by the addition of MoS_2 to SnF_2. The X-ray diffractogram of the second new phase, at 70 mole % SnF_2 contains a great deal of detail associated with the diffractogram of MoS_2, and this may mean that on cooling

Composition Mole % SnF_2	δ (mms^{-1})	Δ (mms^{-1})
100	3.44	1.66
92.5	3.41	1.59
87.5	3.52	1.63
75	3.48	1.63
70	3.45	1.62
60	3.41	1.65

TABLE 6.(4). The ^{119}Sn Mössbauer Parameters for SnF_2 and Selected Cooled Melts of the SnF_2 : MoS_2 System.

this new phase decomposes to molybdenum(IV) sulphide, stannous fluoride or another phase.

6.4. THE SnX_2 : SnS_2 SYSTEM (WHERE X = F, Cl, OR Br).

A study was carried out on the phases obtained from the SnX_2 : SnS_2 systems for X = F, Cl and Br. Phase diagrams constructed from the DTA-TG data (Figures 6.(4). to 6.(6).) did not give conclusive evidence for the existence of new phases but did show the following:

(i) In the SnF_2 : SnS_2 system, two new phases appear to have been formed; one at 95 mole % SnF_2 and the other at 72.5 mole % SnF_2. The eutectic temperature lies at about 204°C at 92.5 mole % SnF_2.

(ii) The $SnCl_2$: SnS_2 system shows two new phases at 85 mole % $SnCl_2$ and 70 mole % $SnCl_2$. A eutectic point is not observed in this system.

(iii) $SnBr_2$: SnS_2 - two new phases are observed at 95 mole % $SnBr_2$ and 70 mole % $SnBr_2$. The eutectic

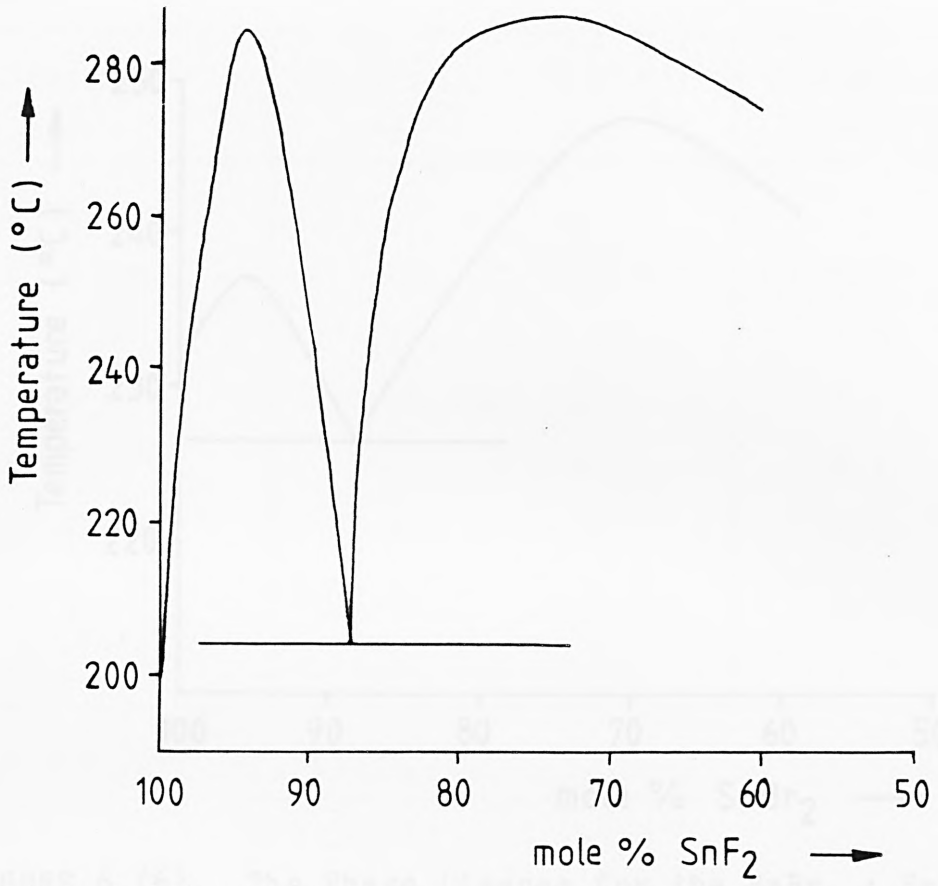

FIGURE 6.(4). The Phase Diagram for the SnF_2 : SnS_2 System.

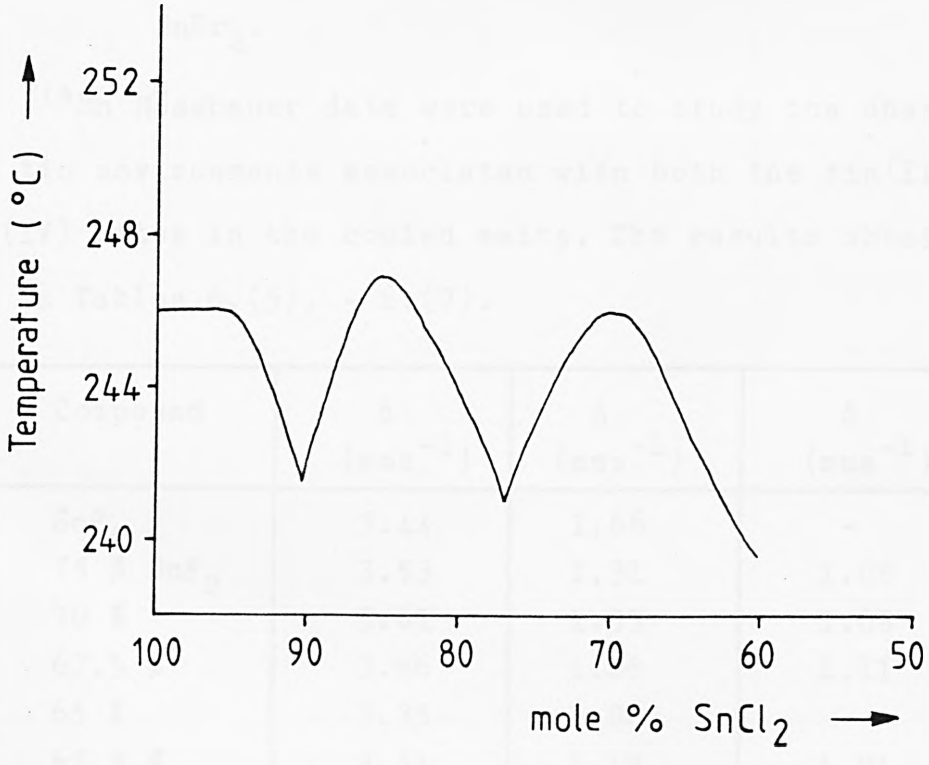

FIGURE 6.(5). The Phase Diagram for the $SnCl_2$: SnS_2 System.

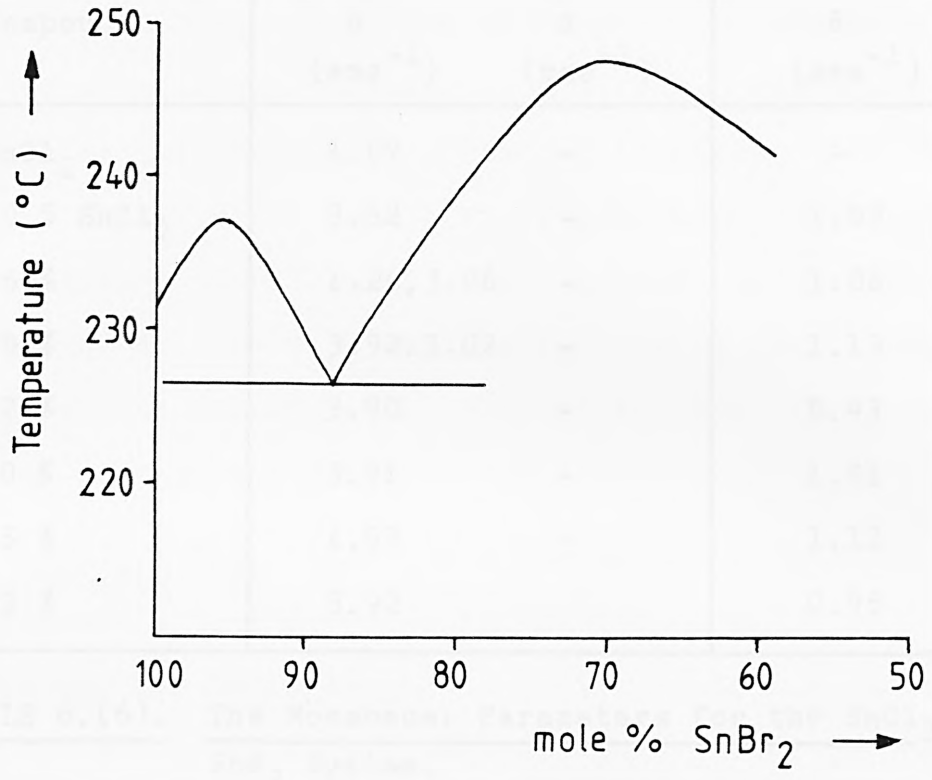

FIGURE 6.(6). The Phase Diagram for the $SnBr_2$: SnS_2 System.

point is at 227°C at approximately 87.5 mole % $SnBr_2$.

^{119}Sn Mössbauer data were used to study the changes in the tin environments associated with both the tin(II) and tin(IV) sites in the cooled melts. The results obtained are in Tables 6.(5). - 6.(7).

Compound	δ (mms^{-1})	Δ (mms^{-1})	δ (mms^{-1})
SnF_2	3.44	1.66	-
75 % SnF_2	3.53	1.31	1.05
70 %	3.61	1.33	1.08
67.5 %	3.66	1.26	1.11
65 %	3.35	1.00	-
62.5 %	3.51	1.19	1.01
60 %	3.61	1.27	1.06
SnS_2	-	-	1.02

TABLE 6.(5). Mössbauer Parameters for the SnF_2 : SnS_2 System.

Compound	δ (mms^{-1})	Δ (mms^{-1})	δ (mms^{-1})
$SnCl_2$	4.07	-	-
80 % $SnCl_2$	3.62	-	1.09
75 %	4.26,3.06	-	1.08
70 %	3.92,3.02	-	1.13
67 %	3.90	-	0.93
50 %	3.91	-	1.01
45 %	4.03	-	1.12
33 %	3.92		0.95

TABLE 6.(6). The Mössbauer Parameters for the $SnCl_2$: SnS_2 System.

Compound	δ (mms^{-1})	Δ (mms^{-1})	δ (mms^{-1})
$SnBr_2$	3.93	-	-
95 % $SnBr_2$	3.95	-	-
90 %	3.94	-	0.46
85 %	3.96	-	1.08
80 %	3.96	-	0.76
75 %	3.90	-	0.92
70 %	3.85,2.92	-	1.10
67 %	3.87	-	0.82
50 %	3.79	-	0.88
33 %	4.09	-	1.01
SnS_2	-	-	1.02

TABLE 6.(7). The Mössbauer Parameters for the $SnBr_2$: SnS_2 System.

(i) $\underline{SnF_2} : \underline{SnS_2}$ - Addition of sulphide to stannous fluoride leads to an increase in the isomer shift and a decrease in the quadrupole splitting (Table 6.(5).). This would be the expected result for replacement of F^- in the environment of tin(II) with sulphide ions, which makes less use of the tin 5s electrons in bonding. There seems to be very little effect on the tin(IV) spectral lines on addition of fluoride ions.

(ii) $\underline{SnCl_2} : \underline{SnS_2}$ - Addition of sulphide to stannous chloride leads to a decrease in the isomer shift of the tin(II) species until 80 mole % $SnCl_2$. At 70 and 75 mole % $SnCl_2$ two Sn(II) sites are observed which could be indicative of a new phase or a mix of Sn-Cl and Sn-S absorptions (SnS: δ = 3.29 mms^{-1}). Below 70 mole % $SnCl_2$ only one phase is seen, this could be a new site or a mixture with $SnCl_2$. Again, there seems to be very little effect on the tin(IV) spectral lines by the addition of chloride.

(iii) $\underline{SnBr_2} : \underline{SnS_2}$ - The Mössbauer parameters of the Sn(II) species (Table 6.(7).) are unaffected up to 80 mole % $SnBr_2$, the spectra show two tin(II) sites for melts with composition at 70 mole % $SnBr_2$. This is accounted for by either a new phase or a mixture of Sn-Br bonding and Sn-S bonding. Below 70 mole % $SnBr_2$, one phase is observed. The Sn(IV) species appears to be affected by the addition of bromine, although there was no clear trend of the effect of addition of bromine on the isomer shift.

6.5. SUMMARY.

The aim of this work was to study the removal of the distortion in a tin(II) species when it is doped with a chalcogenide. The SnF_2 : MoS_2 system was studied in depth and although two new phases were identified at 92.5 mole % SnF_2 and 70 mole % SnF_2, there was no evidence from the electrical conductivity and reflectance measurements and the ^{119}Sn Mössbauer spectral data, to show that the removal of distortion had occurred via the donation of the 5s electrons into the conduction bands.

The tin(II) halide - tin(IV) sulphide systems were studied briefly, but weight losses which occurred both during the preparation and thermal analysis of the cooled melts prevented an accurate description of the systems. Further work to be carried out on these systems should include preparation in sealed ampoules and thermal analysis in sealed pans. Some evidence for the donation of the 5s electron density of the tin(II) species into conduction bands is obtained from the ^{119}Sn Mössbauer data and clearly, a detailed study of this is required.

It was hoped to relate these systems and the results obtained, to the $SnBr_2$: SnS system studied previously[13], in which the new phases were characterised as $Sn_7Br_{10}S_2$ and Sn_4Br_6S. These compounds were obtained from the 75 mole % and 70 mole % $SnBr_2$ ratios, respectively. Therefore, in the SnF_2 : MoS_2 system, the new phase at 70 mole % SnF_2 can be related to Sn_4Br_6S, so that the formula of the new phase is $Sn_3MoF_6S_2$.

REFERENCES.

1. J.D. Donaldson, Progress in Inorganic Chemistry, (1967), 8, 287.
2. D.S. Payne, Q. Rev. Chem. Soc., (1961), 25, 173.
3. T.N. Polynova and M.A. Porai-Koshits, Zh. Strukt. Khim., (1965), 7, 147.
4. J. Barrett, S.R.A. Bird, J.D. Donaldson and J. Silver, J. Chem. Soc. (A), (1971), 3105.
5. J.D. Donaldson, D.R. Laughlin, S.D. Ross and J. Silver, J. Chem. Soc. (A), (1973), 1985.
6. D.S. Urch, J. Chem. Soc., (1964), 5775.
7. T.C. Gibb, R. Greatrex, N.N. Greenwood and A.C. Sarma, J. Chem. Soc. (A), (1970), 212.
8. L. Atkinson and P. Day, J. Chem. Soc. (A), (1969), 2433.
9. D.E. Scaife, P.F. Weller and W.G. Fisher, J. Sol. State Chem., (1974), 9, 308.
10. J.D. Donaldson and J. Silver, Inorg. Nucl. Chem. Lett., (1974), 10, 537.
11. J.D. Donaldson, J. Silver, S. Hadjiminolis and S.D. Ross, J. Chem. Soc., Dalton Trans., (1975), 1500.
12. R.A. Howie, W. Moser and I.C. Trevena, Acta Cryst., (1972), B28, 2965.
13. S.M. Grimes, Ph.D. Thesis, (1982), The City University, London.

APPENDIX I.

Appendix I contains the final calculated and observed structure factors for the following compounds:

(1) Potassium [Hydrogen-bis-(maleato)] - Stannate(II).

(2) Tin(II) malonate.

This information has been reduced onto microfiche and this can be found inside the envelope attached to the back cover of this thesis.